# Proceedings of 2010 AIT-KU Joint Symposium on Human Security Engineering

***in Bangkok***

***November 25-26, 2010***

**Hosted by**

**Asian Institute of Technology**

**Kyoto University**

**Kyoto University Global COE Program**
**Global Center for Education and Research on**
**Human Security Engineering for Asian Megacities**

# Proceedings of
# “2010 AIT-KU Joint Symposium on Human Security Engineering”

---

**25-26 November, 2010**

**Chaophya Park Hotel, Bangkok, Thailand**

**Editors:**
Hiroyasu Ohtsu
Noppadol Pien-Wej

**Organized by:**
Kyoto University
Asian Institute of Technology
Global COE program “Global Center for Education and Research on Human Security Engineering for Asian Megacities”

# Conference Governors

ADVISORY BOARD

COMMITTEE MEMBERS

Yuzo Ohnishi (Kyoto University)

Vilas Wuwongse (AIT)

Yuzuru Matsuoka (Kyoto University)

ORGANIZING COMMITTEE

COMMITTEE MEMBERS

Prof. Hiroyasu Ohtsu (Kyoto University)

Assoc. Prof. Noppadol Phienwej (AIT)

PROGRAM COMMITTEE

CO CHAIRMAN

Prof. Kiyoshi Kobayashi (Kyoto University)

Assoc. Prof. Pennung Warnitchai (AIT)

COMMITTEE MEMBERS

Prof. Eiichi Taniguchi (Kyoto University)

Prof. Toshifumi Matsuoka (Kyoto University)

Prof. Junji Kiyono (Kyoto University)

Prof. Kunitomo Sugiura (Kyoto University)

Prof. Hitoshi Gotoh (Kyoto University)

Assoc. Prof. Yasuto Tachikawa (Kyoto University)

Assist. Prof. Mamoru Yoshida (Kyoto University)

Prof. Suttisak Soralump (Kasetsart University)

Assoc. Prof. Mukand S. Babel (Asian Institute of Technology)

Assist. Prof. Pham Huy Giao (Asian Institute of Technology)

Assist. Prof. Kunnawee Kanitpong(Asian Institute of Technology)

CONFERENCE SECRETATIRATS

Dr. Mamoru Yoshida (Kyoto University)

Mr. Taweephong Suksawat (Asian Institute of Technology)

# FOREWORD

Fulfilling basic human needs and assuring a self-sustainable recovery from environmental pollution and disasters in Asian Megacities has been a major challenge for several decades, and the situation still needs improvements. Along that line, Kyoto University has launched a new program of Global Center Of Excellence (GCOE) entitled “Global Center for Education and Research on Human Security Engineering for Asian Megacities” since 2008. The purpose of the GCOE program is to establish the discipline of “Urban Human Security Engineering” and to provide education for young researchers and high-level practitioners for human security in Asia. “Urban Human Security Engineering” is defined as a system of technology (techniques) for designing and managing cities that will enable the inhabitants to live under better public health conditions, and also be safeguarded against potential threats of large-scale disasters and environmental destructions. In establishment of the discipline, four existing fields, i.e. urban governance, urban infrastructure management, health risk management, and disaster risk management, are integrated into one. In addition, the scope of work of the GCOE program is to implement area-specific researches and educational activities. The program set up 7 overseas bases outside Japan and Asian Institute of Technology (AIT) in Bangkok is one of them.

At AIT oversea base, a variety of collaborative researches related with infrastructure asset management, environment accounting systems for infrastructures, urban water resource management and food supply systems, transportation and logistics system have been conducted. The symposium entitled “2010 AIT-KU Joint Symposium on Human Security Engineering” is to share the research progresses, deepen the understandings on urban human security engineering and develop its policy and implementation. In addition, the symposium contributes to strengthen a broad range of human security network between ASEAN countries through the distinguished speakers who are invited from the countries.

The symposium “2010 AIT-KU Joint Symposium on Human Security Engineering” is jointly organized by Graduate School of Engineering, Kyoto University, Japan and Asian Institute of Technology, Thailand. In addition, the symposium also gets great encouragement and support of the Global COE program “Global Center for Education and Research on Human Security Engineering”, Kyoto University, Japan.

We are grateful to individuals and organizations for their helps and supports during the preparation and hosting the symposium. It is not possible to mention all of them, but their helps are very much appreciated. Specifically, we are grateful to the keynote speaker, authors, participants, the seminar’s advisory board, organizing committee, program committee and the following organizations:

- Graduate School of Engineering, Kyoto University, Japan
- Graduate School of Global Environmental Studies, Kyoto University, Japan
- Asian Institute of Technology
- Department of Highways, Thailand

We are also grateful to Dr.Mamoru Yoshida of Kyoto University and Mr.Taweephong of Asian Institute of Technology for their secretarial duties for the symposium.

## Editors:

Professor Dr. Hiroyasu Ohtsu

Department of Urban Management, Graduate School of Engineering, Graduate School of Management, Kyoto University, Japan

Associate Professor Dr. Noppadol Phienwej

Geotechnical and Geoenvironmental Engineering, Asian Institute of Technology, Thailand

# Table of Contents

2010 AIT-KU JOINT SYMPOSIUM ON HUMAN SECURITY ENGINEERING
Bangkok, Thailand, November 25-26, 2010

# Participatory Approach to Community Based Water Supply System

Kakuya MATSUSHIMA[1], Kiyoshi KOBAYASHI[2]
Kenshiro OGI[3] and, Ismu Rini Dwi ARI[4], Hayeong JEONG[5],

[1]Associate Professor, Dept. of Urban Management, Kyoto University
( Kyoto University Katsura Campus, Nishikyo-ku, Kyoto 615-8540, Japan)
E-mail: kakuya@psa.mbox.media.kyoto-u.ac.jp
[2]Professor, Dept. of Urban Management, Kyoto University
E-mail: kkoba@psa.mbox.media.kyoto-u.ac.jp
[3]Master Student, Dept. of Urban Management, Kyoto University
E-mail: k.ogi@ky4.ecs.kyoto-u.ac.jp
[4]Candidate PhD, Dept. of Urban Management, Kyoto University
E-mail: ismurinidwi.ari@fy5.ecs.kyoto-u.ac.jp
[5]GCOE Researcher, Dept. of Urban Management, Kyoto University
E-mail: hayeong@hse.gcoe.kyoto-u.ac.jp

Water scarcity due to climate change as well as inappropriate water governance is one of the important topics in the world, particularly in developing countries. Most people who live close to the water resource are not always economically-advantaged. Moreover, it might be seems that people living close to "economically-attractive water resource" are classified into lower category according to the standard of living in the country. Community based water supply system is one of strong alternatives to existing water supply system by the public sector. The community based water supply system works more effectively if it is based upon strong community network in the region.

This study conducts an empirical research on community based water supply system in Indonesian rural area. In this paper, we propose a discrete-choice model which describes the mechanism of resident's spontaneous collaboration to access water. We formulate a hypothesis that households with better community tie have ability to organize "community based" management system. In order to test it, we formulate a spatial probit model which can consider the effect of social interaction upon their choices in water supply system. Traditionally, spatial models are estimated with maximum likelihood method, however, in this paper, we adopt Markov chain Monte Carlo (MCMC) method to estimate parameters due to the difficulty in estimation of discrete-choice model with spatial interaction term. Using dataset from a field survey in Indonesia which we conducted in 2008 the spatial probit model is empirically tested to show that social interaction in the community plays an important role on resident's spontaneous collaboration to manage community-based water supply system.

***Key Words :*** *participatory approach, community based, empirical research, discrete choice model*

## 1. INTRODUCTION

Having access to safe drinking water is one of the most indispensable human necessities. WHO (2010) stated that six out of the seven people without access to an improved water source live in rural areas, moreover, regarding WHO/UNICEF (2004) the number of urban residents without adequate water services is increasing rapidly. Consequently, estimates of access to safe drinking water are a cornerstone of most international assessments of progress toward solving global and regional water problems, particularly to reach target 10 of the Millennium Development Goals (MDGs) that reduces by half the proportion of people without sustainable access to safe drinking water by 2015.

There is a mechanism that inhabitants who live near the water resource cannot develop the water resource with their value. In line with the report of Asian Water Development Outlook (AWDO) that the future water crisis in Asian countries, it will not be because of physical scarcity of water, but because of inadequate or inappropriate water governance, including management practices, institutional arrangements, and socio-political conditions, which leave much to be desired (The 1st Asia Pacific Water Summit in 2007).

Under t collaboration activities for water supply system by community members who live close to the water resource has examined in many countries. Collective action may be defined as action on the part of one or more people striving to achieve objective or satisfy common interest of the group, implies devising frameworks that limit the pursuit of individual self interest and sustain the benefit shared by the group. In case of Indonesia, among total 231.6 million inhabitants only around 49.7% of the citizen has access to water which its 10% is obtained through community based water management (Statistic Centre Board, 2005).

In order to support and sustain the participatory approach to community based water supply system, it is necessary to clarify the mechanism and to invent institutional system for support the collaboration activities. However, there are not enough investigations on the participatory approach to community based water supply system. Necessitate of better understanding about local community structure and network is urgent toward encouraging suitable water policy and institutional restructuring.

Therefore this study is questioning: Why people are involved in establishing the community based water supply system in order to access water?, Whether their choices to join the community based water supply system are cooperated or not?, Why people do or do not engage in a kind of collective action? It is important to investigate the mechanism of the spontaneous collaboration to access water. In other words, this study aims to investigate interdependent preference in a choice of clean water of the community on a field survey of Indonesian's water supply system.

Then the paper is structured as follows. Section 2 illustrates the current situation of the respondent and access to water in the study area. Section 3 explains the model consists of a spatial probit model and Markov Chain Monte Carlo (MCMC) for estimation method, and then in section 3 describes the results and discussion of the empirical application. Finally, this paper is concluded with section 5.

## 2. AN EMPIRICAL RESEARCH

### (1) Description of the survey

To illustrate the model in an applied setting, we used data from a field survey which was conducted in 2008. Through systematic sampling, 500 households living at Toyomarto village and Candi Renggo village, Singosari district, Malang regency, East Java Province Indonesia, are selected as the respondents for the study. Data is collected employing face to face interview method that effectively had been done within 10 days by 20 surveyors with interview schedules from 07:00 a.m. to 09:00 p.m. depend on the respondent's readiness.

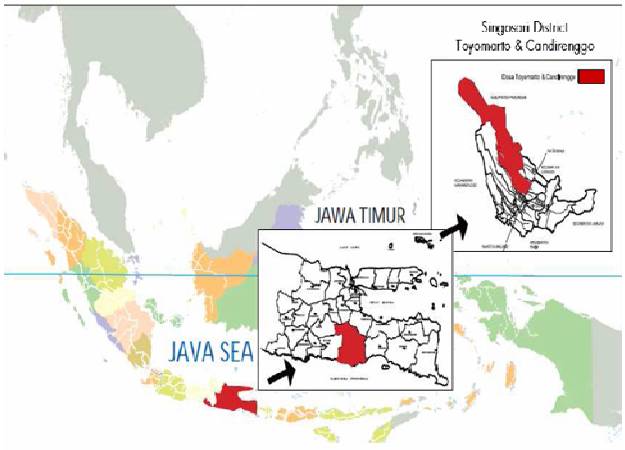


**Fig. 1** Location of the research area

The restraint of the study is that the respondents are selected from total 24,388 inhabitants in the two villages. Hence the results and the substantial assessments replicate the essential characteristics of the contacted people. Furthermore, in order to optimize representativeness of the inhabitants, the respondents selected for the study are the husband, the wife or the head of family that are chosen so as to represent typical precious inhabitants.

Referring to the Instruments of the Social Capital Assessment Tools developed by World Bank (2004) and combining it with preliminary survey information, we developed household questionnaire survey to investigate community network. The questionnaire survey covers questions that concern (i) demographics data of the respondent (gender, age, family size, occupation, length of stay, work place, income, and education), (ii) water issues (water supply issues, water demand issues, rule of water usage), and (iii) community network (participation in community group, trust on lending & borrowing, concern to community welfare, and opinion towards living neighborhood). In this paper, we focus upon the question of participation in community group to explain residents' preferences on water choice of community based.

**(2) Access to Water**

In general, there are two types of fresh water resources utilized by the respondents in the study area, namely surface water and shallow ground water.

Firstly, surface water consists of natural spring and river. There are three natural springs called Candi Sumber Awan Spring and Banyon Spring in Toyomarto village, and Kendedes Pond in Candi Renggo village. The other surface water comes from two rivers named Sumber Awan River and Petung River flowing away through the area of study. Secondly, shallow ground water is utilized by individual household who builds their individual well to get fresh water for domestic purposes. Based on categorization of goods, both types of fresh water resources could be categorized as common-pool resources (CPRs) which share a pair of common characteristics (i) their consumption is rival, but (ii) it is non-excludable (Bruce Wydick, 2008). Rivalry means that consumption by one person/group/ institution precludes consumption by another. In this case, water in the spring or river or shallow ground water that it utilized by A person is one that B person can't consume it. Excludability means that it is easy to control access to a resource, and to exclude others from consuming it. A person can't exclude B person from using water in the spring, river, as well as shallow ground water to fulfill their domestic purposes.

Furthermore, we put more detail explanation of the five type access to water in the research area as follow. First, water services supplied by group of community based water management namely HIPPAM (Resident Association of Drinking Water Users). The HIPPAM serves 42% respondents who become a member of certain group of HIPPAM. These community water providers utilize the three natural wellsprings to supply their member. A group of HIPPAM encompasses around 30 to 300 households living in a certain neighborhood association through direct home water connection. This community group can be categorized as club goods consist of combination of non-rivalry and excludable. Non-rivalry here means that water consumption by one member permit water consumption by another. Excludability means only the member has access to water from HIPPAM and excludes others from consuming it. Structural organization of HIPPAM encompasses 1 leader, 1 treasurer and 2 technician staffs that are selected among the whole member once in a year. Main task of the leader is to maintain management system of HIPPAM. The member goes to treasurer to pay their monthly charge of water usage that the price is set up under their agreement in the community meeting. Water pricing per group employs various fixed monthly price from IDR. 2,000 (¥ 20) up to IDR. 15,000 (¥ 150). For the first physical installation of water connection, each member needs to pay at around IDR. 500,000 (¥ 5,000) to IDR. 1 Million (¥ 10,000). In addition, specific task for technicians are to monitor and maintain water facility, and then try to fix the physical problem if it occurs. Finally, the whole money that compiles in the treasurer functions as capital source to keeping good the performance of water facility, and also to pay a kind of service fee for the committee member that basically their jobs are a type of voluntary work.

Secondly, a drinking water company in Malang regency namely PDAM (Local Company of Drinking Water) serves 22% respondents who become customers. This local water provider employ Candi Sumberawan wellspring to provide water for their customers in the two villages. The respondents who join PDAM's facility are the respondents who officially registered as PDAM's member and pay monthly charge of water usage. Price for the first physical installation of water connection is around IDR. 1,500,000 (¥ 15,000), and there is a fixed price for the first $10m^3$ of water usage at IDR. 11,500 (¥ 115). Then, for the next water usage, the price per cubic meter for domestic purpose is IDR. 1,500 (¥15). A group of respondent who join PDAM is the one who has possibility to obtain fresh water access from PDAM as the local

water provider. In this sense, water from PDAM could be categorized as club goods that it is non-rival among its members but prohibit others from consuming it.

Thirdly is access to clean water through private or individual well. The residents build their own well inside their land property to obtain drinking water and it covers 23% of the respondent as pure private goods. They usually utilize shallow ground water in depth less than 20 meter, where some of them also develop water pipeline installation from the well to the house (e.g. bathroom and kitchen) using electric pump. Meanwhile, others have to draw water from the well manually using plastic bucket and bring it to the kitchen or bathroom.

Then, the fourth type is access to water through public hydrant that serves 12% respondents. There are two types of public hydrant. First, several groups of HIPPAM in addition to serving member, they also build some public taps in vicinity residential area to serve the residents without access to direct water pipeline connection to house, or explicitly reveal that purpose of public tap is to serve non member of the community based water management. And second one is communal well where residents have to draw water using plastic bucket in the public well that is built or provided by someone who like to shares his or her private good with others who cannot afford to have their own wells. This circumstance shows the existence of bridging social capital among groups in the community, as mentioned by Woolcock and Narayan (2000) that bridging social capital refers to the relationships that we have with people who are not like us i.e. relationships with people from different socio-economic status and different ethnic. In this sense, we could also find how the community through their collective action tries to get access to water.

The last type of access to water resources is for the respondents who still use water from rain water or river such as Sumberawan River and Glatik River where the water flows in the two villages (1%).

Table 2 describes the type of access to clean water of the respondents, which 2 respondents are excluded from the sample due to inconsistency of its answer.

**Table 1** Type of Access to Water

| Access to Water | Number Of Respondent | Percentage |
|---|---|---|
| HIPPAM | 210 | 42 |
| PDAM | 109 | 22 |
| Individual Well | 117 | 23 |
| Public Hydrant | 58 | 12 |
| Others | 4 | 1 |
| Total | 498 | |

**Fig. 2** HIPPAM's water reservoir, communal hydrant, PDAM's water reservoir, individual well, river

### (3) Demographic Data of the Respondent

There are majority male respondents (70%) as compared to the females in the study. The average age of the respondents is 46.91 years that around 92% respondents can be classified into productive age (19-65 years). They have an average of 4 members in the household. Thirty percent occupation of the respondents is in agriculture and manufacturing sector. Type of their livelihood is such as food peddler, owner and worker in the small scale sandal industry, farmer, breeder and field hand. Meanwhile, majority occupation could be categorized in services sector which varies from working in the private company (20%), labor industry (15%), and in the range of 1-6% as merchant, driver, teacher, official, military/police, retiree, housewife, and even 4% respondent in unemployment status.

Majority household income of the respondents is less than 1 million rupiah per month (64%) consist of 25% respondents with monthly income less than 500.000 rupiah and another 39% with monthly income between 500.000 - 1 million rupiah. This indicates that the residents are in the lower middle class of socio-economic status that the monthly minimum wage of Malang regency in 2009 is determined at 945.500 rupiah. Elementary level has six years of education; meanwhile it has three years in middle school and also in high school. According to education statistics (source: www.Nation Master.com), average years of schooling of adults in Indonesia is 5 years. It implies that around 56% of the respondents in the study have education level above the national average.

## 3. MODEL AND ESTIMATION METHOD

### (1) Model

This section focuses on a discrete-choice model for whether a household joins HIPPAM conditional on that household's characteristics. We start by introducing main assumptions in the model and the notation that will be used for the rest of the paper. Let $n$ be the number of individual households. Each household has two alternatives, labeled as 1 for joining HIPPAM and 0 for otherwise. For each household we observe whether the household joins HIPPAM or not and model it as the realization of a

random variable $y_i$. Economic theory suggests that the decision to join is primarily made to maximize the discounted value of future profits, so we assume that the choice of whether to join HIPPAM or not is the result of a household's decision to maximize their utility. An event will occur with a certain probability $p$ if the utility derived from choosing that alternative is greater than the utility from the other alternative. Let $z_i$ be the difference in the utility from alternatives 1 and 0. The difference in the utility is modeled as:

$$z_i = x_i'\beta + \theta_i + \varepsilon_i \quad (1)$$

where $i = 1, \cdots n, x_i = (x_{ik}; k = 1, \cdots, K)'$ is a vector of observed household specific attributes, $\beta = (\beta_k; k = 1, \cdots, K)'$ is a vector of unobserved parameters to be estimated, $\theta_i$ is an unobserved random effect component, and $\varepsilon_i$ is a stochastic error term with $\varepsilon_i \sim N(0,1)$. We do not observe $z_i$, but only observe the sign of $z_i$. We observe the household's choice $y_i$ being equal to 1 or 0, depending on whether $z_i$ has a positive sign indicating the higher utility from this alternative or a negative sign associated with the lower utility associated with this alternative. Therefore we observe:

$$y_i = \begin{cases} 1 & if \quad z_i > 0 \\ 0 & if \quad z_i \leq 0 \end{cases} \quad (2)$$

The probability of choosing alternative 1 is given by:

$$P_i = P(y_i = 1) = P(z_i > 0) \quad (3)$$

The distinction between this model and a standard probit model is the term $\theta_i$. The unobserved component $\theta_i$ is constructed such that it allows for spatial interaction among households. This is obtained by specifying $\theta_i$ according to a spatial autoregressive structure:

$$\theta_i = \rho \sum_{j=1}^{n} w_{ij}\theta_j + u_i \quad (4)$$

with $u_i \sim N(0,\sigma^2), W = (w_{ij}; i,j = 1, \cdots n)$ is a row standardized spatial weight matrix such that $\sum_{j=1}^{n} w_{ij} = 1$. ρ can be interpreted as the degree of spatial dependence across households. Positive (negative) value of ρ indicates positive (negative) correlation among households. We can write equation (*.4) in matrix notation:

$$\theta = \rho W\theta + u \quad (5)$$

where $u \sim N_n(0_n, \sigma^2 I_n)$ and $I_n$ is the identity matrix. Letting $S = I_n - \rho W$, we can obtain a solution for $\theta$ using (*.5): (*.1)

$$\theta = S^{-1}u \quad (6)$$

It is worth noting that in our model, there is a network propagation effect captured in equation (*.5). Our model presents a simple test on the existence of propagation effect. If $\rho$ is significantly different from zero, then we conclude thatthere could be some spatial correlation beyond what is captured in the $x_i\beta$ term in the equation (1). From (*.6) we see that the distribution for $\theta_i$ is given by:

$$\theta|(\rho,\sigma^2) \sim N_n(0_n, \sigma^2(S'S)^{-1}) \quad (7)$$

The error term $\varepsilon$ is assumed to be conditionally independent of the spatial unobserved component such that $\varepsilon|\theta \sim N_n(0_n, \sigma_\varepsilon^2 I_n)$ and we assume (*.2) $\sigma_\varepsilon^2 = 1$. The full model in matrix notation is given by:

$$z = X\beta + \vartheta + \varepsilon \quad (8)$$

The likelihood function of this model is as (*.3) follows:

$$L(y|\beta,\theta,\rho,\sigma^2) = \prod_{i=1}^{n} \Phi(x_i'\beta + (S^{-1})_i u)^{y_i}\{1 - \Phi(x_i'\beta + (S^{-1})_i u)\}^{1-y_i} \quad (9)$$

where $\Phi$ and $(S^{-1})_i$ respectively denote a cumulative distribution function of the standard normal and ith row of $S^{-1}$. But it is difficult to estimate this model by maximum likelihood method since the likelihood function has complicated form. Then, we use the Bayesian inference approach to estimate each parameters of equation by using the

Markov Chain Monte Carlo method that sample sequentially from the complete set of conditional posterior distributions for the parameters. The MCMC method provides a powerful tool for simulating complicated posterior distributions.

**(2) Bayesian Inference**

We estimate above spatial probit model by using Markov Chain Monte Carlo (MCMC) method. Gibbs sampler was a first MCMC algorithm and was used in statistics and econometrics popularly, which arrives at the target distribution of unknown parameters by sequentially sampling from a set of conditional distributions of parameters. This is very useful since usually it is difficult to find an analytical result for posterior densities. The MCMC method provides a sample from the posterior density and we can use this sample to draw inferences about the parameters of interest. Under mild regularity conditions satisfied in this application, these samples converge to sample from the posterior distribution.

Most of the parameters can be sampled by using Gibbs sampler, however, sampling the spatial parameter $\rho$ is solely difficult since the conditional posterior distribution is not reducible to a standard distribution. Therefore, we apply a Metropolis-Hastings (MH) sampling method.

To derive the conditional posterior distributions, we use the Bayes theorem.

$$p(\beta,\theta,\rho,\sigma^2,z|y) \propto L(y|\beta,\theta,\rho,\sigma^2,z)\cdot \pi(\beta,\theta,\rho,\sigma^2,z) \tag{10}$$

where $p(\cdot)$ represents posterior densities. The prior distributions of each parameter $\beta,\rho,\sigma^2$ are assumed independent; therefore, the posterior joint density $p(\beta,\theta,\rho,\sigma^2,z|y)$ is given up to a constant of proportionality by

$$p(\beta,\theta,\rho,\sigma^2,z) \propto L(y|z)\cdot\pi(z|\beta,\theta)\cdot \pi(\theta|\rho,\sigma^2)\cdot\pi(\beta)\cdot\pi(\rho)\cdot\pi(\sigma^2) \tag{11}$$

Using this relation, we obtain the appropriate conditional posterior distributions for each parameter in the model and examine MCMC sampling methods in the following section. Before we examine the Bayesian estimation we set each parameter's prior distributions as follows:

$$\pi(\beta)\sim N_k(c,T),\quad \pi(\sigma^2)\sim IG(\alpha,\nu),$$
$$\pi(\rho)\sim U(\lambda_{min}^{-1},\lambda_{max}^{-1})$$
$$\pi(\theta|\rho,\sigma^2)\sim N_n(0_n,\sigma^2(S'S)^{-1}),$$
$$\pi(z|\beta,\theta)\sim N_n(X\beta+\theta,I_n) \tag{12}$$

where $\beta$ has normal conjugate prior distribution with means set to zero and covariance matrix set to $100I_k$, and $\sigma^2$ is assigned a conjugate inverted gamma prior with $\alpha=25$ and $\nu=3$. We employ a uniform prior distribution on $\rho$ over a specified range. The parameter $\rho$ must lie in the interval $[\lambda_{min}^{-1},\lambda_{max}^{-1}]$, where $\lambda_{min}$ and $\lambda_{max}$ denote the minimum and maximum eigenvalues of W, for the matrix $S=I_n-\rho W$ to be invertible (Sun, Tsukawa and Speckman 1999). Introducing each prior distribution (12) into equation (11), we can derive the conditional posterior distributions for each parameter. In the next section, we examine the MCMC sampling method with using these conditional posterior distributions.

**(3) The Markov Chain Monte Carlo (MCMC) sampler**

The MCMC estimation scheme involves starting with arbitrary initial values for the parameters which we denote $\beta^0,\theta^0,\sigma^{2(0)},\rho^0$ and the latent variable $z^0$. We then sample sequentially from the following set of conditional distributions for the parameters in our model.

a) Calculate $p(\beta|\rho^0,\theta^0,\sigma^{2(0)},z^0,y)$ using each initial parameter. We carry out a multivariate random draw to determine $\beta^1$.

$$\beta|(\theta,\rho,\sigma^2,z,y)\sim N_k(A^{-1}b,A^{-1}) \tag{13}$$

where
$A=X'X+T^{-1},b=X'(z-\theta)+T^{-1}c.$

b) Calculate $p(\theta|\beta^1,\rho^0,\sigma^{2(0)},z^0,y)$, we carry out a multivariate random draw to determine $\theta^1$.

$$\theta|(\beta,\rho,\sigma^2,z,y)\sim N_n(A_0^{-1}b_0,A_0^{-1}) \tag{14}$$

where $A_0=\sigma^{-2}S'S+I_n,b_0=z-X\beta$.

c) Calculate $p(\sigma^2|\beta^1,\theta^1,\rho^0,z^0,y)$, we carry out a random draw to determine $\sigma^{2(1)}$.

$$\sigma^2|(\beta,\theta,\rho,z,y)\sim IG(\alpha_0,\nu_0) \tag{15}$$

where $\alpha_0=\frac{n}{2}+\alpha$, $\nu_0=\nu+\frac{1}{2}\theta'S'S\theta$.

d) Calculate $\rho$ using $\theta^1$ and $\sigma^{2(1)}$ from previous steps. We represent the posterior distribution of

$\rho$ as follows,

$$p(\rho|\beta^1,\theta^1,\sigma^{2(1)},z^0,y) \propto |I_n-\rho W| \cdot \exp\left\{-\frac{1}{2\sigma^2}\theta' S' S\theta\right\} \quad (16)$$

It is difficult to sample a draw from this distribution. Therefore, we use the Metropolis-Hastings algorithm with a random walk chain to generate draws (see Chib and Greenberg 1995). Let $\rho^{old}$ denote the previous draw, and then the next draw $\rho^{new}$ is given by:

$$\rho^{new} = \rho^{old} + c^* \phi \qquad \phi \sim N(0,1) \quad (17)$$

where $c^*$ is called tuning parameter. The spatial term $\rho$ is restricted $\lambda_{min}^{-1}, \lambda_{max}^{-1}$. Next, we evaluate the acceptance probability as follows,

$$\Psi(\rho^{old},\rho^{new}) = min\left(1, \frac{p(\rho^{new}|\beta^1,\theta^1,\sigma^{2(1)},z^0,y)}{p(\rho^{old}|\beta^1,\theta^1,\sigma^{2(1)},z^0,y)}\right) \quad (18)$$

Finally, we set $\rho = \rho^{new}$ with probability $\Psi(\rho^{old},\rho^{new})$, otherwise $\rho = \rho^{old}$.

e) We sample $z^1$ draws from a truncated normal distribution using $\beta^1, \theta^1, \sigma^{2(1)}$ and $\rho^1$ as follows,

$$z_t|(\beta,\theta,\rho,\sigma^2,z_{-t},y) \sim \begin{cases} TN_{(0,\infty)}(x_t'\beta+\theta_t,1) & if \quad y_t=1 \\ TN_{(-\infty,0]}(x_t'\beta+\theta_t,1) & if \quad y_t=0 \end{cases} \quad (19)$$

where $z_{-t} = (z_1,\cdots,z_{t-1},z_{t+1},\cdots,z_n)$.

We now return to step 1 employing the updated parameter values in place of the initial values $\beta^1, \theta^1, \sigma^{2(1)}, \rho^1$ and $z^1$. On each pass through the sequence we collect the parameter draws which are used to construct a posterior distribution for the parameters in our model.

## 4. RESULTS AND DISCUSSIONS

### (1) The Explanatory Variables

Since our research aim is to investigate individuals' preference on water choice in the community level, in this paper we define sample of the study with two considerations. First, only the respondent which has more than one option toward access to clean water could be taking into account as the sample. And there are 317 respondents. Secondly, only the respondent in the sample who has complete answer relate to eight demographic data and one psychological data are the respondent in the sample. Thus, the number of sample for this paper is 257 respondents. Then, dependent variable is set to 1 for respondent who participate in CBWM - community based water management (HIPPAM's member and get water from public hydrant), and 0 for respondent who does not participate in community based water management or for those which obtain clean water from different access (PDAM, individual well and others). Table 1 shows the number of respondents as the sample in the paper.

**Table 2** Sample of the Respondent

| Sample of the Respondent | | | |
|---|---|---|---|
| Participate in CBWM | Hippam | 167 | 185 |
| | Public Hydrant | 18 | |
| Not participate in CBWM | PDAM | 18 | 72 |
| | Individual Well | 51 | |
| | Others | 3 | |
| | Total Sample | | 257 |

In detail, number of the respondent who obtains water from HIPPAM is 65%, and the 7% acquires water from public hydrant. Meanwhile, PDAM customers are 7%, the respondents who use individual well are 20%, and others are 1%.

Table 2 illustrates characteristics of respondent from the aspect of water source covering 8 demographic data and one psychological data of the 257 respondents. It is grouped as A – respondent who join community based water management (n = 167) and B - the respondent who does not participate in community based water management (n = 90). In general data in the sample have similar situation with the total 500 respondents.

**Table 3** Characteristics of respondents from the aspect of water source

| | Gender Male | Age | Family Size | Length of Stay | Water Usage |
|---|---|---|---|---|---|
| A | 75% | Av.45.87 | Av.3.96 | Av.30.17 | Av.1789.98 |
| B | 71% | Av.48.61 | Av.4.01 | Av.27.42 | Av.806.89 |

| | Education | | Occupation | | Concern to Com. Welfare | |
|---|---|---|---|---|---|---|
| | M.S. & below | J.S. & upper | Agrc. & Manu. | Serv. & Unempl. | Agree | Dis-agree |
| A | 80% | 20& | 45% | 55% | 30% | 70% |
| B | 72% | 28% | 24% | 76% | 39% | 61% |

| | Income | | | | | | |
|---|---|---|---|---|---|---|---|
| | 0.25 | 0.75 | 1.25 | 1.75 | 2.25 | 2.75 | 3.25 |
| A | 26% | 40% | 19% | 8% | 2% | 3% | 2% |
| B | 28% | 37% | 16% | 8% | 2% | 2% | 8% |

In addition, related to daily water usage, in the questionnaire sheet, we asked the respondent to describe their average household daily water usage. According to Peter Gleick, a standard of minimum water requirements per person per day is 50 liter. Since average family size is 4, then we define daily water usage per household by multiply the standard minimum water requirements with size of the family, as 200 liter/household/day.

In order to investigate concern of the people toward community welfare in the study area, we raised a question to the respondent: "Do you agree or disagree with the following statement: People here look out mainly for the welfare of their own families and they are not much concerned with community welfare" with four categories: Strongly Agree – Agree – Disagree – Strongly Disagree. Then, after grouping in to two classifications - Agree and Disagree – the result shows that majority respondents have concern toward community welfare.

Considering above data, we define explanatory variables as follow:

- *GENDER* : dummy variable which equals 1 if respondent is male
- *AGE* : age of respondent
- *FAM* : number of people in each household
- *LENGTH* : years of living in the area for respondent
- *WATER USAGE :* dummy variable of daily water usage, that is categorized as 1 if respondent consumes less or equal to 200 liters/household/day and categorized as 0 if its consumption more than 200 liters/household/day.
- *EDU* : dummy variable which is recorded as 1 if respondent has educational background in the level of middle school & below, and recorded as 0 if high school & upper.
- *OCCU* : dummy variable which is coded as 1 if occupation of respondent is agriculture or manufacturing and coded as 0 if service or unemployment
- *CONCERN TO COMMUNITY WELFARE :* dummy variable which equals 1 if respondent's answer disagree or strongly disagree and recorded as 0 if its answer is agree or strongly agree.
- *INCOME* : household's monthly income which is divided into 7 items (less than 0.5, 0.5-1.0, 1.0-1.5, 1.5-2.0, 2.0-2.5, 2.5-3.0, more than 3.0 million Rupiah), and we use the medians of each item.

Table 4 shows the standard statistics of each variable.

**Table 4** Standard Statistics

| N= 257 | Mean | STDV. | Max | Min |
|---|---|---|---|---|
| GENDER | 0.74 | 0.440 | 1 | 0 |
| AGE | 46.56 | 11.373 | 75 | 22 |
| FAM | 3.97 | 1.123 | 7 | 2 |
| LENGTH | 29.40 | 18.958 | 75 | 0.02 |
| WATER U. | 0.65 | 0.479 | 1 | 0 |
| EDU | 0.77 | 0.421 | 1 | 0 |
| OCCU | 0.38 | 0.486 | 1 | 0 |
| CONCERN C.W. | 0.67 | 0.471 | 1 | 0 |
| INCOME | 0.98 | 0.751 | 3.25 | 0.25 |

**(2) The Weight Matrix**

Finally, in specifying the weight matrix, we reasoned that households with better community tie have ability to organize community based management system. Therefore, we define a spatial weight matrix using the data about community networks. To investigate participation of the respondent in various types of social organizations and informal networks, and the range of contribution that one gives and receive from them, we asked the respondent to mention their type of community group which they join through 15 following options. The detail options are (1) Religious, (2) Cultural/Social, (3) HIPPAM, (4) PDAM, (5) HIPPA, (6) Ethnic based, (7) Community organization, (8) Finance, (9) Production, (10) Union (labor/trade), (11) Political party, (12) Professional association, (13) Business association, (14) Social movement, and (15) Others (please specify). Table 5 shows the number of respondents in each type of community group.

**Table 5** Number of Respondents in Each Type of Community Group

| | 1 | 2 | 3 | 4 | 5 | 6 | 7 | 8 |
|---|---|---|---|---|---|---|---|---|
| A | 155 | 25 | 0 | 83 | 1 | 5 | 21 | 21 |
| B | 65 | 6 | 4 | 0 | 0 | 0 | 9 | 5 |
| Tot. | 220 | 31 | 4 | 83 | 1 | 5 | 30 | 26 |

| | 9 | 10 | 11 | 12 | 13 | 14 | 15 |
|---|---|---|---|---|---|---|---|
| A | 5 | 1 | 1 | 2 | 1 | 0 | 1 |
| B | 0 | 1 | 1 | 0 | 2 | 1 | 1 |

| | | | | | | | |
|---|---|---|---|---|---|---|---|
| Tot. | 5 | 2 | 2 | 2 | 3 | 1 | 2 |

As you can see, the four popular groups which respondent like to participate are (1) Religious, (2) Cultural/Social, (7) Community organization, and (8) Finance at amount of 75%, 21%, 18%, and 9% among total responses, respectively. Therefore, we focus on these four types of group and get the weight matrix by calculating the social distance between household $i$ and household $j$ as follows:

$$w_{ij}^{g} = \begin{cases} 1 & \text{if household } i \text{ and } j \text{ join the same social group } k \\ 0 & \text{otherwise} \end{cases}$$

$$w_{ij} = \sum_{k=1}^{4} w_{ij}^{g} \qquad (20)$$

The diagonal elements were all set to zero. Next we row standardize the matrix by dividing each element $w_{ij}$ in the matrix by the row sum such that all rows sum to one. The row standardization does not change the relative social interaction among households. Other more complicated weighting schemes are possible, depending on how one wish to quantify the degree of social interaction among households. For the purpose of this paper we simply want to account for social interaction effects in the decision to join HIPPAM, therefore any type of social interaction is acceptable.

**(3) Estimation results**

In addition to the spatial probit model estimates, we also estimated a non-spatial probit model which does not include the spatial interaction term $\theta$. Diffuse or conjugate priors were employed for all of the parameters $\beta, \sigma^2$ and $\rho$ in both models. We iterate MCMC algorithm and sample 5000 parameters respectively and set 1000 samples as burn-in. The chain was considered to have practically converged after 1000 iterations based on a diagnostic proposed by Geweke (1992). The last 4000 draws were used to calculate the posterior mean and standard deviation of the parameters. Table 5 and 6 show the estimation results of each village.

**Table 6** Estimation results (Toyomarto)

| Toyomarto (n=159) | | | | | |
|---|---|---|---|---|---|
| **Probit Model** | | | | | |
| **Variable** | **p.Mean** | **p. Std. Dev.** | **90% Credible Interval** | | **Geweke** |
| Constant | 3.449 | 1.389 | 1.266 | 5.787 | 0.318 |
| FAM | -0.734 | 0.178 | -0.363 | 0.218 | 0.155 |
| GENDER | -0.058 | 0.468 | -0.838 | 0.697 | 0.408 |
| AGE | -0.029 | 0.021 | -0.063 | 0.005 | 1.097 |
| EDU | -0.069 | 0.533 | -0.982 | 0.794 | 0.402 |
| OCCU | -0.289 | 0.428 | -1.007 | 0.383 | 0.236 |
| INCOME | 0.252 | 0.363 | -0.326 | 0.876 | 1.057 |
| LENGTH | 0.024 | 0.013 | 0.002 | 0.046 | 0.476 |
| COST | -0.004 | 0.001 | -0.005 | -0.003 | 0.390 |
| **Spatial Probit Model** | | | | | |
| **Variable** | **p.Mean** | **p. Std. Dev.** | **90% Credible Interval** | | **Geweke** |
| Constant | 3.620 | 1.545 | 1.212 | 6.200 | 1.872 |
| FAM | -0.085 | 0.204 | -0.415 | 0.246 | 0.603 |
| GENDER | 0.035 | 0.509 | -0.801 | 0.861 | 0.607 |
| AGE | -0.031 | 0.023 | -0.069 | 0.006 | 1.680 |
| EDU | -0.136 | 0.579 | -1.112 | 0.788 | 0.322 |
| OCCU | -0.234 | 0.485 | -1.062 | 0.561 | 2.863 |
| INCOME | 0.228 | 0.367 | -0.364 | 0.844 | 0.499 |
| LENGTH | 0.026 | 0.014 | 0.003 | 0.049 | 1.949 |
| COST | -0.004 | 0.001 | -0.005 | -0.003 | 2.224 |
| | 0.128 | 0.027 | 0.092 | 0.177 | 1.220 |
| | -9.016 | 5.486 | -17.345 | 0.175 | 1.203 |

**Table 7** Estimation results (Candi Renggo)

| Candi Renggo (n=142) | | | | | |
|---|---|---|---|---|---|
| **Probit Model** | | | | | |
| **Variable** | **p.Mean** | **p. Std. Dev.** | **90% Credible Interval** | | **Geweke** |
| Constant | -1.272 | 0.749 | -2.501 | -0.045 | 1.634 |
| FAM | 0.199 | 0.119 | 0.006 | 0.394 | 1.360 |
| GENDER | 0.554 | 0.351 | 0.005 | 1.144 | 0.003 |
| AGE | -0.026 | 0.014 | -0.048 | -0.004 | 0.787 |
| EDU | 0.865 | 0.340 | 0.312 | 1.446 | 0.740 |
| OCCU | 1.059 | 0.363 | 0.478 | 1.661 | 1.053 |
| INCOME | 0.129 | 0.181 | -0.168 | 0.426 | 0.059 |
| LENGTH | 0.039 | 0.011 | 0.020 | 0.058 | 0.831 |
| COST | -0.001 | 0.0002 | -0.001 | -0.0003 | 1.147 |
| **Spatial Probit Model** | | | | | |
| **Variable** | **p.Mean** | **p. Std. Dev.** | **90% Credible Interval** | | **Geweke** |
| Constant | -1.376 | 0.800 | -2.714 | -0.092 | 0.509 |
| FAM | 0.196 | 0.123 | 0.002 | 0.404 | 0.711 |
| GENDER | 0.594 | 0.370 | 0.001 | 1.216 | 3.406 |
| AGE | -0.026 | 0.014 | -0.050 | -0.004 | 0.519 |
| EDU | 0.939 | 0.362 | 0.351 | 1.544 | 0.578 |
| OCCU | 1.157 | 0.397 | 0.497 | 1.819 | 1.683 |
| INCOME | 0.149 | 0.193 | -0.170 | 0.476 | 0.544 |
| LENGTH | 0.041 | 0.013 | 0.021 | 0.063 | 0.866 |
| COST | -0.001 | 0.0002 | -0.001 | -0.0004 | 0.903 |
| | 0.127 | 0.026 | 0.091 | 0.175 | 0.274 |
| | -5.092 | 3.222 | -10.121 | 0.067 | 0.412 |

Estimation results are summarized as follows. First, in both the villages, the results indicate very similar inferences would be drawn from the non-spatial probit model versus the spatial probit model. In addition, all of the estimated parameter $\rho$ is negative and insignificant. Therefore, from this result, we cannot confirm the existence of the "social interaction effect" among households.

Second, the estimated parameter *LENGTH* is positive and significant. This result indicates that the longer the respondents stay in the area of study

the higher preference of them to join HIPPAM.

Third, we can find that the estimated parameter *COST* is negative and significant. Then, even the price of monthly water usage is quite cheap, but this price in their point of view are one important demographic neighborhood to put into be consideration whether they have willingness to join or not.

## 4. CONCLUSION

In this paper, we show the spatial probit model with using Bayesian estimation method in order to investigate resident's spontaneous collaboration to manage community based water supply system. We describe the posterior distribution from the Bayes theorem and express the MCMC sampling method. Then, our approach applies to the empirical analysis of the data from a field survey in Indonesia.

From the estimation results, we can say that the length of living in the area and the price of monthly water usage have an important meaning for respondent to make a decision to join community based water supply system. Though, as for the social interaction, we do not have good result for parameter $\rho$ yet. Therefore, we need to use another approach to get weight matrix employing geographical neighbors' data through Social Network Analysis in order to complete the previous analysis of demographic neighbors.

In this paper, we focused on the mechanism of resident's spontaneous collaboration to access water and did not take up the social and economic benefit of community based water supply system. Needless to say, however, it is important to clarify the flow of cost and benefit generated by community based water supply system. These are remained for the future works.

## REFERENCES


1) NARBO Annual Report : Networks of Asian River Basin Organizations, 2007.
2) Asian Development Bank : Asian Water Development Outlook 2007: Achieving Water Security for Asia, Asian Development Bank, 2007.
3) Anselin, L. : Spatial Econometrics: Methods and Models, *Dordrecht: Kluwer Academic Publishers*, 1988.
4) Sun, D., R. K. Tsukawa and P. L. Speckman : Posterior Distribution of Hierarchical Models using CAR (1) Distribution," *Biometrica*, V86, 341-350, 1999.
5) S. Chib and E. Greenburg : Understanding the Metropolis-Hastings Algorithm, *American Statistical Association*, V46(4), 327-336, 1995.
6) Smith, T. E., Lesage J. P. : A Bayesian Probit Model with Spatial Dependencies, *Advances in Econometrics*, V18, 2004.
7) Lesage, J.P. : Introduction to Spatial Econometrics, *CRC Press*, 2009.
8) Lancaster , T. : Introduction to Modern Bayesian Econometrics, *Blackwell Publishing*, 2004.
9) Sha Y. & Greg M.A. : Modeling Interdependent Consumer Preferences.
10) G. Chiristiaan, N. Deepa, J. V. Nyhan, M. Woolcock : World Bank Working Paper No.18: Measuring Social Capital An Integrated Questionnaire", *The World Bank*, Washington DC, 2004.
11) Gelman, A., J.B. Carlin,H.S Stern and D.R. Rubin : Bayesian Data Analysis, *CRC Press*, 2004.
12) Gilks , W.R. , Richardson , S. , Spiegelhalter , D.J. : Markov Chain Monte Carlo in Practice, Chapman & Hall/CRC, 1996.
13) Geweke, J. : Evaluating the Accuracy of Sampling-Based Approaches to the Calculation of Posterior Means, *Bayesian Statistics 4,* 1992.
14) Michael Woolcock & Deepa Narayan : Social Capital: Implications for Development Theory, Research and Policy, *The World Bank Research Observer*, Vol. 15 No. 2, p. 225-249, 2000.
15) Wydick, Bruce : Games in Economic Development, *Cambridge University Press*, 2008.

2010 AIT-KU JOINT SYMPOSIUM ON HUMAN SECURITY ENGINEERING

Bangkok, Thailand, November 25-26, 2010

# Spatial Strategy in Improving Access to Water Supply in Urban Areas

Sri MARYATI[1], Pradono[2]

[1]Assistant Professor, School of Architecture, Planning, and Policy Development, Institute of Technology Bandung
(Labtek IXA, Jl Ganesha No.10 Bandung, 40132, Indonesia)
E-mail: smaryati@pl.itb.ac.id
[2]Associate Professor, School of Architecture, Planning, and Policy Development, Institute of Technology Bandung
(Labtek IXA, Jl Ganesha No.10 Bandung, 40132, Indonesia)
E-mail: pradono@pl.itb.ac.id

The condition of public water services in Indonesia is still not adequate. Decentralization era which was started in 1999 did not improved the condition, even made the service inefficient. Decentralization has raised new-small-scale public water supply. Theoretically, small-scale supply is less efficient compared to the large one. It is because there is economies of scale in water supply. However, the existence of economies of scale in Indonesia has not been known. This paper aims to explore the existence of economies of sacle and economies of density in public water supply in Indonesia context. Based on the analysis result, spatial strategy was proposed in order to improve access to water supply.

***Key Words :*** *water supply, spatial strategy, economies of scale, economies of density*

## 1. INTRODUCTION

Public water supply in Indonesia is basically not sufficient. Based on data from Perpamsi Directory, 2006, the number of customers of public water supply is only 4.6% from total population. The fact showed that not all of the area was serviced by public water supply. But in the area which was serviced by public water supply, only 10% of population was customers. The main reasons not to become a customer for the population in service area were the water tariff which was not affordable for some people and the existence of other sources of water which can be utilized. From the perspective of public water supply company (PDAM), limitation of service was related to ability to invest. The limitation to invest was partly caused by the limitation of revenue to recover the cost.

Public water supply company (PDAM) in Indonesia usually is on district level (kota or kabupaten). Decentralization era which was started in 1999 has raised new province and district. After decentralization in 1999 up to 2008 there were 6 new provinces and 187 new districts. With the same area, but there were more regions, indicates that the region got smaller. Related to water supply, the service area was also got smaller.

Water supply is one type of infrastructure with high capital costs. Theoretically, economies of scale exist in such system. Small-scale PDAM has higher unit cost compared to the big one. If economies of scale exist, the phenomenon of small-scale PDAM will cause inefficiencies. Inefficiencies will influence level of service.

Although theoretically economies of scale exist in water supply provision, some studies suggested that it was not always happened[1]. Study of economies of scale have been developed in other countries, especially in the USA. In developing countries, studies related to the existence of economies of scale was still very limited[2]. These studies produced varying result related to cost model and economies of scale. These indicated that cost model and economies of scale is location and time specific. Study of Nauges and Van den Berg[2] also indicated that the structure of drinking water costs varied significantly between countries and time. Cost models in other countries can not be applied directly to the case in Indonesia. Therefore, it is necesarry to discuss cost model and economies of scale in Indonesia context.

## 2. ECONOMIES OF SCALE IN WATER SUPPLY: LITERATURE REVIEW

The existence of economies of scale can be measured through productivity or cost effectiveness. In productivity approach, scale economies are measured by the elasticity of factor input with respect to output or marginal product of the factor input. In cost effectiveness approach, economies of scale are measured by the elasticity of output with respect to the production cost. In general, for addressing the economies of scale of an industry, the cost function approach can be more effective than the productivity approach due to fewer econometric problems[1].

Neo-classical cost function can be used as reference in forming the cost function. Neo-classical cost function stated that cost is a function of output, factor input prices, technology, and a number of other explanatory variables. Output is generally expressed in quantity of production. For the case of drinking water supply, production and distribution quantities are expressed in production or distribution volume. Factor input prices in the case of water supply consists of retribution, chemicals price, energy prices, wages, and depreciation. According to Maryati et. al.[4),5)] there were several environmental variables affecting water supply cost which can be used as explanatory variables, they are water quality, topography, and customer density. Several empirical studies[1),2),6),7),8)] aimed to assess efficiency and optimal scale of water supply have considered the influence of some environmental variables that have been mentioned, in addition to quantity and input factor price. Environmental variables that have been used are raw water quality and customer density, while topography has not been considered.

Empirical studies of drinking water supply costs in the 70s-era generally use a linear and log linear cost function. The shape of these cost function is relatively easy to use because it has fewer explanatory variables. However, this cost function has several limitations, among others, are the assumption about the elasticity of substitution equal to one, and that the scale of measurement remain constant, regardless of the quantity of output. In economies of scale testing, this assumption becomes important. The translog cost function is more flexible because it varies according to the scale of output. Therefore studies that assess efficiency and optimal scale at this time generally used neo-classical cost function estimated by translog function.

Considering type of data used, empirical data is a common type. The use of empirical data without correction may result in low or no relationship between variables studied, whereas logically and theoretically variables examined closely linked to the cost. If influence of certain factors will be analyzed against costs, other factors must be fixed. If not, the role of these factors must be accommodated as an independent variable.

The unit of analysis in empirical studies that have been conducted can be divided into two, namely company level[1),6),7)] and utility level[8)]. The unit of analysis at company level is less appropriate for application in Indonesia. This is because in one company there are usually several production and distribution systems that operate in different conditions, using different water sources with different quality, even the technology used was sometimes different. If the unit of analysis will be used is at company level, there are many explanatory variables that have to be considered.

Several empirical studies [9),10),11)] using income data for replacing cost data. For the case of drinking water in Indonesia, income does not reflect the cost because income is influenced by the leakage and tariff structures. Income can be used to replace the cost if the rate of water losses is the same for the entire of study object and a flat rate is used.

Previous studies generally examined fixed costs, variable costs or total costs (total cost consist of fixed and variable costs). Only few studies which

was distinguished between production and distribution cost, such as Clark and Stevie[12]. Components and cost structure of production and distribution systems are very different, even Clark and Stevie[12] stated that there was an economies of scale in production system but diseconomies of scale in distribution system in their study area. Therefore, production and distribution system should be differentiated in cost studies.

## 3. METHODOLOGY

In this study neo-classical cost function was used as reference. In this function, cost is a function of output, factor input prices, technology, and other explanatory variables. Cost in this case was operating costs, which consist of fixed costs and variable costs. Output was expressed in quantity of production or distribution. It was expressed as volume of production or volume of distribution per year. Factor input prices in the case of water supply consists of raw water retribution, chemicals prices, energy prices, wages, land rent and depreciation. Input factor prices can be corrected by location index, while technological factors have been accommodated in raw water quality, so these two variables can be ignored. Explanatory variables in this study consisted of raw water quality, topography, and customer density.

Raw water quality affects treatment cost. The greater the deviation between raw water quality with the standards, the higher the treatment costs. Treatment is part of production process, hence raw water quality affects production costs. Quality of water is shown by the composition of the components of physical, chemical, and microbiological from the water. The composition of the components is sometimes variable of the source of water. For example, physically surface water generally has a higher turbidity compared to springs and wells. In estimating water supply cost in Indonesia, water quality parameters used can be limited to turbidity since the main chemicals commonly used in production systems is to eliminate turbidity. Water quality can be expected from the source of water.

Topography in the case of water supply costs affect energy costs and depreciation for transmission and distribution system . Energy costs in pumping system is greater than gravity system. Pumping system requires elevated reservoir and affects the cost of depreciation. Transmission is essentially a part of production process, so that the topography affects cost of production. Distribution is part of distribution process, which also affects cost of distribution. Topography is used in the context of a gravity or pumping system. If service area is lower than water sources, gravity system can be used. If not, than pumping system should be used. The greater the deviation between water sources and service areas (areas of service higher than water source), the greater the energy needed. Topography can be indicated by gravity or pumping system.

Customer density associated with energy costs and depreciation costs on distribution process. The higher the customer density, the lower the cost of distribution. Lower density area, needs a longer pipe than high density. These conditions affect the cost of depreciation in distribution system. Customer density was defined as the number of customers per length of network.

**Table 1** Environmental Variable Affecting Production and Distribution Cost

| System | Environmental Variable | Parameter |
|---|---|---|
| Production | Raw Water Quality | Type of Water Sources (spring, well, surface water) |
| | Topography | Type of Distribution (gravity, pump) |
| Distribution | Topography | Type of Distribution (gravity, pump) |
| | Customer Density | Customers to Network Lenghth (SL/m) |

Environmental variable data were available on the level of production and distribution system. The differences in water quality indicated by the differences in raw water sources, i.e. springs, wells, and surface water. Raw water quality data is expressed in the form of dummy variables well and surface water. Topography was indicated by gravity or pumping system. Topographic data was expressed in the form of a dummy variable pumping or gravity system. Customer density data was expressed by the number of customers per network length (SL / m). Quantity variable was expressed by production and distribution volume per year ($m^3$).

Cost function for production system can be expressed in general form as follows:

$$B_{pro} = f(K, S, Tp) \quad (1)$$

and cost functions for distribution system is defined as:

$$B_{dis} = f(K, Tp, pdt) \quad (2)$$

where $B_{pro}$ is cost of production, $B_{dis}$ is distribution costs, K is quantity, S is raw water quality, Tp is

topography, and pdt is customer density.

Although translog form has several advantages in estimating economies of scale, in this study log linear form was also considered. The use of these two functions were in order to get best function. The best model in explaining the variation in cost was evaluated based on the value of determination coefficient ($R^2$), standard error, and the sign of variables. Log linear and translog form for production cost function can be expressed as equation (3) and (4) as follows.

$$\ln B_{pro(v)} = \alpha + \beta_{pro(v)} \ln K_{pro(v)} + \gamma_{AP} AP + \gamma_{SD} SD + \gamma_{pom} Pom \quad (3)$$

$$\begin{aligned} \ln B_{pro(v)} = {} & \alpha + \beta_{pro(v)} \ln K_{pro(v)} + \gamma_{AP} AP \\ & + \gamma_{SD} SD + \gamma_{pom} Pom \\ & + \tfrac{1}{2} \gamma_{pro(v).pro(v)} (\ln K_{pro(v)})^2 \\ & + \tfrac{1}{2} \gamma_{pro(v).AP} (\ln K_{pro(v)}) (AP) \\ & + \tfrac{1}{2} \gamma_{pro(v).SD} (\ln K_{pro(v)}) (SD) \\ & + \tfrac{1}{2} \gamma_{pro(v).Pom} (\ln K_{pro(v)}) (Pom) \\ & + \tfrac{1}{2} \gamma_{AP.AP} (AP)^2 + \tfrac{1}{2} \gamma_{SD.SD} (SD)^2 \\ & + \tfrac{1}{2} \gamma_{AP.SD} (AP) (SD) \\ & + \tfrac{1}{2} \gamma_{Pom.Pom} (Pom)^2 \\ & + \tfrac{1}{2} \gamma_{AP.Pom} (AP) (Pom) \\ & + \tfrac{1}{2} \gamma_{SD.Pom} (SD) (Pom) \end{aligned} \quad (4)$$

Specification of variables used in production cost function is as follows:

**Tabel 2** Variable in Production Cost Function

| Variable | Unit | Definition |
|---|---|---|
| $B_{pro(v)}$ | Rp/year | Production cost, consists of wage, retribution, chemicals cost, energy cost, land rent, maintenance, and depreciation. |
| $K_{pro(v)}$ | $m^3$/year | Production volume |
| AP | | Surface water *(dummy variable)* |
| SD | | Deep well *(dummy variable)* |
| Pom | | Pumping system *dummy variable)* |

Log linear and translog form for distribution cost function can be expressed as equation (5) and (6) as follows.

$$\ln B_{dis(v)} = \alpha + \beta_{dis(v)} \ln K_{dis(v)} + \gamma_{pdt} \ln pdt + \gamma_{pom} Pom \quad (5)$$

$$\begin{aligned} \ln B_{dis(v)} = {} & \alpha + \beta_{dis(v)} \ln K_{dis(v)} + \gamma_{pdt} \ln pdt \\ & + \gamma_{pom} Pom + \tfrac{1}{2} \gamma_{dis(v).dis(v)} (\ln K_{dis(v)})^2 \\ & + \tfrac{1}{2} \gamma_{pdt.pdt} (\ln pdt)^2 + \tfrac{1}{2} \gamma_{pdt.Pom} (Pom)^2 \\ & + \tfrac{1}{2} \gamma_{dis(v).pdt} (\ln K_{dis(v)}) (\ln pdt) \\ & + \tfrac{1}{2} \gamma_{dis(v).Pom} (\ln K_{dis(v)}) (Pom) \\ & + \tfrac{1}{2} \gamma_{pdt.Pom} (\ln pdt) (Pom) \end{aligned} \quad (6)$$

Specification of variables used in distribution cost function is shown in Table 3. Analytical unit used was production and distribution system in PDAM. In general one PDAM consists of more than one production and distribution system influenced by various environmental variables and other conditions. Therefore production and distribution system are more appropriate to be used instead of PDAM.

To perform parameter estimation, cost data, quantity as well as environment variables were needed. The process and conditions of production and distribution of PDAM in Indonesia are basically referring to the different standards. They include the types of chemicals used, the quality of processed water, types of construction, type of pipe used, the presence of reservoir, the amount of water distributed per capita, and the level of leakage. The implication of such inequalities was on the variation of cost, although they operated in the same condition of environmental variables. To overcome this problem, the cost data that will be processed and analyzed must be standardized in order to make them comparable to each other.

**Tabel 3** Variable in Distribution Cost Function

| Variabel | Unit | Definition |
|---|---|---|
| $B_{dis(v)}$ | Rp/year | Distribution cost, consists of wage, retribution, energy cost, land rent, maintenance, and depreciation. |
| $K_{dis(v)}$ | $m^3$/year | Distribution volume |
| Pdt | SL/m | Customer density; number of customers divided by length of network |
| Pom | | Pumping system |

To standardize the cost data, production and distribution costs have to be elaborated on the basis of its components. In general, production cost consists of raw water retribution, chemical costs, energy costs, wage, land rent, maintenance costs, and depreciation. Distribution cost consists of energy costs, wage, land rent, maintenance costs, and depreciation costs. The components of production and distribution costs in detail is shown in Table 4. In the process of data standardization some assumptions were used. The assumptions were among others related to: type and specification of infrastructure in each production system, chemicals used, type of office building, level of water losses, and the existence of operational vehicle.

According to Kim and Lee[1], the ratio of marginal cost to average cost to measure the

economies of scale is inversely proportional to the elasticity of supply with respect to the cost. The elasticity of supply with respect to the cost is determined by production factors including production level, factor input prices, and environmental variables. Elasticity of supply and elasticity of density can be expressed as equation (7) and equation (8).

$$\varepsilon_S = (dC/C)/(dQ/Q) = (d\ln C)/(d\ln Q) \quad (7)$$

$$\varepsilon_{pdt} = (dC/C)/(dpdt/pdt) = (d\ln C)/(d\ln npdt) \quad (8)$$

**Table 4** Production and Distribution Cost Component

| Production System | Distribution System |
|---|---|
| **Chemicals**<br>SPMA & SPSD: Desinfectant<br>SPAP: Desinfectant & Coagulant | |
| **Energy Cost** (SPMA, SPSD,SPAP)<br>• Treatment Pump<br>• Lighting<br>• Other Electronic Device<br>SPSD: Submersible Pump<br>SPAP: Raw Water Pump | **Energy Cost**<br>• Distribution Pump<br>• Lighting |
| **Raw Water Retribution, Land Rent, Wage, Maintenance Cost** | **Land, Maintenance Cost, Wage,** |
| **Depreciation**<br>• SPMA: Broncaptering, Desinfection Pump<br>• SPSD: Well, Desinfection Pump, Submersible Pump, Generator, Pump and Generator House<br>• SPAP: Intake, Raw Water Pump, WTP, Transmission Pipe, Generator, Pump and Generator House, Equipment Building<br>• Electricity Installment, Office Building, Electricity Installation, Office Equipment, Reqruitment of Employee | **Depreciation**<br>Distribution Pipe, Reservoir (Ground and Elevated Reservoir), Distribution Pump, Generator, Pump and Generator House, Electricity Installment, Office Building, Electricity Installation, Office Equipment, Operational Vehicle, House Connection, Customer Water Meter, Reqruitment of Employee |

Note: SPMA (Spring Production System), SPSD (Well Production System), SPAP (Surface Water Production System).

## 4. DATA

Data was developed from 120 production systems and 53 distribution systems in Kabupaten Bekasi, Kabupaten Subang, Kabupaten Cianjur, Kota Bandung, Kabupaten Bandung, Kabupaten Kuningan, and Kabupaten Ciamis. The data used were based on conditions in 2006.

The range of production volume was between 3,239 $m^3$/year up to 11,000,000 $m^3$/year and the average was 863,042 $m^3$/year. Water sources used consisted of surface water, deep wells, and springs, while transmission system consisted of pumping and gravity. Production costs range from Rp 50,000,000/year to Rp 2,600,000,000/year with an average of Rp 290,000,000/year. Descriptive statistics of production system is showed in Table 5.

**Table 5** Descriptive Statistics of Production System

| Variable | Minimum | Maximum | Average |
|---|---|---|---|
| $K_{pro(v)}$ ($m^3$/yr) | 3,239 | 1.1E+07 | 863,042.3 |
| AP | 0 | 1 | |
| SD | 0 | 1 | |
| Pom | 0 | 1 | |
| $B_{pro}$ (Rp/yr) | 5.0E+07 | 2.6E+09 | 2.9E+08 |

Distribution volume ranged from 26,946 $m^3$/year to 1,727,849 $m^3$/year with an average of 432,012 $m^3$/year. The range of customer density was from 0.0034 customer / m up to 0098 customer / m with an average of 0.02289 customer / m. Distribution system consisted of pumping and gravity system. The range of distribution costs was between Rp 130,000,000/ year to Rp 2,800,000,000 / year with an average of Rp 440,000,000/year.

**Table 6** Descriptive Statistics of Distribution System

| Variable | Minimum | Maximum | Average |
|---|---|---|---|
| $K_{dis(v)}$ ($m^3$/yr) | 26,946 | 1,727,849.57 | 432,012.70 |
| Pdt (customer/m) | 0.0034 | 0.098 | 0.0428 |
| Pom | 0 | 1 | |
| $B_{dis}$ (Rp/yr) | 1.3E+08 | 2.8E+09 | 4.4E+08 |

## 5. RESULTS

Estimation results for production system based on two different models shown in Table 7. Based on the value of $R^2$ and standard error, it can be concluded that translog model has a better value

than log linear model. Based on translog model, the elasticity of production is 0.59. This condition indicates the existence of economies of scale.

**Table 7** Estimation Results for Production System

| Para-meter | Variable | Log Linear | Translog |
|---|---|---|---|
| $\alpha$ | Constant | 13.08<br>(0)<br>[47.08] | 27.21<br>(0.98)<br>[27.68] |
| $\beta_{pro(v)}$ | $K_{pro(v)}$ | 0.42<br>(0.73)<br>[19.09] | -1.84<br>(0.16)<br>[-11.88] |
| $\gamma_{AP}$ | AP | | |
| $\gamma_{SD}$ | SD | 0.05<br>(0.026)<br>[0.62] | |
| $\gamma_{Pom}$ | Pom | 1.01<br>(0.53)<br>[13.26] | |
| $\delta_{pro(v).pro(v)}$ | $K_{pro(v)}$* $K_{pro(v)}$ | | 0.18<br>(0.012)<br>[14.46] |
| $\delta_{pro(v).SD}$ | $K_{pro(v)}$*SD | | 0.54<br>(0.095)<br>[5.73] |
| $\delta_{Pom, Pom}$ | Pom*Pom | | 1.51<br>(0.74)<br>[2.05] |
| $\delta_{pro(v)., Pom}$ | $K_{pro(v)}$* Pom | | 0.019<br>(0.058)<br>[0.032] |
| $\delta_{SD.Pom}$ | SD*Pom | | -5.932<br>(1.134)<br>[-5,23] |
| $R^2$ | | 0.86 | 0.95 |
| *Standard Error* | | 0.34 | 0.20 |

Note: ( ) Standardized parameter, [ ] t-value.

Estimation results for distribution system based on log linear and translog function are shown in Table 8. Based on the value of $R^2$ and standard error, it can be concluded that translog model has a better value than log linear model. Based on translog model, the elasticity of distribution is 0.99, while the elasticity of customer density is 1.70. These conditions indicate the existence of economies of scale and diseconomies of density on distribution system.

## 6. CONCLUSION

Based on the analysis described above it can be concluded that there are economies of scale in production and distribution systems and diseconomies of density in distribution system. These mean, that if the scale of production and distribution is enlarged, the unit cost will decrease. With the decline in unit costs, basically the service would be cheaper and more affordable by the community.

The emergence of small-scale public water supply as a result of decentralization, has caused inefficiency in water supply service . Unit cost of small-scale system is larger compared to the bigger one. Inter-regional cooperation is a strategy in water supply provision that can scale up the services and make services more efficient.

**Table 8** Estimation Results for Distribution System

| Para-meter | Variable | Log Linear | Translog |
|---|---|---|---|
| $\alpha$ | Constant | 8.02<br>(0)<br>[22.82] | -29.7<br>(2.8)<br>[10.58] |
| $\beta_{dis(v)}$ | $K_{dis(v)}$ | 0.78<br>(1.21)<br>[34.98] | -2.20<br>(0.37)<br>[-5.9] |
| $\gamma_{pdt}$ | Pdt | -0.55<br>(-0.62)<br>[-17.89] | 1.007<br>(0.58)<br>[1.73] |
| $\delta_{dis(v).dis(v)}$ | $K_{dis(v)}$* $K_{dis(v)}$ | | 0,207<br>(0,027)<br>[7.80] |
| $\delta_{dis(v).pdt}$ | $K_{dis(v)}$*pdt | | -0.19<br>(0,061)<br>[-3.10] |
| $\delta_{dis(v).pom}$ | $K_{dis(v)}$* Pom | | 0.07<br>(0.071)<br>[0.987] |
| $\delta_{pdt.pom}$ | pdt*Pom | | 0.041<br>(0.108)<br>[0.383] |
| $\delta_{pdt.pdt}$ | pdt*pdt | | 0.092<br>(0.072)<br>[1.275] |
| $\delta_{pom.pom}$ | Pom*Pom | | -0.31<br>(1.17)<br>[-0.27] |
| $R^2$ | | 0.97 | 0.99 |
| *Standard Error* | | 0.11 | 0,066 |

Note: ( ) Standardized parameter, [ ] t-value.

## REFERENCES

1) Mizutani, F., dan Urakami, T. Identifying Network Density and Scale Economies for Japanese Water Supply Organizations, *Regional Science*, Vol. 80: 211-230. 2001.

2) Nauges, C., dan van den Berg, C. Economies of Density, Scale, and Scope in the Water Supply and Sewerage Sector: a Study of Four Developing and Transition Economies, *Regional Economics*, Vol. 34: 144-163. 2008.

3) Kim, E., and H. Lee,. Spatial Integration of Urban Water Services and Economies of Scale, Review of Urban and Regional Development Studies, 10(1), p. 3-18.1998.

4) Maryati, S., Notodarmojo, S., Chatib, B., Widiarto, "Environmental Condition and Cost of Water Production and Distribution", Proceeding the 1st International Conference on Sustainable Infrastructure and Built Environment in Developing Countries; Bandung, 2-3 November 2009.

5) Maryati,S., Widiarto, and Notodarmojo, S. "Environmental Factors and Water Supply Cost", POSITIONING PLANNING IN THE GLOBAL CRISES: International Conference on Urban and Regional Planning Celebratinf 50th Anniversary of Planning Education in Indonesia, Bandung, 12-13 November 2009.

6) Feigenbaum, S. dan Teeples, R. Public versus Private Water Delivery: A Hedonic Cost Approach. *The Review of Economics and Statistics,* 65: 672-678. 1983.

7) Teeples, R. dan David, G. Cost of Water Delivery Systems Specification and Ownership Effects, *The Review of Economics and Statistics*, 69: 399-407.1987.

8) Bhattacharyya, A., Harris, T.R., dan Narayanan, R. Allocative Efficiency of Rural Nevada Water Systems: A Hedonic Shadow Cost Function Approach. *Journal of Regional Science* Vol. 35 No.3: 485-501. 1995.

9) Ford, L.T. dan Warford, L.T.). Cost Function for the Water Industry. *Journal of Industrial Economics,* 18 (Nov): 53-63. 1969.

10) Stevie,R. G., Clark, R. M. dan Adams, J. Q. *Managing Small Water System: a cost study.* US EPA-600/2-79-147a, Vol. 1. 1979.

11) Kirshen, P., McCluskey, M., Vogel, R., dan Strzepek, K. Global Analysis of Changes in Water Supply Yields and Costs Under Climate Change: A Case Study in China, *Climatic Change*, Vol 68, p.303-330. 2005.

12) Clark, R. M. dan Stevie, R.G A Water Supply Cost Model Incorporating Spatial Variables, *Land Economics,* Vol.57 No.1: 18-32. 1981.

2010 AIT-KU JOINT SYMPOSIUM ON HUMAN SECURITY ENGINEERING

Bangkok, Thailand, November 25-26, 2010

# Disclosure Strategy for Critical Infrastructure under Terror Risks

Mamoru YOSHIDA[1] and Kiyoshi KOBAYASHI[2]

[1]Assistant Professor, Dept. of Urban Management, Graduate School of Engineering, Kyoto University
(C1-1-181, Kyoto University Katsura Campus, Nishikyo-ku, Kyoto 615-8540, Japan)
E-mail:yoshida@hse.gcoe.kyoto-u.ac.jp
[2]Professor, Graduate School of Management, Kyoto University
(C2-438, Kyoto University Katsura Campus, Nishikyo-ku, Kyoto 615-8540, Japan)
E-mail:kkoba@psa2.kuciv.kyoto-u.ac.jp

This paper analyzes the government's disclosure strategies for criti cal infrastructure against potential terror attacks. Any event that disrupts the functioning of critical infrastructure su ch as power plants, airports, and water management systems will have a major impact on the society. As such, it is very important for the government to protect such infrastructure from threats by establishing proper disclosure strategies.

The government usually finds it difficult to accuratelyassess the terror risk because thegovernment does not have sufficient information about the terrorists' capabilities and motives. Therefore, implementation of an ant i-terrorism pol icy depends on t he governm ent's subject ive deci sion. C onsidering t his, t he paper formulates the game between the government and the terrorists as a subjective game. It is found that the government's disclosure of the implementation of counter-terrorism measures increases the government's subjective utility, but does not necessarily lead to an increment in the government's objective utility.

***Key Words :*** *terror risk, disclosure, critical infrastructure,subjective game*

## 1. INTRODUCTION

Terror risk is defined as a function of terrorists' capabilities and motives. This is unlike in natural disaster risks, and is one of the distinguishing characteristics of terror risks. As such, it is im portant for the governm ent to elim inate the resources used to carry out terror attacks and de-m otivate potential terrorists. This paper focuses on the government's disclosure strategies against terror attacks. Establishing proper disclosure strategies, the government may be able to reduce the terror risk because its disclosure may affect terrorists' decision making.

On the basis of the Japanese government's policy, potential risks and mitigation measures pertaining to critical infrastructure are not disclosed to the public. The related information is considered confidential by the Japanese government. However, public pressure with regard to the disclosure of related inform ation has been increasing because citizens want a secure society and would like to know about the actual situation of such critical infrastructure. It goes without saying that the governm ent is accountable for tax collections and spending and that the citizens have the right to obtain such related inform ation. However, considering potential terror attacks, the government needs to thoughtfully consider the disclosure strategies for critical infrastructure because wrong disclosure strategies can trigger potential terror attacks. In particular, it should be noted that the im - plementation of an anti-terrorism policy vary ingly depends on the governm ent's subjective decision because the governm ent does not alway s have sufficient inform ation pertaining to the capabilities and motives of potential terrorists. As such, this paper considers a "subjective gam e" between the government and the terrorist [1)]. The paper m odels the situation where the government finds it difficult to assess

the potential terror risk and has to decide on a costly counter-terrorism measure.

There are many published articles that are related to this research. For example, V. Bier *et al.*[2] formulates the game between an attacker and a defender, in which the defender has two objectives that are being targeted by the attacker, and showed that trustworthy disclosure of the defender's strategies can reduce the expected damage caused by the attacker. M. Cremonini and and D. Nizovtsev [3] showed that the higher the defender's signaling ability, the more the welfare obtained by the defender in the situation where several defenders decide the protection level of their own targets against potential terror attacks. These results show that the signaling information by the defender plays an important role in reducing terrorist attacks. In addition, B. Hoffman and G. H. McCormick[4] characterized terrorism as a signaling game where a government are poorly informed about the terrorist groups' objectives, resources, and commitments. It is also argued that given the short-term nature of most terrorist groups, with new groups appearing each year and others splintering, governments are faced with never-ending tasks to assess the threat of terrorism under such incomplete information[5]. These arguments support the model where the government is not able to accurately assess the potential terror risk and it has to subjectively decide whether or not to implement a counter-terrorism measure.

In section 2, the basic model between the government and the terrorist is formulated. The model deals with the situation where the government has one infrastructure site that is targeted by the terrorist, and the terrorist cannot observe as to whether or not the government has implemented a counter-terrorism measure. In section 3, the basic model is developed taking into account the government's disclosure strategy for the implementation of a countermeasure. The terrorist recognizes that the government considers the disclosure strategy. The paper makes it clear that taking account of disclosure strategy by the government affects the subjective or objective government's utility. In section 4, the obtained results are summarized and extensions for future research are discussed.

.

## 2. BASIC MODEL

### (1) Preliminary Settings

The model includes a government and a terrorist. The basic model considers the situation where the government implements a measure to prevent terror attacks. The government has one infrastructure site that can be targeted by the terrorist and it devises a countermeasure against potential terror attacks. Let us define the strategy of the government as $\delta \in [0,1]$. $\delta = 1$ implies that the government implements a counter-terrorism measure, and $\delta = 0$ implies that the government does not do so. Implementing a countermeasure, the government can reduce the probability of the success of a terror attack from 1 to $r$ ($0 < r < 1$). The cost of a counterm easure is given by $c$ and is borne by the government when it decides to implement a countermeasure.

At the same time, the terrorist decides on its strategy to conduct the terror attack. Let us define two types of terrorists: $t \in [\alpha, \beta]$. Let $s^t \in [0,1]$ give the strategy of the type $t$ terrorist. $s^t = 1$ implies that the type $t$ terrorist attacks the infrastructure site and $s^t = 0$ implies that the terrorist does not do so. Let $I$ be the cost of the terror attack, where $I>0$. From the viewpoint of the terrorist, the terror attack is successful if it results in the infrastructure site becoming dysfunctional. If the terror attack succeeds, the type $\beta$ terrorist obtains benefit $U$ while the type $\alpha$ terrorist obtains no benefit 0. That is, the type $\alpha$ terrorist can be regarded as a null player because such a terrorist has no motive to attack the infrastructure site. In what follows, when we write only "terrorist", we are referring to the type $\beta$ terrorist. When the terror attack fails, the terrorist is burdened with a failure cost $D$ that includes the cost pertaining to the terrorist being marked by international authorities.

To simplify the model, it is assumed that

$$U - I > 0 \quad . \tag{1}$$

This inequality implies that the type $\beta$ terrorist has a motive to attack the infrastructure site when it knows that the infrastructure site is not protected and the terror attack is certain to succeed. In addition, it is assumed that

$$rU - I < (1-r)D \quad . \tag{2}$$

This inequality shows that if the terrorist knows that the government implements a counter-terror measure, the expected benefit from the terror attack is negative. These assumptions imply that if the type $\beta$ terrorist is able to observe the government's strategy, its strategy will change in accordance with the government's strategy. The basic model deals with the situation where the terrorist is not able to observe the government's strategy. This game is dealt as a subjective simultaneous game between the government and the terrorist.

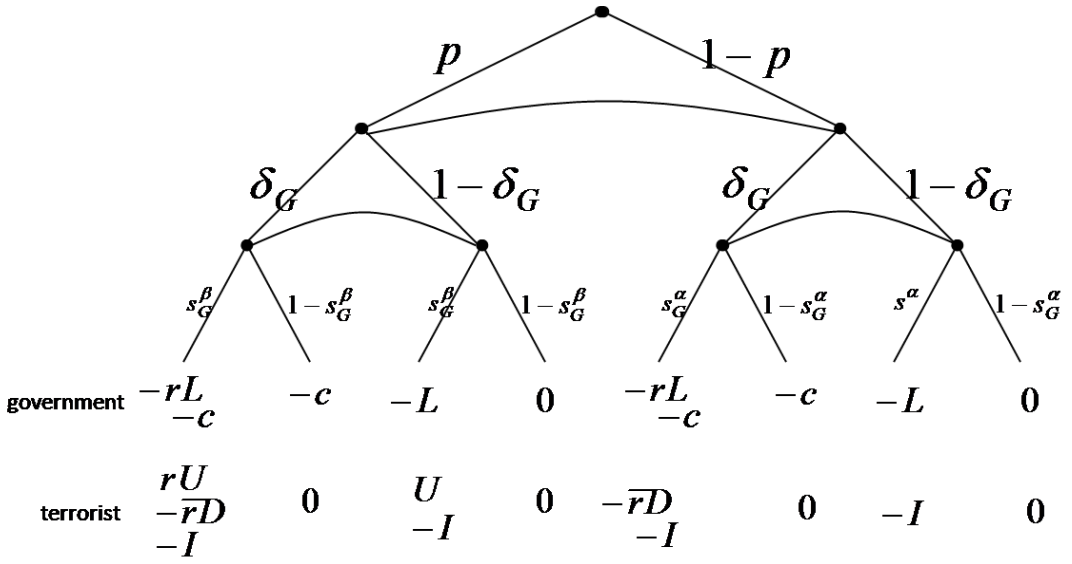


**Fig. 1** Structure of the Government's Subjective Game $\Gamma_G$

Further, it is assumed that both the government and the terrorist do not know the actual ratio of the number of type $\alpha$ terrorists to the actual number of type $\beta$ terrorists. Let $p$ and $q$, respectively, give the government's and the terrorist's belief with regard to the proportion of the type $\beta$ terrorists $0 < p, q < 1$. It is not necessary that $p=q$. The important assumption is that $p$ is private information only for the government and $q$ is private information only for the terrorist. If the belief level of the government $p$ is high (low), it is implied that the government is more (less) concerned about potential terrorists and evaluates the terror risk as high (low). Similarly, if the belief level of the terrorist $q$ is high (low), the terrorist expects that more (less) potential terrorist groups have a motive to attack the infrastructure site. The values of $p$ and $q$ are not common knowledge between the government and the terrorist.

First, consider the game $\Gamma_G$ that the government subjectively plays. Fig.1 shows the structure of the game. In the game $\Gamma_G$, the government has a belief $p$ with regard to the existing proportion of the type $\beta$ terrorists. Let $s_G^\alpha$ and $s_G^\beta$ be the strategies of the type $\alpha$ and type $\beta$ terrorists in the game $\Gamma_G$. With regard to the optimal strategy of the type $\alpha$ terrorist,

$$s_G^{\alpha*} = 0 \tag{3}$$

is always satisfied under the given conditions. With regard to the optimal strategy of the type $\beta$ terrorist, $s_G^{\beta*} = 0$ is induced from the following:

$$s_G^{\beta*} \in \arg\max_{s_G^\beta \in [0,1]} s_G^\beta \{U - I - \delta_G \bar{r}(U + D)\} \tag{4}$$

where $\bar{r} = 1 - r$. From (4), the best response function of the type $\beta$ terrorist is described as follows:

$$\begin{aligned} &If\ \delta_G < \frac{U-I}{\bar{r}(U+D)},\quad s_G^{\beta*} = 1\ . \\ &If\ \delta_G = \frac{U-I}{\bar{r}(U+D)}, s_G^{\beta*} = [0,1]. \\ &If\ \delta_G > \frac{U-I}{\bar{r}(U+D)},\ s_G^{\beta*} = 0. \end{aligned} \tag{5}$$

On the other hand, the optimal strategy of the government is represented by

$$\delta_G^* \in \arg\max_{\delta_G \in [0,1]} \delta_G (p s_G^\beta \bar{r} L - c) - p s_G^\beta L\ . \tag{6}$$

Therefore, the best response function of the government is as follows:

$$\begin{aligned} &If\ s_G^\beta > \frac{c}{p\bar{r}L},\ \delta_G^* = 1\ . \\ &If\ s_G^\beta = \frac{c}{p\bar{r}L},\ \delta_G^* \in [0,1]\ . \\ &If\ s_G^\beta < \frac{c}{p\bar{r}L},\ \delta_G^* = 0\ . \end{aligned} \tag{7}$$

(1) and (2) implies that

$$0 < \frac{U-I}{\bar{r}(U+D)} < 1\ . \tag{8}$$

Thus, the equilibrium of the subjective game played by the government is given as follows:

$$\begin{aligned} &If\ \frac{c}{\bar{r}L} \geq p\ ,\ (\delta_G^*, s_G^{\beta*}) = (0,1). \\ &Otherwise,\ (\delta_G^*, s_G^{\beta*}) = \left( \frac{U-I}{\bar{r}(U+D)}, \frac{c}{p\bar{r}L} \right). \end{aligned} \tag{9}$$

In the case where the government considers the terror risk to be low, the government does not implement a

counter-terrorism measure, and expects that the type $\beta$ terrorist always attacks the infrastructure site. On the other hand, when the government's belief level $p$ is high, the government implements a countermeasure with probability $\frac{U-I}{\bar{r}(U+D)}$, and expects that the type $\beta$ terrorist attacks the infrastructure with probability $c/p\bar{r}L$.

Further let $E[u_G]_G$ and $E[u_T^\beta]_G$ be the utilities of the government and the terrorist in the equilibrium s of the game $\Gamma_G$. Then, $E[u_G]_G$ and $E[u_T^\beta]_G$ are given as follows:

$$\textit{If } \frac{c}{\bar{r}L} \geq p, \quad E[u_G]_G = -pL, \quad E[u_T^\beta]_G = U - I. \tag{10}$$

$$\textit{Otherwise, } \quad E[u_G]_G = -\frac{c}{\bar{r}}, \quad E[u_T^\beta]_G = 0. \tag{11}$$

In the same way, consider the subjective game $\Gamma_T$ that the terrorist plays. In the subjective game $\Gamma_T$, the terrorist holds a belief $q$ with regard to the proportion of the type $\beta$ terrorists. Let $\delta_T \in [0,1]$ be the government's strategy and $s_T^t \in [0,1]$ be the type $t$ terrorist's strategy. The equilibrium of the game $\Gamma_T$ is given as follows:

$$\textit{If } \frac{c}{\bar{r}L} \geq q, \ (\delta_T^*, s_T^{\beta*}) = (0,1).$$

$$\textit{Otherwise, } (\delta_T^*, s_T^{\beta*}) = \left( \frac{U-I}{\bar{r}(U+D)}, \frac{c}{q\bar{r}L} \right). \tag{12}$$

This result implies that if the terrorist's belief level $q$ is low, the terrorist expects that the government does not implement a countermeasure, and always attacks the infrastructure site. Meanwhile, if the terrorist's belief level $q$ is high, the terrorist expects that the government implements a countermeasure with probability $\frac{U-I}{\bar{r}(U+D)}$, and the terrorist attacks with probability $c/q\bar{r}L$, which is based on the terrorist's belief level $q$.

**(2) Equilibrium of the Subjective Game**

The government and the terrorist take their optimal strategies based on the equilibrium strategies in each subjective game. The equilibrium of the subjective game is given as follows:

**Case 1:** $\max[p,q] \leq \frac{c}{\bar{r}L}$

$$(\delta_G^*, s_T^{\beta*}) = (0,1). \tag{13a}$$

**Case 2:** $p < \frac{c}{\bar{r}L} < q$

$$(\delta_G^*, s_T^{\beta*}) = \left(0, \frac{c}{q\bar{r}L}\right). \tag{13b}$$

**Case 3:** $q < \frac{c}{\bar{r}L} < p$

$$(\delta_G^*, s_T^{\beta*}) = \left(\frac{U-I}{\bar{r}(U+D)}, 1\right). \tag{13c}$$

**Case 4:** $\frac{c}{\bar{r}L} \leq \min[p,q]$

$$(\delta_G^*, s_T^{\beta*}) = \left(\frac{U-I}{\bar{r}(U+D)}, \frac{c}{q\bar{r}L}\right). \tag{13d}$$

In case 1, the belief levels of both the government and the terrorist with regard to the proportion of the type $\beta$ terrorist are low. In this case,the government does not implement a countermeasure and the terrorist always attacks the infrastructure site. In Case 2, the belief level of the government is low but that of the terrorist is high. In this case, thegovernment does not implement a countermeasure and the terrorist attacks randomly. Meanwhile, in Case 3, the belief level of the government is high but that of the terrorist is low. In this case,the government implements a countermeasure randomly and the terrorist always attacks. In Case 4, the belief levels of both the government and the terrorist are high. In this case, both the government and the terrorist behave randomly. Note that from the viewpoint of the government, Case 2 is better than Case 1 and Case 4 is better than Case 3.

**(3) Warnining Policy for Terrorist's Synchronized Belief with the Government's Belief**

Let us consider the case where the government has a relatively low belief $p$ that is less than $c/\bar{r}L$. This case corresponds to Case 1 and Case 2. From the government's equilibrium strategy, the government does always not implement a countermeasure. On the other hand, as for the the equilibrium strategy by the terrorist, if the terrorist's belief $q$ is higher than $c/\bar{r}L$, the terrorist attacks infrastructure with probability $c/q\bar{r}L$. Otherwise, the terrorist always attacks. This result implies that the government that has a relatively low belief would like the terrorist to keep a relatively high belief. Thus, the government keep silent with respect to the belief the government forms.

Next, let us consider the case where the government has a relatively high belief $p$ that is higher than $c/\bar{r}L$. This case corresponds to Case 3 and Case 4. In such cases, the government always implements a coun-

ter-terrorism measure with probability $\frac{U-I}{\bar{r}(U+D)}$. On the other hand, if the terrorist forms a higher belief $q$ that is higher than $c/\bar{r}L$, the terrorist attacks with probability $c/q\bar{r}L$; otherwise, the terrorist always attacks the infrastructure site. This result implies that the government would like the terrorist to form a higher belief because the probability the terrorist attack the infrastructure site is lower. Thus, the government has an incentive to make the terrorist's belief high by the disclosure of the government's belief *p*. When the government forms a relatively high belief and the terrorist forms a relatively low belief, the government can reduce the probability the terrorist attacks by disclosing the government's belief and changing the terrorist's belief from *q* to *p*. It is clear that when the terrorist has already formed a high belief, the disclosure of the government's belief does not affect the terrorist's decision on the terror attack; however, when the terrorist forms a low belief, the government can disclose the belief *p* and change the terrorist's belief *q* to *p*. This disclosure policy for the terrorist's synchronized belief with the government's belief can induce the less probability of terror attacks. That is, when the government forms a higher belief, the government should warn the terrorist's threat to the public, but when the government forms a lower belief, the government should keep silent to the public. Adopting this disclosure policy, the equilibria of Case 3 is changed to that of Case 4; therefore Case 1, Case 2 and Case 4 can be actuarized. This is the policy implication from the basic model analysis using subjective game. These results is summarized as the following proposition 1.

**Proposition 1**

*If the government forms a lower belief on the existence of terrorist, the government should keep silent with respect to the belief the government has. If the government forms a higher belief, the government disclose the belief and promote to synchronize the terrorist's belief with the government' belief.*

## 3. DISCLOSURE STRATEGY UNDER TERROR ATTACKS

### (1) Preliminary Settings

The developed model considers the disclosure strategy taken by the government. Let $\Gamma_G^M$ be the subjective game played by the government. Let $m_G(\delta_G^M) \in [0,1]$ be the disclosure strategy taken by the government who chose a countermeasure strategy $\delta_G^M$ in the subjective game $\Gamma_G^M$. $m_G(1)=1$ implies that the government discloses that it is implementing a counter-terrorism measure. $m_G(0)=0$ implies that the government discloses that it is not implementing a counter-terrorism measure. $m_G(1)=m_G(0)=0$ implies that the government declines to disclose any information. Please note that it is assumed that the government is prohibited from lying to the public. That is, in the case where the government did not actually implement a countermeasure, it cannot falsely claim to have implemented a countermeasure, and vice versa. While the lies told by the government can be legitimated on grounds of preventing terror attacks, the government is severely criticized in case the disclosed information turns out to be false. This paper does not deal with this issue, and leaves it for future research. Taking into account the government's disclosure strategy, the terrorist can receive three types of information: $M \in \{1,0,\phi\}$. *M=1* refers to the information that the government implements a counter-terrorism measure. *M=0* refers to the information that the government does not implement a counter-terrorism measure. When the terrorist receives information $M=\phi$, the terrorist does not have any information with regard to the implementation of a countermeasure. On the basis of *M*, let us define the strategy of the type *t* terrorist as $s_G^t(M) \in [0,1]$. $s_G^t(M)=1$ ($s_G^t(M)=0$) implies that the type *t* terrorist receives information *M* and attacks (does not attack) the infrastructure site. Fig.2 shows the structure of the government's subjective game $\Gamma_G^M$.

### (2) Government's Incentive for Disclosure

In the game $\Gamma_G^M$, the optimal strategy with regard to a countermeasure for the type $\alpha$ terrorist is given as

$$s_G^{\alpha*}(1)=s_G^{\alpha*}(0)=s_G^{\alpha*}(\phi)=0. \qquad (14)$$

That is, the type $\alpha$ terrorist's optimal strategy with regard to a countermeasure does not depend on the information it receives. The type $\alpha$ terrorist does not have an incentive to attack the infrastructure site. Meanwhile, the type $\beta$ terrorist's optimal strategy depends on the information it receives. Under the conditions (1) and (2), the optimal strategies $s_G^{\beta*}(1)$ and $s_G^{\beta*}(0)$ are given as

$$s_G^{\beta*}(1)=0, \text{ and}$$

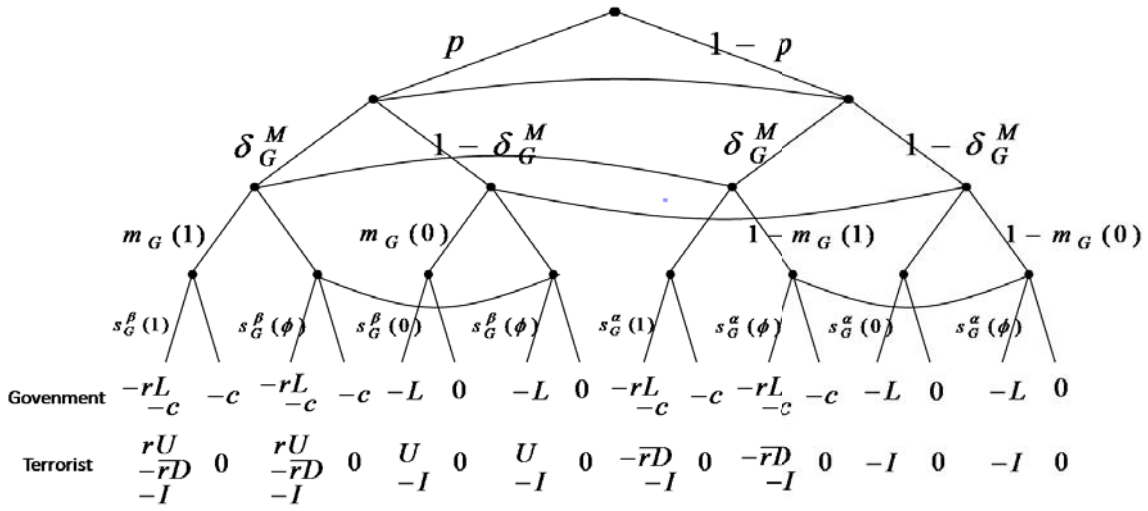


**Fig. 2** The Structure of the Government's Subjective Game Considering Disclosure Strategy $\Gamma_G^M$

$$s_G^{\beta*}(0)=1 \quad . \tag{15}$$

That is, the type $\beta$ terrorist does not attack the infrastructure site when it obtains the inform ation that the governm ent im plemented a counter-terrorism measure; meanwhile, the type $\beta$ terrorist attacks the infrastructure site when it obtains the information that the governm ent did not implement a counter-measure. When the type $\beta$ terrorist does not receive any information, the optimal strategy is given by the following equation:

$$\begin{aligned} s_G^{\beta*}(\phi) &\in \arg\max_{s_G^{\beta}(\phi)\in[0,1]} \\ &\frac{\delta_G^M \bar{m}_G(1)}{\delta_G^M \bar{m}_G(1)+\bar{\delta}_G^M \bar{m}_G(0)} s_G^{\beta}(\phi)(rU-\bar{r}D-I) \\ &+\frac{\bar{\delta}_G^M \bar{m}_G(0)}{\delta_G^M \bar{m}_G(1)+\bar{\delta}_G^M \bar{m}_G(0)} s_G^{\beta}(\phi)(U-I) \end{aligned} \tag{16}$$

where $\bar{\delta}_G^M = 1-\delta_G^M$ , $\bar{m}_G(1)=1-m_G(1)$ , and $\bar{m}_G(0)=1-m_G(0)$ . With regard to the optimal disclosure strategy, when the government implements a countermeasure, the optim al disclosure strategy $m_G^*(1)$ is given by

$$\begin{aligned} m_G^*(1) &= \arg\max_{m_G(1)\in[0,1]} \\ &-\frac{p\delta_G^M}{p\delta_G^M+\bar{p}\delta_G^M}\left\{c+m_G(1)rLs_G^{\beta}(1)+\bar{m}_G(1)rLs_G^{\beta}(\phi)\right\} \\ &-\frac{p\delta_G^M}{p\delta_G^M+\bar{p}\delta_G^M}\left\{c+m_G(1)rLs_G^{\beta}(1)+\bar{m}_G(1)rLs_G^{\beta}(\phi)\right\} \\ &-\frac{\bar{p}\delta_G^M}{p\delta_G^M+\bar{p}\delta_G^M}\left\{c+m_G(1)rLs_G^{\alpha}(1)+\bar{m}_G(1)rLs_G^{\alpha}(\phi)\right\} \\ &= \arg\max_{m_G(1)\in[0,1]} -c-p\bar{m}_G(1)rLs_G^{\beta}(\phi) \end{aligned} \tag{17}$$

where $\bar{p}=1-p$ . That is,

$$m_G^*(1)=1 \quad . \tag{18}$$

Meanwhile, when the government did not implement a countermeasure, the optim al disclosure strategy $m_G^*(0)$ is given by

$$\begin{aligned} m_G^*(0) &\in \arg\max_{m_G(0)\in[0,1]} -p\left\{m_G(0)+\bar{m}_G(0)s_G^{\beta}(\phi)\right\}L \\ &= \arg\max_{m_G(0)\in[0,1]} -p\left\{m_G(0)(1-s_G^{\beta}(\phi))+s_G^{\beta}(\phi)\right\}L \end{aligned} \tag{19}$$

That is,

$$m_G^*(0)=0 \quad . \tag{20}$$

Then, from (18) and (20), the optim al counterm easure strategy $s_G^{\beta*}(\phi)$ is revised as

$$s_G^{\beta*}(\phi)=\arg\max_{s_G^{\beta}(\phi)\in[0,1]} s_G^{\beta}(\phi)(U-I) \tag{21}$$

Then, from (1), the optim al strategy $s_G^{\beta*}(\phi)$ is given as

$$s_G^{\beta*}(\phi)=1 \quad . \tag{22}$$

The government's optim al counterm easure strategy $\delta_G^{M*}$ is given by the following equation:

$$\delta_G^{M*} \in \arg\max_{\delta_G^M\in[0,1]} -p\delta_G^M\left\{m_G(1)s_G^{\beta}(1)+\bar{m}_G(1)s_G^{\beta}(\phi)\right\}rL$$

$$
\begin{aligned}
&- p\bar{\delta}_G^M \left\{ m_G(0) s_G^{\beta}(0) + \bar{m}_G(0) s_G^{\beta}(\phi) \right\} L \\
&- \bar{p}\delta_G^M \left\{ m_G(1) s_G^{\alpha}(1) + \bar{m}_G(1) s_G^{\alpha}(\phi) \right\} rL \\
&- \bar{p}\bar{\delta}_G^M \left\{ m_G(0) s_G^{\alpha}(0) + \bar{m}_G(0) s_G^{\alpha}(\phi) \right\} L \\
&- \delta_G^M c \\
&= \arg\max_{\delta_G^M \in [0,1]} - p(1-\delta_G^M) L - \delta_G c
\end{aligned} \tag{23}
$$

With regard to $\delta_G^{M*}$,

$$
\begin{aligned}
&\text{if } p \geq \frac{c}{L}, \ \delta_G^{M*} = 1 . \\
&\text{Otherwise, } \delta_G^{M*} = 0 .
\end{aligned} \tag{24}
$$

The equilibria of the subjective gam e $\Gamma_G^M$ are summarized as follows:

$$
\begin{aligned}
&\text{if } p \geq \frac{c}{L}, \\
&\quad \left( \delta_G^{M*}, m_G^*(1), m_G^*(0) \right) = (1,1,0) \text{ and} \\
&\quad \left( s_G^{\beta*}(1), s_G^{\beta*}(0), s_G^{\beta*}(\phi) \right) = (0,1,1) .
\end{aligned} \tag{25a}
$$

*Otherwise,* .

$$
\begin{aligned}
&\left( \delta_G^{M*}, m_G^*(1), m_G^*(0) \right) = (0,1,0) \text{ and} \\
&\left( s_G^{\beta*}(1), s_G^{\beta*}(0), s_G^{\beta*}(\phi) \right) = (0,1,1) .
\end{aligned} \tag{25b}
$$

That is, when the government's belief level is high, it implements a counter-terrorism m easure and discloses the sam e to the public. Meanwhile, when the government's belief level is low, it does not implement a counterm easure and does not disclose any information. Then, the governm ent's subjective utility in the equilibrium of the gam e $\Gamma_G^M$ is given as follows:

$$
\begin{aligned}
&\text{if } p \geq \frac{c}{L}, \ E[u_G]_G^M = -c , \\
&\text{Otherwise, } E[u_G]_G^M = -pL .
\end{aligned} \tag{26}
$$

Thus, the following proposition is obtained. The proof of proposition 2 is om itted due to the lim ited space.

**Proposition 2**

*Irrespective of the government's belief with regard to the proportion of the type $\beta$ terrorists, the government's subjective utility increases or remains the same by taking into account the government's disclosure strategy with respect to the implementation of anti-terrorism countermeasure.*

**(3)Equilibria of the Subjective Game Taking into Account the Disclosure Strategy**

Consider the situation where the terrorist recognizes that the governm ent takes the disclosure strategy into account. Then, the terrorist acts in response to the governm ent's disclosure strategy . When the terrorist receives inform ation *M=1*, it considers that the government implemented a counterm easure because the disclosed inform ation is assum ed to be trustworthy. On the other hand, when the terrorist receives no inform ation about a countermeasure strategy, it considers that the governm ent did not implement a counterm easure. Let $s_T^{t*}(M)$ be the optimal strategy of the type *t* terrorist who receives information *M*. Then, the equilibria of the subjective game taking into accountthe government's disclosure strategy are given as follows:

**Case 5:** $p \geq \frac{c}{L}$

$$
\left( \delta_G^{M*}, m_G^*(1), s_T^{\alpha*}(1), s_T^{\beta*}(1) \right) = (1,1,0,0) \tag{27a}
$$

**Case 6:** $p < \frac{c}{L}$

$$
\left( \delta_G^{M*}, m_G^*(0), s_T^{\alpha*}(\phi), s_T^{\beta*}(\phi) \right) = (0,0,0,1) \tag{27b}
$$

In case 5, as the government's belief level *p* is high, it implements a counter-terrorism m easure and discloses inform ation about the sam e; m eanwhile, the type $\beta$ terrorist receives information that the government has implemented a countermeasure and does not attack the infrastructure site. In case 6, the government's belief level *p* is low and it does not im - plement a counter-terrorism m easure and does not disclose any inform ation; m eanwhile, the type $\beta$ terrorist receives no information and decides to attack the infrastructure site. Note that the terrorist's belief level *q* does not play a role in the equilibria of the subjective gam e that takes into account the government's disclosure strategy. The terrorist's recognition of the governm ent's disclosure strategy provides the link between two subjective gam es, and the government's belief level *p* crucially affects the equilibriums.

**(4)Objective Utilities of the Subjective Game**

Let *R* be the true ratio of the type $\beta$ terrorists. Consider the situation in which both the government and the terrorist cannot know the exact value of *R*, and the objective ratio *R* does not necessarily correspond to the governm ent's belief level *p* and the terrorist's belief level *q*. Then, the objective utilities of the government and the terrorist are formulated using the equilibrium strategies of the subjective game. Let us assume that

$$
(RL >) R\bar{r}L > c \tag{28}
$$

The inequality implies that when the terrorist decides to attack the infrastructure site in any strategic situation, the government implement a counter-terrorism measure. Note that the government and the terrorist do not know the exact value of $R$, and as such, this is the hidden condition for both.

Consider the game in which the government and the terrorist have not considered the government's disclosure strategy. This situation corresponds to the basic game in section 2. Let $E[u_G]_o$ be the expected objective utility of the government. Then, the objective utility of the government is described as follows:

**Case 1:** $\max[p,q] \le \frac{c}{\bar{r}L}$

$$E[u_G]_o = -RL \tag{29a}$$

**Case 2:** $p < \frac{c}{\bar{r}L} < q$

$$E[u_G]_o = -\frac{Rc}{q\bar{r}} \tag{29b}$$

**Case 3:** $q < \frac{c}{\bar{r}L} < p$

$$E[u_G]_o = -\frac{RL(I+D)}{U+D} - \frac{U-I}{\bar{r}(U+D)}c \tag{29c}$$

**Case 4:** $\frac{c}{\bar{r}L} \le \min[p,q]$

$$E[u_G]_o = -\frac{Rc(I+D)}{q\bar{r}(U+D)} - \frac{U-I}{\bar{r}(U+D)}c \tag{29d}$$

Next, let us consider the game in which both the government and the terrorist consider the disclosure strategy by the government. Then, the objective utility of the government $E[u_G]_o^M$ is described as follows:

**Case 5:** $p \ge \frac{c}{L}$ $\qquad E[u_G]_o^M = -c$ . (29e)

**Case 6:** $p < \frac{c}{L}$ $\qquad E[u_G]_o^M = -RL$ . (29f)

Thus, the following proposition is obtained. The proof of proposition 3 is omitted due to the limited space.

**Proposition 3**

*Taking into account the government's disclosure strategy with respect to the implementation of anti-terrorism countermeasure does not necessarily lead to an increment in the government's objective utility. When the terrorist's belief level q is relatively high, the government's consideration of the disclosure strategy decreases the government's objective utility.*

## 5. CONCLUSION

This paper analyzed the disclosure strategy with regard to the implementation of countermeasures against terror attacks. In the paper, the game between the government and the terrorist is formulated as a subjective game, and the disclosure strategy by the government plays a role in the linkage between the government's and the terrorist's subjective games. In conclusion, it is shown that the government's objective utility does not always increase by taking the disclosure strategy into account. Of course, the results are obtained in the assumed situation; however, the implication of these results particularly those pertaining to the disclosure of the implementation of a counter-terrorism measure to the public deserves careful and thoughtful consideration. In particular, the disclosure by the government may trigger terror attacks in the case where the terrorist has a relatively high belief of terrorism threat.

To obtain more detailed policy implications about the disclosure strategies, the model needs to be further developed. First, the model deals with the situation where the government takes care of one infrastructure site; however, the government has many infrastructure sites that need to be protected from terrorists. Considering the multiple infrastructure sites, the positive or negative externalities of the countermeasures emerge as problems plaguing the disclosure policy. The allocation of resources to prevent terror attacks is also an important topic. Therefore, we need to extend the model where the government has several types of infrastructure sites. In addition, this paper assumes that the terrorist is rational. However, in the real world, terrorists often behave irrationally. Therefore, robust disclosure strategies should be investigated to prevent irrational terror attacks. These issues will be addressed in future studies.

## REFERENCES


(1) E. Kalai and E. Lehrer, Subjective games and equilibria, Games and Economic Behavior, Vol.8, pp.123-163, 1995.

(2) V. Bier, S. Oliveros, and L. Samuelson, Choosing what to protect: strategic defensive allocation against an unknown attacker, Journal of Public Economic Theory, Vol.9, pp.563-587, 2007.

(3) M. Cremonini and D. Nizovtsev, Risks and Benefits of Signaling Information System Characteristics to Strategic Attackers, Journal of Management Information Systems, Vol.26, pp.241-274, 2009.

(4) B. Hoffman and G. H. McCormick, Terrorism, signalling, and suicide attack, Studies in Conflict & Terrorism, Vol.27, pp.243-281, 2004.

(5) D. G. Arce and T. Sandler, Terrorist signalling and the value of intelligence, British Journal of Political Science, Vol.37, pp.573-586, 2007.

2010 AIT-KU JOINT SYMPOSIUM ON HUMAN SECURITY ENGINEERING

Bangkok, Thailand, November 25-26, 2010

# Drive-by Bridge Monitoring for Short Span Bridges

Chul-Woo KIM[1] and Kunitomo SUGIURA[2]

[1]Professor, Dept. of Civil and Earth Resources Engineering, Kyoto University
(C1-3-183, Kyoto University Katsura Campus, Nishikyo-ku, Kyoto 615-8540, Japan)
E-mail: kim.chulwoo.5u@kyoto-u.ac.jp
[2]Professor, Dept. of Civil and Earth Resources Engineering, Kyoto University
(C1-3-252, Kyoto University Katsura Campus, Nishikyo-ku, Kyoto 615-8540, Japan)
E-mail: sugiura.kunitomo.4n@kyoto-u.ac.jp

This study presents a vibration-based health monitoring of short span bridges by an inspection car so called a drive-by bridge monitoring. This paper also covers brief statements about the level of screening using the inspection car. Feasibility of the drive-by bridge monitoring is investigated through a scaled laboratory moving vehicle experiment. The feasibility of using an instrumented vehicle to detect the natural frequency and changes in structural damping of a model bridge is observed. Observations also demonstrate possibility of diagnosis of bridges by comparing patterns of identified dynamic parameters of bridges through a periodical monitoring. It is confirmed that the method for damage identification under a moving vehicle well identifies the damage location and severity.

***Key Words :*** *bridge health monitoring, drive-by monitoring, inspection car, short span bridges*

## 1. INTRODUCTION

This study presents feasibility investigations for a drive-by bridge health monitoring (BHM) especially for short span bridges which account for the majority of bridge stocks. Actually, large portions of bridges located on municipalities are also short span bridges, but have not been maintained properly because of budget restrictions of local governments. Developing a rapid and cost-effective tool for BHM, therefore, is an important technical issue. How to excite short span bridges is another challenge for the vibration-based BHM because short span bridges are insensitive or sometimes impassive to external dynamic sources such as wind loads, ground vibrations, etc. Of course, the normal traffic excitations are important dynamic sources, but a very cautious approach is required to use traffic-induced vibrations of short span bridges because the traffic-induced vibration is a kind of non-stationary process[1].

Despite of the non-stationary property of the traffic-induced vibration of bridges, the traffic excitation is still an attractive dynamic source for the vibration-based health monitoring of short span bridges. An idea to utilize the traffic-induced vibration for BHM is in the drive-by monitoring using an inspection vehicle. A strong point of the drive-by monitoring is the ready excitement by the inspection vehicle. Another advantage of the drive-by monitoring is its rapidity, because the inspection car can acquire and process the data while traveling on bridges. The inspection car also carries bridges' vibrations. It is expected, therefore, that the inspection car has three major functions like an actuator, data acquisition and message carrier.

The HERMES of FHWA[2] has already been developed just focusing on use of imaging radar for scanning bridge decks. Furukawa et al. [3] employ vehicle's acceleration responses for pavement diagnostic. Interesting attempts to identify bridge frequencies using vehicle's vibration data were theoretically verified [4-6]. However, their approaches are feasible for extracting the natural frequency of

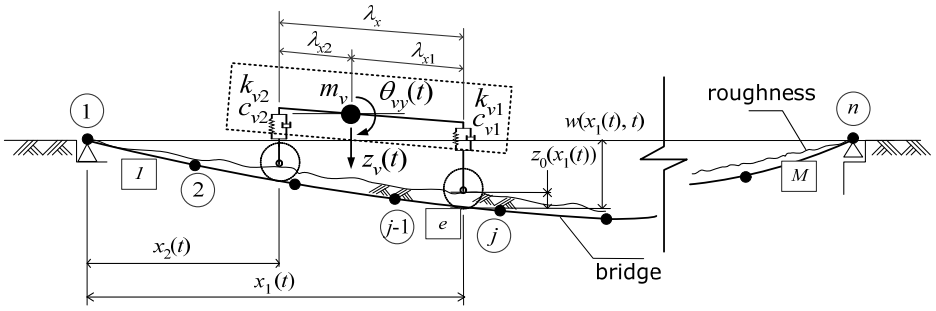


**Fig. 1** Scheme of a bridge-vehicle interactive system in moving vehicle laboratory experiment.

bridges within restricted conditions such as the bridge with very smooth roadway surface profiles.

Three levels of bridge condition screening based on the drive-by monitoring are proposed in this study, and feasibility of the condition screening methods is examined through a scaled laboratory experiment.

## 2. METHODOLOGY

Three major techniques considering in this study to realize the drive-by BHM are the level 1 screening method which monitors the bridge frequency estimated from the vehicle's vibration data, the level 2 screening method based on the modal parameter identification using the data transmitted from the bridge to the inspection car, and the level 3 screening method for the damage identification which uses data both from the vehicle and bridge.

It is noteworthy that the level 1 screening is adopted for a rapid health screening tool with sacrifice of the accuracy. The level 2 screening expecting to offer better information than the level 1 screening is a kind of global condition screening of bridges using identified frequencies, damping constants and mode shapes. The level 3 screening is adopted to identify damage location and severity when some diagnostic symptoms are detected through level 1 or level 2 screening. Theoretically feasibility of all methods is explainable using the dynamic equations of the bridge-vehicle interactive system shown in Fig. 1 and following equations.

To make the problem simple a 2DOF vehicle model is considered as shown in Fig. 1, where $z_v(t)$ and $\theta_{vy}(t)$ respectively represent vehicle's bounce and pitching motions. In that figure, $m_v$ denotes the vehicle mass. Additionally, $k_{vs}$ and $c_{vs}$ respectively denote the spring constant and damping coefficient at the $s$-th axle of the vehicle. The subscript $s$ indicates the position of an axle: that is, $s = 1$ and $s = 2$ respectively signify the first (or front) and second (or rear) axles. Distances from the vehicle's center of gravity to respective axles are denoted by $\lambda_{x1}$ and $\lambda_{x2}$. $z_0(x_s(t))$ indicates the roadway surface roughness at a position of $x_s(t)$ from the bridge entrance which is assumed as the reference position.

Equations of motion for the 2DOF vehicle can be formulated as shown in Eqs. (1) and (2). Therein $w(x_s(t), t)$ represents the time-variant displacement of the bridge at the contact point of the tire located $x_s(t)$ from the reference position.

The combination of the interaction force at the contact point of a vehicle wheel with the dynamic equation of motion of a bridge provides equations of motion for the bridge-vehicle interactive system. The dynamic equation of a bridge under a moving vehicle is definable as

$$\begin{aligned} &m_v\ddot{z}_v(t)+\sum_{s=1}^{2}c_{vs}\left(\dot{z}_v(t)-(-1)^s\lambda_{xs}\dot{\theta}_{vy}(t)-\left(\dot{w}(x_s(t),t)-\dot{z}_0(x_s(t))\right)\right)\\ &+\sum_{s=1}^{2}k_{vs}\left(z_v(t)-(-1)^s\lambda_{xs}\theta_{vy}(t)-\left(w(x_s(t),t)-z_0(x_s(t))\right)\right)=0 \end{aligned} \tag{1}$$

$$\begin{aligned} &m_v\lambda_{x1}\lambda_{x2}\ddot{\theta}_{vy}(t)-\sum_{s=1}^{2}(-1)^s\lambda_{xs}c_{vs}\left(\dot{z}_v(t)-(-1)^s\lambda_{xs}\dot{\theta}_{vy}(t)-\left(\dot{w}(x_s(t),t)-\dot{z}_0(x_s(t))\right)\right)\\ &-\sum_{s=1}^{2}(-1)^s\lambda_{xs}k_{vs}\left(z_v(t)-(-1)^s\lambda_{xs}\theta_{vy}(t)-\left(w(x_s(t),t)-z_0(x_s(t))\right)\right)=0 \end{aligned} \tag{2}$$

$$\mathbf{M}_{br}\ddot{\mathbf{q}}_r(t)+\mathbf{C}_{br}\dot{\mathbf{q}}_r(t)+\mathbf{K}_{br}\mathbf{q}_r(t)=\sum_{s=1}^{2}\boldsymbol{\psi}_s(t)P(t) \tag{3}$$

where $\mathbf{M}_{br}$, $\mathbf{C}_{br}$ and $\mathbf{K}_{br}$ respectively represent the mass, damping, and stiffness matrices of the bridge. $\mathbf{q}_r(t)$ is the displacement vector; over dots denote derivatives with respect to time. $\boldsymbol{\psi}_s(t)$ is a load distribution vector to each node of the element on which a tire contacts.

$P_s(t)$ in Eq. (3) denotes the wheel load at a tire and is definable as

$$P_s(t) = \left(1 - \frac{\lambda_{xs}}{\lambda_x}\right) m_v g + c_{vs}\dot{\delta}_s(t) + k_{vs}\delta_s(t) \tag{4}$$

where, $\delta_s(t)$ denotes the relative vertical displacement at the $s$-th axle of the vehicle and is defined as

$$\delta_s(t) = z_v(t) - (-1)^s \lambda_{xs}\theta_{vy}(t) - \{w(x_s(t),t) - z_0(x_s(t))\} \tag{5}$$

A goal for the level 1 screening is extracting changes of bridge's dynamic features from the vehicle vibrations since dynamic equations of motion of the vehicle traveling on a bridge clearly contain the term relating to bridge's responses such as $w(x_s(t), t)$ as shown in Eqs. (1) and (2). It means that if dynamic properties between the vehicle and bridge are clearly different and moreover the amplitude of the bridge response is big enough then the probability to detect bridge's frequencies increases.

Both level 2 and level 3 screenings basically rely on bridges' vibration data actuated by the inspection vehicle travelling on the bridge. The discrepancy between two methods is in the use of external forces generated by the moving vehicle. In other words, the level 2 screening is an output only method. On the other hand, the level 3 screening needs both bridge's vibration data and vehicle's dynamic wheel loads.

The eigensystem realization algorithm (ERA)[7] based on the state space equation of the dynamic system is adopted for the level 2 screening. Details of the process are obtainable from the reference [8),9)]. From Eq. (3) the state vector $\mathbf{x}(t)$ for the equation of motion of a bridge under a moving vehicle is definable as

$$\mathbf{x}(t) = \begin{bmatrix} \mathbf{q}_r(t) \\ \dot{\mathbf{q}}_r(t) \end{bmatrix} \tag{6}$$

If $\mathbf{y}(t) \in \mathbf{R}^m$ denotes output of the bridge structure taken from $m$ observation points, then the corresponding state equation of a continuous-time system is described as

$$\dot{\mathbf{x}}(t) = \mathbf{A}\mathbf{x}(t) + \mathbf{B}\mathbf{w}(t) \tag{7}$$

$$\mathbf{y}(t) = \mathbf{C}\mathbf{x}(t) \tag{8}$$

where, $\mathbf{A}$, $\mathbf{B}$ and $\mathbf{C}$ respectively denote system, input influence and output influence matrices. Especially, $\mathbf{C}$ is a transformation matrix mapping the position of system degrees of freedom with measured outputs which consists of zero or one. $\mathbf{w}(t)$ denotes external effects (or noise effects) to the system.

This study adopts the AR model[8),9)] to identify dynamic properties of the system $\mathbf{A}$ shown in Eq. (7) assuming white noise excitations. In practice, however, ambient vibration responses observed in operation, which are not white noise excitations actually and are sometimes non-stationary vibrations, are used in the modal parameter identification.

Despite of the non-stationary property of the traffic-induced vibration, the idea of the level 2 screening even using the traffic-induced vibration of short span bridges for their modal identification is that the modal parameters identified repeatedly under a given moving vehicle can provide a pattern or even a statistical one which may give a useful information to make a decision for the bridge's health condition.

The concept of the level 3 screening is based on the fact that the stiffness distribution in the structure is induced to change as a result of damage. This change is detectable by measuring dynamic responses under the inspection vehicle whose dynamic wheel loads or dynamic properties are known. The linear equation for bridge's structural stiffness can also be derived from Eq. (3) as shown in Eq. (9) which is a pseudo-static formulation showing change of structural stiffness.

$$\mathbf{K}_{br}\mathbf{q}_r(t) = \mathbf{f}(t) \tag{9}$$

In that equation, the force vector is definable as

$$\mathbf{f}(t) = \sum_{s=1}^{2} \boldsymbol{\psi}_s(t) P_s(t) + \mathbf{M}_{br}\ddot{\mathbf{q}}_r(t) + \mathbf{C}_{br}\dot{\mathbf{q}}_r(t) \tag{10}$$

The change of stiffness $\mathbf{K}_{br}$ in Eq. (9) provides information about the change of the bridge's stiffness due to damages. Detecting the change in $\mathbf{K}_{br}$ is the basic concept of the damage identification proposed for the level 3 screening. The change of the element stiffness is also obtainable using the element stiffness index (ESI), which is definable as

$$\mu_e = \frac{\mathbf{K}_{be}^d}{\mathbf{K}_{be}^i} \tag{11}$$

(a) model bridge under moving vehicle

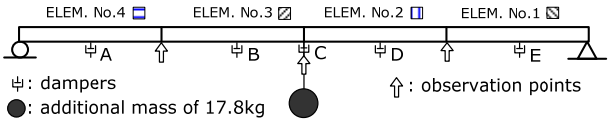


(b) experimental setup for level 1 screening

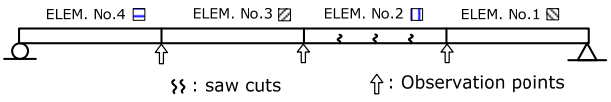


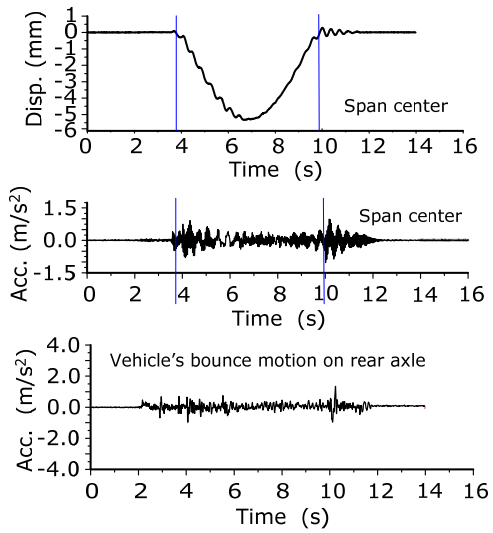


(a) Intact

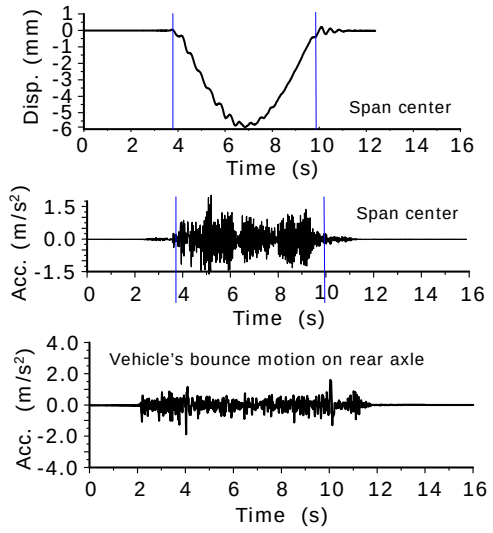


(b) D2

**Fig. 3** Time histories of model bridge and vehicle.

where $\mu_e$ is the element stiffness index, and $\mathbf{K}_{be}^{i}$ and $\mathbf{K}_{be}^{d}$ signify the stiffness of the $e$-th element of an intact and damage states, respectively.

Estimating the ESI is the final goal for the level 3 screening. Details of the methodology can read from the authors' existing research [10]. A noteworthy point is that the ESI value is unity for intact state, meaning that the value is less than unity for damaged members.

## 3. EXPERIMENT

A scaled moving vehicle laboratory experiment is performed to investigate feasibility of the drive-by health monitoring. The experiment setup is summarized in Fig. 2. Roadway profiles are also considered in the experiment.

As for the experiment to examine the feasibility of the level 1 screening, the damping of the bridge is varied in this experiment by applying old displacement transducers at particular points on the bridge in addition to a 17.8kg mass added at midspan. The layout of these transducers is illustrated in Fig. 2 (b), in which the dampers are denoted by the alphabets from A to E. The old transducers are used as they provide frictional resistance to bridge displacements at the chosen locations. The damping constant changes from 1.4% of intact case to 2.1% and 4.3% due to addiotnal damper at the span center and five additional dampers respectively. The additional mass is used to adjust the frequency of the bridge as frequently damage which causes changes in damping may cause some changes in frequency . The additional mass causes change of the natural freqeucny for the first bending mode from 2.7Hz to 2.5Hz.

Two damage scenarios are considered in the experiment to investigate feasibility of the level 2 and level 3 screenings: as for the first damage scenario (hereafter D1), three saw cuts are applied to both sides of web plates at ELEM No.2 of the bridge; the second damage scenario (hereafter D2) considers both saw cuts at ELEM No.2 and cut-out at ELEM. No.4. For damage scenario D1, the bending rigidity of the member decreases to around 89 % of the intact state. About 23 % loss of bending rigidity of the damaged member is observed due to the damage scenario D2. Natural frequencies estimated from free vibrations for the intact bridge is 2.7Hz. The natural frequencies of the damaged bridges according to damage scenarios D1 and D2 are 2.6 Hz and 2.5 Hz, respectively. Apparently the damage causes decrease of natural frequencies.

During the experiment, three different vehicle models of which the natural frequency of the bounce motion is changeable using a different set of mass and spring are considered in the experim ent. Three vehicles, called as VT-A, VT-B and VT-C, are used in the experiment. Natural frequencies for the bounce motion of those vehicle models are respectively 2.93 Hz, 3.76 Hz and 3.03 Hz. Two different speeds of S1=0.93 m/s and S2=1.63 m /s are adopted to investigate the effect of the vehicle speed to the screening results. Six traffic scenarios are considered as: SCN1 of VT-A vehicle traveling with speed S1; SCN2 of VT-A vehicle traveling with speed S2; SCN3 of VT-B vehicle traveling with speed S1; SCN4 of VT-B vehicle traveling with speed S2; SCN5 of VT-C vehicle traveling with speed S1; and SCN6 of VT-C vehicle traveling with speed S2.

Three points at 1/4, 1/2, and 3/4 of the span length are the observation points. As for vehicles, front and rear axles of the vehicle are observation points. The sampling rate of signals is 100Hz. Exam ple time histories of responses at the m idspan as well as the acceleration response for the vehicle' s bounce m otion at the rear axle are shown in Fig. 3. They are the responses under the loading scenario SCN3 which the VT-B vehicle travels on thebridge with speed S1.

## 5. CONDITION SCREENING

### (1) Level 1 screening

Fig. 4 com pares the m ean acceleration spectra of the bridge and vehicle obtained in all scenarios for 5 crossings of vehicle VT-A at speed S1. The bridge frequency peak at 2.44 Hz occurs in both Fig. 4(a) and (b). It can be seen that as the damping increases i.e. from 'Intact' to 'C' to 'ABCDE', the peak magnitude at the bridge frequency in the vehicle spectra decreases. This trend also occurs at the peak in vehicle spectra at 3.91 Hz. This suggests it ispossible to detect changes in bridge dam ping. It is noteworthy that the dom inant frequency of bridge in Fig 4(a) is biased from the natural frequencies of the bridge and vehicle.

For all scenarios investigated but om mited in this paper, the bridge frequency was identified in the vehicle spectra. It is clear that selection of vehicle speed is an im portant factor in the detection of the bridge frequency. The higher speed, S2 = 1.63m/s, provides larger m agnitude peaks in the spectra but the spectral resolution is not as high as for speed S1. For VT-A vehicle and speed of S1, changes in damping are detected in the vehicle spectra. These results indicate that to confirm the feasibility of the system, further investigation of vehicle configuration, speed and girder dam ping scenarios is necessary.

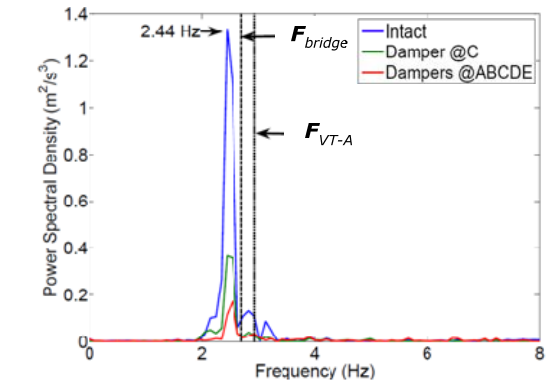


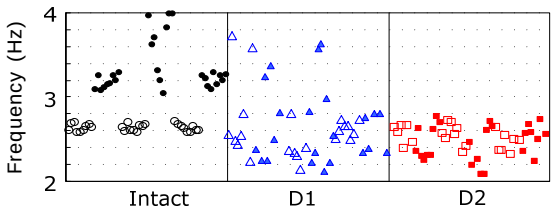


(a) observed frequency near 3Hz

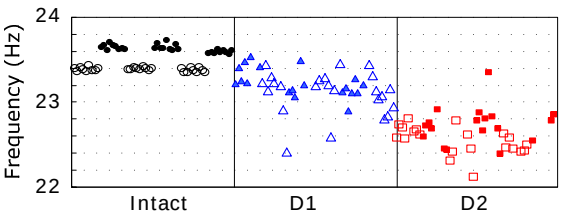


(b) observed freqeucny near 23Hz

**Fig. 5** Variation of identified frequencies for level 2 screening.

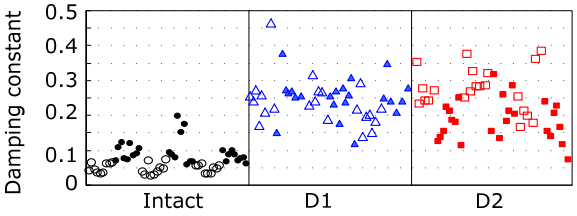


(a) observed damping constant corresponding to the frequency of Fig.5(a)

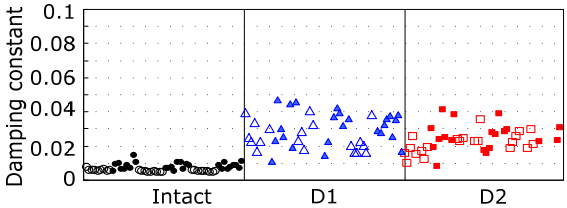


(b) observed damping constant corresponding to the frequency of Fig.5(b)

**Fig. 6** Variation of identified damping constants fro level 2 screening.

### (2) Level 2 screening

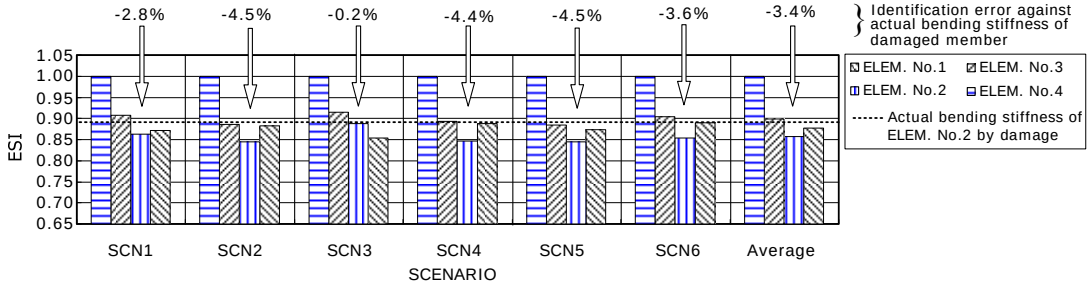


(a) D1

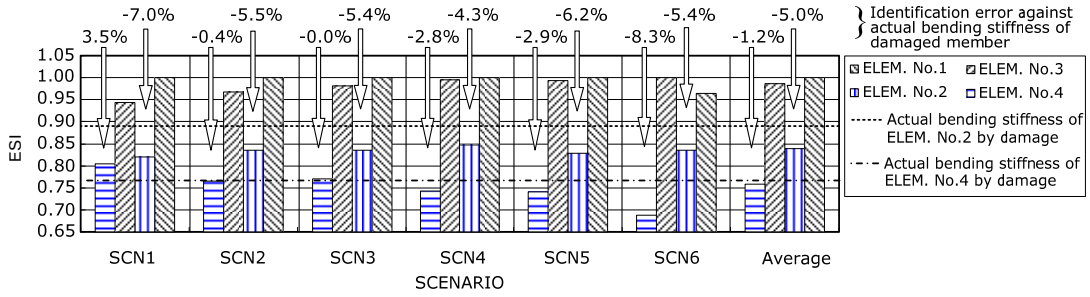


(b) D2

**Fig. 7** Identified damage location and severity by level 3 screening.

Modal parameter identification by the AR model is conducted using experim ental data taken from the intact model bridge and the dam aged m odel bridge under the damage scenarios D1 and D2. The pattern change of identified sy stem m odal parameters such as dominant frequencies and corresponding damping constants is investigated. The reason to take notice of dominant dynamic parameters is that traffic-induced bridge vibrations are usually affected by vehicle's dynamic properties and as a result are not directly linked to natural modal parameters of the bridge itself as already shown in Fig. 4. Therefore this study focuses on the dominant dynamic parameters instead of natural modal parameters.

Dominant frequencies and sy stem dam ping constants estimated from the data taken from the six traffic scenarios are sum marized in Figs. 5 and 6, respectively. Therein the solid circles, solid triangles and solid squares respectively denote the identified parameter from intact and dam aged bridges with D1 and D2 dam ages under vehicle speed S2=1.63m/s. Those of em pty are the identified results under vehicle speed S1=0.93m /s. It demonstrates that the effect of the vehicle sy stem to bridge vibrations, so called traffic-induced vibrations of bridges or non-stationary vibrations, increases with increasing speed, and as a result the identified results under higher vehicle speed yield to more biased results than those of lower speed.

A clear pattern change of identified dominant frequencies can be read from Fig. 5 despite of their severe variations. The higher frequency provides more apparent pattern changes according to the damage as shown in Fig. 5(b).

Usually the dam ping constants derived from eigenvalue of a system m atrix m ay be subject to appreciable error[7], and as a result larger coefficient of variance than that of the identified frequency is observed as shown in Fig. 6. However, despite of their appreciable error the pattern change of identified damping constants due to the damage is apparent.

The point m ade here is that the pattern change of system modal parameters using the traffic-induced vibration data excited by the m oving vehicle can provide information for health condition of short span bridges.

**(3) Level 3 screening**

This section is devoted to discussing the feasibility of the level 3 screening which aim s to identify damages. The identified ESI values for D1 and D2 are summarized in Fig. 7. For D1, the damage on the element No.2 is well identified by the proposed m ethod except SCN3, the loading scenario 3, which identifies ELEM. No.1 as the most suspected damage member rather than ELEM. No.2. Unfortunately the reason for the unsuccessful identification is not clear yet. The percentage term s in Fig. 7 denote the error relating to identifying severity of damages. The error varies up to 4.5 %, and it demonstrates the proposed method can also presum e the dam age severity. Considering D2, suspected dam age locations are also

well identified. The damage severity of each member is identified within the error of 7.0 % for the damaged member ELEM. No.2 and within the error of 8.3 % for the damaged member ELEM. No.4.

Observations from the experimental investigation demonstrate that the location and severityof damages are constantly identified without great variation according to vehicle ty pe and speed, even though the vehicle with sim ilar frequency characteristics with bridge's fundam ental fre quency and higher speed may give better chance to identify both severity and location.

## 6. CONCLUSIONS

This paper investigates feasibility of the drive-by bridge health monitoring through a scaled laboratory moving vehicle experiment. The summarized results are as follows.

The bridge frequency was identified in the vehicle spectra. It is clear that selection of vehicle speed isan important factor in the detection of the bridge frequency. The higher speed, S2 = 1.63m /s, provides larger magnitude peaks in the spectra but the spectral resolution is not as high as for speed S1 = 0.93m/s. For vehicle VT-A and speed S1, changes in damping are detected in the vehicle spectra. These results indicate that it is possible to detect the bridge frequency and changes in dam ping from the acceleration measurements of a m oving vehicle. To confirm the feasibility of the sy stem, further investigation of vehicle configuration, speed and girder damping scenarios is necessary.

Pattern change of sy stem modal parameters using the traffic-induced vibration data excited by the moving inspection vehicle can provide information for health condition of short span bridges. It also demonstrates that the effect of the vehicle sy stem to bridge vibrations, so called traffic-induced vibrations of bridges or non-stationary vibrations, increases with increasing speed, and as a result the identified results under higher vehicle speed y ield more biased results than those of lower speed.

Location and severity of damages are constantly identified without great variation according to vehicle ty pe and speed, even though the vehicle with similar frequency characteristics with bridge' s fundamental frequency and higher speed may give better chance to identify both severity and location.

Many further investigations are necessary to make the method practically applicable, such as how sensitive the method is under various kinds of damages. Another great challenge is realizing data acquisition both from moving vehicle and bridge sim ultaneously. Wireless sensing may be a solution. The schoolof remaining problems is now under investigating.

**ACKNOWLEDGMENT:** A part of this study is supported by the Japan Society for the Promotion of Science (Grant-in-Aid for Scientific Research (C) under project No. 20560443) and Kinki Construction Association (Grant-in-Aid for Scientific Research), which are gratefully acknowledged.

## REFERENCES

1) Kim, C. W. , Kawatani, M. and Kim, K. B. : Three-dimensional Dynamic Analy sis for Bridge-vehicle Interaction with Roadway Roughness, *Computers and Structures* Vol.83, pp. 1627-1645, 2005.
2) FHWA NDE CENTER RESEARCH & DEVELOPMENT, The HERMES Bridge Inspector, http://www.tfhrc.gov/hnr20/nde/hermes.htm/. Accessed November 21, 2009.
3) Furukawa, T. Fujino, Y. Kubota,K. and Ishii, H. : Real-time Diagnostic System for Pavements using Dynamic Response of Road Patrol Vehicles (VIMS). In B. Bakht & A. Mufti (eds), *Structural Health Monitoring & Intelligent Infrastructure,* CD-ROM, 2007.
4) Yang, Y. B., Lin, C. W., and Yau, J. D. Extracting Bridge Frequencies from the Dynamic Response of a Passing Vehicle. *J. of Sound and Vib.*, Vol.272, pp. 471-493, 2005.
5) Oshima, Y. Kobayashi, Y. Yamaguchi, T., and Sugiura, K. : Eigenfrequency Estimation for Bridges using the Response of a Passing Vehicle with Exc itation System. In H.M. Koh & D.M. Frangopol (eds), *Bridge Maintenance, Safety, Management, Health Monitoring and Informatics*, CD-ROM, 2008.
6) McGetrick, P. J., Gonzalez, A. and OBrien, E. J .: Theoretical investigation of the use of a moving vehicle to identify bridge dy namic parameters, *Insight*, V ol.51, N o.8, pp.433-438, 2009.
7) Pappa, R. S. and Ibrahim, S. R. : A Parametric Study of the Ibrahim Tim e Dom ain Modal Identification Algorithm . *Shock and Vibration Bulletin*, No.51, Part 3, pp.43-72, 1981.
8) Gersch, W. , Nielsen, N. N. and Akaike, H. : Maximum Likelihood Estimation of Struct ural Parameters from Random Vibration Data. *J. of Sound and Vib.*, Vol.31, No.3, pp. 295-308, 1973.
9) Wang, Z. and Fang, T. A. : Time-domain Method for Identifying Modal Parameters. *J. Appl. Mech.*, ASME, Vol.53, No.3, pp. 28-32, 1986.
10) Kim, C. W. and Kawa tani M. : Pseudo-static approach for damage identification of bridges based on coupling vibration with a moving vehicle, *Structure and Infrastructure Engineering*, Vol.4, No.5, pp.371-379, 2008.

2010 AIT-KU JOINT SYMPOSIUM ON HUMAN SECURITY ENGINEERING

Bangkok, Thailand, November 25-26, 2010

# Assessment of Steel Flyover Bridges in Bangkok

Tospol PINKAEW, Akhrawat LENWARI, Teerapong SENJUNTICHAI
Taksin THEPCHATRI and Ekasit LIMSUWAN

Dept. of Civil Engineering, Chulalongkorn University
(Phatumwan, Bangkok 10310, Thailand)
E-mail:tospol.p@chula.ac.th

This paper overviews the assessment project that has been recently completed by the Bangkok Metropolitan Administration (BMA) as a part of the maintenance program to investigate the safety, remaining fatigue life, and serviceability of major flyover bridges in Bangkok. A total of eleven steel flyover bridges, which are all the slab-on-girder type, were inspected and were tested by heavy truck loads to investigate the bridge actual behaviors and validate the three dimensional finite element modeling. Then the safety levels of all bridges under certain conditions of loadings are estimated. Their remaining service lifes and the serviceability levels are evaluated based on recorded data obtained from in-service monitoring of traffic and bridge responses for about one week.

***Key Words :*** *steel flyover bridges,bridge load test, fatigue life assessment, bridge servicceability*

## 1. INTRODUCTION

Steel bridges have been commonly employed for flyover bridges over many intersections in Bangkok, Thailand, mainly because the construction time is much faster than the ordinary concrete type. Two basic girder types are I- and box-girders. The I-girders have been utilized for straight or skewed spans, while the box-girders for curved spans as shown in Fig.1. For most bridges, the main spans over the intersection utilize the orthotropic steel decks having span lengths from 35-50 meters and the typical spans employ the composite construction with concrete decks, i.e., pre-cast concrete deck and cast-in-place concrete in conjunction with the formed steel deck, having span lengths of 20-25 meters. Fig.2 shows the composite construction using shear studs to transfer horizontal shear between with the pre-cast concrete and steel I-girders.

Recently, the Bangkok Metropolitan Administration (BMA) has completed an assessment project as a part of the maintenance program to investigate the safety, remaining service life, and serviceability of eleven steel flyover bridges in Bangkok for future decision on modification, strengthening and repair. Most of these bridges have been constructed for over fifteen years. The preliminary investigation indicated some corrosion and distortion of bridge members. Complaints from bridge users about vibration and feeling of unsafe were also reported.

The main objectives of the project were :
(a) to assess the current bridge's condition
(b) to perform the field load test and load rating
(c) to assess the remaining fatigue life
(d) to measure the traffic-induced vibration
(e) to evaluate the existing earthquake resistance

This paper briefly summarizes the project covering field inspection work, the field load test and monitoring, the finite element analysis, the fatigue remaining life estimation and the serviceability evaluation.

(a)

(b)

**Fig.1** Orthotropic steel decks at main spans (a) I girders (b) box girders

(a)

(b)

**Fig.2** Composite girders at typical spans (a) precast concrete and (b) cast-in-place concrete

## 2. FIELD INSPECTION

Field inspection employed both visual inspection and nondestructive testing. Two nondestructive testing methods, namely, the ultrasonic testing (UT) and magnetic particle testing (MPT) were chosen in the project.

The visual inspection aim ed at detecting observable damage such as corrosion in steel deck, pier and girder, warping/misalignment in structural com ponents resulting form accidents, loosening of bolt, and bearing condition. For most of the bridges, the visual inspection revealed no serious corrosion damage in both m ain and secondary structural steel components, e.g., steel decks, girders, diaphragms and piers. However, loosening of bolts at locations such as the girder-diaphragm connection and cross girder-pier connection, as shown in Fig.3, has been reported. These damages are critical as they are related to the structural integrity of the bridge's superstructure. Other types of damage include concrete spalling and collision damage. Fig.4 shows the deform ed bottom flange of the steel girder and the deficient bearing at the girder support.

(a)

(b)

**Fig.3** Loosening of bolts (a) girder-diaphragm connection (b) cross girder-pier connection


(a)

(b)

**Fig.4** Bridge damage examples: (a) defoemed member and (b) deficient bearing movment at girder support

(a)

(b)

**Fig.5** Bridge crack examples: (a) at welded connection near web splice and (b) in the box girder web near support

The magnetic particle testing was utilized to detect the fatigue cracks at fatigue-prone details, while the ultrasonic testing was used to measure the actual thickness of structural steel components at several important locations such as the top and bottom flanges of steel girders and the thickness of the steel pier.

From the field inspection, many cracks have been reported in some bridges. Fig.5(a) shows a visible fatigue crack at welded connection near the web splice location. Fig.5(b) shows the fatigue crack in the box girder web near the support (cross girder). Other crack locations include the diaphragm-web welds and stiffener-flange welds.

In addition to the field inspection, a destructive laboratory test was performed to identify the properties of both steel and concrete materials for the finite element modelling. The steel specimens were cut from the girder's web near the supports, while the concrete specimens were cored from the concrete deck near the sidewalk. The bridge was immediately repaired after the specimens were cut.

## 3. FIELD LOAD TEST AND IN-SERVICE MONITORING

### (1) Field Load Test

A full-scale truck testing was performed to investigate the actual behavior of the bridge structure and to validate the finite element model. One or multiple test trucks advanced across the bridge in several loading cases: (a) static loading where the trucks advanced and stopped at predefined positions (every 5 meters) along the span and (b) dynamic loading where the trucks moved at different predefined velocities (5, 10, 20 and 40 km/hr). Both full and partial lanes loaded by the test trucks were studied. Fig.6 shows the configuration of a standard Thai truck employed in the test program. The total weight of the truck is 25 tons.

All bridges were instrumented with three types of sensors: (1) the 120-$\Omega$ foil strain gages, (2) accelerometers, and (3) linear variable displacement transducers (LVDTs). Fig.7 shows a typical instrumentation layout for strain gages in superstructure and substructure. Basically, the strain gages were attached to the superstructure at the bottom flanges of

all girders (girder G1, G2, and G3) in quarter (SW1 and SW2) and m idspan (MID) locations. All sensor cables were wired into the data acquisition units located beneath the bridge. Each unit contains 48 channels and USB interface online data to PC with the maximum sampling frequency of 1024 Hz.

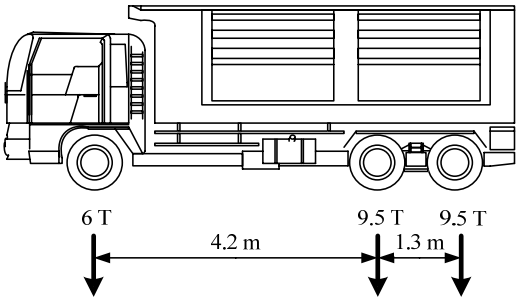


**Fig.6** Test truck configuration (10 wheels with weight of 25 tons)

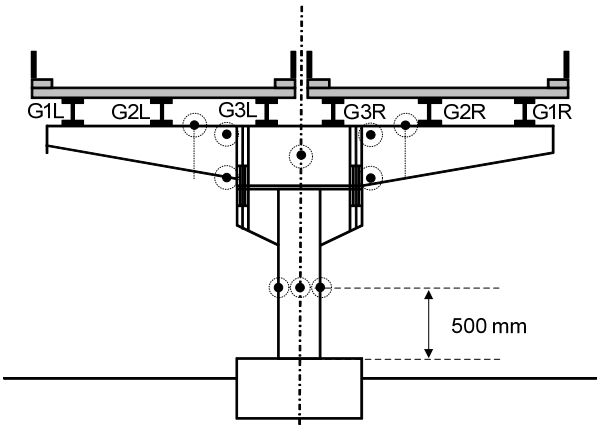


(a) Pier

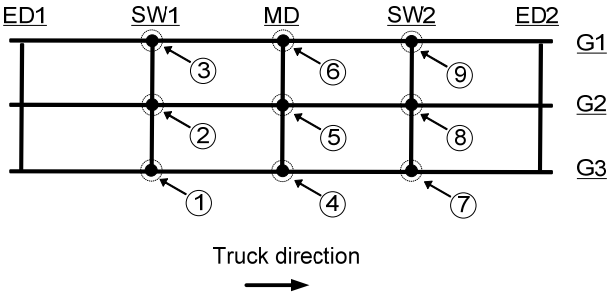


(b) Deck

**Fig.7** Typical instrumentation layout (shows only strain gages)

Fig.8 illustrates an exam ple record of midspan deflection of exterior girder in a 25-m span at different truck velocities. The dy namic am plification factors are calculated to be 1.038,1.096 and 1.221 for truck velocities 5, 10 and 20 km /hr, respectively . Both measured displacements and strains were used to calibrate the finite element model before assessing the existing capacity of the bridge.

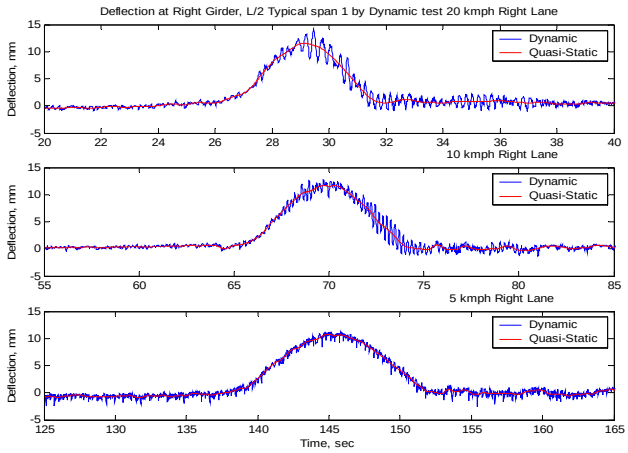


**Fig.8** Typical displacement records at midspan of interior girder

## (2) In-service Bridge Monitoring

In the project, a one-week continuous traffic and strain data m onitoring were perform ed under daily traffic condition. The heavy vehicles were classified into five categories, i.e., bus, 6-wheel truck, 10-wheel truck, sem i-trailor, and trailor. As small personal cars and m otorcycles were considered as less influence on the fatigue life than heavy trucks; they were not included in the fatigue life evaluation.

The traffic m easurement provided the current Average Daily Truck Traffic (ADTT) values ranging from 160 to 1570 trucks/day for the inbound direction. In m ost bridges, the m ajority truck ty pes are 6-wheel trucks followed by the 10-wheel trucks, and buses.

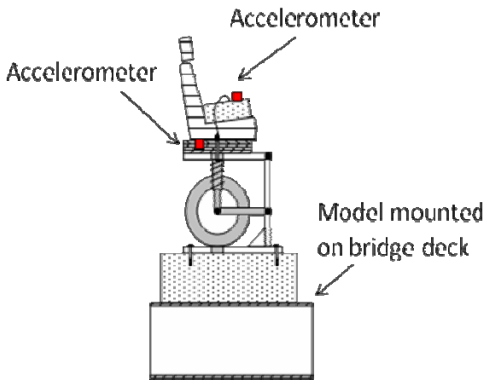


**Fig.9** Typical displacement records at midspan of interior girder

In addition, the simplified quarter car m odel as in Fig.9 is frabricated and installed atthe midspan of the main span of the bridge. The one-week monitoring of

the model car accelerations at the car suspension and passenger seat were recorded in order to use for bridge's serviceability evaluation.

## 4. THE 3-D FINITE ELEMENT MODELS

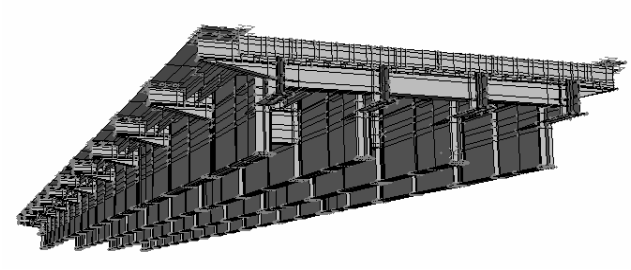

(a) Main span

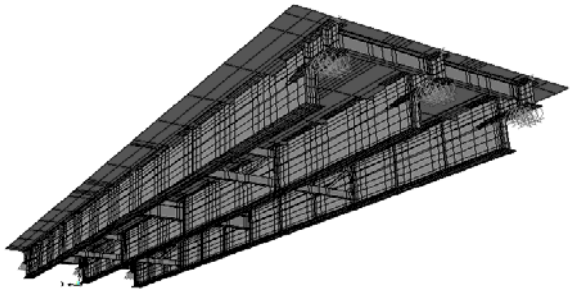

(b) Typical span

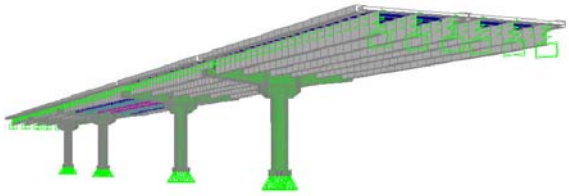

(c) Full model for earthquake analysis

**Fig.10** Finite Element Models of a Bridge

Three-dimensional finite element models were generated using SAP2000[1]. All structural components including the secondary members were modeled with quadrilateral shell elements having six degrees of freedom at each node. For the superstructure, the secondary elements such as diaphragms and cross frames were also modeled. In case of the composite construction, the rigid link elements were employed to represent the interaction between the concrete deck and the top flange of steel girders[2),3)].

Fig.10 shows the finite element mesh for both superstructure and substructure of one bridge. The bridge superstructure has two traffic lanes in one direction. The typical span is simply-supported with a span length of 25 m. The 205-mm-thick concrete deck is supported by three equally-spaced steel girders. The main span over the intersection is a simply-supported span of 35 m long with an orthotropic steel deck. The 12-mm steel deck plate is supported by four equally-spaced steel girders. Total numbers of elements employed were 10,460, 21,900 and 8,000 for the typical span, main span and substructure, respectively.

The finite element models were verified with the field strain and deflection data before used in the load rating of the bridge members. The rating factors were calculated for both inventory level and operating level (absolute maximum load level) for shear and moment capacities of the main (longitudinal) girders and cross girders[4)]. For the steel piers, the interaction diagram was constructed for the rating purpose. The rating factor values suggested that all bridges are sufficient to carry both AASHTO and standard Thai trucks.

## 5. FATIGUE REMAINING LIFE

A 3-D finite element analysis was performed to help identifying the fatigue prone details for the selection of the strain gages locations. The fatigue prone details are those having low fatigue strength and were subjected to high stress ranges. Typical fatigue prone details in steel girders are the diaphragm-web connections, welded transverse stiffeners, and web attachments. Attempt has also been made to investigate the distortion-induced stresses in the web gap area. In the assessment, these fatigue prone details were categorized as Category C or E fatigue strength[5)].

The measured strain data were processed using the rainflow counting method[6)] to obtain the stress range histogram, which represents the cycle counts for each level of stress range. The effective stress range was then calculated as the root-mean-cube value.

Once effective stress range was determined, the total fatigue life in years can be calculated taking into account the traffic data. The remaining fatigue life was then obtained by subtracting the currentage from the total life. Four possible ADTT cases were considered. These include the current ADTT value (no growth), 1%, 5%, and 10% traffic growth per year. The results showed that the remaining fatigue lives of most bridges exceed 50 years for the current ADTT values.

## 6. SERVICEABILITY EVALUATION

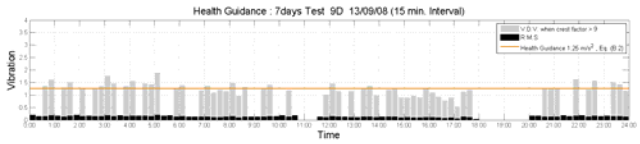


(a) Evaluation for exposure duration = 15 mins.

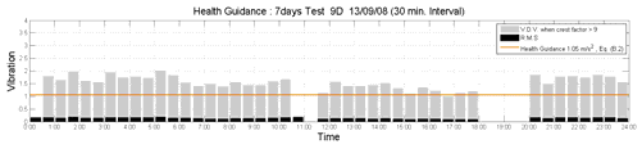


(b) Evaluation for exposure duration = 30 mins.

**Fig.11** Evaluation example of passenger heath per ISO-2631.

The obtained acceleration records from bridge deck and car model were used for serviceability evaluation. The peak, root-mean-square (rms) and vibration dose value (VDV) were calculated. The ISO standards were adopted for evaluation for both pedestrian assessment[7] and passenger health [8]. The obtained results indicate that all considered fly over bridges have excessive vibration level and are not suitable for pedestrian. For passenger, although the vibration level does not seriously induce a feeling of discomfort according to ISO standard, the obtained vibration implies significant effects on passenger's health if the exposure duration becomes longer than about 20 minutes as in Fig11.

## 7. CONCLUSION

As a part of the maintenance program, a field investigation, field load test, in-service monitoring, and finite-element analysis was performed in order to assess the safety, remaining fatigue life, and serviceability of eleven steel fly over bridges in Bangkok. The obtained results indicate repairs of some bridge members, connections and bearings where the significant damages were found. The bridge deck rating factors suggested that existing capacities of all bridges are sufficient to carry both the AASHTO and standard Thai design trucks. However, the in-service monitoring shows that there were illegal heavytrucks crossing the bridges. To prevent this heavy truck problem, the automatic heavy truck detector system is designed and proposed as in Fig.12. This system can enhance not only the bridge safety but also the bridge serviceability. Although the serviceability seems not a serious problem, the installation of conventional MTMD at certain bridge spans is proposed to increase the bridge serviceability and reduce the complaint from bridge users.

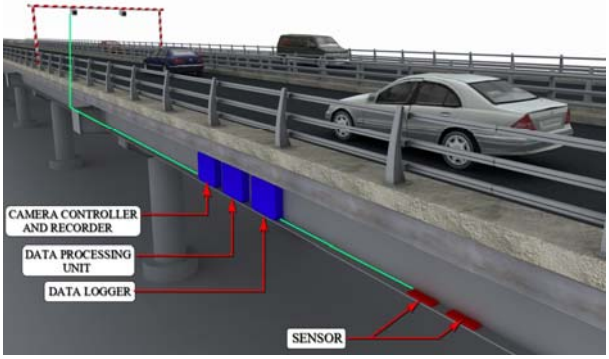


**Fig.12** Automatic heavy truck detector system.

**ACKNOWLEDGMENT:** The authors would liketo acknowledge the Bangkok Metropolitan Administration officers and IETL, Co. Ltd., for the assistance during the field investigation.

## REFERENCES

1) Computers and Structures: *SAP2000 analysis reference*, Computer and Structure, Inc., Berkeley, California, 2005.
2) Mabsout, M. E., Tarhini, K. M., Frederick, G. R., and Tayar, C. : Finite element analysis of steel girder highway bridges, *Journal of Bridge Engineering*, Vol. 2(3), 83-87, 1997.
3) Chung, W., Liu, J., and Sotelino, E. D. : Influence of secondary elements and deck cracking on the lateral load distribution of steel girder bridges, *Journal of Bridge Engineering*, Vol. 11(2), 178-187, 2006.
4) American Association of State Highway and Transportation Officials (AASHTO) : *Manual for condition evaluation of bridges*, 2rd Ed. as revised by 1995, 1996, 1998 and 2000 Interim Revisions, AASHTO, Washington, D.C., 2000.
5) American Association of State Highway and Transportation Officials (AASHTO) : *LRFD bridge specifications*, SI Units 3rd Ed., AASHTO, Washington, D.C., 2005.
6) Downing, S. D., and Socie, D. F. : Simple rainflow counting algorithms, *International Journal of Fatigue*, Vol. 4, Issue 1, January, 31-40, 1982.
7) International Standards Organization, ISO 10137 Bases for design of structures - Serviceability of buildings and walkways against vibrations, Geneva, Switzerland, 2007.
8) International Standard Organization, ISO 2631-1 Mechanical vibration and shock evaluation of human exposure to whole-bofy vibration,Geneva, Switzerland, 1997.

2010 AIT-KU JOINT SYMPOSIUM ON HUMAN SECURITY ENGINEERING

Bangkok, Thailand, November 25-26, 2010

# Optimization of Vehicle Routing and Scheduling Problem with Time Window Constraints in Hazardous Material Transportation

Rojee PRADHANANGA[1], Eiichi TANIGUCHI [2] and Tadashi YAMADA[3]

[1]Researcher, Dept. of Urban Management, Kyoto University
(C1-182, Kyoto University Katsura Campus, Nishikyo-ku, Kyoto 615-8540, Japan)
E-mail: rojee.p@ks3.ecs.kyoto-u.ac.jp
[2] Professor, Dept. of Urban Management, Kyoto University
(C1-335, Kyoto University Katsura Campus, Nishikyo-ku, Kyoto 615-8540, Japan)
E-mail:taniguchi@kiban.kuciv.kyoto-u.ac.jp
[2] Associate Professor, Dept. of Urban Management, Kyoto University
(C1-336, Kyoto University Katsura Campus, Nishikyo-ku, Kyoto 615-8540, Japan)
E-mail: t.yamada@kiban.kuciv.kyoto-u.ac.jp

Unlike widely available literatures in hazardous material (HAZMAT) transportation that basically aim at finding non dominated paths for a given origin-destination pair, our main focus in this study is on vehicle routing problem with time window (VRPTW) aspect of HAZMAT transportation problem that has received very less attention in literatures. We present a new multi-objective optimization model and its meta-heuristic solution technique using Ant Colony System for HAZMAT routing. In contrast to existing local routing models, we consider minimization of risk and transportation cost in both route choice and routing phases of transportation process. Moreover, route choice and routing have been carried out as a single step process. Lastly, the proposed algorithm has been tested for normal VRPTW by testing on Solomon benchmark instances and the results obtained show that the proposed algorithm outperforms while maintaining realistic computation time.

***Key Words :*** *Multi-objective optimization, Hazardous Material, VRPTW, Meta-heuristic*

## 1. INTRODUCTION

A wide class of hazardous materials is produced, transported and used to meet the daily requirements of industrial activities of a country. Due to nature of these materials, every production, storage and transportation activity related to their use inherits many risks for both society and environment. Despite the continuous effort to mitigate the adverse effects of HAZMAT, accidents do happen "Erkut *et al.* (1995)" and though these accidents are very small in numbers the consequences in most cases are undesirable. This is the reason that these accidents are commonly perceived as low probability high consequences (LPHC) events. Data on HAZMAT shipments in most cases are not readily available and are often difficult to access but the sizeable shipments of these materials and their potential adverse conditions are the reason that HAZMAT transportation is a growing issue in logistical decision making.

While risk is the primary ingredient that separates HAZMAT transportation problems from other

transportation problems "Erkut *et al.* (2007)", HAZMAT transportation is a multi-objective issue that involves a number of parties with often conflicting priorities and viewpoints during decision making process. The transporting company for example has priority to minimize the transportation cost while the local government intends to minimize the risk associated with the transportation process. One of the possible methods to resolve this issue is application of a proper routing technique that enables decision maker to come up with safe and economical HAZMAT transport routes, and it is this aspect of HAZMAT transportation that is focused in this study.

A large number of single objective and multi-objective models for finding paths for HAZMAT shipment for a given origin and destination pair are available in literatures. However, in practical situation, HAZMAT shipments specially those based on truck mode like ordinary Vehicle Routing Problems with Time Windows (VRPTW) calls for determination of a set of routes to be used by a fleet of vehicles serving a fixed number of customers. In this study, we present a new multi-objective optimization model for routing and scheduling of a fleet of vehicles carrying HAZMAT from a single common depot and satisfying the demand and time window constraints of a fixed number of customers. Owing to the complexity raised in this study due to our attempt to consider route choice and routing in single step, the dynamic nature of the problem will not be considered in this study. A new heuristic approach using Ant Colony System (ACS) has been developed in order to solve this model. Selection of a path from depot to customer or customer to customer or customer to depot, also known as route choice and finding order of customers to be visited by vehicles for optimal routing called routing are the two terminologies of routing and scheduling of any VRPTW. Unlike in previous studies where route choice is carried out beforehand determining a single path between each customer pair which is then used for routing process to determine order of customers to be visited for optimal routing, both route choice and routing process in this study have been carried out in multi-objective aspects and proceeded as a single step process.

The rest of this paper is organized into five sections. Section 2 provides a thorough review of past researches in HAZMAT routing. A brief description of HAZMAT transportation problem considered in this study, its formulation and the method of assessment of risk involved has been presented in Section 3. Section 4 presents a new heuristic solution technique developed to solve this HAZMAT routing problem. The proposed algorithm has been tested for normal VRPTW in Solomon's benchmark problem and the numerical results obtained are presented in Section 5. Finally, Section 6 provides concluding remarks of the present study and possible future research plans.

## 2. LITERATURE REVIEW

HAZMAT transportation has been a very active area of interest for a large numbers of researchers since last few decades. Erkut *et al.* (2007) have presented an extensive bibliography of the researches on HAZMAT logistics classifying all of them into four different classes - risk assessment, routing, combined facility location and routing and network design. A similar attempt by List *et al.* (1991) resulted in a documentation of research studies since 1980. While a large number risk related researches are available in literatures, our study being focused on multi-objective routing and scheduling of HAZMAT transportation, we would limit our search to the literatures on HAZMAT routing and scheduling only.

A number of both single objective and multi-objective routing models have been presented in the past for HAZMAT routing. All these researches in general are related with two different variants of HAZMAT routing problems (Meng *et al.* 2005). A large number of researches relating to first category of HAZMAT routing are available in literatures that employ a single or multi-objective shortest path algorithms for finding non dominated paths minimizing risks or other attributes in transportation process for a given origin-destination pair. In contrast researches related to second category aiming for optimal routing and scheduling of a fleet of vehicles to distribute HAZMAT from a depot point to a fixed number of customers satisfying their demand and time window requirements are very limited in literatures. Our problem in this study is basically related to second category and here we present a list of available literatures for this category of HAZMAT vehicle routing and scheduling problem.

Cox and Turnquist (1986) were the first to consider scheduling problems of HAZMAT vehicles. They developed a dynamic algorithm considering the effects of presence of locally imposed curfews for identifying an efficient frontier of a bi-objective routing and scheduling problem of HAZMAT truck shipments in graph. However, the problem they considered is more related to first category of Hazmat routing problems. So far known, Tarantilis and Kiranoudis (2001) and Zografos and Androutsopoulos (2004) are the only two studies that explicitly considered the VRPTW prospective of HAZMAT transportation problem. Both of these studies used a bi-objective VRPTW model and ap-

plied heuristic techniques to find solutions for routing vehicles carrying HAZMAT. However, the later study ultimately used a single objective model obtained by transforming the proposed bi-objective model using weighing approach and solved it using insertion based heuristic for routing and used Dijkstra shortest path algorithm for route choice between customers. While the former maintained bi-objective model for routing using a List Based Threshold Accepting (LBTA) meta-heuristic algorithm, they used a risk based single objective approach for route selection using the same Dijkstra algorithm. The model and the heuristic algorithm developed in the later study were extended in Zografos and Androutsopoulos (2008) for developing a GIS based decision support system for integrated hazardous materials routing and emergency response decisions. So far known none of the studies till now are able to represent the multi-objective nature of these problems in both route choice and routing processes. The consideration of multi-objective nature for both route choice and routing processes calls for use of non-dominated paths in both steps of HAZMAT transportation. This emphasizes the requirement of proceeding both these processes in single step to obtain the truly non dominated pareto-optimal paths for routing vehicles carrying HAZMAT.

## 3. HAZMAT TRANSPORTATION PROBLEM

The core concept of HAZMAT transportation problem is similar to that of a Capacitated Vehicle Routing Problem with Time Window (C-VRPTW). C-VRPTW is a variant of VRPTW in which a fleet of delivery vehicles with uniform capacity must service fixed customers demand within pre-defined time windows for a single commodity from a single common depot. VRPTW are topics of a great deal of ongoing research in the operations research community. The details on the topic including its variants, formulations and solution techniques can be referred from Desrosiers *et al.* (1995) and Taniguchi *et al.* (2001). To facilitate prospective readers, attempts have been made during formulation of HAZMAT vehicle routing problem with time window presented in this study to use standard notations used by the later. However, at places where it becomes inconvenient due to introduction of new terms or possibility of creating confusion due to repetition of the notation, efforts have been made to provide more detail information.

**(1)Problem Definition**

Route choice and routing are the two major processes of VRPTW. While solving VRPTW in general, the two processes are completed in two separate steps. A single best path for moving vehicle from a customer to another is first determined in route choice process using some shortest path algorithms for customer-customer or customer-depot node pairs. These pre-defined paths are then used in routing process in which the order of customers to be visited for optimal case is determined. In reality, route choice considering multiple numbers of objectives results into several non dominated paths for each customer node pair including the depot node. Using a pre-defined single route for proceeding routing process would cancel the possibility of a number of non dominated paths to participate in routing process and this at times may hinder decision maker to reach the actual optimal solution. Keeping this in mind, we attempt to process route choice and routing as a single step process thus providing a chance to all non dominated paths of route choice to be part of optimal routing process.

Accordingly, HAZMAT vehicle routing problem here can be defined as a problem of determining a set of pareto-optimal routes for a fleet of vehicles carrying HAZMAT in order to serve a given set of customers satisfying following conditions:

a. Both route choice and routing must be based on multi-objective requirements described below in Section 3.2 and should be carried out as single step process.
b. All vehicles must start and end their routes at depot node.
c. Demand of each customer must be serviced within pre-defined time windows.
d. Waiting at points of early arrival is possible while late arrival is not allowed at all. The final set of routes are however expected to minimize waiting since minimizing total scheduling time that includes waiting at customer nodes is one of the requirement in routing process.

**(2) Objectives**

As previously mentioned, a key reason behind ongoing popularity of HAZMAT transportation study is the risk term associated with the transportation process. While minimizing risk is the primary objective in all HAZMAT transportation problems, HAZMAT shipments are subjected to another important objective of minimizing transportation cost from shipper's point of view. The objectives of

HAZMAT routing problem considered in this study are to minimize both cost and risk associated with transportation process with equal consideration without singling out any preference.

Like normal VRPTW, minimizing transportation cost calls for minimizing fixed cost and operating cost in transportation. Taking this into account, two objectives of minimizing total number of vehicles in use and minimizing total scheduling time including travel time, waiting and service time have been introduced; the first objective being related with former component of transportation cost and the second one being related with the later component.

Risk assessment has been an active area of research study since long and a number of qualitative and quantitative risk modeling are available in literatures. The present study adopts the widely used risk model referred as traditional risk model by Erkut and Ingolfsson (2004) for risk calculation. According to the model, risk associated with a path $R_{path}$ can be presented by equation (1).

$$R_{path} = \sum_{link \in path} [(HAZMAT\ accident\ probability)_{link} \ .\ (consequence\ of\ the\ accident)_{link}] \quad (1)$$

Though a number of consequences in relation to a HAZMAT accident are possible, safety for human life counts for top priority. Therefore in our study, the risk $R^{p(i)}_{n(i)n(i+1)}$ associated with transportation of HAZMAT from customer node $n(i)$ to $n(i+1)$ using path $p(i)$ which consists of numbers of links joining nodes $v(j)$ to $v(j+1)$ is modeled as presented in equation (2).

$$R^{p(i)}_{n(i),n(i+1)} = \sum_{v(j)v(j+1) \in p(i)} AR_{v(j)v(j+1)} . EP_{v(j)v(j+1)} \quad (2)$$

Here $AR_{v(j)v(j+1)}$ is the probability of HAZMAT accident for link connecting node $v(j)$ to $v(j+1)$ and $EP_{v(j)v(j+1)}$ is the exposure population for the same link that is the number of people lying within $\lambda$ distance from the link segment. The distance $\lambda$ is dependent upon the HAZMAT class being transported and has been defined with the assumption that all persons within this distance from the accident spot are subjected to the same consequence of life loss while the consequences outside this distance have been ignored. Detail on this threshold distance $\lambda$ is available in Batta and Chiu (1988).

**(3)Problem Formulation**

A multi-objective VRPTW model for HAZMAT transportation has been formulated based on details provided on Section 3.1 and Section 3.2. The objective function $Z$ which is a multi-objective three dimensional vector for minimizing total number of vehicle in use ($Z_1$), the total scheduling time ($Z_2$) and the total risk exposure associated with the transportation process ($Z_3$), here is dependent upon two decision variables *X and Y*. $X = \{x_l \mid l = 1, m\}$ is the traditional decision variable of order of visiting customer nodes for all vehicles and $Y = \{y_l \mid l = 1, m\}$ is a new decision variable of order of paths to be visited by all vehicles, introduced for proceeding route choice step. The detail formulation is presented here from Equation (3) to (6):

$$Min\ Z(X,Y) = [Z_1(X,Y) \quad Z_2(X,Y) \quad Z_3(X,Y)]^T \quad (3)$$

$$Here,\ Z_1(X,Y) = \sum_{l=1}^{m} \delta(x_l, y_l) \quad (4)$$

$$where \quad \delta(x_l, y_l) = \begin{cases} 1 & if\ vehicle\ l\ is\ used \\ 0 & otherwise \end{cases}$$

$$Z_2(X,Y) = \sum_{l=1}^{m} Z_{tl}(x_l, y_l)$$

$$= \sum_{l=1}^{m} \sum_{i=0}^{\hat{N}_l} (\overline{T}^{p(i)}_{n(i),n(i+1)} + t_{c,n(i+1)} + t_{w,n(i+1)}) \quad (5)$$

$$where \quad t_{w,n(i)} = \begin{cases} (e_{n(i)} - t_{l,n(i)}) & if\ t_{l,n(i)} < e_{n(i)} \\ 0 & otherwise \end{cases}$$

$$Z_3(X,Y) = \sum_{l=1}^{m} Z_{rl}(x_l, y_l)$$

$$= \sum_{l=1}^{m} \sum_{i=0}^{\hat{N}_l} R^{p(i)}_{n(i),n(i+1)} \quad (6)$$

The problem has been defined in a network of nodes and arcs $(V, A)$, where $V = \{v_1, v_2, v_3, ....., v_k\}$ is a finite set of vertices and $A = \{a_1, a_2, a_3, ....., a_k\}$, a finite set of arcs that includes all possible connections between vertices in *V*. The set of customer nodes to be visited which is

subset of $V$ can generally be represented by set $N = \{n_1, n_2, n_3, ....., n_{\hat{N}}\}$. Specifically for this study, $x_l$ which is the order of customers to be visited by vehicle $l$ is represented as $x_l = \{n(i) \mid i = 0, \hat{N}_l\}$. $n(i)$ here is the customer to be visited by vehicle $l$, $m$ being the maximum number of vehicles in use. $\hat{N}_l$ is the total number of customers to be visited by vehicle $l$, $\hat{N}_l + 1$ being zero. Since each vehicle $l$ in use has to start from depot node, it is considered as a temporary customer node $n(0)$ for all vehicles. $[e_{n(i)}, f_{n(i)}]$ is the time window representing earliest and latest possible service time at node $n(i)$. The decision variable $y_l = \{p(i) \mid i = 0, \hat{N}_l\}$ is the order of paths to be used by vehicle $l$ while visiting its customer nodes where path $p(i) \in P$, $P$ being set of all non-dominated paths between customer-customer and customer-depot node pairs. $p(0)$ is the path to be followed from depot node to customer node $n(1)$ and $p(N_l)$ is the path to be used while visiting from customer node $n(N_l)$ back to depot node.

Equation (5) shows detail calculation of total scheduling time where $Z_{tl}$ is total scheduling time associated with vehicle $l$ for hard time window condition and is dependent on the average travel time value from $n(i)$ to $n(i+1)$ that is $\overline{T}^{p(i)}_{n(i)n(i+1)}$ which ultimately relies both on the order of customers and the path used while moving from one customer node to another. Terms $t_{c,n(i)}$, $t_{l,n(i)}$ are the service time and service start time respectively of vehicle $l$ at node $n(i)$. In calculation of risk objective presented in Equation (6), $Z_{rl}$ is the risk value associated with vehicle $l$ which is dependent on $R^{p(i)}_{n(i),n(i+1)}$ that is the risk value associated with each path followed while moving from customer $n(i)$ to $n(i+1)$ of that vehicle, the detail calculation of it being presented in Section (2).

The whole model is subjected to time window, demand-capacity and customer number constraints as in traditional VRPTW. Early time window constraints have been considered during total scheduling time calculation in Equation (5). Equation (7) is the late time window constraint for the model. Mathematical expressions for demand-capacity and customer number constraints are given below in Equation (8) and (9) respectively. $D_{n(i)}$, $W_l(x_l)$ and $W_{c,l}$ here are demand at node $n(i)$, total weight carried by the vehicle $l$ and capacity of vehicle $l$ in use respectively. It should be noted that the two constraints hold true only during routing process and selection of nodes within path $p(i)$ is not subjected to these constraints.

$$t_{l,n(i)} \leq f_{n(i)} \quad (7)$$

$$\sum_{n(i) \in x_l} D(n(i)) = W_l(x_l) \leq W_{c,l} \quad (8)$$

$$\sum_{l=1}^{m} \hat{N}_l = \hat{N} \quad (9)$$

## 4. ANT COLONY SYSTEM FOR HAZMAT ROUTING

VRPTW are related to a class of NP-hard (Non-deterministic Polynomial) combinatorial optimization problems and heuristic or meta-heuristic algorithms must be used to solve problems of larger instances and for timely computation of the solution. A large number of different meta-heuristic approaches have been proposed in recent years for solving different variants of VRPTW. A comprehensive survey on the available approaches can be referred in Toth and Vigo (2002). In this study, we present a new Ant Colony System (ACS) based meta-heuristic solution technique in order to solve the HAZMAT transportation problem presented in Section 3.

Ant Colony Optimization is a meta-heuristic approach inspired by the foraging behavior of real ant colonies. Complete explanation on this meta-heuristic is available in Dorigo and Stutzle (2004). Ant System (AS), a variant of Ant Colony Optimization was first used by Bullnheimer *et al.* (1998) for solving vehicle routing problems. Number of researches focused on improvement and use of the approach for solving a range of problems. Gambardella *et al.* (1999) presented a multi-objective ant colony system MACS-VRPTW algorithm for solving multi-objective vehicle routing problems with time window constraints. The concept was based on Ant Colony System (ACS) and two ant colonies were used, each ant colony being specialized for a particular objective. The algorithm presented however provided precedence for the first objective over the second one. The proposed ACS for this study is adopted version of the MOACS-VRPTW approach presented by Baran *et al.* (2003). The reason behind this particular selection is that the mentioned study

has been found to be able to deal with multiple numbers of objectives using a single ant colony system and each objective has been given equal consideration. Moreover, the approach provides a good convergence to all the pareto front surface which is one of the desirability of this study for coming out with number of solutions to decision making process, the alternative choices of which can lead to equitable distribution of the risk value.

Figure 1 shows the flowchart of proposed ACS for HAZMAT VRPTW. The proposed ACS mainly differs from the MOACS-VRPTW in terms of solution construction process and the local search method. Details on these processes have been provided in Section (1) and Section (2) respectively. As shown in the flowchart, the first step of initialization of trail pheromone value and setting of pareto-optimal set *S* is based on a routing solution obtained using nearest neighborhood (nn) heuristic. The solution obtained itself represents the first member of pareto-optimal set *S*. Equation (10) is the expression for evaluating the initial trail pheromone value $\tau_0$ which is reciprocal of the total scheduling time, total risk value and the average number of nodes (|*N*|) that includes total number of customers and the average number of vehicles for nearest neighborhood solution. The initial pheromone values for subsequent generations are calculated based on average objective values for pareto-optimal set of the previous iteration similar as in MOACS-VRPTW.

$$\tau_0 = \frac{1}{(|N|)_{nn} * (Z_2)_{nn} * (Z_3)_{nn}} \qquad (10)$$

**(1)Solution Construction**

Unlike in MOACS-VRPTW, each of *m* numbers of ants in the proposed ACS employ Labeling Algorithm before proceeding to customer node insertion to find out all non dominated paths from the present node of ant's stay to all feasible customer nodes. Customer node $n(j)$ among feasible set of customer nodes $N'$ for ant at $n(i)$ is then inserted in routing order corresponding to path $p(i)$. This path $p(i)$ is decided based on pseudo-random proportional rule and is added to form an order of routing paths. Choice of path $p(i)$ and thereby customer node $n(j)$ is made based on expression in Equation (11) if $q \le q_0$. The choice otherwise is made randomly based on a probability value presented in Equation (12). $q$ is a random number such that $0 \le q \le 1$ and $q_0$ is a parameter that defines relative importance of exploration and exploitation.

$$\max_{p(i)\in P'} \left(\tau_{p(i)} \cdot [\eta_{p(i)}]^{\theta^\eta \beta} \cdot [\nu_{p(i)}]^{\theta^\nu \mu}\right) \qquad (11)$$

$$\Pr(p(i)) = \frac{\tau_{p(i)} \cdot [\eta_{p(i)}]^{\theta^\eta \beta} \cdot [\nu_{p(i)}]^{\theta^\nu \mu}}{\sum_{p(i)\in P'} \tau_{p(i)} \cdot [\eta_{p(i)}]^{\theta^\eta \beta} \cdot [\nu_{p(i)}]^{\theta^\nu \mu}} \qquad (12)$$

Here $\tau_{p(i)}$, $\eta_{p(i)}$, $\nu_{p(i)}$ are the pheromone value and heuristic values relating to the scheduling time and risk value of path $p(i)$ respectively. $\beta$ and $\mu$ are the parameters that define relative influence of the time and risk objectives. $\theta^\eta$ and $\theta^\nu$ are the ant specific weights/preferences for normalizing time and risk objectives respectively. $P' \in P$ is a set of all non-dominated paths from customer node $n(i)$ to each customer nodes in set $N'$. $\Pr(p(i))$ is the probability of path $p(i)$ to be chosen. Calculation of time related heuristic value is similar to the one for delivery time in MOACS-VRPTW that depends on the waiting time and time window at customer node. The risk related heuristic value depends on the risk value associated with path $p(i)$ that connects customer node $n(i)$ to $n(j)$ and is evaluated as given in equation (13).

$$\nu_{p(i)} = \frac{1}{R^{p(i)}_{n(i),n(j)}} \qquad (13)$$

Basic knowledge on labeling algorithm can be referred from Ahuja *et al.* (1993). The labeling algorithm used in this study is based on the template labeling algorithm proposed by Irnish and Villenuve (2003) for shortest path problem with resource constraint. The concept is to make use of information that the labels created at vertex carry to determine all non-dominated paths in the presence of multiple resource constraints. The label at a vertex in general carries information about a path leading to it by maintaining a linkage with other label at the predecessor vertex. The label in resource constrained shortest path problems are made capable of describing state of the resources at the given node as well. Since labeling algorithm here is basically used for proceeding route choice step, travel time values and the risk values associated with each link of movement along the path constitute the resource constraints of the problem.

**(2)Local Search**

The proposed ACS for HAZMAT VRPTW implements insertion local search procedure to improve quality of the feasible solutions. However being a

time consuming process, we apply local search to only those solutions belonging to pareto-optimal set *S* which is updated at each of the iterations unlike in traditional ACS where local search is carried out to each solution. Update of pareto-optimal set *S* for each iteration is carried out based on a dominance rule in which all the solutions that are dominated in terms of all objectives are discarded. For example, if $\psi_1$ and $\psi_2$ are two solutions belonging to pareto-optimal set *S* with objective values of $Z_1(1), Z_2(1), Z_3(1)$ and $Z_1(2), Z_2(2), Z_3(2)$ respectively, $\psi_1$ is said to be dominated by $\psi_2$ and discarded from the set *S* if Equation (14) to (16) are satisfied except when $Z_1(1) = Z_1(2)\ \&\ Z_2(1) = Z_2(2)\ \&\ Z_3(1) = Z_3(2)$.

$$Z_1(1) \leq Z_1(2) \quad (14)$$
$$Z_2(1) \leq Z_2(2) \quad (15)$$
$$Z_3(1) \leq Z_3(2) \quad (16)$$

Hoos and Stutzle (2004) provide a wide view on local search procedures including their developments, analysis and application. The insertion local search used in this study utilizes insertion neighborhoods of a typical solution. All the nodes of a previously obtained feasible solution are given chances to be inserted to the same vehicle route or to the route of other vehicles without violating feasibility requirements and the newly obtained solutions are checked for improved objective values.

**(4)Pheromone Update**

The present ACS solution algorithm for HAZMAT VRPTW utilizes local and global update of pheromone procedures similar to the one used in MOACS-VRPTW method. Each path used by ant for constructing solution is subjected to local pheromone update as given in Equation (17) where $\rho$ is the evaporation coefficient which powers exploration process by evaporating trail pheromone values for these used paths.

$$\tau_{p(i)}^{new} = (1-\rho)\tau_{p(i)}^{old} + \rho\tau_0 \quad (17)$$

In each iteration, pareto-optimal set *S* is updated after local search process and to each path belonging to pareto-optimal solution $\psi \in S$, global update of pheromone is carried out based on Equation (18) below.

$$\tau_{p(i)}^{new} = (1-\rho)\tau_{p(i)}^{old} + \rho/[(Z_2)_\psi . (Z_3)_\psi] \quad where p(i) \in \psi \quad (18)$$

## 5. NUMERICAL ANALYSIS

Before proceeding to implementation of proposed model and the developed solution algorithm for a particular case of HAZMAT routing, it is essential to compare their performance for a standard case of routing based on earlier available results. However computational tests on HAZMAT transportation problem become unattainable due to lack of availability of standard datasets for the case of HAZMAT transportation. Therefore attempts have been made here to test their performance in standard VRPTW datasets making appropriate modifications for instance removing risk terms, replacing total scheduling time to distance objective etc. The details of the problems that have been considered for testing and the results obtained have been presented in Section 5.1 and Section 5.2 respectively.

**(1)Test Instances**

Solomon (1987) provides a platform for testing efforts in VRPTW by presenting variety of problems for normal vehicle routing problems with time windows. Computational experiments have been conducted for Solomon's benchmark instances for 100 customer problems of R, C and RC classes. All instances provided have a central depot, capacity constraint and time window constraints. While the customers in C type of problems are clustered, those in R type of problems are randomly distributed and those in RC type are of mixed type where customers are both clustered and randomly distributed. For this computational test, random selection of a problem from each problem type has been made.

**(2) Results and Discussions**

In order to adjust proposed model for solving the problem instances, appropriate modifications have been made in the proposed algorithm by removing risk term and changing the second objective of reducing total scheduling time to reducing overall distance. Thus the problem here reduces to bi-objective minimization of number of vehicles and the total distance traveled by these vehicles. The proposed algorithm has been coded using Borland C and is executed in Core 2 Duo desktop PC of 2.67GHz with 2GB RAM. The parameters used are $m=10,\ \theta^\eta = 1, \beta = 1, \rho = 0.1, q_0 = 0.9$ which are

same as in MOACS-VRPTW and MACS-VRPTW. Each problem has been run for 10000 number of iterations and the best solution obtained among 20 test trials has been presented.

The results from proposed ACS presented here are the average objective values of the final pareto-optimal set *S*. It has been found that some test instances for example C101 for 100 customer case are so organized that its optimal solutions is obtainable just by using insertion heuristic along with the initial solution created using nearest neighborhood search. However, the results obtained using this approach for other problems is very poor even for other problems in C type. To check improvement caught with implementation of ACS technique along with nearest neighborhood initialization and insertion heuristic, the results obtained based on only nearest neighborhood and insertion heuristic approach has been also included in the table. It has been observed that the results obtained with the use of proposed ACS technique with nearest neighborhood based solution initialization and insertion based local search are comparatively better than the one without ant approach in terms of both reduction in number of vehicles and distance traveled. A comparison of the results with the best known solutions by exact approach (Kohl *et al.* 1999 referred as KDMSS in C107 problem and Cook and Rich (1999) referred as CR in R110 and RC102 problems in the table) has been also presented. It should be clear to readers that the exact approach referred here is a single objective approach with the main objective of minimizing total distance traveled and its results has been used just as a reference for comparison. It has been observed that the results obtained from the proposed algorithm are quiet satisfactory showing almost negligible deviation from best solution from exact approaches for C type of problems while maintaining an acceptable limit of deviation of around 7.5% for R and RC type of problems. Moreover, the computation time for each case is within 500 seconds which is practical for case of 100 number of customers problems.

For a clearer concept on performance of the approach along various generations, a plot on distance improvement along various generations for the case with number of vehicles being 10 has been created as shown in Figure 1 for C107 problem. Distance improvements with more number of vehicles have also been observed in some generations. However to maintain consistency of the graph, those results have been excluded for this particular plotting. As is clearly observable from the plot, the effect of the approach is found to be quite fast for the first 100 generations, however gradual improvements in the results has been observed even up to 3000$^{th}$ generation. These gradual improvements in later generation can in fact be due to typical features of ACS of exploration in addition to exploitation of the previously obtained best solutions.

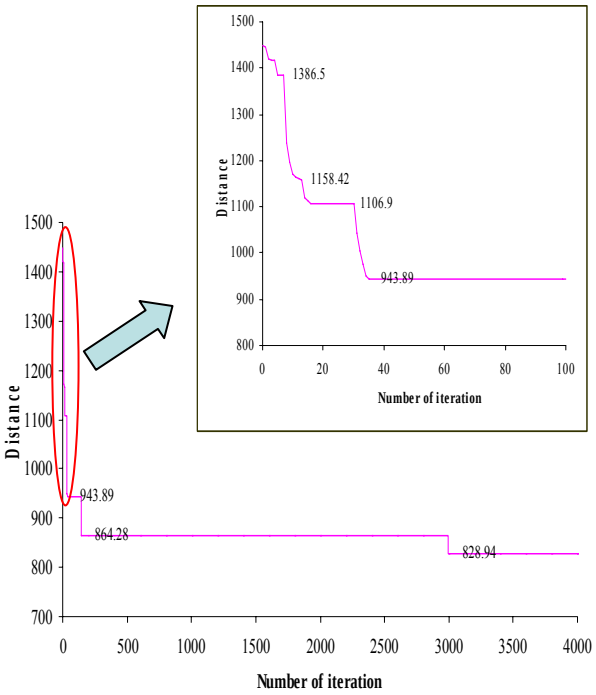


**Figure 1 Distance trend for C107**

## 6. CONCLUSION AND FUTURE WORK

Proper routing being an important aspect for safe and economic logistics of HAZMAT, the main focus in our study is to build an appropriate HAZMAT VRPTW model and develop a suitable algorithm to solve this model which in fact in literatures of HAZMAT has received very less attention. A model illustrating need of multi-objective consideration both for route choice and routing phase of HAZMAT transportation has been presented. A new ACS based meta-heuristic algorithm has been proposed in order to solve this model for optimal case and the performed numerical experiment shows its competency in all type of normal VRPTW problems besides maintaining a good convergence to pareto-front which is one of the main requirements for HAZMAT application. Moreover, the performance for C type of problem has been found to be almost comparable with the best known solution by exact approach.

Normal VRPTW problems though are very different from HAZMAT problems, both of these problems belong to combinatorial optimization problems. With regard to the excellent performance of the algorithm for VRPTW problems in general, similar results can be expected for HAZMAT case too. Besides, the pareto-optimal set consideration in the proposed approach provides numbers of alternative non dominated routing choices which will be more prominent in case of HAZMAT transportation with addition of risk objective. Alternative use of such paths in decision making process assists in maintaining risk equity. Based on its performance on test instances, the next aim of our study is to test its applicability for some test problems of HAZMAT routing. Nevertheless, testing different types of local search methods to make the algorithm more efficient, applying it to some real world problems and including its dynamic nature are other important aspects of the study.

## REFERENCES


Ahuja, R., Magnanti, T. and Orlin, J. (1993) Network Flows: Theory, Algorithms, and Applications, Prentice Hall, New Jersey.

Baran, B. and Schaerer, M. (2003) A multiobjective ant colony system for vehicle routing problem with time windows, Proceeding of 21st IASTED International Conference on Applied Informatics, Austria, 97-102.

Batta, R. and Chiu, S.S. (1988) Optimal obnoxious paths on a network: Transportation of hazardous materials, Operations Research, Vol. 36, No. 1, 84-92.

Bullnheimer, B., Hartl, R.F. and Strauss, C. (1998) Applying the ant system to the vehicle routing problem. In Voss, S., Martello, S., Osman, I.H. and Roucairol, C. (eds.), Meta-Heuristics: Advances and Trends in Local Search Paradigms for Optimization, 109-120. Kluwer, Boston, MA.

Cox, R. and Turnquist, M. (1986) Scheduling truck shipments of hazardous materials in the presence of curfews, Transportation Research Record, No. 1063, 21-26.

Desrosiers, J., Dumas, Y., Solomon, M.M., and Sournis, E. (1995) Time constrained routing and scheduling. In Ball, M.O., Magnanti, T.L., Monma, C.L. and Nemhauser, G.L. (eds.), Network Routing: Handbooks in Operations Research and Management Science, Vol. 8, 35-139. North-Holland, Amsterdam.

Dorigo M. and Stutzle T. (2004) Ant Colony Optimization. MIT Press, Cambridge, MA, USA.

Erkut, E. and Ingolfsson, A. (2004) Transport risk models for hazardous materials: Revisited, Operation Research Letters, Vol. 33, No. 1, 81-89.

Erkut, E., Tjandra, S.A. and Verter, V. (2007) Hazardous material transportation. In Laporte, G. and Barnhart, C. (eds.), Handbooks in Operations Research and Management Science, 539-621. North-Holland.

Erkut, E. and Verter, V. (1995) Hazardous materials logistics. In: Drezner, Z. (eds.), Facility Location: A Survey of Application and Methods, 467-506. Springer-Verlag, New York.

Gambardella L.M., Taillard E. and Agazzi G. (1999) MACS-VRPTW: A multiple ant colony system for vehicle routing problems with time windows. In Corne, D., Dorigo, M. and Glover, F. (eds.), New Ideas in Optimization, 63-79. McGraw-Hill, London.

Hoos, H. and Stutzle T. (2004) Stochastic Local Search: Foundations and Applications. Morgan Kaufmann, San Francisco.

Irnich, S., and Villeneuve, D. (2003) The shortest path problem with k-Cycle elimination ($k \geq 3$): Improving a branch and price algorithm for the VRPTW, Technical Report G-2003-55, GERAD.

Kohl, N., Desrosiers, J., Madsen, O.B.G., Solomon, M.M. and Soumis, F. (1999) 2-Path cuts for the vehicle routing problem with time windows, Transportation Science, Vol. 33, 101-116.

List, G. F., Mirchandani, P. B., Turnquist, M. A., and Zografos, K. G. (1991) Modeling and analysis for hazardous materials transportation: risk analysis, routing/scheduling and facility location, Transportation Science, Vol. 25, 100-114.

Meng, Q., Lee, D., and Cheu, R. L. (2005) Multiobjective vehicle routing and scheduling problem with time window constraints in hazardous material transportation, Journal of Transportation Engineering, Vol. 131, No. 9, 699-707.

Solomon, M.M. (1987) Algorithms for vehicle routing and scheduling problems with time window constraints, Operation Research, Vol. 35, No. 2, 254-265.

Taniguchi, E., Thompson, R.G, Yamada, T. and Duin, R.V. (2001) City Logistics: Network Modeling and Intelligent Transport Systems, Pergamon, Oxford.

Tarantilis, C.D. and Kiranoudis, C.T. (2001) Using the vehicle routing problem for the transportation of hazardous materials, Operational Research - An International Journal, Vol. 1, No.1, 67-78.

Toth P. and Vigo D. (2002) The Vehicle Routing Problem: Siam Monographs on Discrete Mathematics and Applications. SIAM, Philadelphia.

Zografos, K.G., and Androutsopoulos, K.N. (2008) A decision support system for integrated hazardous materials routing and emergency response decisions, Transportation Research Part C, No. 16, 684-703.

Zografos, K.G., and Androutsopoulos, K.N. (2004) A heuristic algorithm for solving hazardous distribution problems, European Journal of Operational Research. Vol. 152, No. 2, 507-519.

GCOE AIT-KU JOINT SYMPOSIUM ON HUMAN SECURITY ENGINEERING

Bangkok, Thailand, November 25-26, 2010

# Driver Typology and Speeding Behavior in Speed Enforcement Zone

Sumethee SONTIKUL[1]

Kunnawee KANITPONG[2]

School of Engineering and Technology, Transportation Engineering Program, Asian Institute of Technology
(P.O. Box 4, Klong Luang, Phathumthani 12120 , Thailand )
E-mail: sumethee@ait.ac.th
kanitpon@ait.ac.th

This paper attempts to gain insights into drivers' speeding behavior upon passing speed enforcement zone. A total of 630 drivers in Thailand were interviewed using a self-reported questionnaire, and they were classified into four types of the Corbett's driver typology: conformers (i.e., those who usually comply with speed limits), deterred drivers (i.e., those who reduce speed all along speed enforcement zone), manipulator (i.e., those who slow down and accelerate after passing speed enforcement zone), and defiers (i.e., those who usually exceed legal speed limit irrespective of the presence of speed enforcement zone. The statistical data tests showed that, manipulators and defiers tend to be those who received a speeding penalty during the past year. It was also found that they are likely to be wealthy and experienced drivers, but have personal attitude against the speed enforcement policy.

***Key Words :*** *speed behavior, speed enforcement, driver typology*

## 1. INTRODUCTION

In Thailand, speeding contributed to 15-23% of all accidents on all types of roads as reported by the police during 2001 to 2009. Despite the potential limitations in identifying the probably causes of accidents by police officers, the magnitude of crash and fatality risks associated with speeding could also be practically reflected by the fact that speed limits are very often violated on a large scale in Thailand. It is therefore necessary to enforce driving within the speed limits by using speed enforcement.The traffic law enforcement as an integral part of the country's speed management policy, physical policing has been the most common method used for speed enforcement on highways located outside cities.

In Thailand, speed offenders along the highway are normally detected by a radar gun within the speed enforcement zone. The speed enforcement zone can be identified by posting speed enforcement warning signs for 1-2 km before entering the enforcement zone. If over speeding is detected by radar gun, the speed offenders will be immediately stopped by the highway police at the police check point which is located about 0.5-1 km. away. The offenders in most cases are then issued the speeding ticket to pay fine as punishment at the check point.

Although previous studies have shown some deterrent effects of speed enforcement at particular locations with the presence of police enforcing (*1, 2*), the general deterrence of speeding on the public appears to have been minimal, and speeding still remains to be very common in Thailand. In 1995, traffic speed surveys in Bangkok and seven other major provinces in all regions of the country were conducted and it was found that the proportion of vehicles exceeding the speed limit ranged from 37% to 54% (*3*). Recently, several survey studies have observed speed

limit violations on major arterial highways outside of cities. Typically, 40% to 70% of the car drivers exceed the speed limit of 90 kph (*4*)

## 2. DRIVER TYPOLOGY AND SPEEDING BEHAVIOR OVERVIEW

Exceeding the speed limit is sometimes considered by the drivers as a minor traffic violation when compared to other traffic crimes (*5*).Some drivers do not see exceeding speed limit as dangerous because they feel that they can safely control their driving (*6*). A study by Corbett (1995) (*5*) and Lex (1997) (*7*) show evidences that some drivers reduce speed only when they are in the speed enforcement area, for example; the presence of speed camera, and then accelerate over speed limit after passing the speed camera.

Different in speeding behavior can be explained by (*8*) with the fact that the drivers' attitude towards exceeding speed limit and the perception of drivers related to the consequences of such speeding are key determinants of intention to speeding behavior. Socio-economic characteristics, driver characteristics and trip preferences are found to be significant factors affecting speeding behavior (*9*).

Previous studies shows the effectiveness of speed camera to control speeding drivers, and the result of this intervention can save over 100 lives and prevent more than 4,000 injuries caused by collisions a year. According to Corbett ( 1995) ( *5*), the drivers' behavioral response to the presence of speed camera can be categorized into four groups, depending on drivers' speed and their driving behavior. Four groups are defined to classify driver's speeding behavior as conformers, deterred, manipulators, and defiers.

In Thailand, the speed camera has not been applied for the speed enforcement program. Instead, the presence of speed enforcement zone by setting police check points along the highway has been used to apprehend drivers who violate the traffic law particularly speeding. In fact, the experience of implementing the police check point has been found to be unsuccessful in reducing the speeding accidents in Thailand. It might be because of the difference in driving behavior in response to the police check points. Thus, most reaction of speeding behavior could be explained based on four types of driver typology as described by (*5*).The definitions of each typology are modified to be applied with the speed enforcement program used in this study which can be described in below.

**(1) Definition of driver typology (*5*)**

The drivers who always comply with speed limit or drive closer to or lower than speed limit were defined as " conformers". Therefore, the speed enforcement zone will make no difference with drivers' speed behavior in this group.

The drivers who reduce speed all along the speed enforcement zone to avoid being stopped by the police so the presence of speed enforcement zone can change behavioral response of drivers to speeding were indentified as " deterred drivers "

The drivers who reduce speed suddenly in the speed enforcement zone and then accelerate after passing the speed enforcement zone were recognized as " manipulators "

The drivers who drive over the speed limit irrespective of the presence of speed enforcement zone were classified as " defiers "

## 3. OBJECTIVES

This study is to evaluate the drivers' speeding behavior in speed enforcement zone and to classify driver typology in responding to the speed enforcement currently used in Thailand. The influencing factors such as driver, trip,and vehicle characteristics are evaluated to determine their effect on the driver typology.

## 4. DATA COLLECTION

Self-reported questionnaire survey was conducted to interview drivers' speed behavior when passing the speed enforcement zone . A total of 630 drivers were interviewed at the superstores and gas stations on Highway No.1 in Wang Noi District, Ayutthaya and Highway No.32 in Bang Pa-in District, Ayutthaya with conditions as follows;

1. The respondents were selected based on the drivers' awareness on the existence of speed enforcement in the study area to ensure that the respondents are aware of the speed enforcement zone.
2. Only the drivers of four-wheel vehicles were interviewed

The data was collected in three months period from November 2008 to January 2009.

## 5. QUESTIONNAIRE DESIGN

The self-reported questionnaire was designed to classify the driver typology according to Corbett (*5*). The drivers were asked to describe their speeding behavior when passing the speed enforcement zone. The questionnaire consists of two sections of the questions. The questions in the first section were designed to classify driver typology into four groups:

conformers, deterred drivers, manipulators and defiers. Table 1 shows the questions designed in the first section. It can be seen that the classification is based on the drivers' behavioral responses to speed enforcement which is the use of radar gun and police speed check point on the road. Firstly, the drivers were asked for their normal driving speed on the same type of roads to cross-check the accuracy of driver typology classification.

From the questions shown in Table 1, drivers who choose answer No.1 (either a or b) and normally use the speed at 100 kph or lower, are classified as "Conformers".

| What speed do you **normally** use on the same type of road? …… kph |
|---|
| Driver Typology Classification |
| **How do you react when passing speed enforcement zone on the road?** (*Choose No.1 or No.2*) |
| ☐ 1) I keep the speed closer to 100 kph or lower in the speed enforcement zone. |
| *(Please choose either a) or b) in which you intend to react after passing speed enforcement zone)* |
| ☐ a) I normally drive using speed lower than 100 kph in both speed enforcement zone and other areas. |
| ☐ b) I reduce the speed when passing speed enforcement zone because of the awareness of speed police check point, and then I maintain the speed at 100 kph and lower. The presence of speed enforcement zone changes my speeding behavior. |
| ☐ 2) I believe that I could manage speed over the limit (100 kph) in the speed enforcement zone. *(Please choose either a) or b) in which you intend to react after passing speed enforcement zone)* |
| ☐ c) I maintain the speed at higher than 100 kph, although there is the speed enforcement zone. |
| ☐ d) I reduce the speed when I approach the speed enforcement zone, and then increase the speed again after passing the speed enforcement zone. I don't want to get the speeding ticket. |
| ☐ e) I don't care with the speed enforcement; therefore, I don't drop my speed in the speed enforcement zone. |

**TABLE 1** Questions to Classify Driver Typology

The second section of the questionnaire includes the questions related to the drivers' characteristics, trip characteristics, and vehicle use characteristics.

## 6. CLASSIFICATION DRIVER TYPOLOGY

From a total of 617 respondents, 237 drivers or 38.4% were classified as conformers, 88 drivers or 14.3% were deterred, 136 drivers or 22% were manipulators, and 156 drivers or 25.3% were defiers. Based on the results, it was found that the highest proportional group of the drivers is conformers, followed by defiers, manipulators, and deterred. Surprisingly, only 14.3% of drivers were classified as deterred in this study, which means that the speed enforcement zone does not change speeding behavior of most drivers.

It is evident from Table 2 that defiers are the drivers who are highly educated and have higher monthly income when comparing to other driver The drivers who choose answer No.1, and then answer b, and only those who normally use the speed higher than 100 kph are classified as "Deterred". The drivers who choose answer No.2, and then answer d, are classified as "Manipulators". Lastly, the drivers who choose answer No.2, and then either c or e are defined as "Defiers". It is noted that 13 drivers gave contradict responses of the normal speed they used and their response to speed enforcement zone; therefore, these data were removed from the study.

The second section of the questionnaire includes the questions related to the drivers' characteristics, trip characteristics, and vehicle use characteristics.

## 6. CLASSIFICATION DRIVER TYPOLOGY

From a total of 617 respondents, 237 drivers or 38.4% were classified as conformers, 88 drivers or 14.3% were deterred, 136 drivers or 22% were manipulators, and 156 drivers or 25.3% were defiers. Based on the results, it was found that the highest proportional group of the drivers is conformers, followed by defiers, manipulators, and deterred. Surprisingly, only 14.3% of drivers were classified as deterred in this study, which means that the speed enforcement zone does not change speeding behavior of most drivers.

It is evident from Table 2 that defiers are the drivers who are highly educated and have higher monthly income when comparing to other driver The drivers who choose answer No.1, and then answer b, and only those who normally use the speed higher than 100 kph are classified as "Deterred". The drivers who choose answer No.2, and then answer d, are classified as "Manipulators". Lastly, the drivers who choose answer No.2, and then either c or e are defined as "Defiers". It is noted that 13 drivers gave contradict responses of the normal speed they used and their response to speed enforcement zone; therefore, these data were removed from the study.

The second section of the questionnaire includes the questions related to the drivers' characteristics, trip characteristics, and vehicle use characteristics.

## 6. CLASSIFICATION DRIVER TYPOLOGY

From a total of 617 respondents, 237 drivers or 38.4% were classified as conformers, 88 drivers or 14.3% were deterred, 136 drivers or 22% were manipulators, and 156 drivers or 25.3% were defiers. Based on the results, it was found that the highest proportional group of the drivers is conformers, followed by defiers, manipulators, and deterred. Surprisingly, only 14.3% of drivers were classified as deterred in this study, which means that the speed typology. Most defiers were found to have life insurance. Similarly, the characteristics of manipulators are also highly educated, high income drivers, and most of them also have life insurance. The finding is somewhat expected as high income drivers are more likely to be a group of people who can afford to buy life insurance. As the income is higher, the value of time tends to be higher as well, and this could be the reason of speeding in defiers group. It is also possible for the high income drivers to be more willing to pay for speeding fine, thus they react as defiers when passing the speed enforcement zone. From the results, defiers are less likely to be aware of the speed limit as shown that only 10% know the legal speed limit of 90 kph. It seems that manipula-

tors travel longer distance in a year when comparing to other driver typology . The passenger car drivers are more likely to be manipulators and defiers.

To evaluate the significant factors affecting the typology of drivers' responses to speed enforcement zone, the multinomial logistic regression (MNL)

**TABLE 2** Characteristics of Drivers in each Typology

| Total Sample (N=617) | Driver Typology | | | |
|---|---|---|---|---|
| | **Conformers** | **Deterred** | **Manipulators** | **Defiers** |
| | **237** | **88** | **136** | **156** |
| **Driver Characteristics** | | | | |
| **Gender** (%) | | | | |
| Male | 78.1 | 84.1 | 88.2 | 82.1 |
| Female | 22.9 | 15.9 | 11.8 | 17.9 |
| **Age** (years) | | | | |
| Mean | 39.5 | 38.2 | 37.7 | 39.4 |
| **Monthly Income** (Thai baht) | | | | |
| Mean | 28,405 ($860) | 22,318 ($676) | 29,207 ($885) | 34,247 ($1,038) |
| **Education** (%) | | | | |
| Bachelor Degree or higher | 49.8 | 55.6 | 62.5 | 62.9 |
| Lower than bachelor Degree | 50.2 | 44.4 | 37.5 | 37.1 |
| **Status** (%) | | | | |
| Single | 34.2 | 43.2 | 39.7 | 37.8 |
| Married | 65.8 | 56.8 | 60.3 | 62.2 |
| **Life Insurance** (%) | | | | |
| With life insurance | 60.3 | 59.1 | 69.9 | 69.9 |
| Without life insurance | 39.7 | 40.9 | 30.1 | 30.1 |
| **Driving Experience** (years) | | | | |
| Mean | 15.0 | 13.5 | 15.0 | 16.3 |
| **Awareness of Speed Limit** (%) | | | | |
| Aware of speed limit of 90 kph | 16.0 | 29.5 | 22.1 | 10.9 |
| Unaware of speed limit of 90 kph | 84.0 | 70.5 | 77.9 | 89.1 |
| **Experience of Receiving Speeding Ticket over a Year** (%) | | | | |
| One time and higher | 9.7 | 19.3 | 30.1 | 25.6 |
| Never | 90.3 | 81.7 | 69.9 | 74.4 |
| **Accident Experience in Recent Two Years** (%) | | | | |
| One time and higher | 25.3 | 21.6 | 26.5 | 24.4 |
| Never | 74.7 | 78.4 | 73.5 | 75.6 |
| **Accident Experience of Family Members** (%) | | | | |
| Ever | 22.4 | 27.3 | 28.7 | 25.6 |
| Never | 77.6 | 72.7 | 71.3 | 74.4 |
| **Trip Characteristics** | | | | |
| **Avg. Total Travel Distance** (km/yr) | | | | |
| Mean | 37,222 | 36,727 | 48,927 | 37,321 |
| **Trip Frequency** (%) | | | | |
| Daily or Weekly | 50.2 | 50.0 | 43.4 | 41.7 |
| Monthly and others | 49.8 | 50.0 | 56.6 | 58.3 |
| **Trip Purpose** (%) | | | | |
| Business Trip | 66.7 | 59.1 | 61.8 | 67.9 |
| Leisure and others | 33.3 | 40.9 | 38.2 | 32.1 |
| **Vehicle Characteristics** | | | | |
| **Vehicle Ages** (years) | | | | |
| Mean | 7.2 | 6.4 | 6.2 | 6.6 |
| **Vehicle Types** (%) | | | | |
| Passenger Car | 55.3 | 52.3 | 64.7 | 64.1 |
| Pickup or Van | 44.7 | 47.7 | 35.3 | 35.9 |
| **Vehicle Status** (%) | | | | |
| Owner | 89.5 | 84.1 | 85.3 | 91.0 |
| Others | 10.5 | 15.9 | 14.7 | 9.0 |

## 7. ANALYSIS

technique has been applied in this study. This model

can be used when the analysis includes more than two dependent variables which one dependent variable is designated as the reference category.

Before the analysis, the test of multicollinearity was conducted and the result indicates that there is no correlation among all variables (i.e. all pair-wise correlation coefficients are lower than 0.6). Table 4 present estimation results from the multinomial logistic regression models. The relative magnitude of estimated coefficients indicates the extent to which driver, trip, and vehicle use characteristics affect the typology of drivers' responses to speed enforcement zone.

**TABLE 3** Definitions of Independent Variables

| Variables | Definition | Avg. |
|---|---|---|
| Gender | 1= male; 0 otherwise | 0.82 |
| Age | Continuous variable | 38.9 |
| Income (baht) | Continuous variable | 29,191 |
| Status | 1= married; 0 otherwise | 0.62 |
| Life Insurance | 1 = with life insurance; 0 otherwise | 0.65 |
| Education | 1= bachelor degree or higher; 0 otherwise | 0.57 |
| Driving Experience (yr) | Continuous variable | 15 |
| Awareness of Speed Limit | 1= unawareness; 0 otherwise | 0.82 |
| Speeding Ticket Experience in the Past Year | 1 = at least one times; 0 = otherwise | 0.20 |
| Accident Experience in Recent Two Years | 1 = at least one accident; 0 = otherwise | 0.25 |
| Accident Experience of Family Members | 1 = at least one accident; 0 otherwise | 0.25 |
| Avg.Total Travel Distances (km/yr) | Continuous variable | 39,756 |
| Trip Frequency | 1 = daily or weekly; 0 otherwise | 0.47 |
| Trip Purpose | 1 = business trip; 0 otherwise | 0.65 |
| Age of Vehicle (yr) | Continuous variable | 6.7 |
| Type of Vehicle | 1 = passenger car; 0 otherwise | 0.59 |
| Ownership of Vehicle | 1 = ownership; 0 otherwise | 0.88 |

## 8. RESULTS OF ANALYSIS

In Table 4, the deterred was designated as the reference category and was compared to other groups of driver typology. The results of analysis were reported in three groups including the comparison between conformers, manipulators, and defiers with deterred a driver which is the base category.

For group 1 (conformers), the coefficients of independent variables "gender, income, awareness of speed limit, and experience of receiving speeding ticket in the past year" are statistically significant at 1-10%. It was found that female drivers are more likely to be conformers rather than deterred. Drivers with high monthly income are more likely to be conformers rather than deterred. There is the likelihood of conformers to be unaware of the speed limit used on the highways as opposed to deterred. It is possible that conformers always drive using the speed close to or under the speed limit, thus they are not aware of the speed limit on this highway. Unsurprisingly, conformers tend to have less experience in receiving the speed ticket over a year when comparing to deterred because conformers normally use the speed closer to the limit, thus have less opportunity to be stopped in the speed enforcement zone.

The comparison between manipulators and deterred in group 2 (manipulators) shows the significant level of independent variables "income, driving experience, trip frequency, awareness of speed limit, experience of receiving speeding ticket in the past year, and vehicle type" at 1-10%. It is evident that drivers who have higher monthly income and those who have more driving experience are more likely to be manipulators rather than deterred. The results can be also found that manipulators were more likely to travel less often on the highway with speed enforcement zone when comparing to deterred. As manipulators are less likely to aware of the speed limit, their reaction to the speed enforcement zone is perhaps the reason of receiving more speeding ticket in a year than deterred. Furthermore, the drivers who drive passenger car tend to be manipulators rather than deterred drivers.

Group 3 (defiers) which is the analysis comparing between defiers and deterred shows that income, driving experience, trip frequency, trip purpose, awareness of speed limit, and experience of receiving speeding ticket in the past year are significant factors at 1-10% level. Similar results to group 2 (manipulators) were found in this analysis as shown that high income and experienced drivers are more likely to be defiers rather than deterred. Drivers who travel less, unaware of speed limit, and have experiences of receiving speed ticket tend to be defiers. It is also interesting to see that driver whose trip purpose is business trip tend to drive over speed limit irrespective of the presence of speed enforcement zone.

According to table 4, defiers group was deter-

mined as the reference category and was compared to conformers and manipulators. The analysis shows that in the comparison between conformers and defiers (Group 4), the independent variables "driving experience, trip frequency, awareness of speed limit, and experience of receiving speeding ticket in the past year" are significant at levels of 1-10%. The coefficients of these variables indicate that drivers with less driving experience, travel more often, unaware of speed limit, no experience of receiving speed ticket tend to be conformers rather than defiers. When the manipulators were compared with defiers(Group 5), average travel distance, trip purpose, and awareness of speed limit were found to be significant.

The last comparison was made between conformers and manipulators (Group 6) as shown in Table4. In this group, the manipulators group was designated as the reference category.

Note: *, **, *** indicate significant levels at 10%, 5%, and 1%, respectively.

It is found that gender, average travel distance, trip frequency, and experience of receiving speeding ticket in the past year are significant at a level of 1-10%. The results can be interpreted that female drivers, those who travel longer distance in a year, those who travel more often, and those who have less experience in receiving speed ticket are more likely

**TABLE 4** Coefficients of Multinomial Logistic Regression Model for the Typology of Drivers' Responses to Speed Enforcement Zone

| Variables | Conformers Group 1 | | Manipulators Group 2 | | Defier Group 3 | | Conformers Group 4 | | Manipulators Group 5 | | Conformers Group 6 | |
|---|---|---|---|---|---|---|---|---|---|---|---|---|
| | Coeff. | | Coeff. | | Coeff. | | Coeff. | | Coeff. | | Coeff. | |
| Gender | -0.608 | * | 0.260 | | -0.304 | | -0.304 | | 0.564 | | -0.868 | ** |
| Age | -0.025 | | -0.038 | | -0.029 | | 0.004 | | -0.009 | | 0.013 | |
| Income | 0.000 | ** | 0.000 | * | 0.000 | ** | 0.000 | | 0.000 | | 0.000 | |
| Status | 0.289 | | 0.246 | | 0.100 | | 0.188 | | 0.145 | | 0.043 | |
| Life Insurance | -0.001 | | 0.326 | | 0.191 | | -0.192 | | 0.135 | | -0.327 | |
| Education | -0.492 | | -0.075 | | -0.118 | | -0.374 | | 0.043 | | -0.417 | |
| Driving Experience | 0.024 | | 0.042 | * | 0.054 | ** | -0.030 | * | -0.013 | | -0.018 | |
| Avg.Total Travel Distances (km/yr) | 0.000 | | 0.000 | | 0.000 | | 0.000 | | 0.000 | * | 0.000 | ** |
| Trip Frequency | -0.190 | | -0.665 | ** | -0.835 | *** | 0.645 | *** | 0.169 | | 0.476 | * |
| Trip Purpose | 0.481 | | 0.171 | | 0.758 | ** | -0.278 | | -0.588 | ** | 0.310 | |
| Awareness of Speed Limit | 0.900 | *** | 0.542 | * | 1.519 | *** | -0.618 | * | -0.977 | *** | 0.359 | |
| Speeding Ticket Experience in the Past Year | -0.636 | * | 0.706 | ** | 0.615 | * | -1.250 | *** | 0.092 | | -1.342 | *** |
| Accident Experience in Recent Two Years | 0.264 | | 0.197 | | 0.147 | | 0.117 | | 0.050 | | 0.067 | |
| Accident Experience of Family Members | -0.338 | | -0.233 | | -0.296 | | -0.043 | | 0.063 | | -0.106 | |
| Age of Vehicle | 0.026 | | 0.002 | | 0.010 | | 0.017 | | -0.008 | | 0.024 | |
| Type of Vehicle | 0.173 | | 0.580 | * | 0.440 | | -0.267 | | 0.140 | | -0.407 | |
| Ownership of Vehicle | 0.251 | | -0.173 | | 0.263 | | -0.012 | | -0.436 | | 0.424 | |
| Constant | 0.631 | | -0.365 | | -1.257 | | 1.889 | | 0.892 | | 0.997 | |
| Reference Category | Deterred Drivers | | | | | | Defiers | | | | Manipulators | |
| *Summary of Statistics:* | | | | | | | | | | | | |
| No. of observation | 617 | | | | | | 617 | | | | 617 | |
| Log likelihood | -759.33865 | | | | | | -759.33865 | | | | -759.33865 | |

to be conformers rather than manipulators

## 9. SUMMARY

In this study, the drivers' speed attitude under speed enforcement program was conducted to evaluated driving speed while passing the police check point zone base on difference of demographic background, trip characteristics and the characteristics of the vehicle had an influential correlation for the four types of driver typology. The main findings from the study are summarized as follows:

The wealthy drivers, those with a high driving experience, were most likely to violate the speed limits on rural roads and to oppose the speed law enforcement using the police check points. However, the penalty structure could possibly not control the behavior of the defiers who tend to have committed at least one or repeated offenses, compared to conformers and deterred. Therefore, the concerned agency should determine countermeasures such as high imposition for offenders, and more severe penalties for the repeated violators.

The manipulators and defiers are likely to have lack of perception of the relationship between the higher speed and increased severity of road accidents (i.e., collision and the likes). Both believed that they could well manage driving speeds of above 100 kph on rural roads. Moreover, the defiers had a negative attitude against the police check point policy. Therefore, the campaigns encouraged them to assess the impact of serious crashes due to excessive speeds so that they might show a positive attitude regarding the speed enforcement objective and adjust their speeding behavior.

The respondents' statements were used in classifying the groups of driver typology. It is highly possible that some respondents gave wrong answers about their general speed and driving behavior on the speed enforcement routes. For example, some drivers who exceed the speed limits might give information which underestimate their general speed on those routes Also slower drivers overestimated their general speed Therefore, the incorrect response obviously affected their erroneous speed behavior upon passing a police check point.

## REFERENCES


1) Kulleab, S., Jirawak, S., and Kaewkanya, K., *Model development for traffic injury prevention by speed control on Highway No. 2 in Khon Kaen province*, Report No.147-2006-11, Khon Kaen Trauma and Critical Care Center, Khon Kaen Hospital, Thailand, 2006
2) Ponboon, S., Kanitpong, K., Kachathong, S., Boontob, N., Aniwattakulchai, P., and Jiwattanakulpaisarn, P., *Effectiveness of speed enforcement with police intervention on a national highway in Thailand*, Working paper, Thailand Accident Research Center (TARC), 2009
3) Chongsuvivatwong, V., Ritsmitchai, S., Suriyawongpaisal, P., Chariyalertsak, S., Kosuwan, W., Punyaratabandhu, P., and Sutiwipakorn, W., *High prevalence of drink-driving in Thailand*, Drug and Alcohol Review, Vol. 18, pp. 293-298, 1999
4) Jiwattanakulpaisarn, P., Kanitpong, K., and Suriyawongpaisal, P., *On the Effectiveness of Speed Enforcement in Thailand: Current Issues and need for Changes and new Approaches*, the Transport and Communication Bulletin for Asia and the Pacific, No.79, 2009, pp. 31-46.
5) Corbett, C., *Road Traffic Offending and the Introduction of Speed Cameras in England: the First Self- Report Survey*, Accident Analysis and Prevention, Vol. 27, No. 3, pp. 345-354, 1995
6) Corbett, C., Simon, F., and O'Connell, M., The Deterrence of High Speed Driving: A Criminological Perspective, Contract Report No.296, Transport Research Laboratory, 1998.
7) Lex, Driving for Safety, Lex Report on Motoring, Lex Service Plc. London, 1997
8) Kimura, I., The relationship between drivers' attitudes to speeding and their speeding behavior in hypothetical situations, Hiroshima Forum Psychol. 15, 51-60, 1993
9) Fildes, B.N., Rumbold, G., and Leening, A., *Speed Behavior and Drivers' Attitude to Speeding*," Report No.16, Monash University Accident Research Centre, Victoria, Australia, 1991
10) Corbett, C., 2000, *A Typology of drivers' responses to speed cameras: implications for speed limit enforcement and road safety*, Psychol. Crime Law *6, 305-330*, 2000.

2010 AIT-KU JOINT SYMPOSIUM ON HUMAN SECURITY ENGINEERING

Bangkok, Thailand, November 25-26, 2010

# Conflict Analysis for Traffic Flow Dominated by Motorcycles Based on Video Image Data

Yasuhiro SHIOMI[1], Teruaki HANAMORI[2] and Nobuhiro UNO[3]

[1]Assistant Professor, Dept. of Urban Management, Kyoto University
(C2-434, Kyoto University Katsura Campus, Nishikyo-ku, Kyoto 615-8540, Japan)
E-mail:shiomi@trans.kuciv.kyoto-u.ac.jp
[2]Master Course Student, Dept. of Urban Management, Kyoto University
(C2-438, Kyoto University Katsura Campus, Nishikyo-ku, Kyoto 615-8540, Japan)
E-mail:hanamori@trans.kuciv.kyoto-u.ac.jp
[3]Associate Professor, Graduate School of Management, Kyoto University
(C2-436, Kyoto University Katsura Campus, Nishikyo-ku, Kyoto 615-8540, Japan)
E-mail:uno@trans.kuciv.kyoto-u.ac.jp

This study proposes a traffic conflict index for motorcycle-dominant traffic flow and establishes a method for quantitatively evaluating traffic safety in a mixed traffic flow. In South-east Asian cities, motorcycles have comprised substantial portions of road traffic. Because the traffic management and operation systems are not well developed, both traffic efficiency and safety are severely deficient. Thus, this study proposes a method for evaluating traffic safety as a first step towards establishing traffic management and operation systems for a mixed traffic flow. Due to the difficulty in observing actual traffic accidents, this study focuses on traffic conflict situations, which are regarded as underlying factors in traffic accidents. It is confirmed that the proposed index can appropriately present the risk situation in a traffic flow dominated by motorcycles.

***Key Words :*** *mixed traffic flow, motorcycles, conflict analysis, traffic accident, video image data*

## 1. INTRODUCTION

In South-east Asian countries such as Vietnam, Cambodia and Thailand, motorcycles are mainly used as a mode of urban transportation. With the recent growth in the respective economies of these countries, the proportion of passenger cars has also increased, resulting in traffic flow situations with a mix of motorcycles and passenger cars. Because such mixed traffic situations are relatively unique to South-east Asian cities, the traffic management and operation systems targeting the traffic flow comprising passenger cars are no longer suitable; as a result, both traffic efficiency and safety are severely deficient. For example, in terms of the safety issue, the number of fatalities in Vietnam (population: approximately 86 million) is 11,500 in the year 2009, whereas in Japan (population: approximately 127 million), the number of fatalities is about 4,914 in the year 2009. The number of fatalities per capita in Vietnam is 3.5 times higher than that in Japan, and more than 80% of fatalities are related to motorcycles [1)]. It suggests that the traffic safety issue in developing countries, where there is a mix of motorcycles and passenger cars in the traffic flow, is critical to human security. To improve this situation, some policies and measures have been proposed and implemented. For example, in Hsu[2)] and Hsu et al. [3)], a time and space segregation policy of motorcycles from passenger cars was proposed. On the basis of field surveys, the authors reported that the segregation policy could improve the traffic situation in

terms of both efficiency and safety. However, each policy has both merits and demerits. To achieve the optimal traffic flow situation, both merits and demerits should be quantified, and then the criteria—whether each motorcycle-oriented policy is effective or not—must be determined in relation to the proportion of motorcycles to passenger cars, roadway configuration and other factors.

Therefore, as a first step to finding the criteria for installing motorcycle-oriented policies, this study establishes a method for quantitatively evaluating traffic safety. Due to the difficulty in observing actual traffic accidents, this study focused on traffic conflicts, which are regarded as the underlying factors in traffic accidents. Then a traffic conflict index suitable for mixed traffic flow is established. After obtaining vehicle trajectory data through video images taken at a signalized intersection in Hanoi City, the proposed index is applied to the trajectory data and validated.

## 2. CONCEPT OF CONFLICT ANALYSIS

Traffic accidents are considered rare events. It is difficult to directly observe the details of vehicle movements in traffic accidents. Therefore, it is necessary to understand the underlying mechanism in traffic accidents. Generally, the mechanism for traffic accidents comprises the following three factors: hazards, risks and accidents; these are defined by the hierarchical structure shown in **Fig. 1** (Wakabayashi et al.[4]). This means that a traffic conflict situation occurs from some dangerous situation with a certain probability; it also indicates that traffic accidents occur from traffic conflict situations with a certain probability. In other words, the risks can be defined as potential situations for the occurrence traffic accidents. Traffic safety can be evaluated by quantifying the risks. With respect to the traffic conflict pertaining to passenger cars traffic flow, some indices have been proposed. Hayward[5] has proposed a TTC (time to collision) indicator. Allen et al.[6] have proposed a PET indicator: PET is the 'post-encroachment time', the time taken by a vehicle to arrive at a place previously occupied by another vehicle. Uno et al.[7] have established the PICUD (possibility index for collision with urgent deceleration) indicator, which evaluates the possibility that two consecutive vehicles might collide, assuming that the leading vehicle applies its emergency brake. These indices, however, were targeted for traffic flow composed of passenger cars and assumed that each vehicle moves on a deter mined lane.


**Fig. 1** Hierarchical structure of three factors in traffic accidents

The manoeuvres specific to motorcycles in avoiding collisions, such as an urgent change in moving direction, can never be considered. Thus, this study proposed a conflict index considering moving manoeuvres with a high degree of freedom, which is relatively unique to motorcycles.

## 3. PROPOSITION OF CONFLICT INDEX FOR MIXED TRAFFIC FLOW

### (1) Definition of Proposed Conflict Index

Given the maximum acceleration and deceleration rate and the maximum angle for direction change within which a vehicle can safely maintain its balance and moving stability, an area can be defined where a vehicle potentially reaches after a certain time, $\Delta t$. The area is named 'potential area', which can be determined for every vehicle. If a potential area of a vehicle is unique, i.e. if there is no area overlapping with potential areas of other vehicles, the vehicle has no risk of collision with other vehicles surrounding it. On the other hand, if a potential area of a vehicle is not unique, i.e. if there is some area overlapping with potential areas of other vehicles, as shown in **Fig. 2**, a vehicle has the possibility of collision after $\Delta t$ seconds, though the vehicle does not always collide with other vehicles. The subset area within a potential area unique to a vehicle is named 'potentially safe area'. It can be naturally concluded that the smaller the proportion of the potentially safe area to the whole potential area, the higher is the risk of colliding with other vehicles. Then, the conflict index is defined as the 'proportion of potentially safe area (PPSA)' to the whole potential area. It is concretely expressed by Eq. (1).

$$PPSA_i(t) = 1 - \frac{\bigcup_{\forall j (j \neq i)} \left\{ PA_i(t) \cap PA_j(t) \right\}}{PA_i(t)}, \qquad (1)$$

where

$PPSA_i(t)$: Proportion of potentially safe area of vehicle $i$ at time $t$.

$PA_i(t)$: A set of the area including vehicle $i$'s potential area at time $t$.

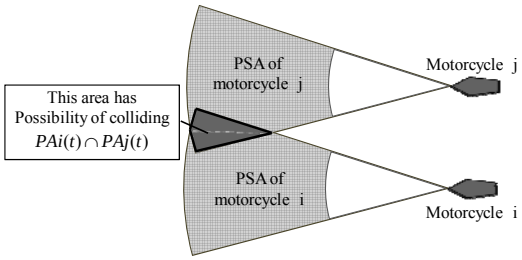


**Fig. 2** Image of potential safety areas

The higher the PPSA index of a vehicle, the smaller is the risk of collision; in other words, the safer is the vehicle. Hereafter, potential areas of motorcycles and passenger cars are explained.

### (2) Definition of Potential Area for Motorcycle

Assuming that a motorcycle determines its moving direction and acceleration/deceleration rate every $\Delta t$ second, the potential area for a motorcycle can be expressed as a gap between two fan-shaped areas as shown in **Fig. 3**. If a motorcycle takes the maximal acceleration, it reaches the left side of the potential area arc, whereas for maximal deceleration, it reaches the right side. Thus, $L_{\max}^{MC}$ and $L_{\min}^{MC}$ are expressed as Eqs. (2) and (3), where it is assumed that a motorcycle never goes back upstream during $\Delta t$ seconds.

$$L_{\max}^{MC} = v_t \cdot \Delta t + \frac{1}{2} \cdot a_{\max}^{MC} \cdot (\Delta t)^2 , \qquad (2)$$

$$L_{\min}^{MC} = \begin{cases} \dfrac{v_t^{\,2}}{2 \cdot d_{\max}^{MC}} & if \ v_t < \dfrac{1}{2} \cdot d_{\max}^{MC} \cdot \Delta t \\ v_t \cdot \Delta t - \dfrac{1}{2} \cdot d_{\max}^{MC} \cdot (\Delta t)^2 & otherwise \end{cases} , \qquad (3)$$

where $v_t$ indicates a speed of a subject motorcycle at time $t$, $\alpha_{\max}^{MC}$ indicates the maximum acceleration of motorcycles and $d_{\max}^{MC}$ indicates the maximum deceleration of motorcycles. In **Fig. 3**, $\alpha$ represents the maximum angle a motorcycle can take during $\Delta t$ seconds when it changes its moving direction without any risks of skidding. It is difficult to accurately determine the angle because motorcycle behaviour is affected by numerous factors such as the type of motorcycle, weight of riders and road surface condition. Therefore, the angle $\alpha$ is approximately defined as follows:

For changing the moving direction, a motorcycle leans its body to the side rather than turning the handle. When a motorcycle turns, it balances the angle of bank with the centrifugal force. The dynamical balance of a motorcycle while turning can be illustrated through **Fig. 4**. To avoid skidding, dotted and solid lines should maintain balance. Focussing particularly on the vertical direction with respect to the motorcycles, the balance equation can be written as Eq. (4).

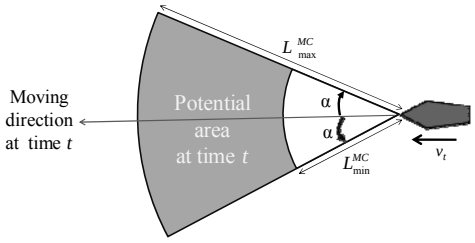


**Fig. 3** Potential area for motorcycle

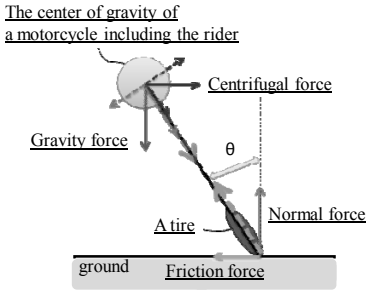


**Fig. 4** Dynamical balance of motorcycle in turning

$$m \cdot g \cdot \sin\theta - \frac{m \cdot v_t^{\,2}}{r} \cdot \cos\theta = 0 , \qquad (4)$$

where

$m$: mass of motorcycle including the rider,
$g$: gravity acceleration,
$\theta$: angle of bank,
$r$: turning radius.

Thus, when a motorcycle is turning at a speed $v_t$, the turning radius $r$ can be defined as given in Eq.(5).

$$r = \frac{v_t^{\,2}}{g} \cdot \tan\theta . \qquad (5)$$

Then, $\alpha$ is approximately defined as the interior angle between the moving direction vector at time $t$ and the vector from the origin to the destination reached after $\Delta t$ seconds by turning during the $\Delta t$ seconds, maintaining the speed at time $t$ constant and with the maximum angle of bank $\theta_{\max}$. **Fig. 5** also gives the definition of $\alpha$. Note that, strictly speaking, a motorcycle moves on the broken line. Given $\omega$, the line length can be expressed in two ways, as shown in Eq. (6).

$$\text{The broken line length} \equiv v_t \cdot \Delta t = r_{\min} \cdot \omega, \qquad (6)$$

where $r_{\min}$ indicates the minimum turning radius if a motorcycle takes the maximum angle of bank while turning, and $\omega$ indicates the rotation angle of the turning circle. Note that $r_{\min}$ is not smaller than a certain value $r_{MIN}$, which is specific to each type of motorcycles. Namely, $r_{\min}$ is written as

$$r_{\min} = \max\left( \frac{v_t^{\,2}}{g} \cdot \tan\theta_{\max} , r_{MIN} \right) . \qquad (7)$$

Due to the geometric theory, the relationship between $\alpha$ and $\omega$ can be written as Eq. (8).

$$\alpha = \frac{\omega}{2} . \qquad (8)$$

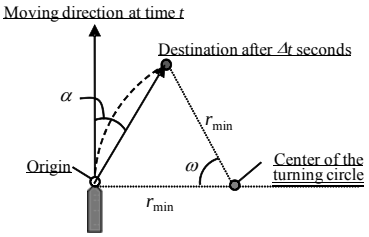


**Fig. 5** Definition of maximum turning angle $\alpha$

Then, according to the speed $v_t$ and the maximum angle of bank $\theta_{\max}$, $\alpha$ can be expressed as

$$\alpha = \min\left( \frac{g \cdot \tan\theta_{\max}}{2 \cdot v_t} \cdot \Delta t,\ \frac{v_t}{2 \cdot r_{MIN}} \cdot \Delta t \right). \qquad (9)$$

Although $\alpha$ is based on some strong assumptions, it is rational that Eq. (9) can express the relationship that if $v_t$ reduces, $\theta_{max}$ increases and when $\Delta t$ increases, $\alpha$ also increases.

### (3) Definition of Potential Area for Passenger Cars

For passenger cars, the length and width of vehicles should be considered. Supposing that a passenger car will not change the moving direction during $\Delta t$ seconds, the potential area for a passenger car can be illustrated as a rectangular area shown in **Fig. 6**. In the figure, the vehicle A indicates the position after $\Delta t$ seconds in case the vehicle accelerates at the maximum acceleration rate $a_{\max}^{PC}$, whereas the vehicle B indicates the position after $\Delta t$ seconds in case the vehicle decelerates at the maximum deceleration rate $d_{\max}^{PC}$. The potential area of the vehicle at time $t$ is defined as the rectangular area, i.e. $\left(L_{\max}^{PC} - L_{\min}^{PC}\right)$ long and $W$ wide. $L_{\max}^{PC}$ and $L_{\min}^{PC}$ are written as Eq. (10) and (11). In Eq. (11), it is assumed that a passenger never goes back upstream.

$$L_{\max}^{PC} = v_t \cdot \Delta t + \frac{1}{2} \cdot a_{\max}^{PC} \cdot (\Delta t)^2 + L, \qquad (10)$$

$$L_{\min}^{PC} = \begin{cases} \dfrac{{v_t}^2}{2 \cdot d_{\max}^{PC}} & \text{if } v_t < \dfrac{1}{2} \cdot d_{\max}^{PC} \cdot \Delta t \\ v_t \cdot \Delta t - \dfrac{1}{2} \cdot d_{\max}^{PC} \cdot (\Delta t)^2 & \text{otherwise} \end{cases}, \qquad (11)$$

where $L$ is the vehicle length.

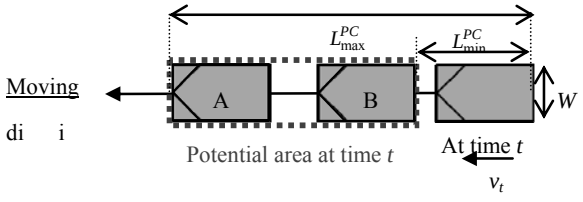


**Fig. 6** Potential area for a passenger car

## 4. DATA COLLECTION

### (1) Data Collection Site

To validate the proposed conflict index PPSA, traffic surveys were conducted using a DV camera at an intersection in Hanoi City. The intersection was selected to satisfy the following requirements: 1) passenger car and motorcycle volumes should be sufficiently large to observe mutually mixed traffic flow; 2) a DV camera can be set from a high position; and 3) the position should be near obstacles in traffic flow, such as bus stops and parking lots. As a result, the western approach of Kim-MA St. - Nguyen Chi Thanh St. intersection was selected. By setting a DV camera at the JICA office, located on the 16th floor of the building at the north-west of the intersection, traffic flow was observed on 29 Sept., 2009 from 0900 to 1100 h. Among all the observed signal cycles, three cycles, during which there were not many large vehicles present, were selected for the analysis.

### (2) Data Extraction

The vehicle trajectory data is extracted from the DV image data. According to Khan et al.[7], every screen coordinate pair $u$ and $v$ can be written as Eq. (12) in relation to the roadway coordinate pair $x$ and $y$.

$$u = \frac{a_3 x + a_4 y + a_5}{a_1 x + a_2 y + 1},\ v = \frac{a_6 x + a_7 y + a_8}{a_1 x + a_2 y + 1}, \qquad (12)$$

where $a_i$ ($i$ = 1,2,3,4,5,6,7,8) are unknown parameters.

To match the coordinates between the screen and roadway, all parameters will be estimated by solving Eq. (12). This process requires at least four base points. In this case, 11 points were set for estimating the parameters. As shown in **Fig. 7**, $x$ axis was set as the flow direction and $y$ axis as the vertical direction against the flow direction. Next, the coordinates of all vehicles on a screen are obtained by clicking the point of the front tyre on grounding for motorcycles and the left-front and the left-back edge for passenger cars every 0.25 s using a manual trajectory acquisition system developed for this analysis. As a result, a total of 314 motorcycles and 70 passenger car (in cluding large vehicles) trajectories were extracted. The extracted trajectories contain some errors caused

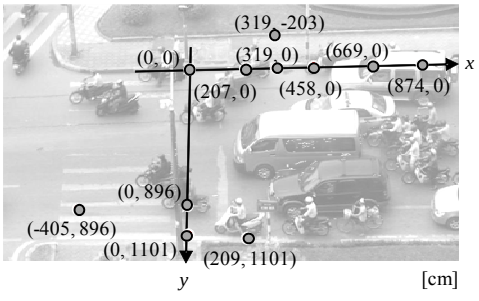


**Fig. 7** Roadway coordinate and base points

by the manual clicking and the coordinate transition from the screen to the real world. As a result, some trajectories exhibit relatively unrealistic movements. Thus, to correct these errors, a smoothing spline algorithm was applied.

## 5. NUMERICAL EXAMPLE OF PPSA INDEX

### (1) Calculation Algorithm

It is difficult to accurately calculate the proposed PPSA index because the potentially safe areas of each vehicle are complicatedly overlapped. In this study, an algorithm for calculating PPSA index is established. The observation field, where $x_{min} < x < x_{max}$ and $y_{min} < y < y_{max}$, is expressed as a grid with the intervals $\Delta x$ and $\Delta y$. Then, suppose a matrix $\mathbf{X}_{it}$ with $n$ rows and $m$ columns, where $n$ and $m$ stand for the number of grids in the $x$ and $y$ directions. Hence, each matrix element stands for the information of each grid point, and the matrix $\mathbf{X}_{it} = \left[x_{pq}^{it}\right] \in \Re^{n \times m}$ is defined for each vehicle $i$ at time $t$ as

$$x_{pq}^{it} = \begin{cases} 1 \left(if\ \left((p-1)\Delta x + x_{min}, (q-1)\Delta y + y_{min}\right) \in PA_i(t)\right) \\ 0 \left(otherwise\right) \end{cases}. \tag{13}$$

Here, a matrix $\mathbf{Y}_{it}$ is defined as

$$\mathbf{Y}_{it} = \left[y_{pq}^{it}\right] = \coprod_{\forall j,\, j \neq i} \mathbf{X}_{jt} \in \Re^{n \times m}, \tag{14}$$

where $\coprod$ indicates logical addition for all vehicles on the observation field at time $t$, except for vehicle $i$. The element of $\mathbf{Y}_{it}$, $y_{pq}^{it}$, stands for the dummy, which is 1 if the grid point $(p, q)$ is included in potential areas of all other vehicles, and 0 otherwise. Hence, the overlapping area of potential areas of all other vehicles with vehicle $i$'s potential area, $\mathbf{Z}_{it}$, can be written as

$$\mathbf{Z}_{it} = \left[z_{pq}^{it}\right] = \mathbf{Y}_{it} \wedge \mathbf{X}_{it} \in \Re^{n \times m}, \tag{15}$$

where $\wedge$ means logical multiplication.

Thus, PPSA index value of vehicle $i$ at time $t$, $PPSA_i(t)$, can be approximately calculated by Eq. (16)

$$PPSA_i(t) \approx 1 - \left( \sum_{p=1}^{n} \sum_{q=1}^{m} z_{pq}^{it} \Big/ \sum_{p=1}^{n} \sum_{q=1}^{m} x_{pq}^{it} \right). \tag{16}$$

### (2) Parameter Settings

To calculate the PPSA, each parameter is set as follows: first, the scanning interval $\Delta t$ is set as 0.75 [sec] and the maximum angle of bank is set as 15 degrees. According to Sekine[8], the maximum acceleration and deceleration rate of motorcycles are set as $g/3$ [m/s$^2$] and $g/2$ [m/s$^2$], and those of passenger cars are set as $g/5$ [m/s$^2$] and $g/2$ [m/s$^2$] by referring to 'Explanation and Operation of Road Structure Regulations[9]. Moreover, the minimum turning radius $r_{MIN}$ is equal to 2.0 m by referring to specifications for Honda motorcycles. The subject field is defined as the rectangle area where −200 cm < $x$ < 800 cm and 0 cm < $y$ < 1,000 cm, and both $\Delta x$ and $\Delta y$ are set as 5 cm.

### (3) Calculation Results

At first, to grasp the distribution of each vehicle's potential area, time-series change of the distribution is focused upon. **Fig. 8** summarizes the potential area within the observation area at (a) 2.5 s; (b) 5 s; and (c) 10 s after the signal turns green. The rectangular areas show potential areas of passenger cars and triangular and trapezoidal areas show those of motorcycles. It can be seen that in **Fig. 8** (a) potential areas of motorcycles are narrow because they move at slow speed, just after the signal turns green. With the passing of time, potential areas of motorcycles get wider, whereas motorcycles just behind passenger cars tend to have narrower potential areas. Because the speed of these motorcycles is restricted by passenger cars, it can be concluded that this result is relatively rational.

Second, a motorcycle which takes risky manoeuver is focused upon. The target situation is as follows: A motorcycle was moving behind a passenger car, but at around 13 sec, the passenger car suddenly stopped; then, the motorcycle urgently changed its moving direction. **Fig. 9** shows the time-series change in the motorcycle's PPSA value and **Fig. 10** the video images at each moment. It can be seen that just after sudden stop of a passenger car, PPSA value dramatically decreases and gets to about 0.1. After avoiding safely, PPSA value recovers to be high. From theses analysis, it can be concluded that the proposed conflict index can indicate the risky behavior and conflict situation appropriately.

## 6. CONCLLUSION

In this study, which focuses on traffic flow mainly comprising motorcycles, a safety evaluation method was proposed by building a traffic conflict index. This index considers the difference in the characteristics of passenger car traffic flow and mixed traffic flow. For example: 1) motorcycles are not restricted by driving lanes for passenger cars; 2) motorcycles

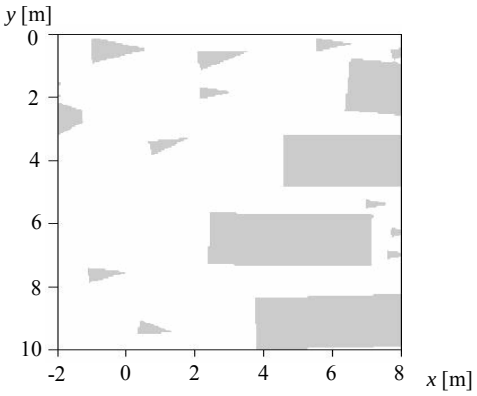


(a) 2.5 seconds after turning green

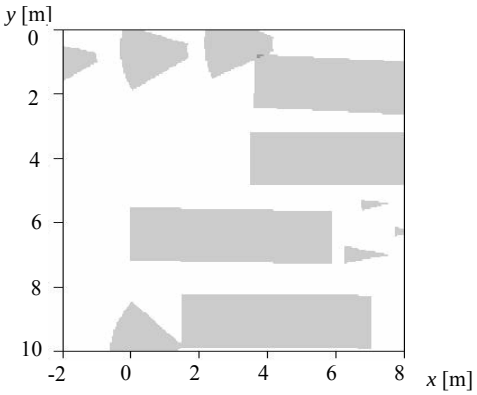


(b) 5 seconds after turning green

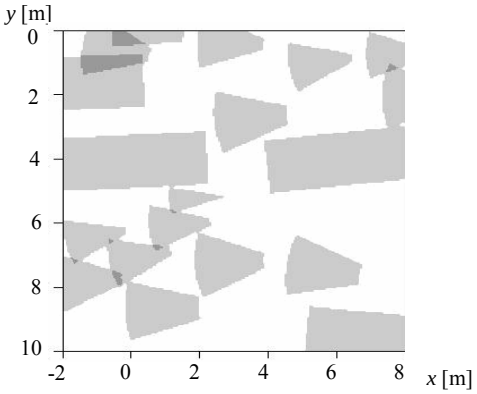


(c) 10 seconds after turning green

**Fig. 8** Time-series change of potential area distribution

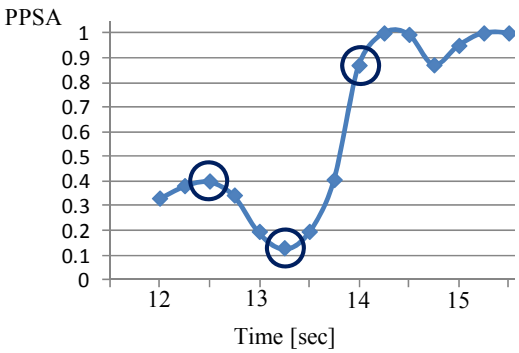


**Fig. 9** Time-series change in PPSA

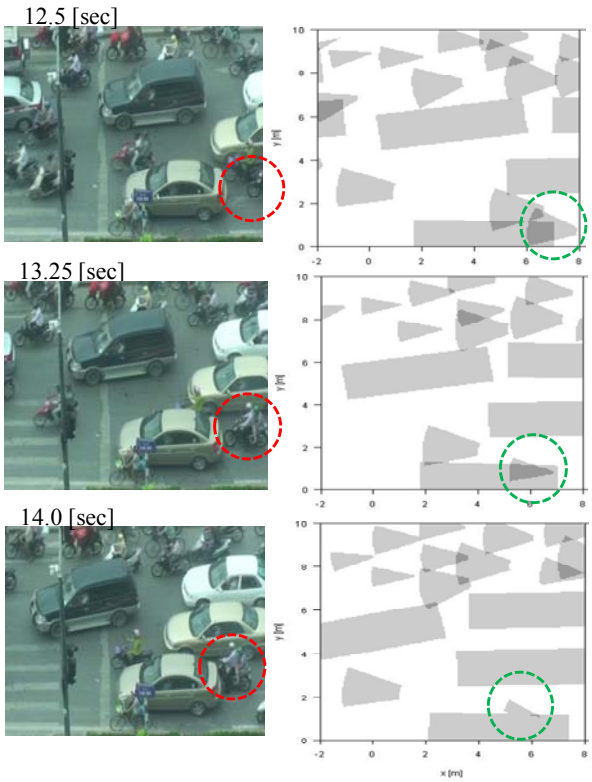


**Fig. 10** video images of conflict situation

can change the moving direction suddenly and rapidly; 3) different acceleration and deceleration characteristics of motorcycles and passenger cars; and 4) the area occupied by a vehicle is different. After defining the conflict index, PPSA, and establishing the method for calculating it, the index was applied to the real-world traffic flow data. It was confirmed that the PPSA index can appropriately present traffic conflict situations.

In future work, traffic situations in which traffic safety and efficiency are low should be analyzed in detail. In particular, it can be assumed that a mix of passenger cars into motorcycles platoon severely decrease the traffic efficiency and safety. The mechanisms needed to reduce the efficiency and safety must be quantitatively clarified furthermore. Based on these results, it can be stated that there is a significant need for traffic operation and management policies which improve both traffic safety.

## REFERENCES

1) JICA-NTSC: Final report of the survey for planning the master plan of road traffic safety in Vietnam, 2009.
2) Hsu, TP.: Segregated Flow Concept for Motorcycle Traffic, IATTS Review Vol. 29, No. 3, pp. 188-198, 2004.
3) Hsu, TP., Dao, N.X. and Sadullah, A.: A Comparative Study on Motorcycle Traffic Development of Taiwan, Malaysia and Vietnam. Journal of the Eastern Asia Society for Transportation Studies. Vol. 5, pp. 179-193, 2003.
4) Wakabayashi, T., Kojima, N. and Oishi, S.: Development of Vehicle Tracking System using Digital VCR and Its Application to Traffic Conflict Analysis, Infrastructure Plan-

ning Review Vol. 19, pp. 765-775, 2002 (in Japanese).
5) Hayward, J.C.: Near-miss determination through use of a scale of danger. Highway Research Record, 24-34, 1972.
6) Allen, B.L., Shin, B.T. and Cooper, D.J.: Analysis of traffic conflicts and collision. Transportation Research, 1978
7) Uno, N., Iida, Y., Itsubo, S. and Yasuhara, S.: A Microscopic Analysis of Traffic Conflict Caused by Lane-Changing Vehicle at Weaving Section. Proceedings of the 13th Mini-Euro Conference "Handling Uncertainty in Transportation Analysis of Traffic and Transportation Systems", pp. 143-148, 2002.
8) Khan, S.I., Raksuntorn, W.: Accuracy of numerical rectification of video images to analyze bicycle traffic scenes, Journal of the Transportation Research Board, No. 177, TRB, pp. 220-228, 2001.
9) Sekine, T.: Fact Surrounding Motorcycle Accidents and Proposal for Safety Educational Guide in Asia, IATTS Review Vol. 29, No. 3, pp. 219-228, 2004.
10) Japan Road Association: Explanation and Operation of Road Structure Regulations (Douro Kouzou Rei No Kaisetsu To Unyou), 2009.

GCOE AIT-KU JOINT SYMPOSIUM ON HUMAN SECURITY ENGINEERING

Bangkok, Thailand, November 25-26, 2010

# Geotechnical Infrastructure Asset Management -Field Monitoring in Nakhon Nayok, Thailand-

Hiroyasu OHTSU[1]

[1]Professor, Dept. of Urban Management, Kyoto University

(C1-182, Kyoto University Katsura Campus, Nishikyo-ku, Kyoto 615-8540, Japan)

E-mail:civil@hse.gcoe.kyoto-u.ac.jp

Landslide/slope failure caused by heavy rainfall is one of the most serious natural disasters all over the worlds. Recently, the number of landslide events has drastically been increasing in Asian countries, because of disorderly land-use development for residential areas and agricultural areas and/or climate change. The occurrence of landslide causes huge losses to individual and society; therefore, the risk mitigation against landslide should be one of the most urgent tasks from a viewpoint of "Human Security Engineering".

Among various measures for risk mitigation, this study focuses on early warning system by aiming at evacuation and road service interruption. In general, the early warning system is established based on the method associating historical records of landslide events with corresponding rainfall records. Therefore, the applicability and reliability of the system heavily rely on the precision of observed precipitation in the past and the kinds of rainfall records, which are selected as indexes associated with decision-making for issuing evacuation and road service interruption. At present, for rainfall observation, conventional tipping bucket type rainfall gauge is mainly used. For indexes of rainfall, the system in Thailand adopts both daily rainfall and accumulated rainfall by taking account of the effect of antecedent rainfall on slope stability in Thailand. It should be discussed that the current system may be revised under the situation that landslide event is currently increasing due to climate change.

From such a viewpoint, this paper discusses the precision of conventional rainfall gauge for monitoring of torrential rainfall and the physical meanings for considering the effect of antecedent rainfall based on results of field monitoring, which the authors have conducted in Nakhon Nayok, Thailand to monitor the variation of moisture content and suction due to heavy rainfall, so-called squall. Finally, the necessity considering the effect of antecedent rainfall on slope stability is presented.

***Key Words :*** *landslide, torrential rainfall, rainfall gauge, early warning system*

## 1. INTRODUCTION

Recently, frequency of landslide occurrence caused by torrential rainfall such as tropical monsoon/squall is drastically increasing in Asian countries. Specially, number of landslide occurrence in Thailand has been increasing since 2000 as shown in **Fig.1**. For the reason of it, so far, many researchers have suggested that it is due to climate change or disorderly infrastructure development such as housing areas, highway and so on. However, clear understanding has not been obtained until now.

Also in Japan, the guerilla-like rainfall, which is the locally-high intensity rainfall, so-called, which may be regarded as one of significant phenomenon caused by climate change, has been frequently observed, and has caused landslide and associated mudslide damaging individual properties and societies. The feature of guerilla-like rainfall observed in Japan this past a few year is that high intensity rainfall, which exceeds 10 mm/10 minute, concentrates during relatively short periods as shown in **Fig.2**.

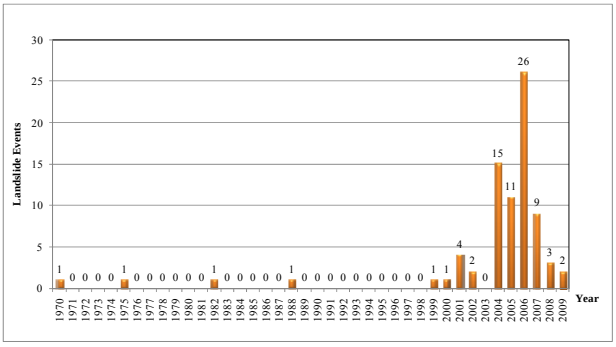


**Fig.1** Frequency of landslide event in Thailand[1)]

Here, the typical measures to mitigate landslide disaster risk can be classified into two types. The first one is to carry out countermeasures such as slope reinforcement, for examples, ground improvement using ground anchors, rock bolts and so on, which requires additional investment/budget. The other is the establishment of early warning system aiming at the evacuation and the interruption of road service. Generally speaking, officials have to manage so many instable slopes that it is very difficult to make decision of priority of slopes to be reinforced. On the other hand, basic concept on establishment of early warning system is relatively simple. Because, it can be empirically established by collecting historical rainfall records observed in a certain area when a slope failure occurred. **Fig.3** shows an example of the system adopted in Japan, which clarifies a warning envelop in a plane consisting of accumulated rainfall and hourly rainfall, based on historical rainfall records.

Here, the occurrence of torrential rainfall such as guerilla-like rainfall is relatively new in Japan so the collected data is very limited. Therefore, it is wondered whether the conventional method can be applied for torrential rainfall such as guerilla-like rainfall. In addition, there is doubt whether the system requires taking account of the effect of antecedent rainfall on slope stability as proposed in Thailand, in which torrential rainfall, so-called squall is frequently observed.

In order to cope with the problems above mentioned, it is necessary to investigate the feature of moisture infiltration into subsoil during torrential rainfall by field monitoring. However, the lack of data collection associated with the prediction of both timing and location of torrential rainfall events make it difficult to select suitable sites for conducting field monitoring in Japan.

From such a viewpoint, authors[3)] have initiated the field monitoring of moisture infiltration caused by torrential rainfall in Nakhon Nayok, Thailand by focusing on similarity of rainfall characteristics between guerilla-like rainfall observed in Japan and

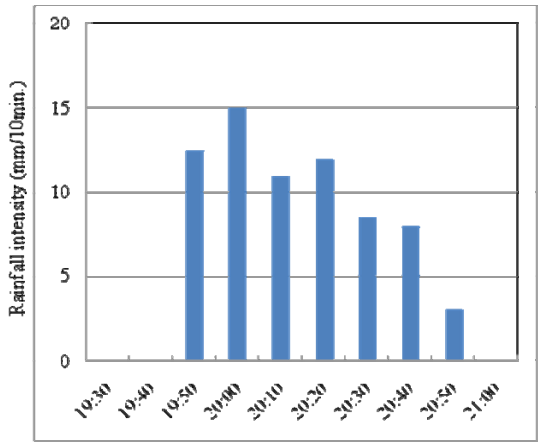


**Fig. 2** An example of rainfall records of guerilla-like rainfall observed in Japan ( Nerima, Tokyo, July 5,2010 )

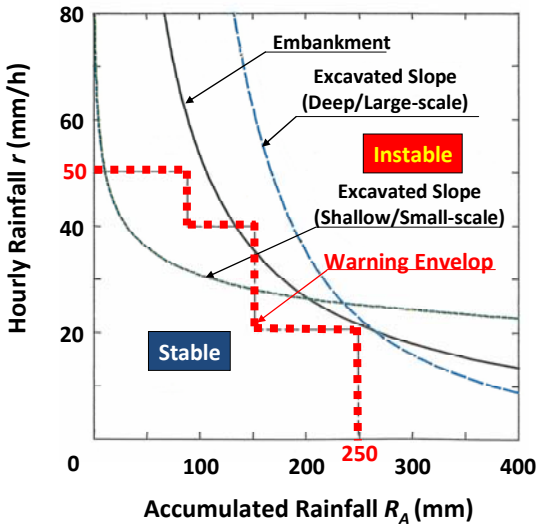


**Fig.3** An example of early warning system adopted in Japan[2)]

tropical torrential rainfall, so-called squall. The feature of the investigation is to directly measure surface flow, which does not infiltrate into subsoil in addition to volumetric moisture content and suction near slope surface.

This paper introduces the outline of the field monitoring conducting in Nakhon Nayok and presents the observed results and relating consideration. The discussion focuses on the effect of antecedent rainfall on slope stability whether is required for establishment of early warning system against torrential rainfall.

## 2. EXAMPLES OF EARLY WARNING SYSTEM AGAINST LANDSLIDE

As mentioned in **1.**, the early warning system adopted in Japan deals with accumulated rainfall and hourly rainfall. On the other hand, **Fig.4** shows an

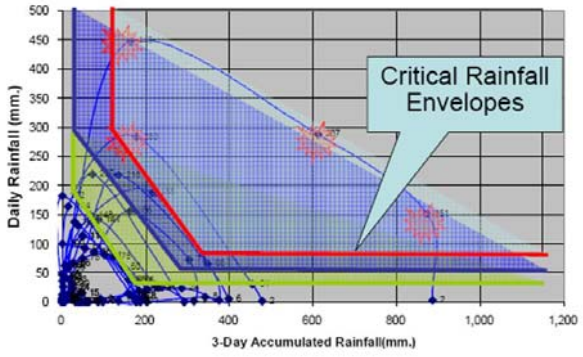


**Fig.4** An example of early warning system [4)]

example of the sy stem proposed in Thailand, in which warning envelop is established by combining 3 days accumulated rainfall and daily rainfall in order to consider the effect of antecedent rainfall on slope stability implicitly[4)].

However, it is reported that slope failure occurred at point F shown in **Fig.5**(a) before snake curve plotting rainfall record on a plane, which consists of 3 days accumulated rainfall and daily rainfall reaches pre-determined critical rainfall envelop. The finding implies the necessity to consider the effect of antecedent rainfall effect on slope stability. Therefore, in order to cope with the above problem , the following index called Antecedent Precipitation Index[5)], API, is introduced:

$$\mathrm{API}_t = \left(\mathrm{K}_t \times \mathrm{API}_{t-1}\right) + \mathrm{P}_t \qquad (1)$$

In which, API $_t$ denotes Antecedent Precipitation Index on day $t$, $\mathrm{K}_t$ denotes reduction rate on day $t$, and $\mathrm{P}_t$ denotes precipitation on day $t$.

It is needless to say that API explicitly takes account of the effect of antecedent rainfall. Therefore, as shown in **Fig.5**(b), it can be m odeled that snake curve plotted on a plane consisting of API and daily rainfall starts from point S in **Fig.5**(b) instead of point O in **Fig.5**(a), and reaches pre-determ ined critical rainfall envelop when slope failure occurs.

The concept of API is relatively effective to solve the shortcomings associated with conventional early warning system by focusing on accumulated rainfall. Current API sy stem is established based on the observed daily rainfall. The reliability of the API sy stem heavily relies on the precision of reduction rate, $\mathrm{K}_t$, involved in eq.(1) , which is akey index that takes account of infiltration into subsoil by considering antecedent rainfall and evaporation. Therefore, in this study, the modified reduction rate, which is evaluated based on field m onitoring results, is proposed later.

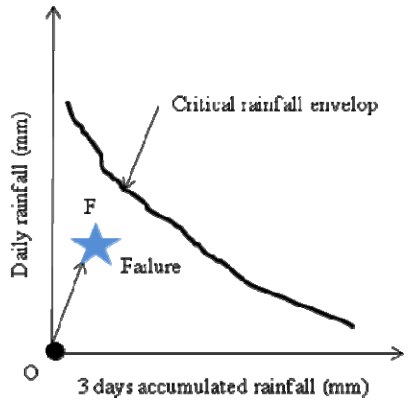


(a) Accumulated rainfall type

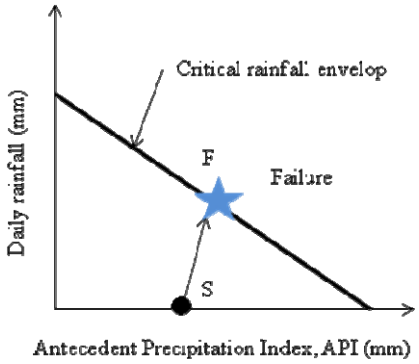


(b) Antecedent Precipitation Index, API, type

**Fig.5** Critical rainfall envelop[5)]

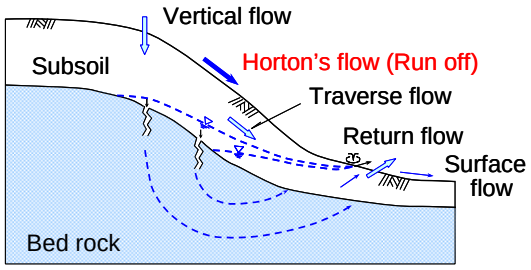


**Fig.6** Water circulation at a slope during rainfall[6)]

## 3. FEATURE OF FIELD MONITORING

### (1) Basic concept

The continuous equation associated with water circulation at slopes due to rainfall described in **Fig.6** can be shown as follow:

$$P = Q_E + Q_S + Q_{IN} \qquad (2)$$

In which, $P$ denotes precipitation, $Q_E$, $Q_S$ , $Q_{IN}$ denote amount of evaporation, am ount of surface flow along a slope, am ount of m oisture infiltration into subsoil, respectively.

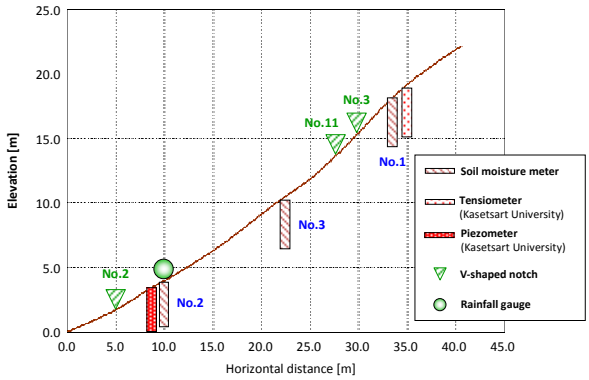


(a) Cross section

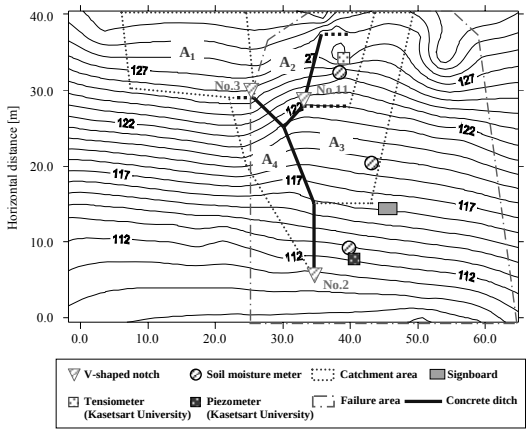


(b) Plane view

**Fig.7** Layout of measurement instruments and catchment areas for run-off [7)]

In eq.(2), amount of evaporation, $Q_E$, can be negligible during rainfall, and surface flow along a slope is generally called Horton's flow and/or run-off as shown in **Fig.6**. Among terms involved in eq. (2), amount of moisture infiltration into subsoil, $Q_{IN}$, has dominated over slope stability , causing change of resisting force acting slip plane. Therefore, this study aims at directly measuring variation of surface flow, in order to clarify amount of moisture infiltration into subsoil from amount of rainfall.

### (2) Layout of Field monitoring equipments

**Fig.7**(a) and **Fig.7**(b) show lay out of field instruments at monitoring site in Nakhon Nay ok, Thailand[7)]. In **Fig.7**(b), catchment areas, $A_i$ for run-off, which was specified by field survey, are also shown. Monitoring equipments installed at the site are the moisture meters to measure volumetric moisture contents, the tension-meters to measure suction, the water level sensors to measure surface flow, and the tipping bucket type rainfall gauge.

Among them, measurement principle of moisture meter shown in **Fig.8** is to measure voltage, which is related to electricity resistance of surrounding subsoil

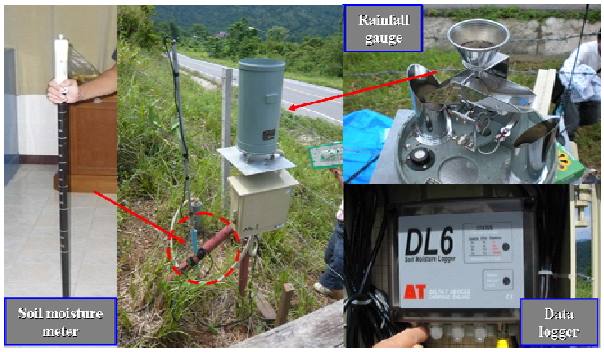


**Fig.8** Moisture meter

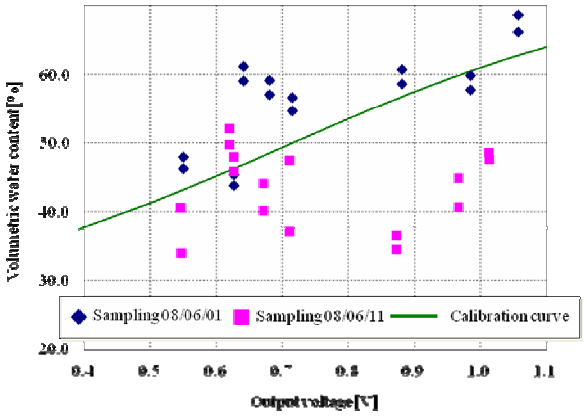


**Fig.9** Calibration curve between measured voltage and volumetric moisture content

measured by using magnetic wave system, and then the measured voltage will be converted to volumetric moisture content in accordance with the following regression curve (eq.(3)). It is the calibration result between the output voltage that was measured by moisture meter and the volumetric moisture content of soil that was sampled from monitoring site, as shown in **Fig.9**:

$$\theta = 0.32 - 0.09V + 0.72V^2 - 0.34V^3 \qquad (3)$$

In which, $\theta$ and $V$ denote output voltage and volumetric moisture content, respectively.

On the other hand, surface flow is measured in accordance with following procedures. First, after construction of a V-shaped notch as shown in **Fig.10**(a) along water lane, a water level sensor is attached as shown in **Fig.10**(b). Second, water level measured by the sensor shown in **Fig.10**(c) is converted to surface flow in accordance with the following equation, which is specified by Japanese Industrial Standard, JIS, code B8302:

$$Q = 0.00084 \times H_w^{0.25} \qquad (4)$$

(a) V-shaped notch No.2

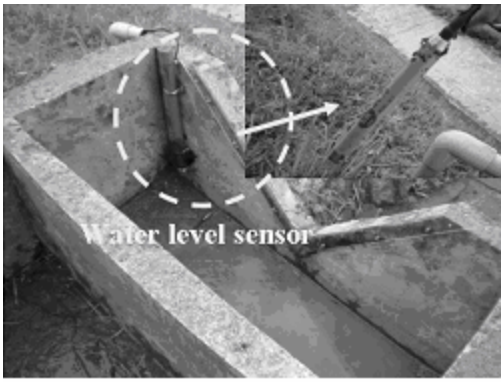


(b) Water level sensor attached at V-shaped notch No.2

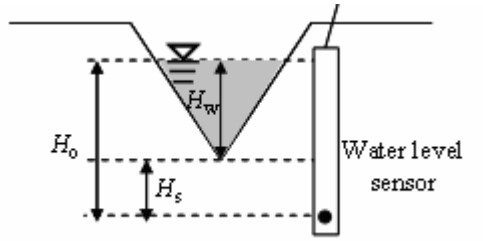


(c) Measurement system

**Fig.10** V-shaped notch No.2 and measurement system

$$H_w = H_0 - H_s \tag{5}$$

In which, $H_w$, $H_0$ and $H_s$ denote height of water level from bottom of V-shaped notch, height of water level measured by water level sensor and distance between bottom of V-shaped notch and level of sensor, respectively.

**(3) Geological condition at monitoring site**

Geological condition of monitoring site comprises weathered ryolite, which is one of typical volcanic rock, as shown in **Fig.11**. The geotechnical properties obtained by laboratory test are summarized in **Table 1**. As shown in the table, subsoil, which covers relatively shallow region at the monitoring site is classified as medium plastic clay.

**Table 1** Soil properties

| | |
|---|---|
| Unit weight, $\gamma$ | 17.66 kN/m$^3$ |
| Plastic limit | 46-51% |
| Liquid limit | 6-18% |
| Plasticity index | 33-40 |
| Cohesion, $c$' | 14.5 kPa |
| Frictional angle, $\phi$' | 33.9 degree |
| Coefficient of permeability at saturated condition | $10^{-5}$ ~ $10^{-6}$ cm/sec |

**Fig.11** Weathered ryolite exposed on surface of slope

## 4. COMPARION OF PRECIPITATION OBSERVED BY TWO TYPES OF RAINFALL GAUGE

**(1) Rainfall gauge**

Tipping bucket type rain gauge has been used commonly all over the world to observe precipitation. Its principle of measurement is to sum up the frequency of pulse signal during a unit period such as 1 min., 10 min., 1 hour, which is caused whenever raindrop accumulating into tipping bucket exceeds just 0.5 mm. Therefore, the measured result provides discreet values, which are multiples of 0.5 mm.

On the other hand, Doppler radar rainfall shown in **Fig. 12**, which is recently developed, can measure amount of rainfall continuously . Its principle of the gauge is to measure velocity of raindrop by receiving frequency of reflection wave corresponding to wave that is transmitted from the top of probe shown in **Fig.12**. Velocity of raindrop can be correlated to a size of raindrop based on following equation:

$$V = 9.65 - 0.3\exp(-0.6D) \tag{6}$$

In which, $V$ denotes velocity of raindrop (m/s), and $D$ denotes size of raindrop (mm).

Doppler radar rainfall gauge can clearly detect the timing of both the beginning of rainfall and the end of rainfall, and requires less maintenance than conven-

**Fig.12** Doppler radar type rainfall gauge

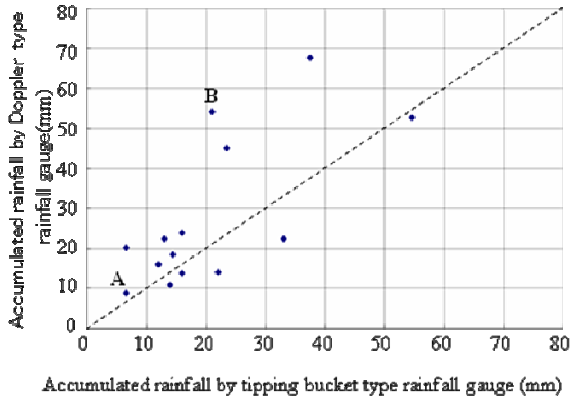


**Fig.13** Comparison of accumulated rainfall observed by two type of rainfall gauge

tional rainfall gauges.

### (2) Comparison of observed precipitation

**Fig.13** shows comparison of accum ulated rainfall observed by two types of rainfall gauge, which are14 rainfall records observed from June, 2010 to September, 2010. The plotted points are relatively scattered. However, the points except 3 rainfall records are m ainly plotted around the correlation line, of which ratio is 1:1. In order to investigate the difference between them in detail, observed rainfall intensity is discussed by focusing on two rainfall records, which are denoted as Rainfall A and Rainfall B in **Fig.13**.

**Fig.14** and **Fig.15** show the com parisons of rainfall intensity observed by two types of rainfall gauge on June 24, 2010 (Rainfall A) and on June 25, 2010 (Rainfall B), respectively.

First, as shown in **Fig.14**(a) and **Fig.14** (b), the comparisons of both one-m inute rainfall intensity and ten-m inutes rainfall intensity observed by two gauges show relatively good agreement. Therefore, it is pointed out that in the case of Rainfall A of which intensity is relatively low, the difference between accumulated rainfall observed by two rainfall gauges

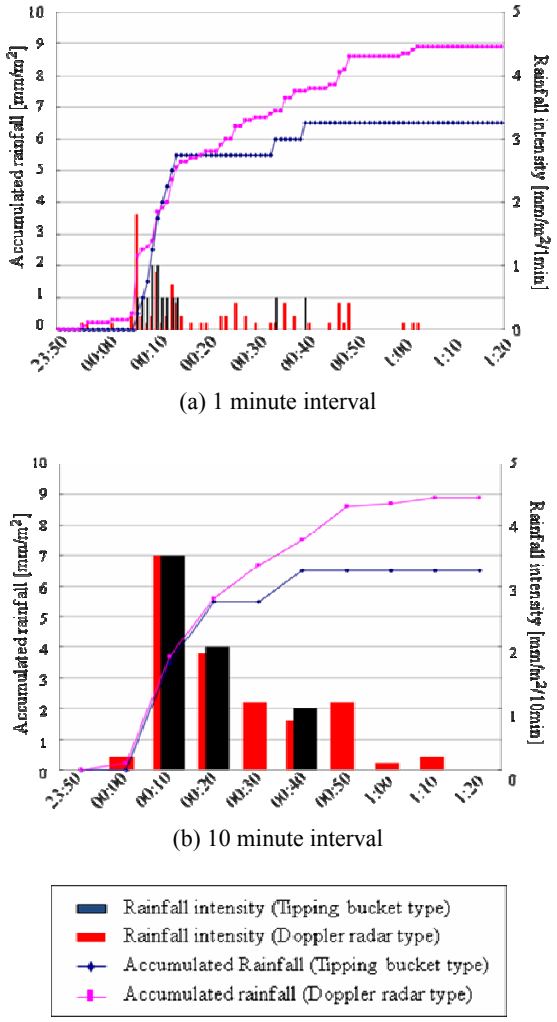


(a) 1 minute interval

(b) 10 minute interval

**Fig.14** Comparisons of rainfall observed by two types of rainfall gauge (Rainfall A; June 24, 2010)

is relatively small.

On the other hand, in the case of Rainfall B of which intensity is relatively high, it is found out that there is big difference between results observed by two rainfall gauges as shown in **Fig.15**. Focusing on one-minute rainfall intensity shown in **Fig.15(**a), high rainfall intensity ranging from 1.0 m m to 3.0 mm was observed before precipitation observed by tipping bucket type rainfall gauge. Later, while tipping bucket ty pe rainfall gauge was observing rainfall intensity ranging from 1.0 mm to 1.5 mm around 3:30 am. discretely, Doppler radar rainfall gauge was measuring very high rainfall intensity ranging from 2.0 mm to 4.4 m m continuously at corresponding period. Again, huge difference between results observed by two gauges around 3:40 pm was found as well. It is considered that the accum ulation of the above difference corresponding to the m easurement of high intensity raindrop in very short periods causes significant difference shown in **Fig.15**.

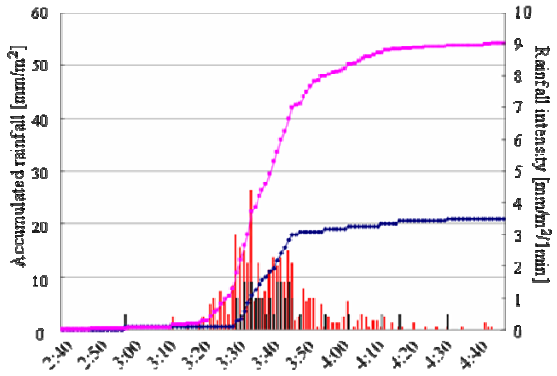


(a) 1 minute interval

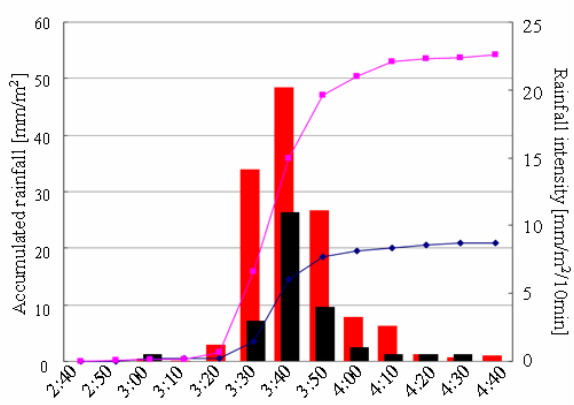


(b) 10 minute interval

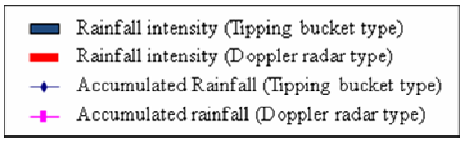


**Fig.15** Comparisons of rainfall observed by two types of rainfall gauge (Rainfall B; June 25, 2010)

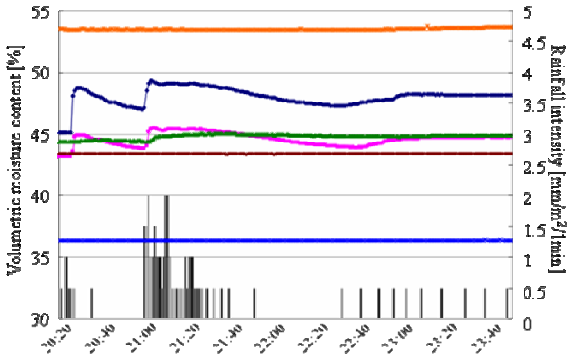


(a) Tipping bucket type rainfall gauge

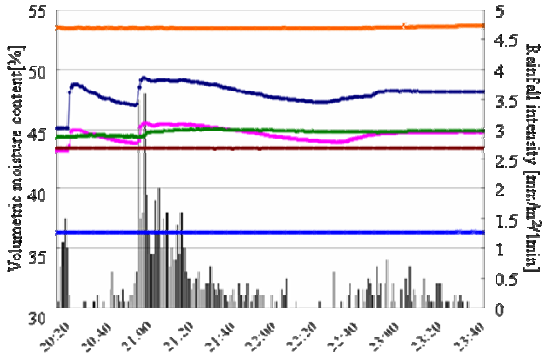


(b) Doppler radar rainfall gauge

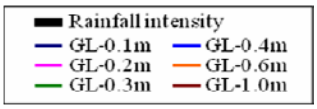


**Fig.16** Correlation of variation of moisture content with rainfall intensity by two types of rainfall gauges (Moisture meter No.1; September 2, 2010)

However, the above results just show comparisons of result observed by two ty pes of rainfall gauge, which have different m easurement principles. Therefore, additional discussion is required to investigate which rainfall gauge can observe torrential rainfall suitably. In response to the requirem ent, **Fig.16** shows the correlation of variation of volumetric moisture content observed from m oisture meter No.1 with rainfall intensity observed by two types of rainfall gauge. As shown in **Fig.16**, volumetric moisture content at shallow area shows drastic increase in response to rainfall event around 21:00. Rainfall intensity observed by tipping bucket type rainfall gauge shows va riation ranging from 1.0 mm/min. to 2.0 mm/min. On the other hand, rainfall intensity by Doppler ra dar rainfall gauge shows rainfall intensity ranging from 2.0 m m/min. to 3.5 mm/min, which is m uch higher than that one. In addition, focusing on the variation m ode of rainfall intensity, the correlation of variation between volumetric m oisture content and rainfall from Doppler radar rainfall gauge shows much better agreement than the other also. Specially , during 21:00-21:10, volumetric moisture content decreases in spite of continuity of rainfall event, rainfall variation observed by Doppler radar rainfall gauge shows m uch better agreem ent with volum etric m oisture content. Therefore, it can be im plied that Doppler radar rainfall gauge can catch variation of am ount of raindrop during torrential rainfall event m ore precisely than tipping bucket ty pe rainfall gauge and that the conventional rainfall gauge may provide smaller amount of rainfall to torrential rainfall.

Based on the above discussions, it is revealed that the fact that tipping bucket type rainfall gauge cannot catch very high intensity raindrop during a very short period as shown in **Fig.15** causes the difference of accumulated rainfall between two ty pe gauges m entioned above. In other words, it is pointed out that in the case of torrential rainfall, accumulated rainfall observed by conventional tipping ty pe gauge m ay provide underestimated results.

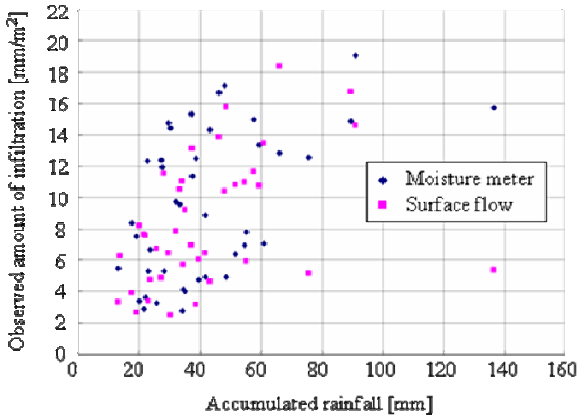


**Fig.17** Comparison of amount of infiltration into subsoil

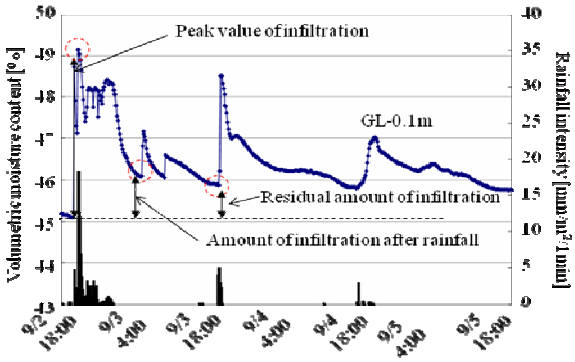


**Fig.18** An example of the variation of volumetric moisture content

## 5. INVESTIGATION OF THE EFFECT OF ANTECEDENT RAINFALL

### (1) Investigation of precision of observed results

Before discussing variation of volumetric moisture content due to rainfall observed at the monitoring site, the preciseness of observed results is verified by focusing on amount of infiltration into subsoil. As described previously, in this study, both change of volumetric moisture content and surface flow, that is to say, run-off is measured. Therefore, amount of moisture infiltration into subsoil can be calculated by following two methods:

1) Method 1

Calculation based on change of moisture contents observed by moisture meter during rainfall

2) Method 2

Calculation using run-off observed by V-shaped notch

For method 2, considering catchment areas shown in **Fig.7,** which was specified by field survey, amount of moisture infiltration into subsoil can be derived as following equation:

$$q_{IN} = (P - Q_s)/A$$
$$A = \sum A_i \quad (7)$$

In which, $q_{IN}$ denotes averaged amount of moisture infiltration into subsoil corresponding to unit area ($m^2$), and $A$ denotes catchment areas, which is the summation of corresponding to each catchment area $A_i$.

Here, it should be considered that while the amount obtained by method 2 is corresponding to an average value, the amount obtained by method 1 is corresponding to a value observed at a spot where moisture meter was installed. **Fig.17** shows the comparison of amount of moisture infiltration into subsoil between two methods. Amount of infiltration obtained by both methods increases in proportion to accumulated rainfall, and finally reaches constant value, which is amounted 18mm approximately. The trend of scattered values in both methods shows relatively good agreement. Therefore, it can be pointed out that the preciseness of obtained results is verified through the above comparison.

### (2) Investigation of effect of antecedent rainfall

As mentioned in **1.**, for establishment of early warning system against torrential rainfall event, it is of engineering concern whether the effect of antecedent rainfall on slope stability should be considered or not. In this section, the effect of antecedent rainfall is investigated based on the results of field monitoring shown in **Fig.7**.

**Fig.18** shows an example of the variation of volumetric moisture content observed during September 2-September 7, 2010. In **Fig. 18**, following two kinds of moisture variation in subsoil are considered. The first one is amount of moisture stored into subsoil during rainfall, and the other one is amount of moisture reduced during the end of rainfall and the beginning of following rainfall event. Both are evaluated based on results of field monitoring.

Here, reduction rate of moisture in subsoil is defined as follow:

$$K^* = Q_D / Q_S \quad (8)$$

In which, $K^*$ denotes modified reduction rate of moisture, $Q_S$ denotes the amount of moisture content stored into subsoil during rainfall, $Q_D$ denotes the amount of moisture content dissipated during the end of rainfall and the beginning of following rainfall event due to moisture movement in subsoil and evaporation.

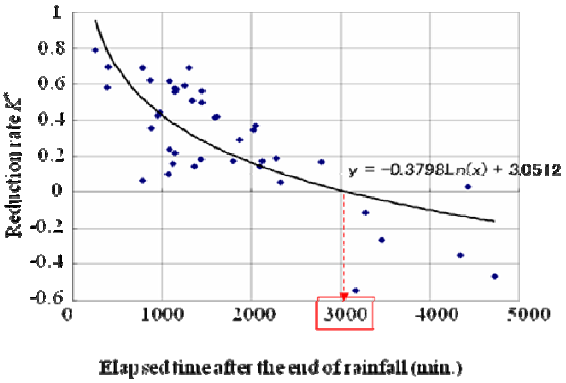


**Fig.19** Variation of reduction rate $K^*$ due to elapsed time

First, for the amount of moisture storing into subsoil during rainfall, $Q_S$, involved in eq.(5), results corresponding to all rainfall events at field monitoring site are already shown in **Fig.17**. Second, the amount of moisture dissipating during the end of rainfall and the beginning of following rainfall event, $Q_D$, involved in eq.(5) corresponding to all rainfall events at field monitoring site are obtained based on monitoring results of moister meter in a same manner as $Q_S$.

**Fig.19** shows the variation of reduction rate $K^*$ due to elapsed time. The reduction rate, $K^*$ decreases gradually with the increasing of period between the end of rainfall and the beginning of following rainfall event. According to regression curve shown in **Fig.19**, reduction rate $K^*$ at 3,000 minutes (50 hours, approximately 2 days) is corresponding to 0. The result points out that when rainfall event occurs within 2 days, the effect of antecedent rainfall on slope stability should be considered.

Here, it should be noticed that the finding on reduction rate $K^*$ evaluated is based on a site-specific data. In addition, it is needless to say that the timing when the effect of antecedent rainfall disappears depends on various conditions such as soil type, vegetation and so on. However, as mentioned above, subsoil condition at the monitoring site comprises relatively low permeable clay. Therefore, it is considered that it takes relatively longer time to dissipate volumetric moisture content after the end of rainfall event than other subsoil condition. For example, in the case of slopes comprising weathered granite, in which landslide event has often been recorded, it is supposed that higher permeability of subsoil may shorten time to disappear the effect of antecedent rainfall stored into subsoil.

Finally, it is pointed out that investigation based on field monitoring at various places to investigate effect of antecedent rainfall stored into subsoil helps to establish comprehensive early warning system.

## 5. CONCLUDING REMARKS

In this paper, the precision of conventional rainfall gauge for monitoring of torrential rainfall, and the physical meanings for considering of the effect of antecedent rainfall on slope stability are presented based on results of field monitoring in Nakhon Nayok, Thailand. The findings obtained are summarized as follows:

1) Rainfall variation observed by Doppler radar rainfall gauge shows much better agreement with variation of volumetric moisture content. Therefore, Doppler radar rainfall gauge can catch variation of amount of raindrop during torrential rainfall event more precisely than tipping bucket type rainfall gauge. In addition, the conventional rainfall gauge may provide smaller amount of rainfall to torrential rainfall.
2) According to modified reduction rate $K^*$, which was evaluated based on the results obtained from the field monitoring in Nakhon Nayok, the effect of antecedent rainfall on slope stability should be considered when rainfall event occurs within 2 days.
3) The finding on reduction rate $K^*$ evaluated is based on a site-specific data. In addition, it is needless to say that the timing when the effect of antecedent rainfall disappears depends on various conditions such as soil type, vegetation and so on. Investigation based on field monitoring at various places to investigate effect of antecedent rainfall stored into subsoil helps establishing of comprehensive early warning system.

## REFERENCES

1) Soralump, S.: Corporation of geotechnical engineering data for landslide hazard map in Thailand, Proceeding of EIT-JSCE Joint Seminar on Rock Engineering 2007, pp.143-148, 2007.
2) Okada, K. et al.: Statistical estimating method of railway embankment damage due to rainfall. In proceeding of JSCE, No.448/III-19, 1992.
3) Suwanishwong, T., Ohtsu, H. and Takahashi, K.: Application of Kalman filter algorithm in Parameters identification of modified Multi Tank Model system, Journal of the Southeast Asian Geotechnical Society, pp.113-121, 2008.
4) Mairaing, W., and Thaiyuenwong, S., : Dynamic Landslide Warning from Rainfall and Soil Suction Measurement. International Conference on Slope 2010. Geotechnique and Geosynthetics for Slopes, 27-30 July , 2010 Chiangmai, Thailand. Organized by th e Department of Highways, Thailand (DOH) (in Thai).
5) Soralump, S.: Landslide Risk Management in Thailand using API model, Proceeding of EIT-JSCE Joint International Symposium 2009, pp.42-81, 2009.
6) Ohtsu, H., Takahashi, K. and Ohnishi, Y: A Study on Development of Methodology to Simulate Variation of

Moisture Content Caused by Rainfall in Slopes, Journal of the Southeast Asian Geotechnical Society , Vol. 40, No.3, pp.201-208, 2009.
7) Ohtsu, H., Hotta, Y., Takahashi, K. and Nakamura, K.: A Study on Applicability of Modified Multi-Tank Model for Unsaturated Soil Slope, Proceedings of the EIT-JSCE Joint International Seminar on Rock Engineering 2008, pp.184-191, 2008.

2010 AIT-KU JOINT SYMPOSIUM ON HUMAN SECURITY ENGINEERING

Bangkok, Thailand, November 25-26, 2010

# Estimation of the deep underground structure and physical properties from geophysical surveys for a Spent Fuel Interim Storage Facility

Yasushi Okajima[1] , Keiji Mizukami[2], Dai Nobuoka[3] and Takeshi Iwamoto[4]

[1,2]Recyclable-Fuel Storage Company
(596-1, Mizukawame, Sekine, Mutsu, Aomori 035-0022, Japan)
E-mail:okajima-yasushi@rfsco.co.jp, mizukami-keiji@rfsco.co.jp
[3,4]OYO Corporation
(2-2-19, Daitakubo, Minami, Saitama, Saitama 336-0015, Japan)
E-mail:nobuoka-dai@oyonet.oyo.co.jp, iwamoto-takeshi@oyonet.oyo.co.jp

The Niigataken Chuetsu-oki Earthquake which occurred at July 16, 2007 in Japan caused substantial damage to the Kashiwazaki Kariwa Nuclear Power Station. At this site, the acceleration of the ground had exceeded the value that was expected by the seismic design. This was because the wave produced by the earthquake was amplified and focused by the physical properties of the sedimentary rock and the deep underground structure. After this earthquake, the Japanese government (METI) notified companies related to the atomic energy that the analysis of the site properties should be determined by considering a deep underground structure from a point of seismic design. As the contrasts of the physical properties are much higher in the sedimentary rock, this is more important to nuclear power plant sites that are covered with a soft sedimentary rock than for sites that are covered with volcanic rock. The authors implemented a seismic reflection and a refraction surveys and a microtremor array survey at the Spent Fuel Interim Storage Facility site to delineate a deep underground structure and presume physical properties at this site. The results of these surveys derived from deep underground structure resulted in the validity of both surveys. As a result, we estimated the physical properties at this site up to a depth of 2500m.

***Key Words :*** *deep underground structure, seismic reflection survey, seismic refraction survey, microtremor array survey*

## 1. INTRODUCTION

The Niigataken Chuetsu-oki Earthquake (M6.8), which occurred at July 16, 2007 in Japan, caused substantial damage to the Kashiwazaki Kariwa Nuclear Power Station. Although the safety of the reactor was secured in this earthquake, there was a lot of damage to the facilities related to the operation of the power station.

The main cause of this damage was the huge acceleration of the ground, which had exceeded the value that was estimated by the numerical calculation for the seismic design. After this earthquake, it was proven that this phenomenon was affected by the following factors.

- Deep underground structure
- Thick sedimentary rocks

At this site, there is a syncline structure, which related to the focus of the wave produced by the earthquake. In addition, the thickness of the sedimentary rock is also related to the amplification of the wave at the surface. This is because the contrasts

of the physical properties are much higher in the sedimentary rock than in the volcanic rock.

This earthquake showed that it is important to take into account the deep underground structure in order to estimate the ground acceleration and its effects on seismic design. Therefore, the Japanese government (METI) notified to the companies related to atomic energy that the analysis of the site properties should be determined by considering a deep underground structure.

In this study, we applied a seismic reflection survey and a microtoremor array survey at the Spent Fuel Interim Storage Facility site to delineate a deep underground structure and to determine its physical properties.

As a result of this survey, we succeeded in delineating the underground structure up to a depth of 2500m, and estimated the physical properties at this site.

In this paper, we introduce the results of our survey and its applicability to other sites.

## 2. SEISMIC DESIGN OF THE NUCLEAR POWER STATIONS IN JAPAN

In Japan, there is a "Regulatory Guide for Reviewing the Seismic Design of Nuclear Power Reactor Facilities" which was issued by the Nuclear Safety Commission of Japan. This guide was issued in 1978 as a first revision and revised in 1981. After the Great Hanshin-Awaji Earthquake in 1995, the latest seismological and earthquake knowledge was accumulated and resulted in the revision of this guide in 2006. The next year, The Niigataken Chuetsu-oki Earthquake caused substantial damage to the Kashiwazaki Kariwa Nuclear Power Station. This earthquake showed that the deep underground structure above the seismic bedrock affect to the acceleration of the ground at the surface.

For this reason, companies related to the atomic energy were required to confirm the deep underground structure in detail, and precisely estimate the physical properties related to seismic design.

As it is difficult to delineate and estimate deep underground structures, geophysical techniques are now receiving much attention in this field.

Seismic reflection surveys and microtremor array surveys have especially received much attention recently because these surveys offer an effective technique in determining important aspects of seismic design.

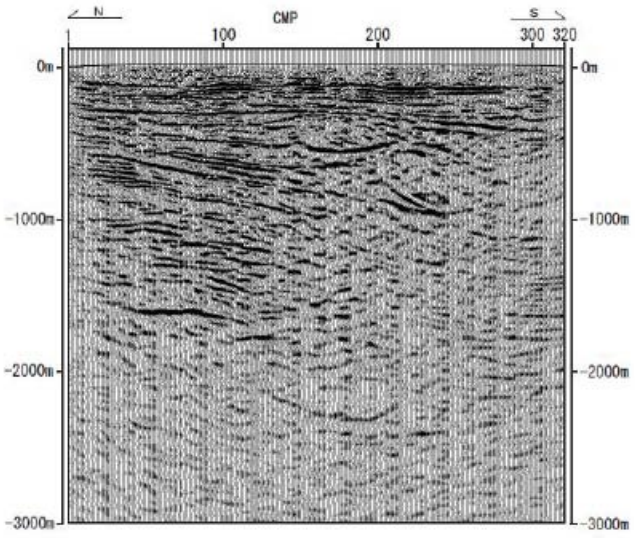


**Fig.1** The result of seismic reflection survey（C line）.

## 3. PLAN FOR THE INVESTIGATION AT THE SPENT FUEL INTERIM STORAGE FACILITY SITE

The geology of the Spent Fuel Interim Storage Facility site consists of neogene and quaternary sand layers, which was confirmed by a well bore investigation whose target depth was about 300m just beneath the site. To confirm the deep underground structure, we conducted a seismic reflection survey and determined that the thickness of the sedimentary rock was at about the depth of 1700m (Fig.1).

From the aspect of seismic design, we must consider more carefully the deep underground structure at sites that are covered with sedimentary rock than at sites covered with volcanic rock, because the contrasts of the physical properties are much higher in the sites that are covered by sedimentary rock.

We examined the geological investigation techniques that could be applied to our site to confirm the deep underground structure around the site. As it was not realistic to drill the well to a depth of around 1700m, other techniques that could accurately estimate deep underground structures were required. We concluded that geophysical techniques were the most suitable to investigate the deep underground structure at this site.

In regard to the seismic design, S wave velocity is an important physical parameter in calculating the amplification of the wave at the surface, as well as the spatial distribution of the sedimentary rock.

Microtremor array surveys can estimate S wave velocity values and boundaries in depth direction easily, so we adopted this technique at this site, as well as seismic reflection and refraction surveys that

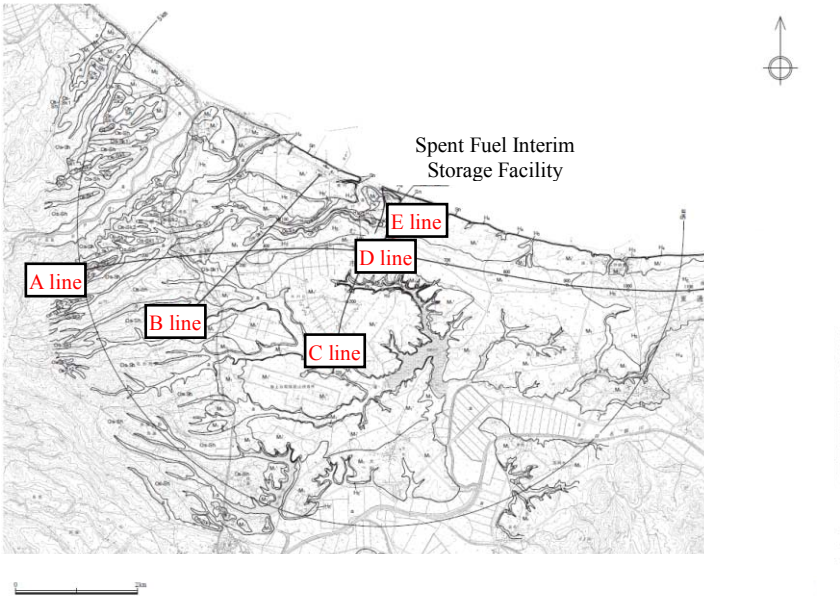


**Fig.2** Location map of the seismic reflection and seismic refraction surveys.

could delineate the deep underground structure in a spatial manner (See Fig.1: The result of the seismic reflection survey).

## 4. GEOPHYSICAL SURVEYS

At the Spent Fuel Interim Storage Facility site, we conducted a seismic reflection survey, a seismic refraction survey, and a microtremor array survey to delineate the deep underground structure. The details of each survey are as follows.

### (1) Seismic reflection survey

The location map of the seismic reflection survey is shown in Fig.2, and the parameter of the survey is shown in Table 1 respectively.

As the aim of this survey was to delineate the deep underground structure, we conducted a seismic reflection survey using Vibroseis as a source. The total profile length was 12.4km, which covered the area of 5km radius from the facility.

The results of this survey are shown in Fig.3. From these results, we could confirm clear reflection layers that correspond to the sedimentary rock in the eastern part of this section. The maximum depth of the sedimentary rock was estimated to be about 1700m, and the construction of our facility was planned to be located at this position. Although the fault was presumed at a distance of 5km, it was not thought to affect the construction of the facility because the quaternary sediments were not affected by this fault.

However, the deep underground structure in the western part of this section was not as clear as in the eastern part. It was thus determined that there was no large structural gap between the eastern area and the western area, but the dispersion layer existed around this area. To confirm this, we conducted a seismic refraction survey to delineate the P wave velocity structure.

### (2) Seismic refraction survey

The location of the seismic refraction survey was the same as the seismic reflection survey. The parameters of the survey are shown in Table 1.

The aim of this survey was to delineate the deep underground structure as a P wave velocity and to confirm the fact that the results of the seismic reflection survey in the western part was caused by the existence of the dispersion layer. We also conducted a seismic refraction survey using Vibroseis as a source.

The results of this survey are shown in Fig.4. From these results, we were able to confirm that the depth of the layer whose P wave velocity was higher

**Table 1** The parameter of the seismic reflection and refraction surveys.

| | Seismic reflection survey | Seismic refraction survey |
|---|---|---|
| Profile Length | 12.4km | 12.4km |
| Sampling interval | 4ms | 4ms |
| Record length | 8sec | 20sec |
| Source | Vibroseis | Vibroseis |
| Num. of source | 246 | 5 |
| Source interval | 40m | 5km |
| Sweep parameter | 8-60Hz | 6-40Hz |
| Receiver | SM-7 (10Hz) | SM-7 (10Hz) |
| Num. of receiver | 621 | 621 |
| Receiver interval | 20m | 20m |

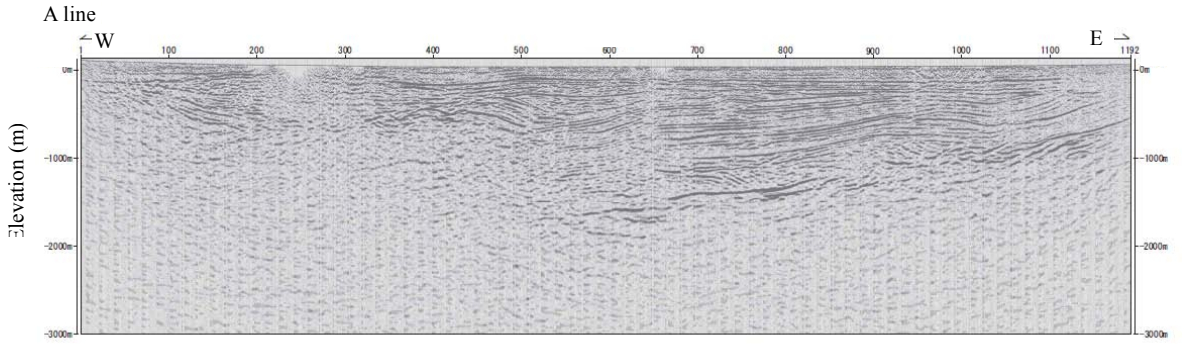


**Fig.3** The results of the seismic reflection survey.

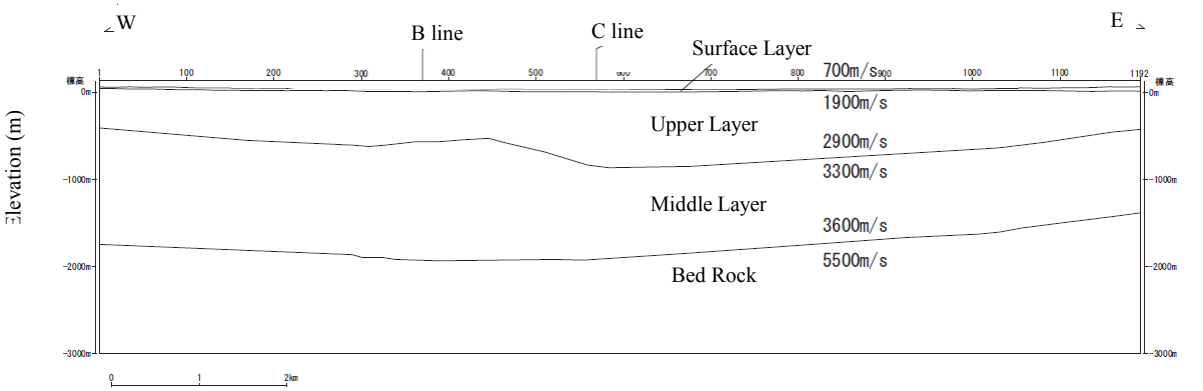


**Fig.4** The results of the seismic refraction survey (P wave).

than 5km/sec was almost flat in this section. This layer corresponds to the layer that could not be detected clearly by the seismic reflection survey. This result shows that the deep underground structure has no large structural gap caused by the fault.

### (3) Microtremor array survey

In determining seismic design, it is important to understand the S wave structure in detail. For this purpose, we conducted a microtremor array survey at this site.

The location map of the microtremor array survey is shown in Fig.5, and the parameters of the survey are shown in Table 2 respectively.

The Microtremor array survey was conducted at the two areas shown in Fig.5. This is because we aimed to confirm that there is no large structural gap between both the eastern part and the western part of the facility.

As the depth of the sedimentary rock was assumed to be at a depth of about 1700m based on the results of the seismic reflection and the seismic refraction surveys, the maximum array size was set to detect the basement rock. The size of the array was also considered to in determining the topographical conditions and the measurement restrictions.

The results of this survey are shown in Fig.6. These results showed that the depth of the basement

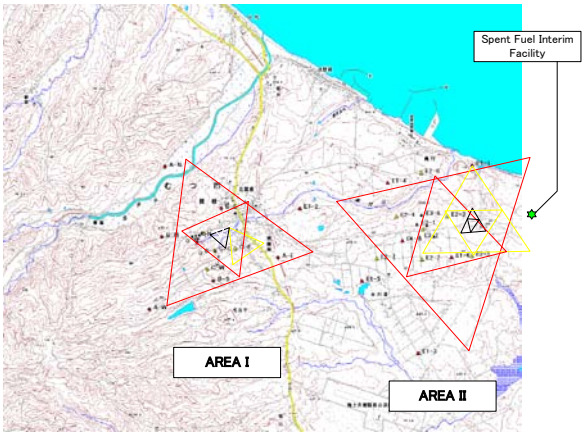


**Fig.5** Location map of the microtremor array survey.

**Table 2** The parameter the microtremor array survey.

AREA I (west)

| Array | Array size (Base lengh) | Record lengh | Samping frequency | Num. of data (Analysis) | Frequency range (Analysis) |
|---|---|---|---|---|---|
| A | 2000m | 4hour | 100Hz | 126 | 0.3～0.576Hz |
| B | 1000m | | | | |
| C | 500m | 2hour | | 70 | 0.588～1.008Hz |
| D | 250m | 1hour | | 35 | 1.02～2.004Hz |
| E | 100m | | | 28 | 2.064Hz～3.504Hz |
| F | 50m | | | | |

AREA II (east)

| Array | Array size (Radius) | Record lengh | Samping frequency | Num. of data (Analysis) | Frequency range (Analysis) |
|---|---|---|---|---|---|
| E1 | 1600m | 1hour | 100Hz | 15 | 0.24～0.30Hz |
| E2 | 800m | | | 36 | 0.32～0.72Hz |
| E3 | 200m | | | 36 | 0.76～2.96Hz |

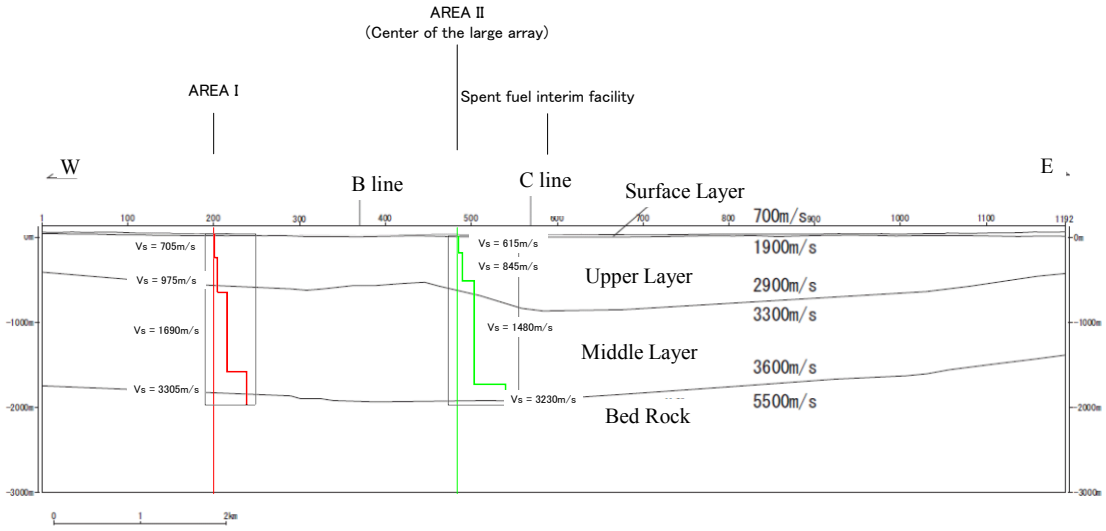


**Fig.6** The results of the microtremor array survey(Displayed with the result of seismic refraction survey).

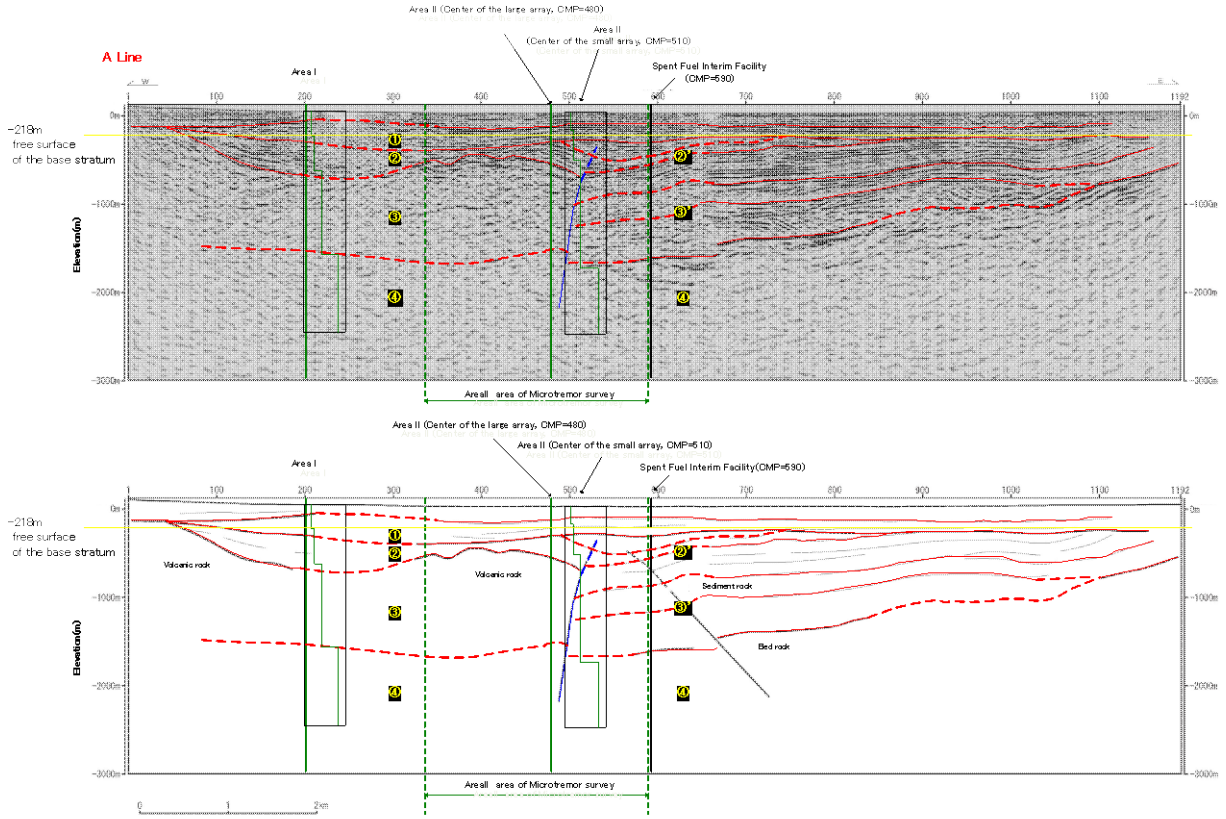


**Fig.7** The interpretation of the deep underground structure at the Spent Fuel Interim Storage Facility.

rock was slightly shallower in the western part of the facility than in eastern part. This structure corresponds to the activity of the reverse fault, which was determined from the results of the seismic reflection survey. However, the structural gap of the fault was small, so these results are consistent with the results of the seismic refraction survey. The results derived in eastern part also correspond to the results of the seismic reflection survey.

## 5. INTERPRETATION OF THE GEOLOGICAL STRUCTURE

From the results of the geophysical surveys which were analyzed using geological information, we determined the deep underground structure shown in Fig.7.

We determined that there is a fault at this site at a distance of 1km. It was confirmed, however, that this

fault does not affect the quaternary sediment, and the depth of the basement rock was almost flat from the results of the seismic refraction survey and the microtremor array survey, so we were able to confirm the safety of the facility. In addition, it was determined from the results of the surveys that there would be no large focusing of the wave caused by the shape of the deep underground structure at this site.

However, since we confirmed that there is a thick sediment layer that would cause an amplification of the wave beneath the facility, we must take its effects into account when determining seismic design.

To calculate and estimate the effect of the amplification of the sedimentary rock, we tried to set the physical properties of the sedimentary rock and the basement rock.

## 6. ESTIMATION OF THE PHYSICAL PROPERTIES

To calculate and estimate of the seismic ground motion characteristics which are caused by the deep underground structures, the model of physical properties was made using geophysical surveys.

The geological classifications were estimated from the seismic reflection survey and geological information, and the S wave velocity of each layers were estimated from microtoremor array survey and S wave reflection survey. The damping ratio was estimated using information from free surface of the base stratum. The other properties were estimated using the relation of Ludwig et. al.[1].

The estimation of physical properties is shown in Table 3.

**Table 3** Estimation of physical properties.

| location | classification | Density $\rho$ t (g/cm$^3$) | S wave velocity Vs (m/s) | P wave velocity Vp (m/s) | Damping ratio h |
|---|---|---|---|---|---|
| eastern part | ① | 1.97 | 705 | 2,075 | 0.01 |
| | ②' | 2.04 | 900 | 2,285 | 0.01 |
| | ③' | 2.16 | 1,300 | 2,760 | 0.01 |
| | ④ | 2.69 | 3,305 | 5,720 | 0.01 |
| western part | ① | 1.97 | 705 | 2,075 | 0.01 |
| | ② | 2.05 | 975 | 2,375 | 0.01 |
| | ③ | 2.26 | 1,690 | 3,165 | 0.01 |
| | ④ | 2.69 | 3,305 | 5,720 | 0.01 |

The result that the calculated seismic ground motion using this model was less than the design basis earthquake ground motion shows there is no focus effect caused by geological structure at this site.

## 7. CONCLUSIONS

We implemented a seismic reflection and a refraction surveys and a microtremor array survey at the Spent Fuel Interim Storage Facility site to delineate a deep underground structure and presume physical properties at this site.

These results show that the geophysical technique is effective to delineate deep underground structures in detail. We also confirmed that the physical properties can be modeled using results of the geophysical surveys.

This result shows the applicability of this technique to other sites in the aspect of seismic design.

## REFERENCES

1) Ludwig,W.J., J.E.Nafe, and C.L.Drake: Seismic refraction, *in The Sea*, Vol.4, Part 1, Wiely-interscience, New York, pp.53-84, 1970

2010 AIT-KU JOINT SYMPOSIUM ON HUMAN SECURITY ENGINEERING

Bangkok, Thailand, November 25-26, 2010

# Estimation of relative permeability of single fracture by using Multi-phase Lattice Boltzmann Method

Takashi AKAI[1], Shumihiko MURATA[2], Hiroshi OKABE[3]

[1]Researcher, Japan Oil, Gas and Metals National Corporation (JOGMEC)
(1-2-2 Hamada, Mihama-ku, Chiba-city 261-0025 Japan)
E-mail: akai-takashi@jogmec.go.jp
[2]Associate Professor, Graduate School of Engineering, Kyoto University
(Room 356, Bldg. C1, Katsura Campus, Nishikyo-ku, Kyoto 615-8540, Japan)
E-mail: murata@mbox.kudpc.kyoto-u.ac.jp
[3]Researcher, Japan Oil, Gas and Metals National Corporation (JOGMEC)
(1-2-2 Hamada, Mihama-ku, Chiba-city 261-0025 Japan)
E-mail: okabe-hiroshi@jogmec.go.jp

For the successful and efficient development of a fractured oil/gas reservoir, it is important to estimate multi-phase fluid flow behavior in the single fracture. In many cases, the fluid flow in the fracture has been studied by the simplified model as parallel smooth plates. Therefore, the anisotropy of the fluid flow behavior inside the fracture has not been estimated accurately. Moreover, it is not well understood how the wettability of the fracture surfaces, the interfacial tension between water and oil, and the geometries of the fracture surfaces affect the multi-phase flow behavior in the single fracture

In this study, in order to understand these phenomena, we investigated the multi-phase flow behavior in the single fracture model and try to determine the fracture relative permeability of oil and water by performing water flooding simulations using Multi-phase Lattice Boltzmann Method. By this study, the effect of the wettability and the interfacial tension on the multi-phase flow behavior and the relative permeability in the fracture has been clarified.

***Key Words :*** *fracture, cubic low, relative permeability ,Lattice Boltzmann Method, wettability, interfacial tension*

## 1. INTRODUCTION

In the oil/gas exploration and production business, production from the fractured reservoirs has been increasing. McNaughton and Grab estimated that ultimate recovery from currently producing fractured reservoirs will be exceeded 40 billion stock tank barrels of oil[1)]. However, in spite of theimportance of fractured reservoirs, many technical problems are still unsolved. The problems can be classified into three groups. The first is the detection and quantification of fracture distribution, the second is the evaluation of fracture communication and the third is the understanding of multi-phase flow phenomena in a fracture. In this paper, we focus on the understanding of multi-phase fluid flow in the fracture.

### (1) Single phase fluid flow in the fracture

Generally, the fracture permeability is estimated by the cubic law, that is, the volumetric flow rate in a fracture is directly proportional to the cubic of its aperture. This law is valid for the laminar flow between two perfectly smooth parallel plates. However, the fractures have complicated rough surfaces. This makes the fluid flow through them

anisotropic and their permeability deviate from the cubic law. **Fig.1** shows the single phase fluid flow simulation result carried out by Watanabe, et al[2]. They conducted single phsae fluid flow simulations by solving local cubic law to a fracture model constructed by X-ray CT image. In this figure, an anisotropic and preferencial flow path can be observed and the evaluated permeability was deviated from the cubic law.

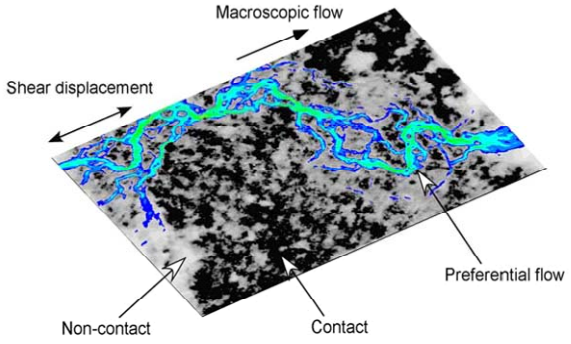


**Fig.1** The result of single phase fluid flow simulation by Watanabe et al. (2010)

**(2) Multi-phase flow in the fracture**

When we deal with the multi-phase flow phenomena in the oil/gas reservoir, the generalized Darcy's law to the multi-phase flow defined as equation (1) is applied.

$$\mathbf{v}_i = \left( \frac{k k_{ri}}{\mu_i} \right) \nabla P_i \qquad (1)$$

where $\mathbf{V}_i=(\delta Q_i/\delta A)\mathbf{n}$, with $Q$ the volumetric flow rate and $\mathbf{n}$ the unit normal vector of the surface $\delta A$, $k$ is the absolute permeability, $k_r$ is the relative peremabiltiy, $\mu$ is the viscosity of fluid, $P$ is the pressure, and subscript $i$ indicates non-wetting phase and wetting phase respectively. By combining this equation with the continuity equation, the governing equation of fluid flow is obtained. Based on this governing equation, the fluid flow simultions for the forcast of oil/gas produciton are carried out.

Typical relative permeabilty curvses of oil and water for the porous media are shown in **Fig.2**. Generally, $k_{ro}$ and $k_{rw}$ are treated as a function of the saturation, $k_{rw}$ starts to increase from the irreduible water saturation and $k_{ro}$ becomes 0 at the residual oil condition. Since the shapes of the curves and those endpoits have a significant impact on the multi-phase fluid flow, the accurate estimation of relative permeability is important.

Meanwhile, in the case of multi-phase flow in the fracture, the two straight lines satisfying the relation of $k_{r,nw}+k_{r,w}=1$ as shown in **Fig.3** have been widely used for the fracture relative permeability curves based on the experimental works by Romm (1966), where $k_{r,nw}$ and $k_{r,w}$ are the relative permeability of non-wetting phase and wetting phase respectively. This type of relative permeability curves physically means that the each phase flows in its own flow path without interference. But, some theoretical or experimental works and some numerical simulations to the two-phase flow in a single fracturehave shown that each phase flows with strong phase interference[3-6]. However, these works are not sufficient to understand the phase interference flow behavior for the correct estimation of the fracture relative permeability. Therefore, additional detail research on the multi-phase flow in a single fracture must be performed.

In this study, we try to simulate and to estimate the relative permeability to the single fracture model having complex surface geometry by performing two-phase flow simulations using the Lattice Boltzmann method (LBM). Moreover, we investigate the effect of the wettability and the interfacial tension on the multi-phase flow behavior and the relative permeability by the multi-phase LBM flow simulations.

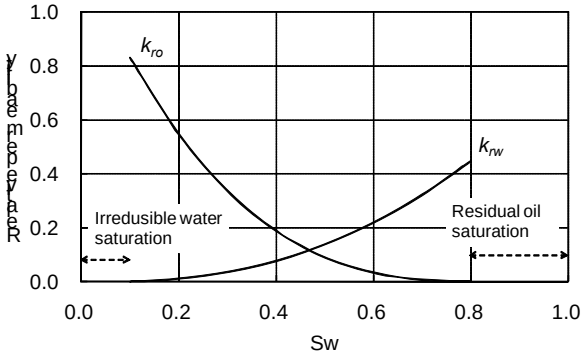


**Fig.2** Typical relative permeability for the porous media

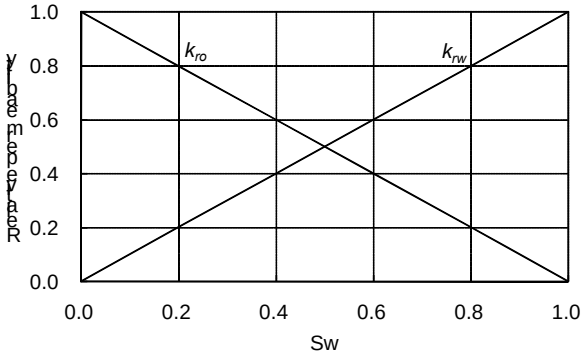


**Fig.3** The fracture relative permeability curves based on experimental works by Romm. (1966)

## 2. CONSTRUCTION OF MULTI-PHASE LATTICE BOLZMANN MODEL

### (1) Multi-phase LBM

The Lattice Boltzmann Method (LBM) is based on cellular automata, which describes a complex system by the interaction of a massive number of cells following simple local rules [7]. While other methods, such as the FEM or the FDM, discretize the model and the governing equations, the LBM method recovers the governing equation from the rule in the discrete model.

In order to simulate the immiscible two-phase flow of oil and water, the Boltzmann equation for the colored particles, red (oil) and blue (water) was used in this study. It is given by the following equation.

$$f_i^k\left(\mathbf{x}+\mathbf{c}_i\Delta t, t+\Delta t\right) = f_i^k\left(\mathbf{x},t\right)+\Omega_i^k\left(\mathbf{x},t\right) \quad (2)$$

where $f_i^k(\mathbf{x}, t)$ and $\Omega_i^k(\mathbf{x},t)$ are the particle distribution function and the collision function respectively. They are defined to every kind of particle $k$, red and blue, and to every direction of particle motion $i$ at the position $\mathbf{x}$ and time $t$. In Equation (2), $\boldsymbol{c}_i$ is the particle velocity in $i$ direction on the lattice, and $\Delta t$ is the time step during which the particles travel one lattice spacing. The particle velocity vectors on the D3Q15 (3D-LBM with 15 velocities) lattice used in this study is given by

$$\mathbf{c}=\begin{bmatrix} 0 & 1 & 0 & 0 & -1 & 0 & 0 & 1 & -1 & 1 & 1 & -1 & 1 & -1 & -1 \\ 0 & 0 & 1 & 0 & 0 & -1 & 0 & 1 & 1 & -1 & 1 & -1 & -1 & 1 & -1 \\ 0 & 0 & 0 & 1 & 0 & 0 & -1 & 1 & 1 & 1 & -1 & -1 & -1 & -1 & 1 \end{bmatrix} \quad (3)$$

The collision function is decomposed into two terms as Equation (4).

$$\Omega_i^k\left(\mathbf{x},t\right) = \left(\Omega_i^k\left(\mathbf{x},t\right)\right)^A + \left(\Omega_i^k\left(\mathbf{x},t\right)\right)^B \quad (4)$$

The first term of the right side of Equation (4) represents the relaxation from the collision perturbing condition to the local equilibrium condition. This term determines the effect of fluid viscosity in the LBM simulation. The second term represents the surface tension between the two kinds of immiscible fluid.

The first term of the collision function is defined as Equation (5) applying BGK (Bhatnagar-Gross-Krook) collision operator.

$$\left(\Omega_i^k\left(\mathbf{x},t\right)\right)^A = -\frac{1}{\tau^k}\left(f_i^k\left(\mathbf{x},t\right)-f_i^{k(eq)}\left(\mathbf{x},t\right)\right) \quad (5)$$

where $\tau^k$ is the relaxation time to the local equilibrium condition after collision, and $f_i^{k(eq)}$ is the local equilibrium particle distribution function. In this study, in order to get the numerical stability, the value of $\tau^k$ is set to 1. On the other hand, the second term of the collision function is defined by Equation (6) applying the interfacial tension model proposed by Grunau *et al*[8].

$$\left(\Omega_i^k\left(\mathbf{x},t\right)\right)^B = A\left|\mathbf{F}\right|\left(\frac{\left(\mathbf{c}_i\cdot\mathbf{F}\right)^2}{\left|\mathbf{c}_i\right|^2\left|\mathbf{F}\right|^2}-K\right) \quad (6)$$

where $A$ is the coefficient which controls the magnitude of interfacial tension, and $K$ is the coefficient determined from the mass conservation depending on the lattice model. In this study, $A$ is set to $1.0\times10^{-3}$ for the base case of interfacial tension. $K$ is 1/3 for the 3D15Q lattice model. $\mathbf{F}$ is a function called local color gradient. It is defined by Equation (7).

$$\mathbf{F}(\mathbf{x},t) = \sum_i \mathbf{c}_i\left(\rho_r(\mathbf{x}+\mathbf{c}_i\Delta t,t)-\rho_b(\mathbf{x}+\mathbf{c}_i\Delta t,t)\right) \quad (7)$$

where $\rho_r$ and $\rho_b$ are the density of red fluid and blue fluid respectively. This function has a contribution at the interface of immiscible fluids.

### (2) Verification of multi-phase LBM

The change of contact angle depending on the wettability and the Young-Laplace relation were simulated in order to confirm the validity of the interfacial tension model used in the multi-phase LBM.

Wettability is an index how the solid surface has a tendency to be wet with the contacting fluid. It is estimated by the contact angle, $\theta_c$, of a droplet on the solid surface. When a droplet of oil contacts a rock surface in water and the contact angle measured through the oil is less than 90 degrees, the rock surface must be oil wet. Conversely, when it is more than 90 degrees, the rock surface must be water wet. Moreover, when it is just 90 degrees, the rocksurface must be neutral wet.

Supposing the following relations among the interfacial tensions between the rock surface and the oil, $\gamma_{s\text{-}o}$, the oil and the water, $\gamma_{o\text{-}w}$ and the rock surface and the water, $\gamma_{s\text{-}w}$,

$$\gamma_{s-o} = \lambda\gamma_{o-w} \quad (8)$$

$$\gamma_{s-w} = (1-\lambda)\gamma_{o-w} \quad (9)$$

where $\lambda$ is the scaling parameter ranging from 0.0 to 1.0. The contact angle can be obtained from the Young's equation as

$$\cos\theta_c = 1-2\lambda \quad (10)$$

Therefore, any contact angle of rock surface can be realized by setting $\lambda$ according the Equation (10).

Then, the contact angle of an oil droplet on a flat rock surface in water was simulated to the case of the perfectly water wet, $\lambda$=1.0, the neutral wet, $\lambda$=0.5, and the perfectly oil wet, $\lambda$=0.0. The results of the simulation are shown in **Fig.4**. In the case of the perfectly water wet, the oil droplet changed its shape from the initial condition in **Fig.4(a)** to be a sphere as shown in **Fig.4(b)**. In the case of the neutral wet, the oil droplet changed its shape to be a semi-sphere as

shown in **Fig.4(c)**. In the case of the perfectly oil wet, the oil droplet spread itself on the rock surface as shown in **Fig.4(d)**. From these results, we can recognized that the contact angles are well simulated, although it looks larger than 0 degree in the case of the perfectly oil wet.

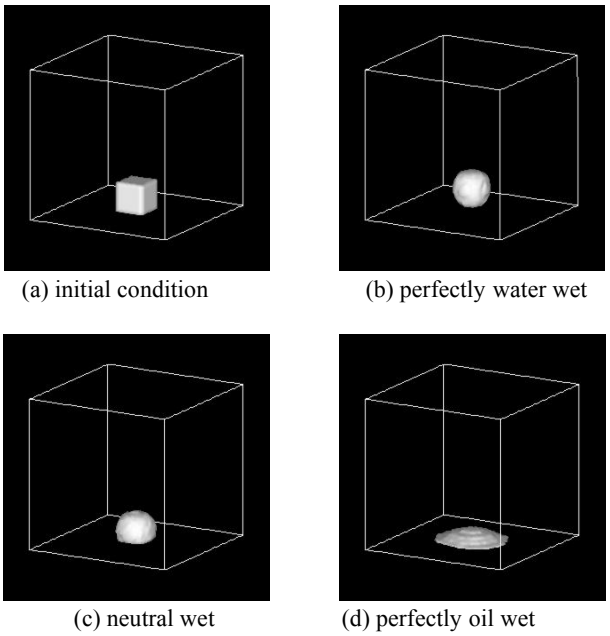

(a) initial condition (b) perfectly water wet

(c) neutral wet (d) perfectly oil wet

**Fig.4** The realization of wettability condition of rock surface in the LBM

Next, the Young-Laplace relation described by Equation (11) must be satisfied when a droplet of one phase exists in another immiscible phase under the static condition.

$$\Delta p = p_{in} - p_{out} = \frac{2\gamma}{R} \qquad (11)$$

where $p_{in}$ is the inside phase pressure of the droplet; $p_{out}$ is the outside phase pressure of the droplet; $\gamma$ is the interfacial tension, $R$ is the radius of the droplet.

Then, a square oil droplet was put in the water, and the pressure difference between the oil and the water, $\Delta p$, and the radius of the oil droplet, $R$, was evaluated under the static equilibrium condition. The relation between the $\Delta p$ and the reciprocal of the radius, $1/R$, was plotted by changing the volume of the square oil droplet. The simulation was carried out to the two cases of interfacial tension by setting the coefficient of $A$ $1.0\text{x}10^{-3}$ and $0.5\text{x}10^{-3}$. They are the base case of interfacial tension and the half of the base case. The result of the plot is shown in **Fig.5**. From this figure, it can be recognized that the $\Delta p$ is directly proportional to the $1/R$, and the Young-Laplace relation is satisfied.

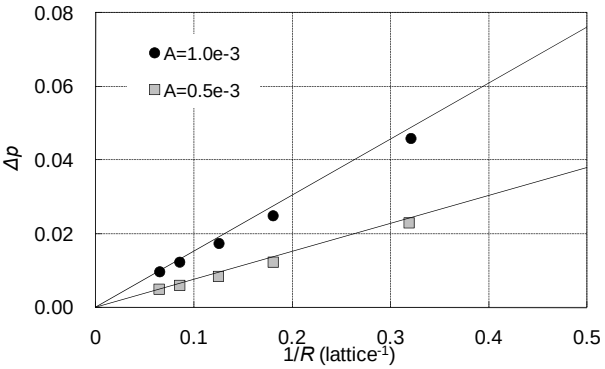


**Fig.5** The realization of Young-Laplace relation the pressure difference between oil and water and the reciprocal of the radius of the oil droplet, R.

## 3. WATER FLOODING SIMULATION IN A SINGLE FRACTURE

### (1) Single fracture model used for the simulation

It has been shown that the topography of a fracture surface is a self-affine fractal and the power spectral density function of the fracture surface profile, $G(f)$, shows a decaying power law that can be described as

$$G(f) = Cf^{-(5-2D)} \qquad (12)$$

where $D$ is the fractal dimension; $C$ is a constant; $f$ is the spatial frequency [9,10]. The two meeting surfaces of a single fracture correlate each other in the lower spatial frequency band and do not correlate in the higher spatial frequency band. The fracture surfaces interlock and the aperture distribution is generated by this frequency dependent correlation.

In order to generate such a fracture numerically, we used the Glover's method[11]. The fractal dimension and the roughness of the generated fracture surfaces are set by changing the slope and the intersection of the decaying power law respectively. We generated a square single fracture model of 1024 lattices in side length and 64 lattices in thickness. Then, a single fracture model of 100 lattices in side length and 64 lattices in thickness was cut out and the 10 lattices in length and 64 lattices in thickness of fluid buffer regions were added to the both sides of inlet and outlet. The single fracture model is shown in **Fig.6** and its descriptions are listed in **Table 1**.

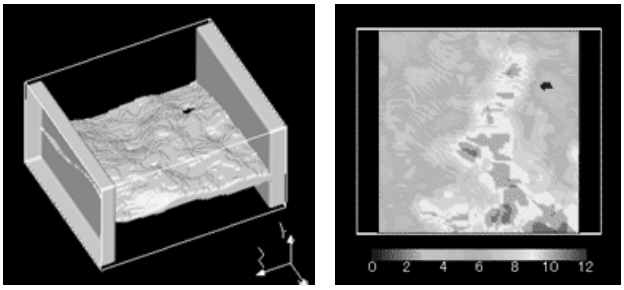


(a) bird view (b) aperture distribution

**Fig.6** The single fracture m odel used for the multi-phase simulation.

**Table 1** The description of the fracture model used in the study.

| | |
|---|---|
| Lattice interval | 0.05 (mm/lattice) |
| Size of Fracture area | 120 x 100 (lattice) |
| Contact ratio | 0.8 (%) |
| Max. aperture | 12 (lattice) |
| Mean aperture | 4.2 (lattice) |

**(2) Relative permeability estimation of a single fracture**

By conducting Multi-phase LBM simulation to the fracture model, the relative permeability of the single fracture model was estimated from the average flux of each phase and the water saturation. In this simulation, the fracture was perfectly saturated with water at first, and then oil was injected under the constant pressure gradient until the irreducible water saturation was accomplished. After that, the water flooding was carried out. The simulation conditions are summarized in **Table 2**.

The snapshots during the simulation are show in **Fig.7**. At first, water invades even in the small aperture regions avoiding the oil saturated large aperture regions. Then, as result of water breakthrough, two isolated oil islands are formed (20,000 steps). After that, one of them is swept by the injected water, but the other is remained.

Oil and water relative permeability curves concaving downward are obtained as shown in **Fig.8**. It can be recognized that the relative permeability curves of a single fracture are not straight lines satisfying the relation of $k_{r,nw}+k_{r,w}=1$. This is probably because the each phase of fluid flows avoiding or pushing each other in the complex aperture distribution of the fracture, and the flow pass consequently becomes as tortuous as the porous reservoir rocks.

**Table 2** The simulation condition.

| | | |
|---|---|---|
| Density | Water | 1.0 x $10^3$kg/m$^3$ |
| | Oil | 0.9 x $10^3$kg/m$^3$ |
| Viscosity | Water | 1.0 x $10^{-3}$Pa・s |
| | Oil | 4.5 x $10^{-3}$Pa・s |
| Wettability | | Perfectly water wet |
| Interfacial tension | | $A$=1.0 x $10^{-3}$ (Base case) |
| Boundary condition | | Constant pressure boundary |

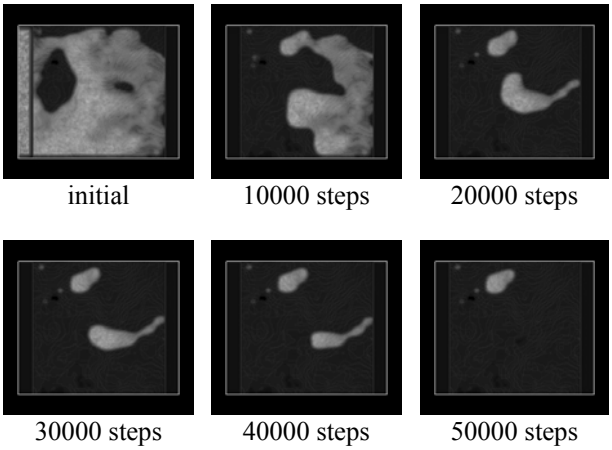


**Fig.7** The change of oil saturation during the water flooding. (Gray color represents oil, block color represents water.)

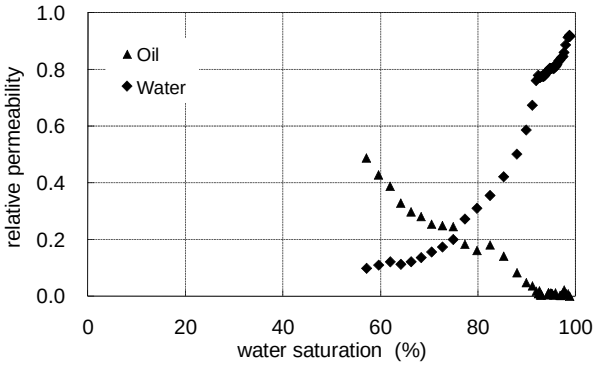


**Fig.8** The fracture relative permeability curves of oil and water obtained from the water flooding simulation.

**a) Effect of wettability on relative permeability**

Water flooding simulations were performed to the perfectly water wet, the neutral wet, andthe perfectly oil wet to the same single fracture model as mentioned above. However, the viscosity ratio was set to one in order to diminish the effect of viscosity. The initial water saturation is 57.2% to the water wet, 42.6% to the neutral wet, and 20.7% to the oil wet (**Fig.9**). From this initial water saturation condition, water was injected into the fracture under the con-

stant pressure gradient.

The change of the oil saturation is shown in**Fig.10** to each case of the wettability in the progress of time step. In the case of the perfectly water wet, it is shown in **Fig.10(a)**, the aspect of the flooding is the same as above mentioned. The residual oil saturation is 1.5%. In the case of the neutral wet, it is shown in **Fig.10(b)**, the alm ost all of oil is flooded out continuously without form ing the independent oil islands. The residual oil saturation is 0.74% . In the case of the perfectly oil wet, it is shown in **Fig.10(c)**, the water invades selectively the large aperture regions. Two flow paths are form ed as the result of avoiding the surface contact region, and the two flow paths surround the sm all aperture region around the surface contact region. The oil in that small aperture region is left finally. The residual oil saturation is 5.7% that is the highest am ong the three cases of wettability (**Fig.11**).

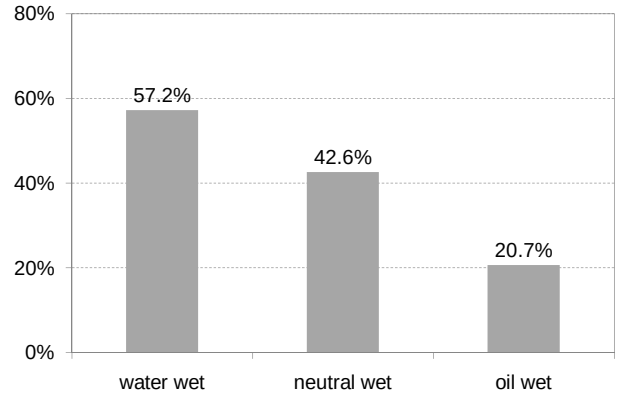


**Fig.9** The initial water saturation of each wettability condition. (Before water flooding)

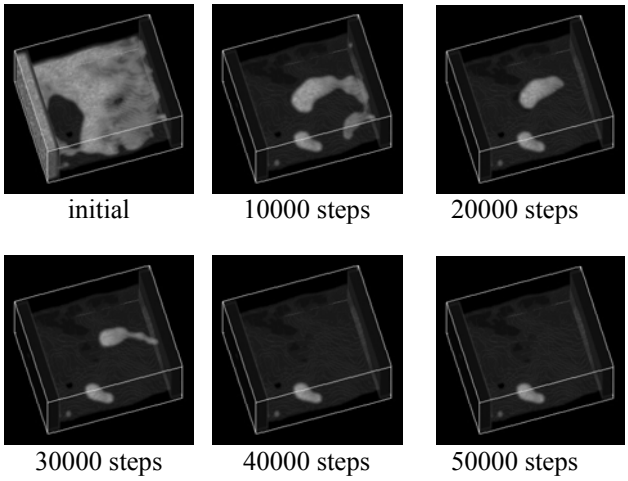


(a) perfectly water wet

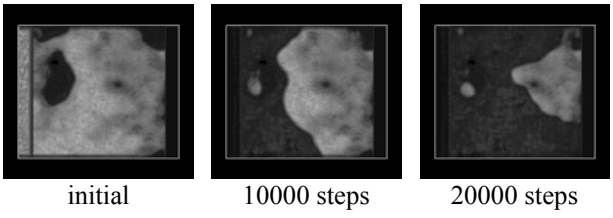


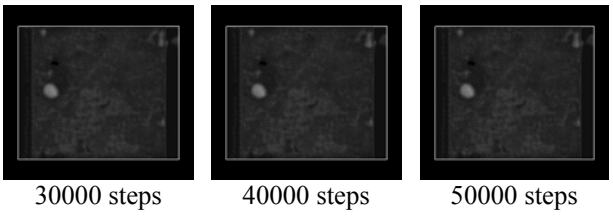


(b) neutral wet

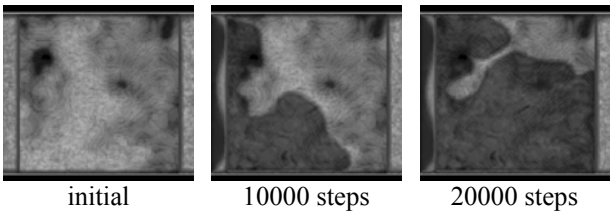


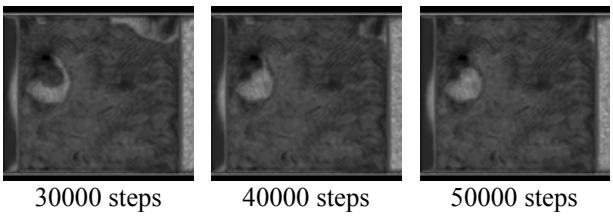


(c) perfectly oil wet

**Fig.10** The change of oil saturation during the water flooding. (Gray color represents oil, block color represents water.)

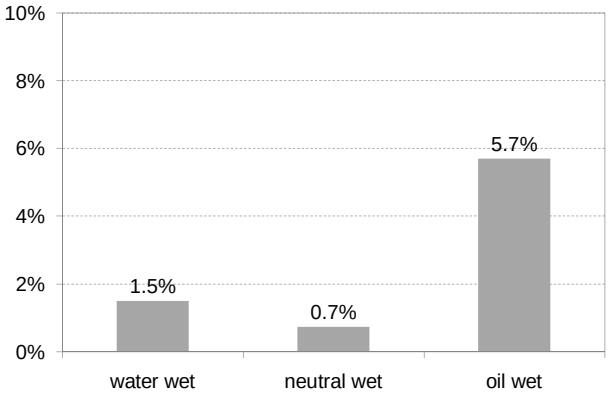


**Fig.11** The residual oil saturation of each wettability condition. (After water flooding)

The relative permeability curves are shown in **Fig.12** to each case of the wettability. In the case of the perfectly water wet, the water relative permeability is difficult to increase during the small water

saturation, because the water flows by avoiding the oil occupying large aperture region. But it rapidly increases with the increase in the water saturation, as the water flows through almost the whole fracture. Consequently, the water relative permeability curve concaves downward. In the case of the neutral wet, the both relative permeability curves of oil and water become almost straight line. This is because the each phase of the fluid can flow without capillary force. In the case of the perfectly oil wet, the relative permeability of water concaving upward is obtained. This is because the water invades selectively the large aperture regions at first and then it spreads into the small aperture regions. The flow rate of the water decreases as the result.

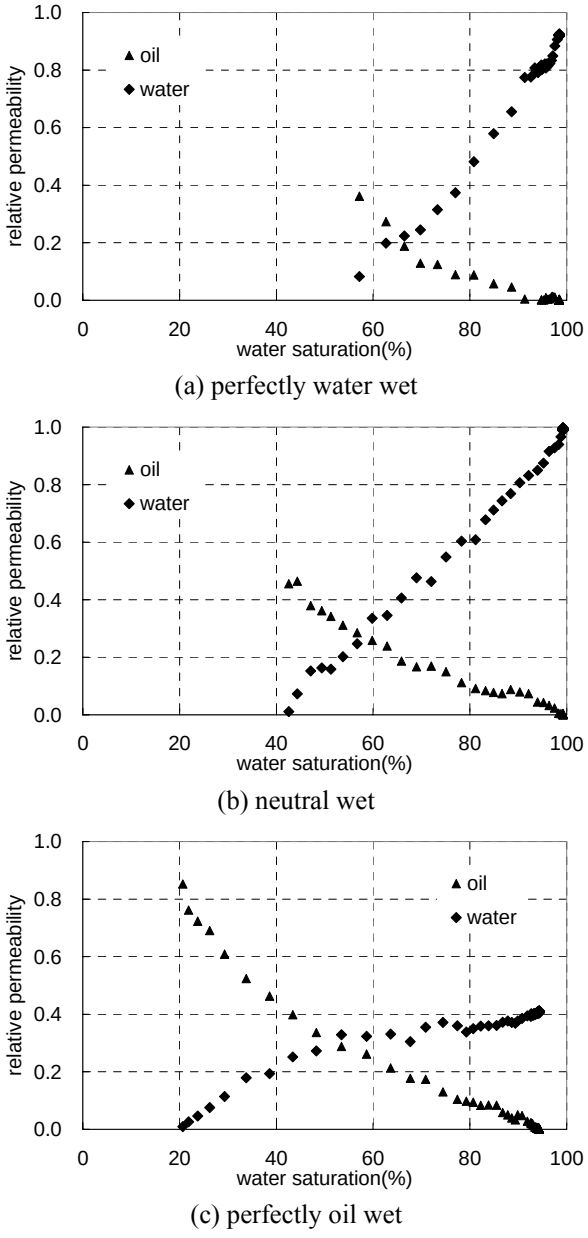


**Fig.12** The relative permeability curves of each wettability condition.

**b) Effect of interfacial tension on relative permeability**

The effect of the interfacial tension on the relative permeability was secondly investigated. We set the value of interfacial tension controlling coefficient, $A$, 1/10 of the base case, and performed the water flooding simulation to the cases of perfectly water wet and the perfectly oil wet. The pressure gradient and viscosity ratio are the same with the previous simulations.

Although the flow pattern of the both cases of the wettability is almost the same with the base case of the interfacial tension, the formed oil islands become smaller in the case of the perfectly water wet and the water invades into the smaller aperture regions in the case of the perfectly oil wet by reducing the interfacial tension. The residual oil saturation decreases in the both cases of the wettability. The residual oil saturation is 0.04% to the perfectly water wet and 4.2% to the perfectly oil wet.

The relative permeability curves are shown in **Fig.13** to each case of the wettability. In the both cases of wettability, the relative permeability curves approach the straight line which is shown in **Fig.3**. This is probably because the capillary effect becomes small and the flow behavior of the both fluids becomes independent of the aperture distribution.

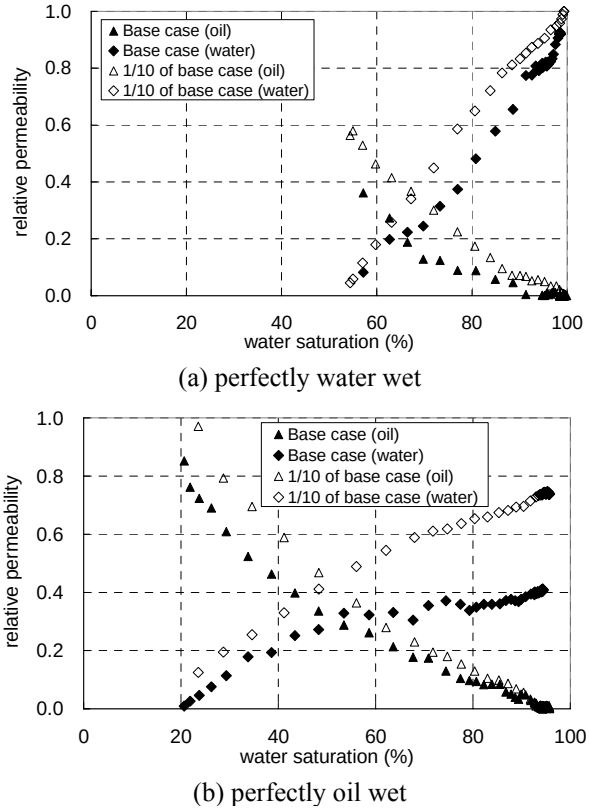


**Fig.13** The change of relative permeability curves due to the decrease of interfacial tension.

## 4. CONCLUSION

Multi-phase flow behavior is simulated by the LBM used in the study, and the relative permeability of oil and water for the single fracture is estimated.

As a result of the water flooding simulation in the fracture having a complex topography of surface, residual oil is observed clearly.

In the case of perfectly water wet surface, the residual oil is remained in isolated droplet shape from the flow path of water phase.

In the case of perfectly oil wet surface, the residual oil is remained at the small aperture region around the surface contact region.

The fracture relative permeability curves of oil and water are not the straight lines but the curves whose shape depend on the wettability of the fracture surface and interfacial tension between oil and water.

The water relative permeability curve concaves downward when the wettability is perfectly water wet , and it concaves upward when the wettability is perfectly oil wet.

The relative permeability curves of oil and water approach a straight line regardless of the wettability when the interfacial tension between oil and water is reduced.

**ACKNOWLEDGMENT:** We would like to appreciate JOGMEC's support and Dr. Murata's technical supervision to this study and the permission to submit this paper.

**REFERENCES**

1) Roberto Aguilera : Naturally Fractured Reservoirs, pp.1-2, 1980.
2) N. Watanabe, Y. Osaki, Y.Thuchiya, T. Tamagawa, N. Hirano, H. Okabe, N. Thuchiya, Analysis of fracture flow by numerical modeling coupled with X-ray CT computed tomography, Japan Geoscience Union Meeting 23-28 May 2010 (Japanese)
3) Rossen, W. R., and Kumar, A. T. K., 1992, Single- and two-phase flow in natural fractures, Proc. of the 67th SPE ATC, paper SPE-24195.
4) Persoff, P., and Pruess, K., 1995, Two-phase flow visualization and relative permeability measurement in natural rough-walled rock fractures, Water Resour. Res., 31(5), p. 1175-1186.
5) Iwai, T., and Tosaka, H., 2003, Laboratory measurement of relative permeability of air-water two-phase flow in a single fracture (in Japanese), Shigen-to-Sozai, 119., p. 593-598.
6) Speyer, N., Li, K., and Horne, R., 2007, Experimental measurement of two-phase relative permeability in vertical fractures, Proc. of 32nd workshop on geothermal reservoir engineering Stanford University, SGP-TR-183.
7) Youngseuk Keehm :COMPUTATIONAL ROCK PHYSICS: TRANPORT PROPERTIES IN POROUS MEDIA AND APPLICATIONS, pp.12-21, 2003.
8) Grunau, D., Chen, S. and Eggert, K., 1993, A lattice Boltzmann model for multiphase fluid flows, Phys. Fluids A, 5(10), p. 2557-2562.
9) Brown, S. R., and Scholz ,C. H., 1985, Broad bandwidth study of the topography of natural rock surfaces. J. Geophys. Res., 90, p. 12575-12582.
10) Power, W. L., and Tullis, T. E., 1991, Euclidean and fractal models for the description of rock surface roughness, J. Geophys. Res., 96, p. 415-424.
11) Glover, P. W., J., Matsuki, K., Hikima, R. and Hayashi, K., 1997, Fluid flow in fractally rough synthetic fractures, Geophys. Res, Lett., 24, p. 1803-1806.

2010 AIT-KU JOINT SYMPOSIUM ON HUMAN SECURITY ENGINEERING

Bangkok, Thailand, November 25-26, 2010

# Effective Utilization of CO2 for Oil and Gas Field Development in Vietnam

S. Takagi , Y. Suehiro, K. Katakura, H. Okabe, H. Mitsuishi[1]
Phan Ngoc Trung, Nguyen Huu Trung, Nguyen Hai An, Nguyen Manh Hung[2]

1. Japan Oil, Gas and Metals National Corporation (JOGMEC)
2. Vietnam Petroleum Institute (VPI)

In southern Vietnam, there has continued to increase number of industrial plants, which are becoming the large amount of CO2 emission sorces. Some offshore CO2 gas fields have already been developed by separating CO2 from the produced gas and more offshore CO2 contained gas fields are waiting for the development. Through these activities, CO2 emission will be more and more increased and its immediate reduction has to be considered from environmental protection point of view. It is apparent to take this action in quicker manner. JOGMEC and VPI have been cooperated to tackle this issue through the joint studies since 2007. CO2 EOR application to the oil field(s) will increase oil production as well as contributing CO2 sequestration by transporting CO2 from industrial plants or CO2 contained gas field. In addition, unique Japan technology of Gas To Liquid (JAPAN-GTL) can handle CO2 directly to produce liquid from produced gas including CO2 without separating CO2. An integrated design of CO2 related development is overviewed in the paper.

***Key Words :*** *Offshore Vietnam, CO2 Emission Reduction, CO2 EOR, JAPAN-GTL*

## 1. INTRODUCTION

Japan Oil, Gas and Metals National Corporation (JOGMEC) specializes in technology related to oil and natural gas exploration and development as shown in Fig.1, and deploys its expertise to find solutions to technical problems at oil and gas fields operated by Japanese companies. JOGMEC also collaborates on projects globally, having technical partnerships with oil- and gas-producing countries. JOGMEC develops the basic and advanced technologies necessary for these solutions, and provide the technologies and the latest technical information to private industry.

From 2007, JOGMEC, Vietnam Oil and Gas Group (PVN) and Vietnam Petroleum Institute (VPI) have been cooperated in the technical studies intensively for EOR and Gas utilization technologies. Those technologies are aimed to develop the oil and gas fields considering the reduction of CO2 emission. The paper separeately focuses on the CO2 EOR and GTL, however, the integration is considered since both technologies can be combined well for the effective utilization of CO2.

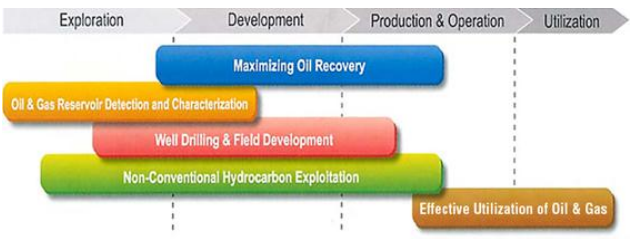


**Fig.1** JOGMEC Current Technology Area

## 2. FEASIBILITY STUDY ON CO2 EOR APPLICATION TO OFFSHORE VIETNAM OIL FIELD

In one of the oil field producing from sandstone reservoir, JOGMEC started CO2 EOR study in 2007 as the joint study among JOGMEC, PVN (VPI) and JX Nippon Oil & Gas Exploration Corporation and completed in 2010.

The target reservoir is characterized as a thin-layered sandstone with the depth of 2,100 mss and 50m gross thickness. Structure map is shown in Fig. 2. Average reservoir permeability is in the range of several tens of md with wide variety from several md to thousands md. Average porosity is about 25%. Initial reservoir pressure is 3,100 psi with the oil gravity of 38°API. Since water injection has been started step by step, the reservoir pressure has not been increased field-wide yet and the current reservoir pressure has depleted in the range of 2,000 - 2,500 psi. The field operator is planning to expand the number of water injectors to sweep oil and to increase reservoir pressure for preparing possible gas flooding (i.e. CO2 EOR).

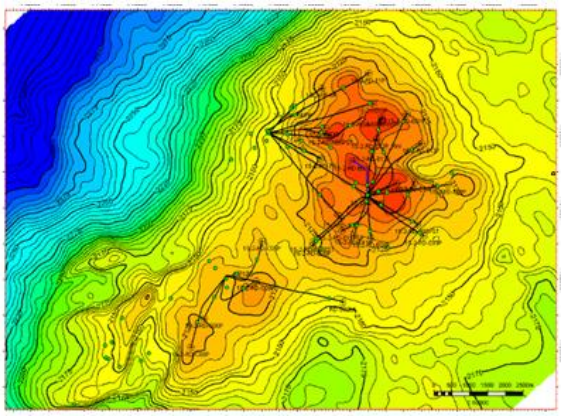

**Fig. 2** Study Target Reservoir Map

The success of CO2 EOR project relies on the following several key issues;

- Reliable Reservoir Simulation Model
- MMP (Minimum Miscible Pressure) and Core Flood Test
- Evaluation of Field Incremental Recovery Factor (Vertical and areal sweep efficiency)
- CO2 injection related cost and economics

The above four technical issues have been studied in detail and described below.

(a) Reliable Reservoir Simulation Model:

Black oil (Oil – Gas – Water immiscible system) reservoir simulation model has been constructed by upscaling the geological model. After tuning the reservoir parameters, mainly permeability distribution has been reviewed and modified by the careful investigation of porosity-permeability correlation, reasonable history matching has been achieved. Fig. 3 shows the geological model in the representative layer and Fig. 4 shows the history matching results.

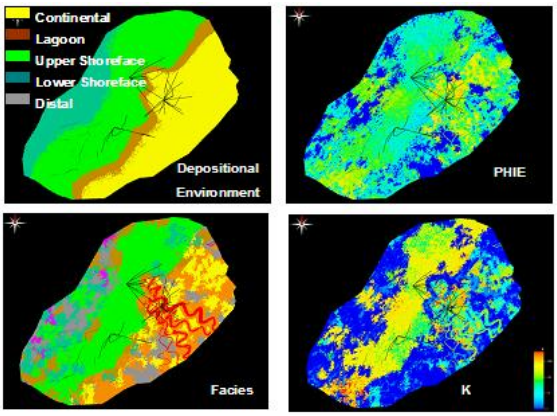


**Fig. 3** Geological Model

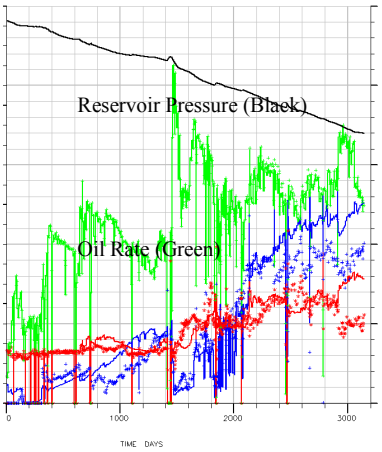


**Fig. 4** History Matching Results

(b) MMP (Minimum Miscible Pressure) and Core Flood Test:

A series of laboratory study was conducted to obtain reservoir Oil-CO2 interaction function by using recombined oil from fresh surface samples. Conventional PVT test, slimtube test, solubility swelling test, core flood test and interfacial tension measurement were conducted mainly at the Technology Research Center (TRC) of JOGMEC.

- Slimtube test for MMP Measurement

Slim tube is composed of the long pipe (4.6 mm diameter and 12.2 m length) with packed beads.

Porosity is around 37% with 9 Darcy of Permeability (Refer to Fig. 5). Before injecting CO2, Slim tube is filled with reservoir fluid. By maintaining the target pressure, the recovery factor is plotted at 1.2 pore volume of CO2 injection as shown in Fig. 6. In addition, the fluid flow condition is visually monitored at the sight cell. By measuring oil recovery at several points of pressure, pressure-oil recovery cross plot is created as shown in Fig. 6. At the pressure above MMP, oil recovery does not increase any more as miscible condition achieved. The MMP is estimated by the bending point in Fig. 6.

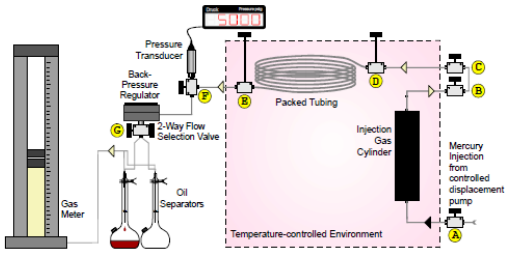


**Fig. 5** Apparatus of slimtube test

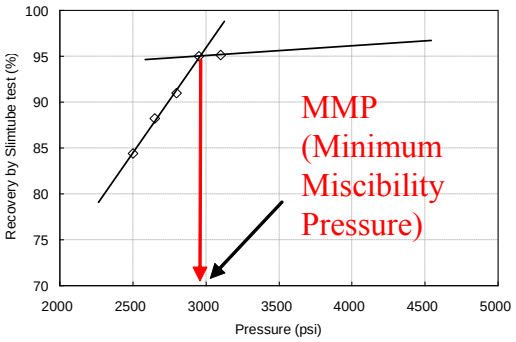


**Fig. 6** Slimtube Test Results

Separately from Slim tube test, Interfacial Tension between reservoir fluid and CO2 was measured to compare MMP. Slimtube test results and Interfacial tension (IFT) measurements were plotted in the same figure as a function of the pressure in Fig. 7, which indicated the similar MMP. By this comparison, the MMP is believed to be more reliable.

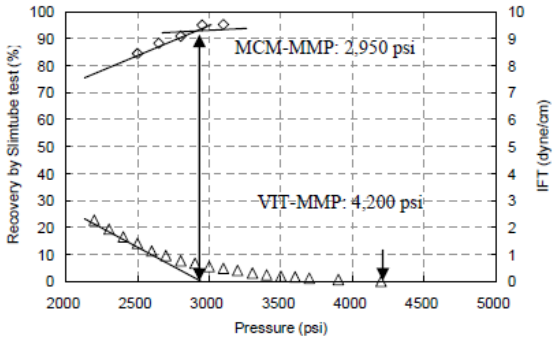


**Fig. 7** Comparison of Slimtube Test and IFT Measurement in terms of Minimum Miscibility Pressure (MMP) estimation.

- Core flood test

In order to estimate the recovery factor at the heterogeneous reservoir rock, the the core sample taken from the field has been flooded by CO2 after careful examination of the cores by X-ray CT scan (to examine whether fracture or damage inside or not). Core flood test by CO2 was conducted from the top of the composite core with the injection rate of 0.1 cc/mins in order to minimize the effect of the gravity. The results showed more than 85 % of core scale (micro-scale) recovery factor by CO2 injection (93.1% by secondary mode and 88.6% by tertiary mode). By this study, more realistic oil recovery efficiency has been measured, but still at the core scale evaluation.

(c) Evaluation of Field Incremental Recovery Factor (Vertical and areal sweep efficiency)

In order to evaluate incremental recovery factor by CO2 injection in this field, we have to rely on the reservoir simulation technique including reservoir fluid-CO2 physics. This reservoir fluid-CO2 compositional modeling technique is called as EOS Modeling. For the Equation Of State (EOS) modeling, the Peng-Robinson EOS method (1978) was used.

After the parameter tuning, the EOS simulation results successfully matched with experimental data of constant composition expansion, differential liberation, separator test, viscosity measurement, CO2 swelling test, and CO2 slim-tube test. For the CO2 slim-tube test, comparison between the measured and the calculated is shown in Fig. 8; oil recovery at 1.2 PV-injected for each pressure setting is plotted (A sufficiently good match was attained).

**Fig. 8** Comparison of Slimtube Test and EOS model simulation

The plane view of the grid system for the simulation model is shown in Fig. 9. The model is com-

posed of 97 x 116 x 40 (corresponding to divisions in the x, y, and z directions) grid-blocks.

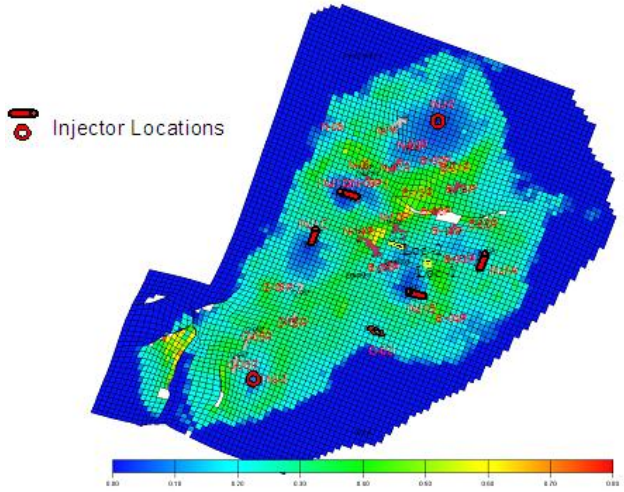


**Fig. 9** Simulation Model and Injector Location

The well locations for the base case of CO2 injection are shown in Fig. 9. Simulation settings are summarized as follows.

- The number of CO2 injectors : 6
- CO2 and Water Injection : 3-month CO2 injection, then 6-month water injection as 1 cycle
- CO2 injection period : total 7.5 years

Before CO2 injection, water injection is planned to raise the reservoir pressure for 3 years since a higher reservoir pressure promotes the development of miscibility or near-miscibility with CO2. The field total CO2 injection rate is planned to be 52 MMSCF/D (about 2,700 ton/d) and all produced CO2 is to be recycled to minimize CO2 emission to the atmosphere.

The calculated oil production performance by CO2 injection case is shown in Fig. 10, compared with that of waterflood case. Fig. 11 shows the change of oil saturation distribution at a layer of the model in simulation. In this figure, it is clearly observed oil around CO2 injector is swept well by CO2 injection.

CO2 injection brought a field cumulative oil production equivalent to 42% of OOIP. CO2 injection project is summarized as follows.

- Total CO2 Injection : 7.5 million ton (8 years)
- Oil Recovery Increment against Waterflood : 8%

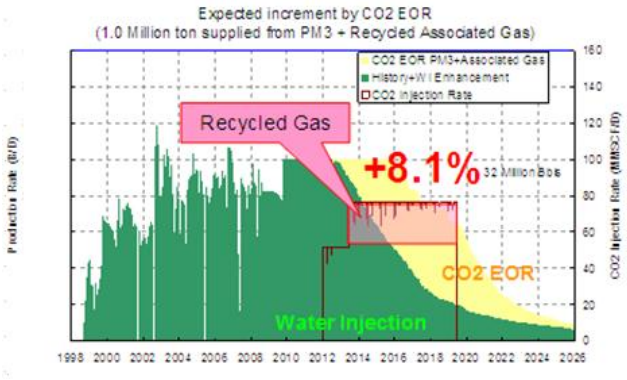


**Fig.10** Field oil production forecast by waterflood and CO2 WAG (Base Case)

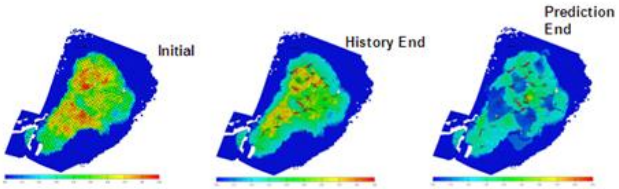


**Fig. 11** Change of oil saturation distribution in CO2 Injection Case

(d) CO2 injection related cost and economics

In order to inject sufficient amount of CO2 into the reservoir in the offshore field, a site survey of CO2 sources was carried out by visiting cement plant, power plants and fertilizer plant. Separately from the industrial plants, a gas field with CO2 was also nominated as a CO2 source. As a result, some of the visited industrial plants seemed not suitable due to the distance (the cement plant is over 300 km away from the field), low concentration of CO2 (CO2 concentration of power plant is 3% only) and insufficient volume of CO2 availability. Finally, two CO2 sources were selected for the preliminary feasibility study. One is the gas field with separated CO2 emitted to the atmosphere, which is far from the field (over 500 km CO2 transportation pipeline is required) and the other is the fertilizer plant.

In order to receive/inject CO2 and to protect from corrosion by breakthrough CO2, new platform with CO2 compressor and CO2 treatment system is considered to be required nearby current facility. Produced CO2 rich associated gas is assumed to be recycled without CO2 capture process (re-injection and no CO2 emission). Their rough costs including CO2 Capture/Transportation, new platform and well drilling/workover are estimated in the order of 700 – 1,000 MMUS$.

(e) Current Situation and Further Plan

Through this study, it is concluded the technical feasibility is very high, dependent on the field pilot test results, however, economical feasibility seems not so high due to the cost. All the joint study party including PVN is considering the importance of the field pilot test as well as economics improvement. As a next step, a field pilot test is planned in this field to evaluate the effectiveness in the real field application and the expansion of CO2 EOR application not only to this field but to the surrounding filed(s) to share CO2 injection/treatment cost each other.

## 3. APPLICABILITY STUDY ON JAPAN-GTL TECHNOLOGY TO OFFSHORE VIETNAM GAS FIELD

There are several gas field development methods to be selected, i.e. transportation of the gas to the onshore to be used as a city gas or power/chemical plants and LNG. Recent years, GTL (Gas to Liquid) technology has been studied and applied worldwide by several different methods. GTL is one of the emerging gas technologies, with which natural gas as a raw material can be converted into petroleum products. It is an extremely effective method to gain alternative fuel sources to petroleum and achieve the diversification of primary energy supplies. Besides, GTL has a variety of advantages: e.g.; it is available to monetize stranded gas reserves and contribute flaring reduction for upstream business and it has environmental advantages such as sulfur/aromatic free and realizes efficient performance of diesel engines due to very high Cetane Number and furthermore enables to utilize the existing infrastructure and facilities for downstream business. It is known GTL is anticipated to increase the share of Global Liquid Production in the future as shown in Fig. 12.

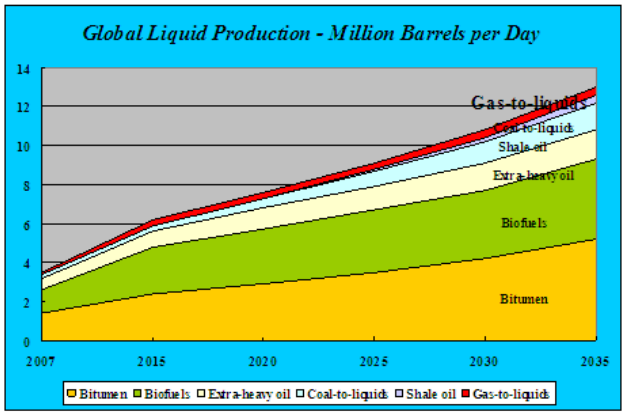


**Fig.12** Global Liquid Production (2007 – 2035) from International Energy Outlook 2010

(1) JAPAN-GTL Technology

JOGMEC has been tackling the research and development of the natural gas conversion technology since 1998. JOGMEC made the "Joint Research Contract" with Nippon GTL Association established by six private firms in 2006, following the Yufutsu Pilot Test Project (2001 to 2004), in order to conduct the Demonstration Project (500BPD) scheduled 5 years with an eye toward potential international gas field development with the capacity of 15,000 to 20,000 BPD per train (refer to Fig. 13)

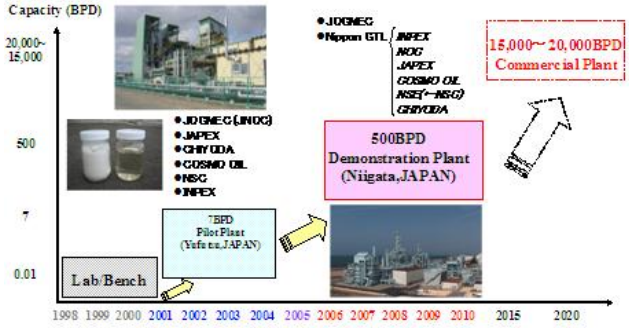


**Fig.13** JAPAN-GTL History of R&D Activities

The construction of the JAPAN-GTL Demonstration Plant in Niigata (refer to as "Demonstration Plant") was completed in March 2009 and it has been in operation since 16th April 2009. The production of 500 barrels (about 80 kiloliters) per day was achieved.

The JAPAN-GTL process contains three core processes as shown in Fig.14: synthetic gas production section (refer to as "Syngas"), FT (Fischer-Tropsch) production section (refer to as "FT") and Upgrading (hydrocracking) section (refer to as "UG"), which equip with proper catalysts developed by Chiyoda, Nippon Steel Eng. and NOE (formerly known as NOC), respectively. They have been tested in the Demonstration Plant. Naphtha, Kerosene and Gas Oil are produced from natural gas including CO2.

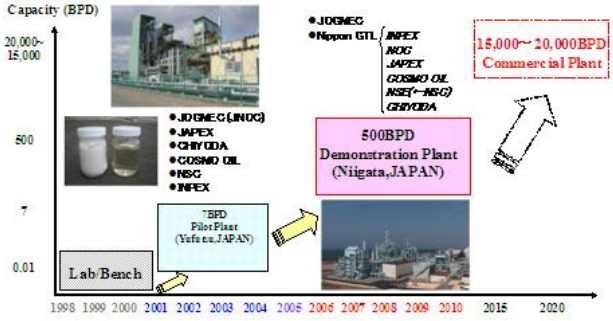


**Fig.14** Characteristics of JAPAN-GTL Process

(a) Technical and Cost Advantages of JAPAN-GTL Process

Steam/CO2 reforming in the Syngas reformer is one of particularities of JAPAN-GTL process as appears in Fig. 14, which illustrates main distinction between JAPAN-GTL process and conventional GTL processes. The Syngas Reformer efficiently uses CO2 included in the natural gas feedstock and it enables to produce Syngas, which consists of H2 and CO with the composition molar ratio of H2/CO=2/1. Thus, JAPAN-GTL process is capable to utilize CO2 contained in the natural gas directly and does not require any O2 supply. In summary, the characteristics of JAPAN-GTL process in contrast to those of the existing ones using ATR or POx are (1) no use of the O2 generator, (2) no use of the CO2 removal unit, and (3) no use of the H2 conditioning unit for Syngas. The Syngas will be introduced to the subsequent FT Reactor to convert it to GTL production oil.

GTL product is light oil and heavy oil. Fig. 15 shows samples of produced at Yufutsu GTL pilot plant. The analyzed property of light oil shown in Table 1 demonstrated that they are super clean fuels, because of no sulfur and no aromatic contained.

**Fig.15** Produced Heavy Oil (Left) and Light Oil (Right) by Yufutsu GTL Plant

**Table 1** Property of Light Oil

| Item | | A | B |
|---|---|---|---|
| Density | 15℃, g/cm$^3$ | 0.7566 | 0.7525 |
| Kinematic Viscosity | 30℃,mm$^2$/s | 1.853 | 1.616 |
| Distillation | 10%, ℃ | 131.0 | 129.5 |
| | 50%, ℃ | 221.0 | 207.5 |
| | 90%, ℃ | 302.0 | 286.5 |
| Aromatic | mass ppm | <1 | <1 |
| Sulfur | mass ppm | <10 | <10 |

(b) JAPAN-GTL Advantage in terms of CO2 Emission

As for CO2 emission, JAPAN-GTL has more advantage than the existing GTL technologies.

Fig. 16 shows the comparison of CO2 emission by the different technologies.

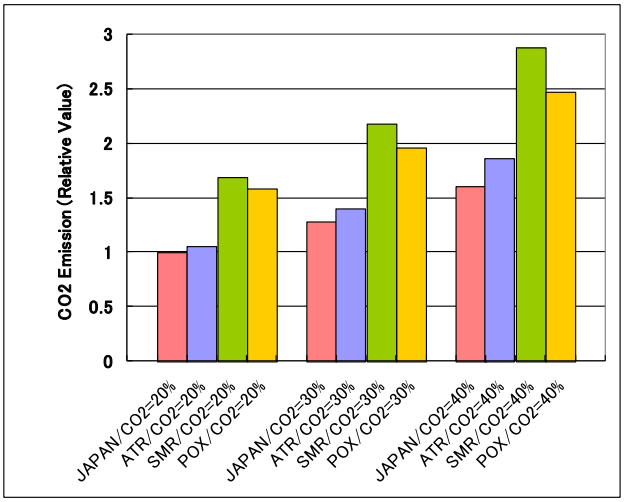


**Fig.16** Comparison of CO2 emission

In this figure, the amount of CO2 emission expresses the relative values to the JAPAN-GTL for CO2 20% case. As clearly seen in this figure, JAPAN-GTL has the smallest CO2 emission compared with SMR, ATR, and POX in all the cases. Especially, more CO2 case has much less CO2 emission than the other methods.

(2) **Joint Study on the Applicability of JAPAN-GTL Process to Offshore Vietnam Gas Field**

Preliminary Feasibility Study has been conducted from 2007 to 2009 among JOGMEC, PVN and VPI.

The aim of the study is to clarify the availability of JAPAN-GTL process to offshore gas fields in Vietnam. As specific offshore gas fields were not nominated in the study, JOGMEC assumed applying imaginary offshore gas field in Vietnam as the target gas field by the following assumptions.

- Distances from shore (50, 100 and 150km) and water depths (50, 100 and 200m)
- GTL Plant capacities (7,500, 15,000 and 30,000BPD)
- CO2 contents (0, 20 and 40%)

As a result, it was concluded JAPAN-GTL will be a candidates to apply to Vietnam offshore gas field. Further detailed feasibility study for a specified gas field is planned.

## 5. CONCLUSIONS

- JOGMEC and VPI have been jointly conducting studies on CO2 EOR and JAPAN-GTL technologies.

- The field pilot test of CO2 EOR is planned in

southern Vietnam offshore oil field before field-wide application. CO2 EOR project is considered to be environmental-friendly technology by increase oil production as well as reducing CO2 emission, however, this project seems sub-economical due to huge investment for CO2 separation/transportation and corrosion protection for the field.

- JAPAN-GTL technology is potentially an application technology for stranded CO2 contained offshore gas field in Vietnam. This technology seems to have environmental advantages by utilizing CO2 directly for GTL process up to 40mol%.

- JOGMEC and VPI are considering the emerging technologies of CO2 EOR and JAPAN-GTL to develop Vietnam offshore oil/gas fields as well as CO2 reduction technologies. The integration of the technologies can contribute the effective utilization of CO2.

**ACKNOWLEDGMENT:**

We would like to take this occasion to express our sincere gratitude to PVN, VPI, JOGMEC and JX NOEX, who performed great efforts to the Collaborative Study from 2007 to 2010 and gave us the permission to submit the paper.

**REFERENCES:**

(1) Danesh, A., 1998; "PVT AND PHASE BEHAVIOR OF PETROLEUM RESERVOIR FLUIDS", DEVELOP- MENTS IN PETROLEUM SCIENCE 47, Elsevier Ltd.

(2) Baljit S. S., Scott M. F. and Akanni S. L., 2001; "Analysis of Factors Affecting Microscopic Displacement Efficiency in CO2 Floods", SPE 70022

(3) Lake, L. W., 1989: "Enhanced Oil Recovery", Prentice- Hall Englewood Cliffs, NJ.

(4) Rao D.N., Lee J.I.: "Evaluation of Minimum Miscibility Pressure and Composition for Terra Nova Offshore Project Using the Vanishing Interfacial Tension Technique", Society of Petroleum Engineers (SPE) 59338, Louisiana State University, Petro-Canada Oil and Gas

(5) Stern D., 1991,:"Mechanisms of Miscible Oil Recovery: Effects of Pore-Level Fluid Distribution", SPE 22652

(6) Kawahara.Y., An.N.H, Hung.N.M., Ueda.Y., Mitsuishi.H., Takagi.S., Okabe.H., Trung.P.N.: "Comprehensive CO2 EOR Study - Study on Applicability of CO2 EOR to Block 15-2, Offshore Vietnam, Rang Dong Field - Part I Laboratory Study, Articles for "PETROVIETNAM Journal", 2009

(7) Matsumoto.Y., Long.N.H., Thanh.D.A., Ueda.Y., Uchiyama.T., Kawahara.Y., Mitsuishi.H., Takagi.S., Okabe.H., Binh.C.H.: "Comprehensive CO2 EOR Study - Study on Applicability of CO2 EOR to Block 15-2, Offshore Vietnam, Rang Dong Field - Part II Compositional Simulation Study", Articles for "PETROVIETNAM Journal", 2009

(8) Coats, K.H.: "An Equation of State Compositional Model", paper SPE 8284, Oct. 1980.

(9) Takagi S., Mitsuishi H.,Okatsu K., Okabe H., Kawahara Y., NguyenVan Toan, Phan Ngoc Trung , Ueda Y. and Uchiyama T.: "International Joint Study on CO2-EOR - Study on Applicability of CO2-EOR to Rang Dong Field, offshore Vietnam", IEA Collaborative Project on Enhanced Oil Recovery, 30th Annual Workshop and Symposium, 21-23, September, 2009, Australia

(10) Suehiro, Y.: "Development of JNOC GTL technology", JAPT, vol.68, No.6, 2003 (in Japanese).

(11) Suehiro, Y., Ihara, M., Katakura, K., Nakamura, A., Sakamoto, A., Kawazuishi, K., Kajiyama, R., Fujimoto, KI. , Ohnishi, Y., Okado, H., Simizu, T.: "New GTLProcess – Best Candidate for Reduction of CO2 in Natural Gas Utilization-", SPE88628, 2004

(12) Shimura, M., Yagi, F., Nagumo, A., Wakamatsu, S., Suzuki, S.: "Development of a new H2O/CO2 Reforming Catalyst and Process for natural gas utilization", ACS Div. Petro Chem Prepr. 47(4), 363, 2002.

(13) Yagi, F., Wakamatsu, S., Kanai, R., Kajiyama, R., Suehiro, Y., Shimura, M., "Development of Synthesis Gas Production Catalyst and Process", ACS Div. Fuel Chem Prepr. , 49(2), 652, 2004.

(14) Fujimoto, KI. , Suzuki, K., Kageyama, M., Ohnishi, Y., Yamane, N., Jitsuhara, I., Suehiro, Y.: "Development of high-performance F-T synthesis catalyst and demonstrative operation of a pilot plant with the catalyst by JOGMEC-GTL project in Japan", ACS Div. Fuel Chem Prepr. 49(2), 710, 2004.

2010 AIT-KU JOINT SYMPOSIUM ON HUMAN SECURITY ENGINEERING

Bangkok, Thailand, November 25-26, 2010

# Projection of River Discharge in Thailand under Climate Change and its Impact on Water Resources

Yasuto TACHIKAWA[1], P. B. HUNUKUMBURA[2], Kazuaki YOROZU[3], and Somkiat APIPATTANAVIS[4]

[1]Associate Professor, Department of Civil and Earth Resources Engineering, Kyoto University
(C1-116, Kyoto University Katsura Campus, Nishikyo-ku, Kyoto 615-8540, Japan)
E-mail: tachikawa@hywr.kuciv.kyoto-u.ac.jp
[2]Research Associate, Department of Civil and Earth Resources Engineering, Kyoto University
(C1-116, Kyoto University Katsura Campus, Nishikyo-ku, Kyoto 615-8540, Japan)
E-mail: hunu@hywr.kuciv.kyoto-u.ac.jp
[3]Assistant Professor, Department of Civil and Earth Resources Engineering, Kyoto University
(C1-116, Kyoto University Katsura Campus, Nishikyo-ku, Kyoto 615-8540, Japan)
E-mail: yorozu@hywr.kuciv.kyoto-u.ac.jp
[4]Researcher, Office of Research and Development, Royal Irrigation Department
200 Tivanon Road, Pakkred, Nonthaburi 11120, Thailand
E-mail:skavis@yahoo.com

The impact of climate change on river flow in Thailand is analyzed by feeding future climate projection data into a distributed rainfall-runoff model. The projection data used consists of daily hydrologic data downscaled by hourly precipitation for the present climate (1979-2003), the near future climate (2015-2039), and the future climate (2075-2099), which were simulated by a 20km spatial resolution general circulation model (MRI-AM20km) developed by the Meteorological Research Institute, Japan Meteorological Agency. It is found that a change of river flow appears at the tributaries of the Chao Phraya River. The change pattern differs according to location, and it is expected to decrease of water resources at the Pasak River basin. Thus, we develop a water resources assessment model at the Pasak River basin, which includes a distributed hydrologic model, a dam reservoir water storage prediction model, and a plant growth model for rice production assessment.

***Key Words :*** *Thailand, Chao Phraya River, Pasak River, water resources, climate change, river flow, rice production*

## 1. INTRODUCTION

Global warming will give us a serious impact on our life. Frequencies and magnitudes of floods and sedimentation disasters are predicted to increase due to the change of precipitation extremes. The IPCC, the Intergovernmental Panel on Climate Change, 4th assessment report (WG1, WG2; 2007) describes increase of global average surface temperatures, and potential increase of frequency of heavy rainfall, and so on based on long term observations. The report also shows the projections of climate change ac-

cording to several greenhouse gas emission scenarios and the impacts of climate change on water-related disasters and water resources.

To cope with water-related disasters induced by climate change, both mitigation measures and adaptation measures are essential. For adaptation measures, prediction of future water resources is a key issue. In this paper, a distributed hydrologic model of the Chao Phraya River basin is developed. Then, future river discharge is projected using the latest GCM output to detect the hotspots of river discharge change. It is found a change of flow characteristics at the tributaries of the Chao Phraya River, and water resource at the Pasak River basin is decreased. Thus, we develop a water resources assessment model at the Pasak River basin, which includes a distributed hydrologic model, a dam reservoir water storage prediction model, and a plant growth model for rice production assessment.

## 2. DISTRIBUTED HYDROLOGIC MODEL

### (1) Watershed model

The topography of the catchment is modeled using the eight direction method which assumes the flow direction one-dimensionally to the steepest gradient direction illustrated in Fig. 1. Each slope element determined by the flow direction is represented by a rectangle formed by the two adjacent nodes of grid cells. The watershed model is developed using a digital elevation model, DEM, included in HydroSHED, which cover the globe with about 100m spatial resolution. Figure 2 shows the delineated catchments of the Chao Phraya River basin (160,400km $^2$), Thailand using the DEM. The area, length, and gradient of each rectangular slope element used for runoff and channel routing are calculated according to the watershed model.

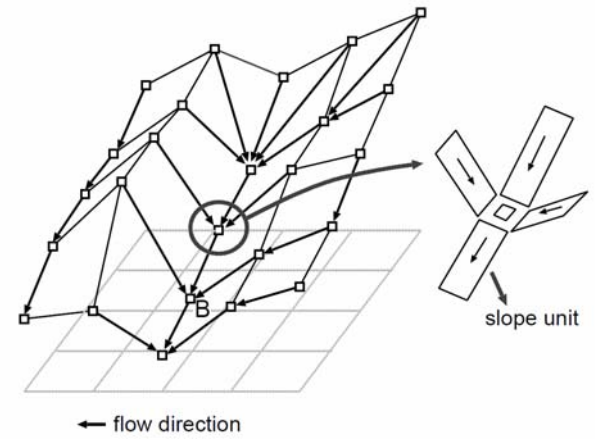


**Fig. 1** Schematic drawing of a catchment modelling using DEMs.

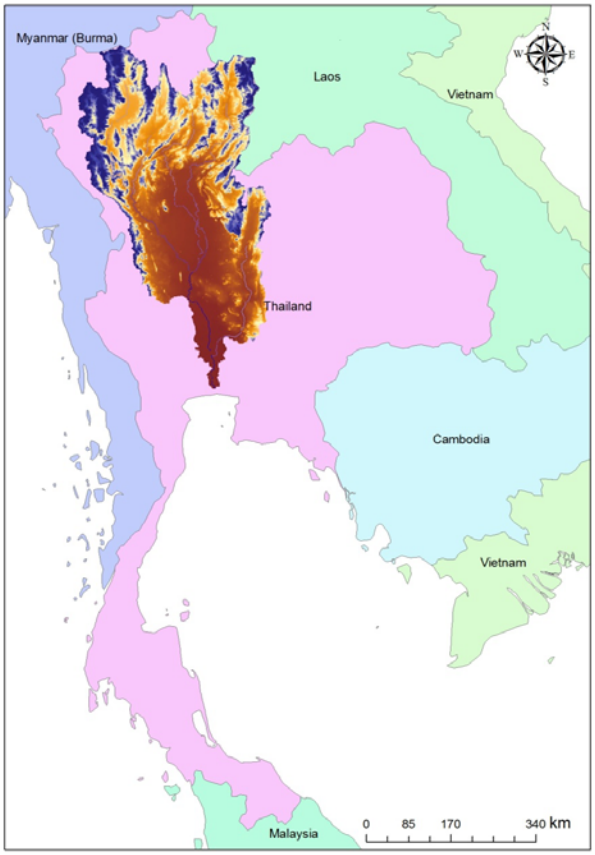


**Fig. 2** Chao Phraya River basin in Thailand derived from DEM.

### (2) Flow model

The kinematic wave model is applied to all rectangular slope elements to route the water to downstream according to the derived watershed model. The continuity equation for each rectangular slope element is:

$$\frac{\partial A}{\partial t}+\frac{\partial Q}{\partial x}=q(t) \qquad (1)$$

where $t$ is time; $x$ is distance; $A$ is cross-sectional area; $Q$ is discharge; and $q(t)$ is the lateral inflow per unit length of slope or channel given as runoff generation provided by MRI-AM20km. The Manning type relation of the discharge and the cross-sectional area:

$$Q=\alpha A^m, \quad \alpha=\frac{\sqrt{i_0}}{n}\left(\frac{1}{B}\right)^{m-1}, \quad m=5/3 \qquad (2)$$

is combined with the continuity equation to route the water, where $i_0$ is slope; $n$ is roughness coefficient; and $B$ is width of the flow. The slope $i_0$ is determined according to the watershed model. The model parameters of the flow model are $B$ and $n$. The value of $B$ is determined using the regression relationship $B=aS^c$, where $S$ is the catchment area, and $a$ and $c$ is constant parameters. The value of $n$ is determined to 0.03m$^{-1/3}$s when the size of the catchment is larger

than 250km $^2$ and 11.0m $^{-1/3}$s when sm aller than 250km$^2$. These values were tuned to reproduce the observed data at two different catchm ents and applied to all basins.

The flow model was applied to all catchments and 75 years runoff sim ulations were conducted. The simulated river discharge data of daily maximum and daily mean were stored for each day with about 1km spatial resolution.

## 3. GCM DATA USED FOR RIVER FLOW PROJECTION

The projection data used here is sim ulated by the general circulation m odel (MRI-AM20km ) developed by the Meteorological Research Institute in Japan. MRI-AM20km realizes 1920×960 of grid cells of about 20 km spatial resolutions (Kitoh *et al.*, 2009). The products of MRI-AM20km consists of various atmospheric and hydrologic variables of the present climate experim ent (1979-2003), the near future clim ate experim ent (2015-2039), and the future climate experim ent (2075-2099), which were simulated under the SRES A1B scenario.

The river discharge for the Chao Phray a River basins is predicted by feeding the future climate projection data into the 1km -spatial resolution distributed hydrologic model. The hy drologic projection variables related to river discharge is shown in Figure 3. The inputted data to the distributed hy - drologic model is daily surface runoff generation and daily sub-surface runoff generation data, which are simulated by the land-surface process m odel em - bedded in the MRI-AM20km.

The time-scale of daily runoff generation data is insufficient to reproduce the hourly flood peak discharge, thus it was downscaled using the time-series of hourly precipitation data of MRI-AM20km to add the same hourly distribution pattern into the daily surface runoff generation data. We confirm ed that river discharge simulation with the tim ely downscaled surface runoff generation and daily subsurface runoff generation data successfully reproduced almost sim ilar river discharge sim ulated by using hourly precipitation, daily snowmelt, daily evaporation and daily transpiraion (Takino *et al.*, 2010). Thus, the tim ely downscaled surface runoff generation data and daily subsurface runoff generation data were used as inputted data to the distributed hydrologic model.

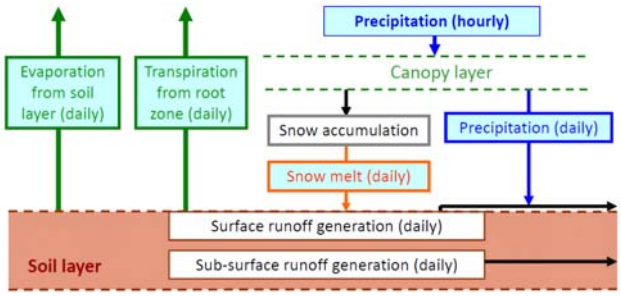


**Fig. 3** Hydrologic projection data provided by MRI-AM20km used for river discharge simulation.

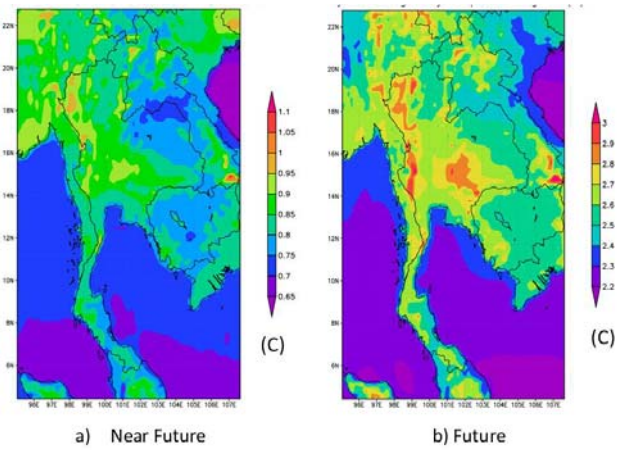


**Fig. 4** Change of the difference ofthe mean of the annual average daily temperature in near future and future clim ate with respect to the present climate.

## 4. CHANGE OF BASIC METEOROLOGI -CAL PARAMETERS

According to the MRI-AM20km projection data for the near future clim ate experim ent, the surface temperature found to increase roughly by 0.5 to 1 degree from the present tem perature whereas the temperature increased by about 2.5 to 3 degreesin the future climate. Figure 4 shows a spatial pattern ofthe change of the difference of the mean of the annual average daily temperature in the near future and the future climate experiment with respect to the present climate experiment.

Figure 5 shows a spatial pattern of the change of the percentage difference of the mean annual rainfall in the near future and the future climate experiment with respect to the present clim ate experiment. The percentage difference *PD* is obtained as

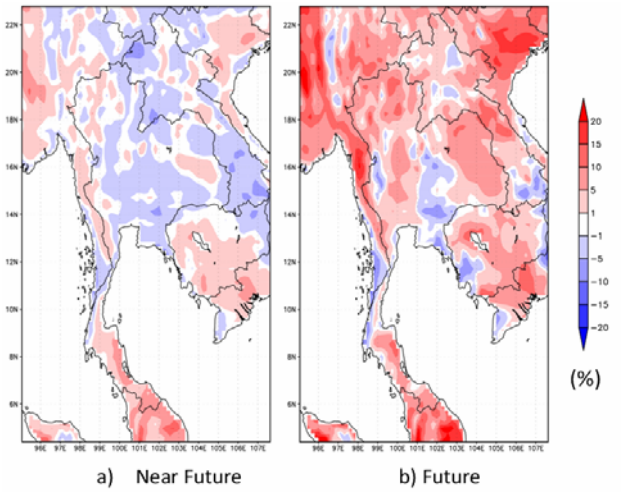


**Fig. 5** Change of the percentage difference of the mean annual precipitation in the near future and the future climate experiment with respect to the present climate experiment.

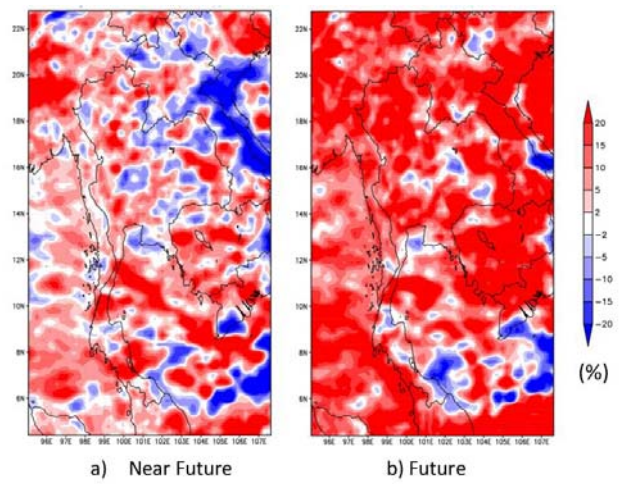


**Fig. 6** Change of the percentage difference of the mean annual maximum hourly rainfall in the near futureand the future climate experiment with respect to the present climate experiment.

$$PD = 100 \times \frac{r_f - r_p}{r_p} \qquad (3)$$

where $r_f$ is the annual mean precipitation in the near future or the future climate experiment and $r_p$ is the annual mean precipitation in the present climate experiment. 1% to 5% decreases of annual precipitation is observed in the central region of Thailand and 1% to 10% of increase inannual precipitation is observed in the southern region in the near future climate experiment. In the future climate conditions, it is expected to have 1% to 10% of increase in annual precipitation in the north mountainous region and 5% to 10% increase in the northeast region.

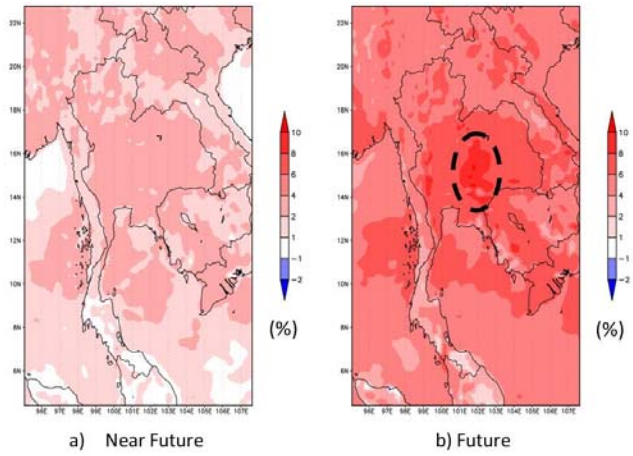


**Fig. 7** Change of the percentage difference of the mean annual daily potential evapotranspiration in the near future and the future climate experiment with respect to the present climate.

Figure 6 shows a spatial pattern of the change of the percentage difference of the annual maximum hourly rainfall in the near future and the future climate experiment with respect to the present climate experiment. It is observed that a clear increasing trend of the annual maximum hourly rainfall over Thailand for both time periods of the climate experiments. Notably, in the future climate experiment, about 20% increase of the annual maximum hourly rainfall in many parts of the region.

Figure 7 shows a spatial pattern of the change of the percentage difference of the mean annual daily potential evapotranspiration in the near future and the future climate experiment with respect to the present climate experiment. It is noticed that the potential evappotranspiration increase by 4% to 6% in the near future climate experiment and 4% to 10% in the future climate experiment.

## 5. IMPACT OF CLIMATE CHANGE ON RIVER FLOW REGIME

Runoff simulations of 75 years for the present climate experiment (1979-2003), the near future climate experiment (2015-2039), and the future climate experiment (2075- 2099) were conducted. Runoff simulation data of hourly maximum and daily mean are stored for each day with about 1km spatial resolution. The simulated discharge data were analyzed to discuss the change of the flood risk and water resources.

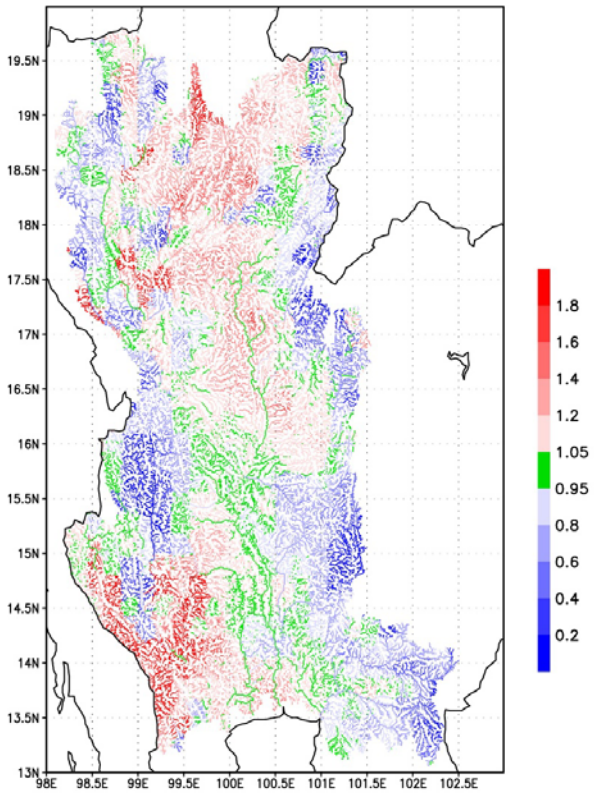


**Fig. 8** Change of the ratio of the mean of the annual maximum hourly discharge in the future climate experiment with respect to the present climate experiment.

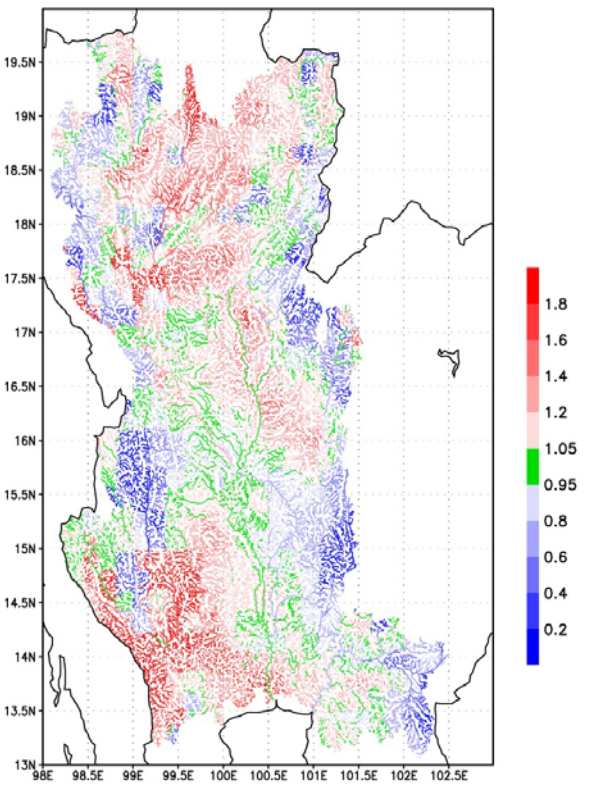


**Fig. 9** Change of the ratio of the 10-y ears return period river discharge in the future clim ate experim ent with respect to the present climate experiment.

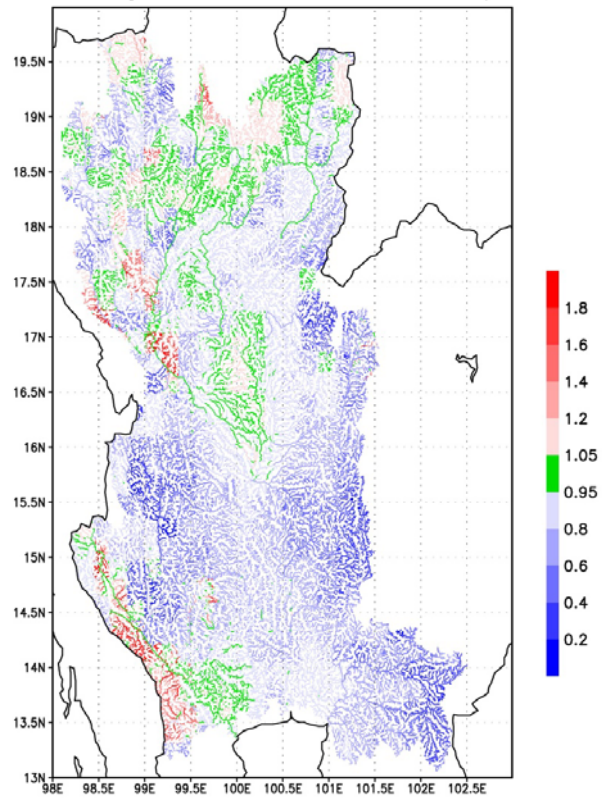


**Fig. 10** Change of the ratio of the mean October river discharge in the future clim ate experim ent with res pect to the pres ent climate experiment.

### (1) Change of flood

Annual maximum hourly discharge data was compiled and the statistical characteristics were analyzed. Figure 8 shows the changeratio of the mean of the annual maximum hourly discharge for the present climate experim ent and the near future climate experiment. Generally, the annual maximum discharge of the main stream of the Chao Phraya River does not change, however the one of the tributaries changes location to location.

Figure 9 shows the change ratio of the 10-year return period river discharge in the future clim ate experiment with respect to the future clim ate experiment using the Gum bel distribution. The spatial pattern is sim ilar to the change of the m ean of the annual m aximum river discharge. It is im portant to recognize that the change of the discharge would appear especially at the tributaries.

### (2) Change of water resources

Figure 10 shows the change ratio of the mean October dischar ge in the future clim ate experim ent with respect to the present clim ate experim ent. Generally, the m onthly dischar ge on October decreases in the middle and lower part of the Chao Phraya River basin.

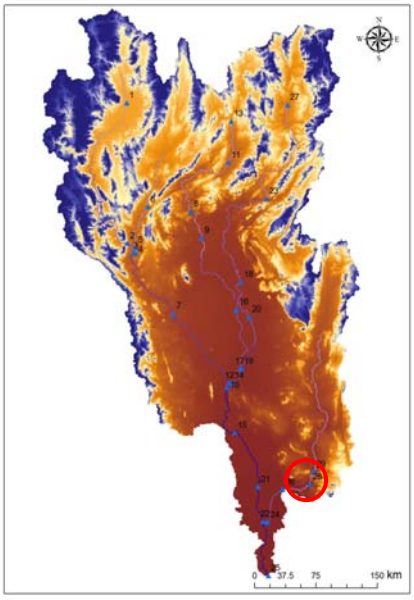


**Fig. 11** The location of the Pasak Dam reservoir which is located at the Pasak River, a tributary of the Chao Phraya River.

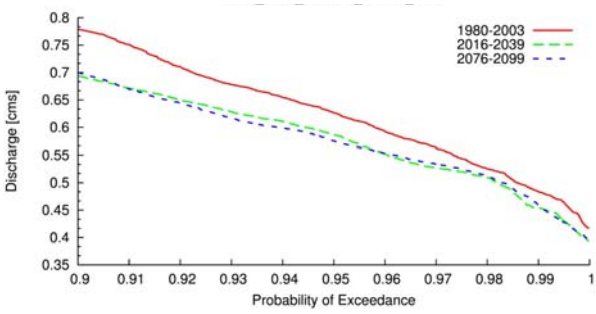


**Fig. 12** Change of the ratio of the mean October river discharge in the future climate experiment with respect to the present climate experiment.

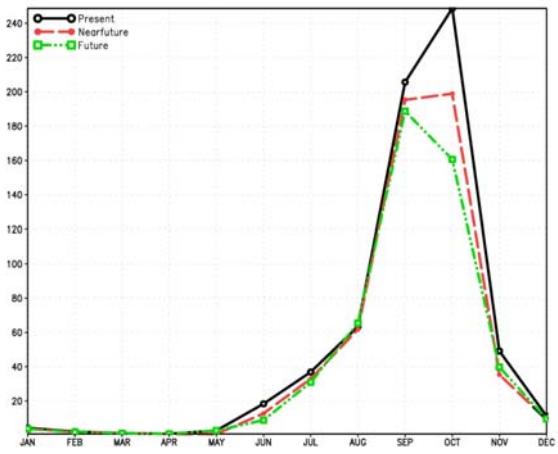


**Fig. 13** Change of the monthly discharge at the lower reach of the Pasak River.

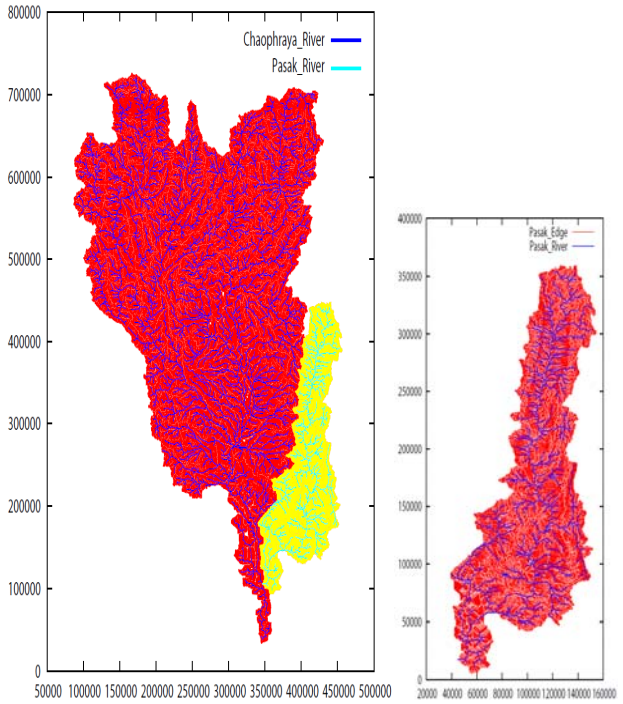


**Fig. 14** Detail topographic modeling using HydroSHED for a distributed hydrologic model. Left shows the entire Chao Phraya River basin and Right shows the Pasak River basin.

Figure 12 shows the last 10% daily flow duration curve for each 25 years climate experiment at the lower reach of the Pasak River shown in Figure11 in the red circle. The figure shows the decrease tendency of the low discharge at the area. Figure 13 shows the projected monthly discharge at the lower reach of the Pasak River. The figure shows the clear pattern of the decrease of the October discharge.

## 6. WATER RESOURSES ASSESSMENT MODEL AT THE PASAK RIVER BASIN

Through the river discharge projection research of the entire Chao Phraya River, it was revealed that the Pasak River basin would be one of the hotspot basins for the river discharge change. Thus, we focus the catchment and develop a water resources assessment model to analyze the change of hydrologic cycle, water resources, and its impact on rice production (Tachikawa and Yorozu, 2009). Figure 14 shows the detail topographic modeling using HydroSHED. Left figure shows the entire Chao Phraya River basin and right figure shows the Pasak River basin. The topography data is used for a detail distributed hydrologic model.

**Fig. 15** Irrigated area extended over the lower part of the Pasak dam reservoir.

**Fig. 16** A hydro-meteorological observation instrument installed at the Rama VI office, RID.

Figure 15 shows the irrigated area at thelower part of the Pasak Dam , where water is taken from the lower reach of the Pasak River for paddy fields extended over the lower part of the Pasak River basin. To predict a potential rice crop yield for the irrigated area, a developm ent of a crop production model combined with a distributed hydrologic model and a dam storage prediction model is in progress. We have installed a hy dro-meteorological observation instrument at the Ram a VI office, RID to develop a crop yield model (Fig. 16).

## 7. SUMARRY

The im pact of clim ate change on river flow regimes in the Chao Phraya River basin was analyzed. A possible change of water resources are indicated in the near future clim ate experim ent and it becomes clearer in the future clim ate experim ent. We found the Pasak River basin would be one of hotspots of river discharge change. Thus, the following researches are in progress at the Pasak River basin:

- Development of a detailed distributed hydrologic model at the Pasak River basin,
- Development of the Pasak Dam storage prediction model,
- In-situ observation of crop production cy cle at the irrigation area of the Pasak dam reservoir,
- Development of crop production model, and
- Hydro-meteorological observation at the study area.

**ACKNOWLEDGMENT:** The hy drologic projection data used for the river flow sim ulations was provided by the Meteorological Research Institute, Japan. The hydrologic observation data at the Pasak River basin was provided by the Roy al Irrigation Department, Thailand.

## REFERENCES

IPCC WG I : Climate Change 2007 : The Physical Science Basis, Contribution of Working Group I to the Fourth Assessment Report of the Intergovernmental Panel on Climate Change (IPCC), Cambridge Univ. Press, Cambridge, UK, 2007.

IPCC WG II : Climate Change 2007 : Impacts, Adaptation and Vulnerability, Contribution of Working Group II to the Fourth Assessment Report of the IntergovernmentalPanel on Climate Change (IPCC), Cambridge Univ. Press, Cambridge, UK, 2007.

Kitoh, A., Ose, T., Kurihara, K., Kusunoki, S., Sugi, M. and KAKUSHIN Team-3 Modeling Group : Projection of changes in future weather extrem es us ing super-high-resolution global and regional atmospheric models in the KAKUSHIN Program: Results of preliminary experiments, Hydrological Research Letters, Vol. 3, pp. 49-53, 2009.

Takino, S ., Tachikaw a, Y ., S hiiba, M ., Y amaguchi, C., and Yorozu, K. : Estimation of changes of river flow regimes in Japanese river basins under climate change, *Annual Journal of Hydraulic Engineering, JSCE*, 54, pp. 475-480, 2009 (in Japanese) .

Tachikawa, Y. and Yorozu, K.: Im pact Analy sis of Clim ate Change on Water Resources in Japan and Thailand using a GCM Hy drologic Projections and a Distributed Rainfall-Runoff Model, Proc. of 2009 AIT-KU Joint Symposium on Human Security Engineering, Bangkok, Thailand, November 19-20, pp. 149-156, 2009.

2010 AIT-KU JOINT SYMPOSIUM ON HUMAN SECURITY ENGINEERING

Bangkok, Thailand, November 25-26, 2010

# Integrated Flood Risk Assessment for the Day River Flood Diversion Area in the Red River, Vietnam

NGUYEN Mai Dang[1] and Mukand S. BABEL[2]

[1] Hydrology and Water Resources Faculty, Water Resources University
(175 Tay Son Str, Dong Da Dist, Hanoi, Vietnam)
Email: dang@wru.edu.vn

[2] Water Engineering and Management, School of Engineering and Technology, Asian Institute of Technology
(Klong Luang, Pathumthani 12120, Thailand)
Email: msbabel@ait.asia

The study has presented an integrated approach to flood risk assessment for the flood diversion area in the Red River. The Analytical Hierarchy Process (AHP) was appraised as quite satisfactory for quantifying the weights to parameters contributing to flood risk. The Decision Tree Analysis (DTA), in conjunction with dummy simulation skills, was an effective tool in the operation of a complex flood control system created using the MIKE 11 model. The outputs of integrated flood risk assessment provide valuable information for policy-makers, responsible authorities, and local residents in planning for flood risk reduction in the study area.

***Key Words :*** *Flood Simulation, Flood Control Operation, DTA, AHP, Flood Hazard, Flood Vulnerability, Integrated Flood Risk Assessment*

Flood disasters are increasing worldwide due to numerous reasons such as global changes (land use and climate), urbanization, industrialization, and socioeconomic development. The Red River Delta (RRD) in Vietnam is one of the most flood-prone areas in the world and also densely populated. The RRD suffers increased risk due to frequent floods and the rise in sea level, especially in the Day River Flood Diversion Area (DRFDA) and Hanoi city. Other factors causing increased flood vulnerability in the DRFDA include high population growth, increased infrastructure development, and social and environmental implications. An integrated approach to flood risk assessment is, therefore, essential for the DRFDA to improve flood management in the Red River.

The study developed here provides a methodology to define the flood risk parameters and quantify weights to them. A review of the literature on this subject, in conjunction with expert analysis, has been employed in this research to define and select flood risk parameters, while a household survey has investigated flood risk perception and flood preparedness and mitigation in the DRFDA. The Analytical Hierarchy Process (AHP) method has been applied to convert qualitative scores (which were rated by experts) to the quantitative value of weights to each parameter. The data processing has been done using the SPSS. The research recognizes that integrated flood risk is a product of both multi-indicator flood hazard and comprehensive flood vulnerability. The hierarchy of flood risk components is developed to build the matrices for applied AHP. Components, subcomponents, indicators and categories are arranged like a tree root with four levels, as illustrated in Figure 1.

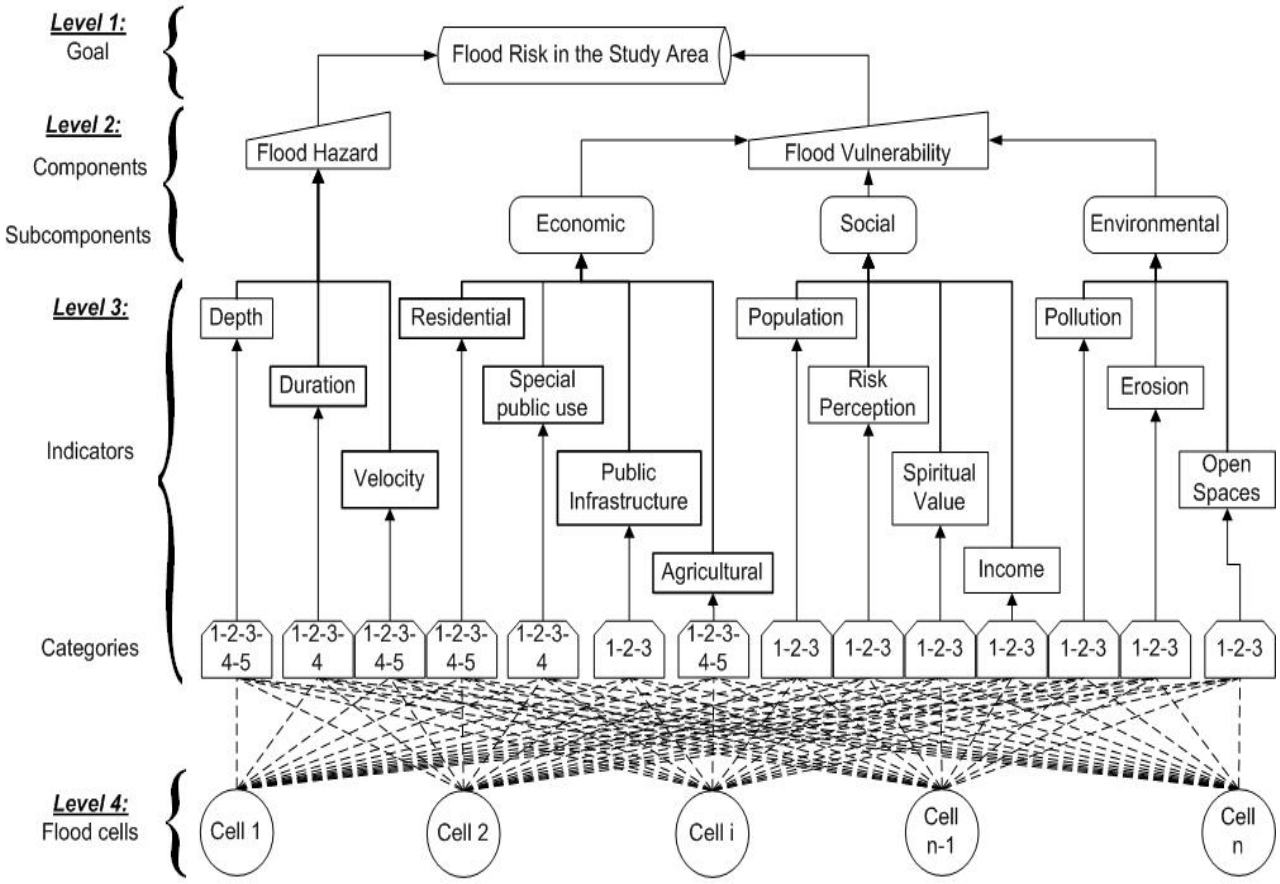


Figure 1. Hierarchy for the quantification of flood risk

The goal level represents flood risk analysis of a region or a community from synthesizing land units (hamlets, communes, or flood cells which are used in this study). The second level depicts the two main components, such as flood hazard and flood vulnerability. The third level presents the indicators for hazard and vulnerability, whereas the fourth level represents flood cells.

Flood hazard is assessed using depth, duration, and velocity indicators. Flood vulnerability is analyzed from economic, social, and environmental points of view. Here, economic susceptibility is represented by parameters such as residential buildings, special public use buildings, public infrastructure, and agriculture; social susceptibility is contributed to by factors like population, flood risk perception, spiritual values, and income; environmental susceptibility is represented by such indicators as pollution, erosion, and open spaces. These parameters were assessed through the mechanism of weighted contribution to flood risk. The relationships and contributions of flood risk parameters were estimated through mean index (MI), coefficient of determination (R2); root mean square error (RMSE), mean overall contribution (MOC).

An assessment of potential flood in Hanoi and the DRFDA in the RRD has been carried out by analyzing flood trends, future flood frequencies, and the rise in sea level. The techniques of linear regression, exponential smoothing, Data-Fit functions, stochastic modeling, and artificial neural network (ANN) have been investigated. The modeling of flood propagation in the Red River System (RRS) - including the flood diversion zones as well as the operation of the flood control system - was carried out using the 1-D hydrodynamic model (MIKE 11) and the 2-D hydrodynamic model (MIKE 21). The Decision Tree Analysis (DTA) method, in conjunction with dummy simulation skills, was applied to describe the flood control system and its rules of operation. As will be seen, results of the trend analysis indicate an increase in flood peak discharge in the Red River by 4.4, 9.9, and 20.9% and the rise in sea level by 0.10, 0.22, and 0.46 m in 2025, 2050, and 2100 correspondingly (compared to 2005). The maximum water level in Hanoi is likely to increase by 0.95 m by the end of this century. Hanoi will, however, not be affected by the rise in sea level even in the worst case scenario of an increase by 1.0 m. In

Table 1. Correlation and contribution of parameters to flood hazard, vulnerability and risk in the study area

| Risk Parameters | Weight | The Head Zone | | | | The Middle Zone | | | |
|---|---|---|---|---|---|---|---|---|---|
| | | MI | $R^2$ | RMSE | MOC (%) | MI | $R^2$ | RMSE | MOC (%) |
| **Hazard** | | 0.448 | | | | 0.444 | | | |
| Depth | 0.0974 | 0.964 | 0.090 | 0.579 | 17 | 0.592 | 0.901 | 0.225 | 10 |
| Duration | 0.5695 | 0.580 | 0.997 | 0.208 | 79 | 0.629 | 0.998 | 0.232 | 87 |
| Velocity | 0.3331 | 0.055 | 0.003 | 0.473 | 4 | 0.039 | 0.635 | 0.505 | 3 |
| **Economic** | | 0.077 | | | | 0.053 | | | |
| Residential building | 0.6087 | 0.016 | 0.364 | 0.088 | 20 | 0.013 | 0.318 | 0.059 | 22 |
| Special Public Use | 0.2485 | 0.078 | 0.450 | 0.224 | 18 | 0.017 | 0.242 | 0.119 | 6 |
| Public Infrastructure | 0.1014 | 0.172 | 0.258 | 0.194 | 43 | 0.116 | 0.461 | 0.160 | 42 |
| Agriculture | 0.0414 | 0.248 | 0.104 | 0.278 | 19 | 0.269 | 0.015 | 0.279 | 30 |
| **Social** | | 0.214 | | | | 0.413 | | | |
| Population | 0.4673 | 0.152 | 0.970 | 0.192 | 35 | 0.139 | 0.618 | 0.355 | 17 |
| Risk Perception | 0.2772 | 0.123 | 0.000 | 0.201 | 18 | 0.779 | 0.119 | 0.477 | 59 |
| Spiritual Value | 0.1601 | 0.024 | 0.010 | 0.293 | 1 | 0.006 | 0.000 | 0.454 | 0 |
| Income | 0.0954 | 0.898 | 0.025 | 0.741 | 46 | 0.916 | 0.046 | 0.574 | 24 |
| **Environmental** | | 0.206 | | | | 0.142 | | | |
| Pollution | 0.6738 | 0.073 | 0.848 | 0.138 | 28 | 0.082 | 0.721 | 0.088 | 45 |
| Erosion | 0.2255 | 0.934 | 0.262 | 0.751 | 72 | 0.453 | 0.563 | 0.458 | 51 |
| Open Space | 0.1007 | 0.0 | 0.000 | 0.223 | 0 | 0.093 | 0.000 | 0.267 | 4 |
| **Vulnerability** | | 0.244 | | | | 0.244 | | | |
| Economic | 0.4000 | 0.077 | 0.272 | 0.197 | 10 | 0.053 | 0.227 | 0.223 | 7 |
| Social | 0.2000 | 0.214 | 0.846 | 0.087 | 25 | 0.413 | 0.538 | 0.212 | 48 |
| Environment | 0.4000 | 0.206 | 0.875 | 0.064 | 65 | 0.142 | 0.767 | 0.120 | 45 |
| **Risk** | | 0.164 | | | | 0.181 | | | |
| Hazard | 0.3333 | 0.448 | 0.612 | 0.336 | 55 | 0.444 | 0.606 | 0.341 | 55 |
| Vulnerability | 0.6667 | 0.244 | 0.450 | 0.132 | 45 | 0.244 | 0.686 | 0.113 | 45 |

contrast, the DRFDA can be greatly influenced by both flood from the upstream catchment area and the rise in sea level because of topographical conditions. For example, as predicted for 2100, the flood volume diverted to the Day River will increase by 48.7% due to flood increase in the Red River, and the water level will rise by an average of 0.54 m due to a combination of flood waters from the upstream and the rise in sea level.

Based on flood simulation for various scenarios in the RRS, the hydrographs of flood divergence to the DRFDA have been computed using the MIKE 11 model. Accordingly, flood risk in the flood diversion zones has been assessed for each flood-cell (90 by 90m) using the MIKE 21 model, GIS software, and statistical techniques. The digital maps of flood hazard, food vulnerability, and flood risk in the flood diversion zones have also been developed.

Results for two zones in the study area are summarized in Table 1. In both flood diversion zones - the Head Zone and Middle Zone - the overall contribution to flood risk of the flood hazard component is 55%, and the flood vulnerability component is 45%, even though the weight given to hazard is only half of that given to vulnerability. Flood duration dominates other indicators (flood depth and flood velocity) due to high weight and long duration. The overall contribution to flood hazard by the depth indicator is higher than that by the velocity indicator, even though the weight to depth indicator is much lower than that to velocity.

For flood vulnerability, the Head Zone faces maximum risk from environmental factors (65% contribution) such as erosion and social factors (25% contribution) such as dense inhabitation and low income. Inversely, the Middle Zone is most susceptible from the angle of social issues (48% of the overall contribution), especially since there is poor flood risk awareness and low income. Moreover, this zone is also susceptible to environmental factors by a considerable level (45%) under which erosion and pollution are primary. Noticeably, economic susceptibility has been weighted equal to environmental vulnerability and is the double of social vulnerability, but its overall contribution in both the Head and Middle Zones is less than 10%, much lower than the contribution of social and environmental implications.

The sensitivity of flood hazard and vulnerability parameters of flood risk for future scenarios has been analyzed during the course of research and in conjunction with that, a questionnaire survey was also carried out to determine suitable measures to reduce flood risk in the DRFDA. It has been found that flood crease by 8% in the year 2100, and flood duration hazard in the flood diversion zones is likely to in always dominates other indicators although acceleration of the relative increase of the depth indicator is most rapid. Two structural measures, namely improving the drainage capacity and strengthening the dyke system, have been suggested to mitigate flood hazard in the flood diversion zones. The development of residential buildings and agricultural activities in flood diversion zones increases economic vulnerability. Population growth and lessening/increasing spiritual values result in more social vulnerability, whereas an improving income helps lessen social susceptibility. Pollution due to industrialization also leads to more environmental susceptibility. In general, the increase of flood vulnerability will be higher than the increase of flood hazard in the future, though flood hazard is always greater than flood vulnerability. On the other hand, the weight to vulnerability is double that of the weight to hazard; thus, several nonstructural measures such as evacuation, public awareness about flood risk, land use management etc. are recommended to decrease flood vulnerability.

The study has presented an integrated approach to flood risk assessment for the flood diversion area in the Red River. The AHP was appraised as quite satisfactory for quantifying the weights to parameters contributing to flood risk. The DTA, in conjunction with dummy simulation skills, was an effective tool in the operation of a complex flood control system created using the MIKE 11 model. The outputs of integrated flood risk assessment provide valuable information for policy-makers, responsible authorities, and local residents in planning for flood risk reduction in the study area.

2010 AIT-KU JOINT SYMPOSIUM ON HUMAN SECURITY ENGINEERING

Bangkok, Thailand, November 25-26, 2010

# Nonparametric Conditional Flood Frequency Estimator on Climate Variability

Somkiat APIPATTANAVIS[1], Balaji RAJAGOPALAN[2] and Upmanu LALL[3]

[1]Researcher, Office of Research and Development, Royal Irrigation Department
(200 Tivanon Road, Pakkred, Nonthaburi 11120, Thailand)
E-mail:apipatta@colorado.edu
[2]Associate Professor, Department of Civil Environment and Architectural Engineering, University of Colorado
(ECOT 541, Campus Box 428, Boulder, CO 80309, USA)
E-mail:balajir@colorado.edu
[3]Professor, Department of Earth and Environmental Engineering, Columbia University
(500 West 120th Street, 918 Mudd, Columbai University, MC 4711, New York, NY 10027, USA)
E-mail:ula2@columbia.edu

The traditional flood frequency analysis has been challenged by the growing evidence that annual maximum flood frequency at a given location is not independent and identically distributed, and its underlying process is not stationary but changes over time in response to the underlying climate state modulated by structured low-frequency climate variation. In this paper, we propose a nonparametric local polynomial likelihood approach for estimating flood quantiles conditional on climate indices that represent the underlying climate states. Requiring no prior assumption of distribution function, the proposed nonparametric approach has advantage over the parametric and semiparametric approaches (e.g. quantile regression and local likelihood) on providing a flexible and general framework that being able to capture a wider range of tail behavior. Performance of the proposed method is compared to those of parametric and semiparametric methods on both synthetic data sets and observed annual flood data from gauging stations in the United States.

***Key Words :*** *Conditional Flood Frequency Estimator,Climate Variability*

## 1. BACKGROUND

The traditional flood frequency analysis assumes that the annual maximum floods are independently and identically distributed (Kite, 1975; Bobee and Ashkar, 1991), however, there is growing evidence that frequency distribution at a given location is not identical but depends on the underlying climate state modulated by structured low frequency climate fluctuations (Lins and Slack, 1999; Baldwind and Lall, 1999; Jain and Lall, 2000; Pizaro and Lall, 2002; Franks and Kuczera, 2002; Anctil and Coulibaly, 2004). The variation in climate can markedly change patterns of atmospheric moisture transport in the flood season, consequently, change the probabilities of floods in a given year at that particular location.

Applying to an entire flood record which is a representative of different climate states, the traditional flood frequency analysis can only provide long-term or unconditional flood estimates, however, the unconditional distribution may seriously underestimate or overestimate flood for the current climate state that possibly persists several years, consequently, may affect the flood risk estimates and flood protection plans. In contrast, the flood frequency analysis conditional on the underlying climate state provides short-term flood estimates that are more

accurate for a given period but a good understanding of the causal mechanisms of the well organized variability is required.

It is now widely acknowledged that well organized low-frequency climate modes, such as interannual El Nino Southern Oscillation (ENSO) and interdecadal Pacific Decadal Oscillation (PDO) modulate regional climates on annual and interannual timescales around the globe. Therefore, these climate indices can be useful precursors for estimating short-term flood risk.

The objective of this paper is to propose a non-parametric approach for modeling flood frequency at a given location assuming the underlying process is nonstationary in time and conditional on teleconnected climate indices. The focus is on providing better short-term flood estimation conditional on the current underlying climate state.

A brief overview of relationship between low-frequency oscillation modes in climate and flood variability is first provided. Methodologies of different approaches for conditional flood quantile estimation are next presented. Performances of models on synthetic data are then compared. Application to data from gauging stations is next presented.

## 2. RELATION BETWEEN LOW-FREQUENCY CLIMATE VARIABILITY AND FLOOD VARIABILITY

Low-frequency climate variability influences flood variability through ocean-atmosphere interactions that are key drivers of large-scale moisture delivery pathways and their variability around the globe (Wendland and Bryson, 1981; Hirschboeck, 1991). Structured low-frequency modes of interannual and interdecadal variability in climate modulate the moisture delivery pathways (Trenberth and Guillemont, 1996; Cayan et al., 1999). El Nino-Southern Oscillation (ENSO) and Pacific Decadal Oscillation (PDO) and hence modulate the temperature, precipitation, and streamflow patterns across the United States (Cayan et al., 1999; Ropeleweski and Halpert, 1987; Drecup and Kahya, 1994; Mantua et al., 1997; Gershunov and Barnett, 1998; Dettinger et al., 1999; Rajagopalan et al., 2000).

ENSO represents the dominant coupled ocean-atmosphere mode of the tropical Pacific (Cane, 1992) with a characteristic 3-7 year narrow band of variability, and has two phases; El Nino and La Nina. The global impacts of ENSO primarily stem from changes in the strength and location of tropical Pacific convection, consequently, changes in the global atmosphere circulation (Cane and Clement, 1999). Several studies have shown that major extremes of floods and droughts around the globe are associated with the state of ENSO (Trenberth and Guillemot, 1996; Piechota and Dracup, 1996; Jain and Lall, 2000; Pizaro and Lall, 2002). Several researchers have reported that ENSO also has significant effects on interdecadal and century scale variations (e.g., Rajagopalan et al., 1997; Cole and Cook, 1998; McCabe and Dettinger, 1999; Mann et al., 2000).

PDO with a characteristic narrow band width of 18-22 years is identified as the leading eigenvector of North Pacific sea surface temperature variability (Mantua et al., 1997) and shows strong associations with snowpack variability and winter surface climate over the western United States (Mantua et al., 1997; Cayan, 1996; Jain and Lall, 2000, 2001; Pizaro and Lall, 2002; Gershunov and Barnett, 1998; McCabe and Dettinger, 1999).

The mean position of the jet stream, modulated by the ENSO phase, can be shifted by the modulation of the PDO phase. Since the jet stream brings moisture into the continents, therefore, the effects of ENSO can be reduced or enhanced by the PDO.

## 3. METHODOLOGY

The conditional probability density function $f(Q_t|X_t)$, or the conditional distribution function $F(Q_t|X_t)$ summaries the whole picture of flood quantiles conditional on climate indices ($X_t$). These functions can be derived from historical data $\{Q_t, X_t, t = 1,2,\ldots,n\}$:

$$F_p(Q_t|X_t) = \int_{-\infty}^{Q_{pt}} f(Q_t|X_t)\,dQ = p \quad (1)$$

$$Q_{pt} = F_p^{-1}(Q_t|X_t) \quad (2)$$

where Q is a flood variable of interest, e.g., the annual maximum flow, the annual maximum n-day flow, etc at a given location. $Q_{pt}$ is the inference of the pth quantile of Q for year t conditioned on some set of climate indices. $X_t = [x_{1t},x_{2t},\ldots,x_{mt}]$ is set of m climate indices or other predictors. However, the functions are usually difficult to estimate for small sample size and high-dimensional indices.

(1). Conditional Quantile Estimation

The conditional distribution function $F(Q_t|X_t)$ can be estimated by assuming that the joint probability density function $f(Q_t,X_t)$ and the marginal density function $f(X_t)$ follows a particular distribution and then estimating their parameters accordingly. However, conditional tail quantile estimates vary widely due to sensitivity to the choices of the parametric forms of the distributions. Often it is assumed that $f(Q_t|X_t)$ is log-normal, with its mean and variance varying in time conditional on the state of ENSO and PDO (Jain and

Lall, 2000). Another way to estimate the conditional distribution function $F(Q_t|X_t)$ nonparametrically is to use kernel and *k*-Nearest Neighbor (*k*-NN) methods (Yu and Jones, 1998; Bhattacharya and Gangopadhyay, 1990). But both methods have limitations. The kernel based approach may be difficult to implement in practice for multiple predictors and leads to highly biased estimates in the tails, whereas the *k*-NN approach performs poorly near the boundaries of predictors (Yu, 1999). Yu (1999) suggested the combination of these two methods by first estimating the quantile using a *k*–NN approach and then smoothing the estimated quantiles using a kernel function. However, the combined model required for higher dimension data (for increased number of predictors) tends to be computationally intensive and requires a very large data set to be effective.

(2). Quantile Regression

A subset of this approach is the use of Quantile Regression that was implemented by Koenker and Bassett (1978) and reviewed recently by Yu et al (2003) The general model is of the form:

$$Q_{pt} = \psi_p(X_t) + \upsilon_{pt} \tag{4}$$

where $\psi_p(.)$ is a linear or nonlinear function relating the pth conditional quantile to the climate indices and $\upsilon_{pt}$ is a noise process with the pth quantile zero and variance $\sigma_p^2$. The noise process can be homoskedastic ($\sigma_p^2$ is a constant) or heteroskedastic ($\mathrm{Var}(\upsilon_{pt}) = \sigma_p^2(X_t)$). The parametric function $\psi_p(.)$ is estimated by solving the following minimization problem

$$\min_{\psi_p(X_t)} \sum_{t=1}^{n} \rho_p\left(Q_{pt} - \psi_p(X_t)\right) \tag{5}$$

where the check function $\rho_p(u)$ is defined by $\rho_p(u) = u(p - I\{u\}) = \dfrac{|u| + (2p-1)u}{2}$ and $I\{u\}$ denotes the indicator function with

$$I\{u\} = \begin{cases} 1 & \text{if } u < 0 \\ 0 & \text{otherwise} \end{cases} \tag{6}$$

For example if a linear function is assumed for (4) and median (p=0.5) is considered, then $\psi_p(X_t)=\beta^T X_t$ where $\beta^T = [\beta_0, \beta_1, \ldots, \beta_m]$ and $X^T_t = [1, x_{1t}, x_{2t}, \ldots, x_{mt}]$. There is no explicit solution for the regression coefficients under this parametric quantile regression model since the check function is not differentiable at the origin. However, using recent advances in interior point methods for solving linear programming problems discussed by Portnoy and Koenker (1997), this minimization can be performed by using the algorithm that was provided by Koenker and D'Orey (1987). An 'interior' algorithm for general quantile regression fitting has been developed by Koenker and Park (1996).

The conditional quantiles are estimated by minimizing the sum of asymmetrically weighted absolute deviation by giving different weights for positive and negative residuals. The advantage of this method is that it is easy to implement and can be extend to nonlinear functions as well. However, the main disadvantages are (i) a functional form has to be assumed and (ii) there is no guarantee that the quantiles do not cross – i.e., the 95$^{th}$ quantile can be lower than the 90$^{th}$ quantile.

(3). Local Likelihood Model

Recently, Davison and Ramesh (2000) suggested a semiparametric approach to estimate the parameters of the assumed flood frequency distribution conditional on predictors using local likelihood estimation and based on local neighborhood in the predictor state-spaces. They were concerned with a time trend in the parameters and used a time index as a predictor. Later, Sankarasubramanian and Lall (2003) extended this approach to consider multiple climate indices as predictors using the conditional PDF $f(Q_t|X_t)$ with parameters $\theta(X_t)$. They assumed a log normal distribution but with varying parameters $\theta(X_t)$ which are assumed to depend on the conditional variables (in this case ENSO and PDO). The parameter $\theta(X_t)$ carrying the 'conditional information' of the probability model $f(Q_t|X_t)$ are approximated through a linear function in the neighborhood of $X_t$. For instance, in the case of a two parameter distribution, if $\theta(X_t) = [\mu(X_t)\ \sigma(X_t)]$ represent the location ($\mu(Xt)$) and the scale ($\sigma(Xt)$) parameters of the distribution, then $\mu(X_t) = \lambda_0 + \sum_{k=1}^{m} \lambda_k (x_{kj} - x_{kt})$ and $\sigma(X_t) = \lambda_0 + \sum_{k=1}^{m} \gamma_k (x_{kj} - x_{kt})$ can be represented as a linear function of m predictors where j denotes all the data points (X) that receives a weight – i.e. within a certain neighborhood of $X_t$. The local likelihood method estimates $\theta(X_t)$ by maximizing the likelihood of the sample in such a way that data points ($X_j$) lying closer to $X_t$ receive more weightage. Epanechnikov kernel (Pagan and Ullah, 1999) was used for weighing each $X_j$ in this extended study.

The parameters of the method are thus *m* bandwidths and then *2m+2* coefficients ($\lambda_k$, $\gamma_k$, k=0,1,…,m ) in estimating $\theta(X_t) = [\mu(X_t)\ \sigma(X_t)]$) for the neighborhood of the point of estimate. The bandwidths $h_k$ can be obtained by specifying that each point of estimate have at least *2m+2* observations. Cross-validated maximum likelihood in (6) is used to choose the bandwidths.

$$\ell_{cv}\left(\hat{\theta}_{-t}(X_t), \hat{h}\right) = \sum_{\substack{j=1 \\ j \neq t}}^{n} w_j(X_t)\, log\left(fQ_t \middle| X_t; \hat{\theta}_{-t}(X_t)\right) \tag{7}$$

The entire set of parameters and bandwidths can be obtained by maximizing the cross-validated local log

likelihood with respect to $\hat{\theta}_{-t}(X_t)$ and $\hat{h}$. The cross-validated local log likelihood in (6) estimates the distribution of Qt conditioned on the predictors Xt by estimating the parameters $\hat{\theta}_{-t}(X_t)$. Sankarasubramanian and Lall (2003) used the shuffled complex evolution algorithm (Duan et al., 1992) to perform the maximization of (6) at each candidate point of estimate $X_t$.

It showed better performance than the quantile regression. However, this approach also suffers from several drawbacks (i) a form of the PDF (i.e. log normal in their case) has to be assumed and this can be hard to verify (ii) bandwidth estimation in higher dimensions is typically plagued by high variability (Sankarasubramanian and Lall, 2003) and (iii) For each point several parameters have to estimated from limited sample size and this can induce high variability.

To alleviate the drawbacks mentioned above, we propose a fully nonparametric approach based on local polynomials to the conditional flood frequency problem described in the following section. We also compare the performance of the proposed approach with those of two approaches tested by Sankarasubramanian and Lall (2003).

(4). Local Polynomial likelihood Model

Nonparametric flood frequency approach proposed in this study is to use local polynomial likelihood function for estimating joint probability density function of flood variable and its predictors, $f(Q_t,X_t)$ and joint probability density function of the predictors $f(X_t)$, then use conditional probability (7) to obtain pdf $f(Q_t|X_t)$ and finally $Q_{pt}$ can be obtained using (1) and (2).

$$f(Q_t|X_t)=\frac{f(Q_t,X_t)}{f(X_t)} \tag{8}$$

Suppose we have climate indices $X_1,X_2,\ldots,X_n$ lying in a subset $\chi$ where $\chi$ is the domain of density, having unknown density *f*. The log-likelihood function is

$$\ell(f)=\sum_{j=1}^{n} log\left(f(X_j)\right)-n\left(\int_{\chi} f(u)du-1\right) \tag{9}$$

The definition (8) of the log-likelihood is unusual, with the added a penalty term $\int_{\chi}\left(f(u)du-1\right)$. If *f* is a density, the penalty is 0, therefore in this case (8) coincides with the usual log-likelihood. The reason for adding the penalty to (8) is that $\ell(f)$ can be treated as a likelihood for any non-negative function *f* without imposing the constraint $\int f(x)dx=1$.

Frequently, we do not have sufficient information to specify a global family for *f*, but local smoothness assumptions may be reasonable. In this case, it is useful to consider a localized version of the log-likelihood:

$$\ell(f,x)=\sum_{j=1}^{n} K\left(\frac{X_j-x}{h}\right) log\left(f(X_j)\right)-n\int_{\chi} K\left(\frac{u-x}{h}\right) f(u)du \tag{10}$$

where $x$ is the considered point, $n$ is number of points, $K$ is a suitable nonnegative weight function and $h$ is a bandwidth.

The local polynomial approximation supposes that log(*f*(u)) can be well approximated by a low-degree polynomial in a neighborhood of the fitting point x that is, $log\ f(u)\approx P(u-x)$, for instant, in one dimension $P(u-x)=a_0+a_1(u-x)+a_2(u-x)^2+\ldots+a_p(u-x)^p$ with this approximation, we get the local polynomial likelihood as

$$\ell(f,x)=\sum_{j=1}^{n} K\left(\frac{X_j-x}{h}\right) P(X_j-x)-n\int_{\chi} K\left(\frac{u-x}{h}\right) exp(P(u-x))du \tag{11}$$

For weighing each point, tricube weight function (11) is used.

$$K(u)=(1-|u|^3)^3 \tag{12}$$

For selecting the best bandwidth (h), Generalised Cross Validation (GCV) criteria (12) is used.

$$GCV=n\frac{\sum_{i=1}^{n}\left(Y_i-\hat{Y}_i\right)^2}{(n-\upsilon_1)^2} \tag{13}$$

where $Y_i$ is true density value, $\hat{Y}_i$ is estimated density value, $\upsilon_1$ is fitted degree of freedom defined as trace(H) and H is hat matrix.

## 4. MODEL EVALUATION

The proposed nonparametric model is evaluated by applying to a Monte Carlo simulation experiment with synthetic data sets designed by Sankarasubramanian and Lall (2003) and then compared the performance of this model with those of quantile regression approach and local likelihood smoothing approach.

4.1. Synthetic Data

An idealized setting of synthetic data designed by Sankarasubramanian and Lall (2003) is to replicate the cyclostationary behavior expected to be present under ENSO and PDO. Two cases are considered: (1) homoskedastic case where nonstationary in the mean of the annual flood variable with a constant variance of the noise process, and (2) heteroskedastic case where nonstationary in the mean and variance of the annual maximum peak.

Consider that the annual maximum flood $Q_t$ in year t arises from a lognormal distribution. This corresponds to a model:

$$y_t \approx N\left(\mu_t(t),\sigma_y(t)\right) \tag{14}$$

where $y_t=\log(Q_t)$, $\mu_{yt}$ and $\sigma_{yt}$ are the mean and the variance of year t.

The parameters of the distribution, for the homoskedastic case, are assumed to vary as:

$$\mu_{yt} = C_1 x_{1t} + C_2 x_{2t} \quad (15a)$$

$$\sigma_{yt} = C \quad (15b)$$

where C is a constant variance, $C_1$ and $C_2$ are coefficients and $x_1$ and $x_2$ are two climate predictors.

Similarly, the corresponding parameters for the heteroskedastic case are:

$$\mu_{yt} = C_1 x_{1t} + C_2 x_{2t} \quad (16a)$$

$$\sigma_{yt} = C_v \mu_{yt} \quad (16b)$$

where $C_v$ is a constant coefficient of variation.

The two predictors are modeled as periodic modes with different frequencies $\omega_1$ and $\omega_2$:

$$x_{1t} = a \sin(\omega_1 t + \phi_1) \quad (17)$$

$$x_{2t} = b \sin(\omega_2 t + \phi_2) \quad (18)$$

where $\phi_1$ and $\phi_2$ are the phase angles, and a and b are the amplitudes of two climate signals. For this study, a=1.352, b=1.743, $\phi_1$=180, $\phi_2$=0, $T_1$=5, $\omega_1=(2*\pi/T_1)$, $T_2$=18, $\omega_2=(2*\pi/T_2)$, $C_1$=1.352, $C_2$=-0.678, C=2 and $C_v$=0.12.

Using these parameters, we generate 1000 realizations of $Q_t$, $x_{1t}$, and $x_{2t}$ with record length of 100 years. Then using the proposed nonparametric approach, we obtain cross-validated estimates of the pth quantile $[\hat{Q}_{pt}]_{-t}$ that correspond to each year. The data are log transformed before application.

The cross-validated Bias and Root mean square error (RMSE) averaged over the 1000 realizations are computed at each time t:

$$\text{Bias}(\hat{Q}_{pt}) = \frac{1}{1000}\sum_{i=1}^{1000}\left[\hat{Q}_{pt}\right]_{-it} - Q_{pt} \quad (19)$$

$$RMSE(\hat{Q}_{pt}) = \sqrt{\frac{1}{1000}\sum_{i=1}^{1000}\left(\left[\hat{Q}_{pt}\right]_{-it} - Q_{pt}\right)^2} \quad (20)$$

## 4.2. Results

The cross-validated performances for homoskedastic and heteroskedastic cases, in terms of Bias and RMSE, are illustrated in Figures 1 and 2, for the 20 year flood (p=0.95). Furthermore, the Bias and RMSE that are averaged over 1000 realizations from the proposed method are shown and compared with ones from Quantile Regression method and Local Likelihood method taken from Sankarasubramanian and Lall (2003) in Table 1.

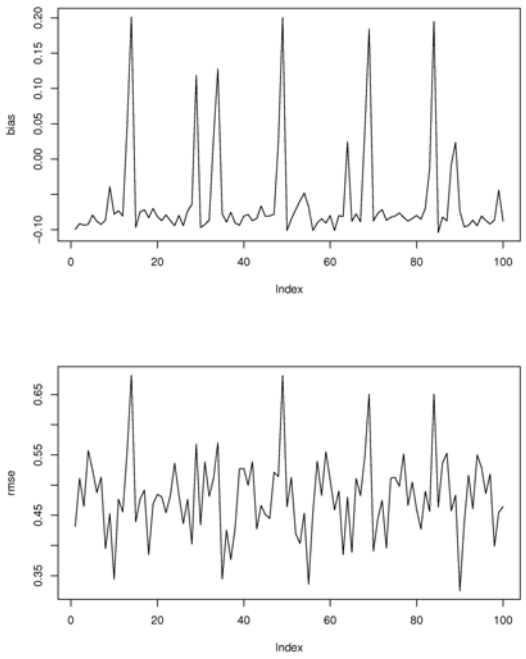


**Fig. 1** (a) Bias($Q_{0.95t}$) and (b) RMSE($Q_{0.95t}$) from leave one out cross validation for homoskedastic synthetic model.

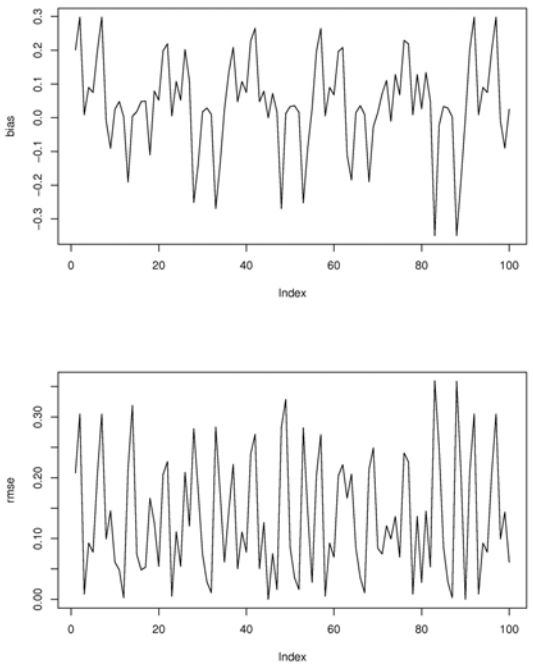


**Fig. 2** Same as Figure 1 but for heteroskedastic synthetic model.

As expected, in homoskedastic case, the higher absolute bias of local likelihood and local polynomial likelihood are apparent at points of high curvature in the target function. The bias of quantile regression is purely due to sampling (Buchinsky, 1995). Consequently, local polynomial likelihood performs worse on

RMSE but surprisingly, local likelihood performs better than quantile regression on RMSE (Sankarasubramanian and Lall, 2003). For heteroskedastic case, local likelihood and local polynomial likelihood have better performance than quantile regression in terms of both bias and RMSE. However, local polynomial likelihood provides much low RMSE.

**Table 1.** The average Bias and RMSE relative to the population conditional quantiles across 100 years.

| Method | Homoskedastic | | Heteroskedastic | |
|---|---|---|---|---|
| | Bias | RMSE | Bias | RMSE |
| Quantile Regression | 0.010 | 0.348 | -0.120 | 0.679 |
| Local Likelihood | -0.030 | 0.214 | 0.034 | 0.635 |
| Local Polynomial Likelihood | -0.039 | 0.377 | 0.041 | 0.166 |

Therefore, considering both Bias and RMSE, it can be concluded that Local Polynomial Likelihood performs better than the others, especially, in the heteroskedastic case that often happens in the nature. Furthermore, the proposed fully nonparametric approach provides a flexible and general framework in being able to capture a wide range of tail behavior.

## 5. APPLICATION

### (1) Study Area

The proposed nonparametric approach is also applied to data from three gauging stations whose flood flows have rather strong correlation with the climate indices i.e. ENSO and PDO. Two stations are in the western US and one is in New Zealand.

The first flood data set is from the gage at Clark Fork River below Missoula, Montana (USGS Station No: 12353000) with the drainage area of 9,003 $mi^2$. The annual flood data are available from 1930-2000. According the USGS standards, the record flows are considered as minimally affected by upstream activities, diversions and human influence. The winter (January-February-March-April) average of the NINO3 and PDO indices are used as the predictors of the flood flows (see Figure 3). The correlations; $\rho$(Q,NINO3) and $\rho$(Q,PDO) are -0.37 and -0.39 respectively. Note that this data set is the same data set used by Sankarasubramanian and Lall (2003) and we use it because we can easily compare the performance of our proposed approach with those of two approaches in their study.

The second flood data set is from the gage at Umpqua River near Elkton, Oregon (USGS Station No: 14321000) with the drainage area of 3,683 $mi^2$. The annual flood data are available from 1908-2004. The records are considered as minimally affected by upstream activities, diversions and human influence as well. The correlations; $\rho$(Q,NINO3) and $\rho$(Q,PDO) are -0.26 and -0.30 respectively.

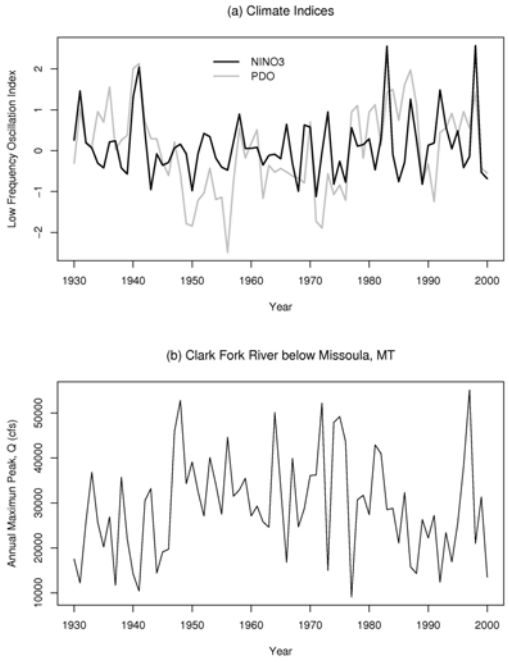


**Fig. 3** (a) Winter average (Jan-Feb-Mar-Apr) of the NINO3 and PDO indices, (b) Observed annual maximum peak at Clark Fork River below Missoula, MT.

### (2) Conditional Flood Quantile Estimation

Local Polynomial Likelihood is applied to the log transformed flows at various stations stated in 6.5.1 for estimating cross-validated conditional flood quantiles for p=0.1, 0.5 and 0.9. For comparison, estimations of the corresponding unconditional flood quantile using Local Polynomial technique (Apipattanavis et al., 2008) are performed. Figure 4 shows the results from the two stations. The conditional PDFs for high and low years for various sites are also shown in Figure 5.

### (3) Reconstruction of Flood Records

For illustrate the potential for forecasting flood risk, Local polynomial likelihood method with NINO3 and PDO are used for reconstructing the conditional flood quantiles for 1900-1929, a period prior to the earliest year of record at the Clark Fork River site. Annual maximum peak data from two nearby sites on the Clark Fork River is available for part of the prior period for a pseudovalidation. The correlation between the annual maximum peak at Clark Fork River below Missoula, MT (study site)

and the annual maximum peak at Clark Fork River near Plains, MT (USGS 12389000) is 0.986 over the 1930-2000. Similarly, the correlation between the annual maximum peaks at study site and the annual maximum peak at Clark Fork River at St. Regis, MT (USGS 12354500) is 0.911 for observed peaks during 1930-2000. The conditional flood quantiles reconstructed at the study site for the 1900-1929 period are shown in Figure 4(b), and their correlation with the two sites that have data for part of the period is provided in Table 2. The correlations resulted from local likelihood method are also shown in Table 2. It can be seen that the local polynomial likelihood provides a relatively higher correlation.

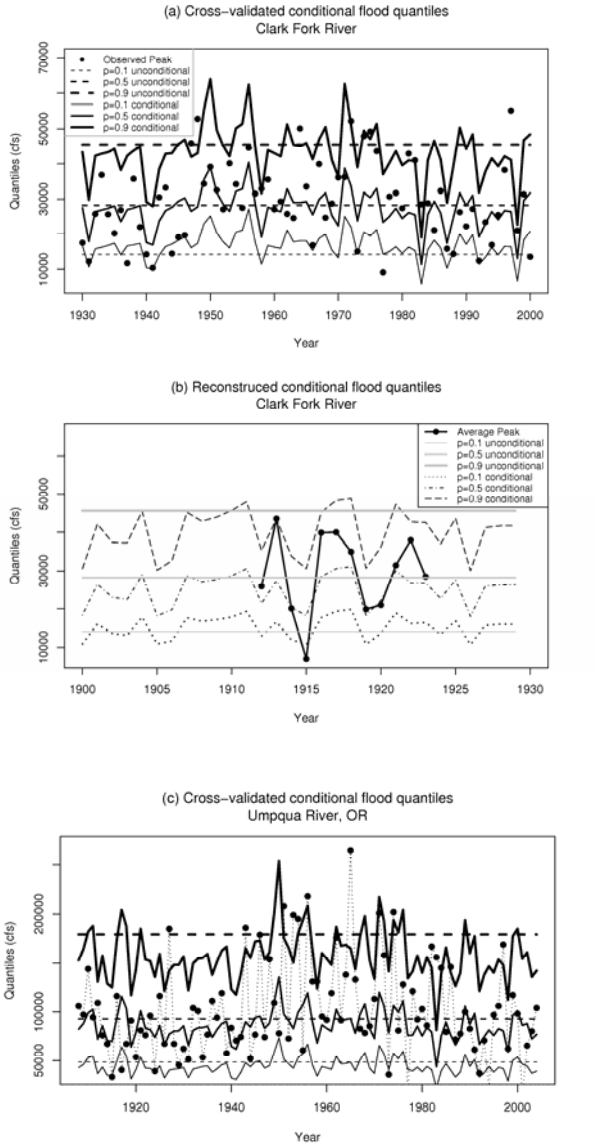


**Figure 4.** (a) Cross-validated conditional flood quantile estimates for the Clark Fork River, (b) Reconstructed conditional flood quantiles for period prior record for 1900-1929. (c) Cross-validated conditional flood quantile estimates for the Umpqua River, OR,

**Table 2.** Correlation of reconstructed flood quantiles with the observed annual maximum peak at nearby sites on the Clark Fork River

| Methods | Station 12389000 | | | Station 12354500 | | |
|---|---|---|---|---|---|---|
| | $\rho_{Q,Qp1}$ | | | $\rho_{Q,Qp2}$ | | |
| | p=0.1 | p=0.5 | p=0.9 | p=0.1 | p=0.5 | p=0.9 |
| Local likelihood | 0.64 | 0.54 | 0.33 | 0.53 | 0.48 | 0.37 |
| Local polynomial likelihood | 0.76 | 0.79 | 0.79 | 0.63 | 0.66 | 0.67 |

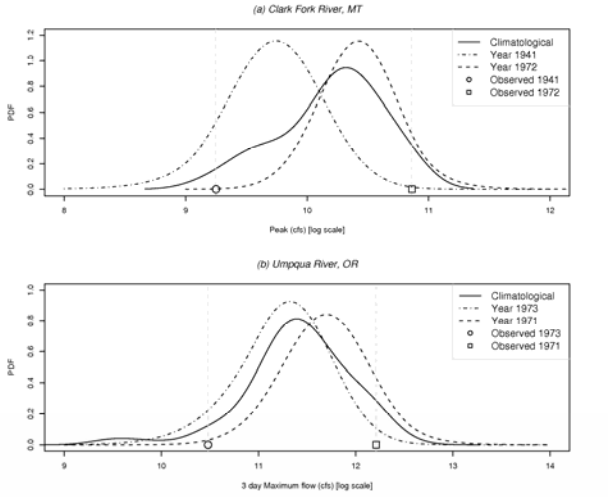


**Fig. 5.** Conditional PDF of high and low flow years for (a) Clark Fork River, (b) Umpqua River.

## 6. CONCLUSION

Local polynomial likelihood function performs well in estimating joint probability density function of annual maximum floods and predictors (e.g. ENSO, PDO, etc.), and joint probability density function of the predictors. Then, conditional probability density function and those joint probability functions are together used for calculation of conditional flood quantiles. Requiring no prior assumption of distribution function, the proposed nonparametric approach has advantage over the parametric and semiparametric approaches such as quantile regression and local likelihood respectively, on providing a flexible and general framework that being able to capture a wider range of tail behavior

The local polynomial estimation of the conditional density function was shown to be an effective competitor for the estimation of flood frequencies in the presence of nonstationarity. The applications provided here focused on the use of climate indices derived for representing known low frequency hydroclimatic variations. However, if appropriate atmospheric circulation indices can be identified for floods at a given site, then a projection of changing flood frequency can be

developed even for the case where scenarios using ocean-atmosphere General Circulation Models (GCMs) are developed for $CO_2$ or other forcings.

## REFERENCES


1) Anctil, F. and Coulibaly, P. : Wavelet analysis of the interannual variability in Southern Quebec streamflow, *J. Climate* **1** (2004), pp. 163–173, 2004.
2) Apipattanavis, S., B. Rajagopalan, and U. Lall, Local Polynomial Based Flood Frequency Estimator for Mixed Population, *Journal of Hydrologic Engineering*, 15(9), 680-691, 2010.
3) Baldwin, C. K., and Lall, U. : Seasonality of streamflow: The upper Mississippi River, *Water Resour. Res*., *35*, 1143–1154, 1999.
4) Bobee, B. and Ashkar, F. : The Gamma Family and Derived Distributions Applied in Hydrology. Water Resources Publications, Littleton, Colorado, USA, 1991.
5) Buchinsky, M. : Estimating the asymptotic covariance matrix for quantile regression models, Journal of Econometrics 68, 303–338, 1995.
6) Cane, M. and Clement, A. C. : A role for the Tropical Pacific coupled ocean–atmosphere system on Milankovitch and millennial timescales, Part II: global impacts. In: P. U. Clark, R. S. Webb and L. D. Keigwin, Editors, Mechanisms of Global Climate Change at Millennial Time Scales. Geophysical Monograph, vol. 112, American Geophysical Union, Washington, D.C., pp. 373–383, 1999.
7) Cayan, D. R. : Interannual climate variability and snowpack in the western United States. Journal of Climate, 9: 928–948, 1996.
8) Cayan, D. R., Redmond, K. T. and Riddle, L. G. : ENSO and hydrologic extremes in the Western United States. Journal of Climate, 12(9): 2881-2893, 1999.
9) Cole, J. E. and Cook, E. R. : The changing relationship between ENSO variability and moisture balance in the continental United States. Geophysical Research Letters, 25: 4529-4532, 1998.
10) Davison, A. C., and Ramesh, N.I. : Local likelihood smoothing of sample extremes, Journal of the Royal Statistical Society: Series B., 62(1): 191-208, 2000.
11) Dettinger, M. D., Cayan, D. R. and Redmond, K. T. : United States streamflow probabilities based on forecasted La Nina, winter–spring 2000. *Experimental Long-Lead Forecast Bulletin*, **8**(4), 57-61, 1999.
12) Dracup, J. A., and Kahya, E. : The relationships between U.S. streamflow and La Nin˜a events. *Water Resour. Res.,* **30,** 2133–2141, 1994.
13) Duan, Q., Sorooshian, S. and Gupta, V. K. : Effective and efficient global optimization for conceptual rainfall-runoff models, Water Resour. Res., 28(4): 1015-1091, 1992.
14) Franks, S. W. and Kuczera, G. : Flood frequency analysis: Evidence and implications of secular climate variability, New South Wales, Water Resour. Res., 38(5), 1062, 2002.
15) Gershunov, A. and Barnett, T. P. : Interdecadal modulation of ENSO teleconnections, Bulletimof American Meteorological Society, 79: 2715-2725, 1998.
16) Hirschboeck, K. K. : Climate and Floods," in R. W. Paulson, Chase, E.B. and Moody, D.W. eds., National Water Summary 1988–89, Floods and Droughts, U. S. Geological Survey Water-Supply Paper 2375, Denver, CO, 1991.
17) Jain, S. and Lall, U. : Magnitude and timing of annual maximum floods: Trends and large-scale climatic associations for the Blacksmith Fork River, Utah, Water Resour. Res., 36(12), 3641–3651, 2000.
18) Jain, S. and Lall, U. : Floods in a changing climate: Does the past represent the future?, Water Resour. Res., 37(12), 3193–3205, 2001.
19) Kite, G.W. : Confidence limits for design events, Water Resources Research 11: 48–53, 1975.
20) Koenker, R. and D'Orey, V. : Computing regression quantiles. Applied Statistics, 36: 383–393, 1987.
21) Koenker, R. and Park, B. : An interior point algorithm for nonlinear quantile regression. Journal of econometrics, 71:265-283, 1996.
22) Lins, H. F., and Slack, J. R. : Streamflow trends in the United States, *Geophys. Res. Lett*., *26*, 227–230, 1999.
23) Mann, M. E., Bradley, R. S. and Hughes, M. K. : Long-term variability in the El Nino Southern Oscillation and associated teleconnections, , Diaz, H.F. and Markgraf, V. (eds) El Nino and the Southern Oscillation: Multiscale Variability and its Impacts on Natural Ecosystems and Society, Cambridge University Press, Cambridge, UK, 357-412, 2000.
24) Mantua, N. J., Hare, S. R., Zhang, Y., Wallace, J. M. and Francis, R. C. : A Pacific decadal climate oscillation with impacts on salmon. Bulletin of the American Meteorological Society, 78: 1069-1079, 1997.
25) McCabe, G. J., Jr. and Dettinger, M. D. : Decadal variability in the relations between ENSO and precipitation in the western United States: International Journal of Climatology , 19, 1399-1410, 1999.
26) Pagan, A. and Ullah, A. : Nonparametric Econometrics, New York: Cambridge University Press, 1999.
27) Piechota, T. C. and Dracup, J. A. : Drought and regional hydrologic variation in the United States: Associations with El Niño–Southern Oscillation. *Water Resour. Res.*, **32**:1359–1373, 1996.
28) Pizaro, G. and Lall, U. : El Nino and Floods in the US West: What can we expect?, Eos Trans. AGU, 83(32), 349– 352, 2002.
29) Portnoy, S., and Koenker, R. : The Gaussian hare and the Laplacian tortoise: computability of squared-error versus absolute-error estimators. Statististical Science 12: 279–300, 1997.
30) Rajagopalan, B., Lall, U. and Cane, M.A. 1997. Anomalous ENSO occurrences: an alternate view, Journal of Climate, 10(9):2351-2357, 1997.
31) Rajagopalan, B., Cook, E., Lall, U. and Ray, B. : Temporal Variability of ENSO-drought association in the South West US, Journal of Climate, 13: 4244-4255, 2000.
32) Ropelewski, C. F. and Halpert, M. S. : Global and regional scale patterns associated with the El Niño/Southern Oscillation. Monthly Weather Review, 115: 1606-1626, 1987.
33) Sankarasubramanian, A. and Lall, U. : Flood quantiles in a changing climate: Seasonal forecasts and causal relations. Water Resources Research, 39(15):1134, 2003.
34) Trenberth, K. E., and Guillemot, C. J. : Physical processes involved in the 1988 drought and 1993 floods in North America. Journal of Climate, 9: 1288–1298, 1996.
35) Yu, K. : Smoothing regression quantiles by combining k-NN estimation with local linear kernel fitting, Statistica Sinica, 9: 759-774, 1999.
36) Wendland, W.M. and Bryson, R.A. : Northern Hemisphere airstream regions. Monthly Weather Review, 109: 255-270, 1981.

2010 AIT-KU JOINT SYMPOSIUM ON HUMAN SECURITY ENGINEERING

Bangkok, Thailand, November 25-26, 2010

# Estimation of Ground Profile in Padang City by Using Microtremor Observations

Junji Kiyono[1], Yusuke Ono[2], Rusnardi Rahmat Putra[3] and Tatsuya Noguchi[4]

[1]Professor, Dept. of Urban Management, Kyoto University
(Kyoto University Katsura Campus, Nishikyo-ku, Kyoto 615-8540, Japan)
E-mail: kiyono@quake.kuciv.kyoto-u.ac.jp
[2]Assistant Professor, Dept. of Urban Management, Kyoto University
(Kyoto University Katsura Campus, Nishikyo-ku, Kyoto 615-8540, Japan)
E-mail: ysk@quake.kuciv.kyoto-u.ac.jp
[3]Ph.D candidate, Dept. of Urban Management, Kyoto University
(Kyoto University Katsura Campus, Nishikyo-ku, Kyoto 615-8540, Japan)
[4]Assistant Professor, Faculty of Engineering, Tottori University
(Koyama-cho Minami, Tottori 680-8550, Japan)

Padang City is located in the high seismicity region of western Sumatra and often affected by such a massive earthquake. Earthquake damages are governed by the intensity of ground motion. The intensity of ground motion is dependent on the magnitude of the event, the source distance and the site amplification. In the present study we have investigated the characteristics of the site amplification in Padang City. A technique by use of microtremor have been widely used in recent years. In this study, microtremor at 62 sites in Padang City was measured. The two horizontal and vertical components of the microtremor were recorded at all 62 sites and array observations with 4 stations were performed for 11 sites of them. Two analyses were conducted using the recorded microtremor. First the Horizontal to Vertical Spectrum Ratios (HVSR) were computed for all sites. The results suggest that the thick alluvium is situated in the coastal area and its depth is decreasing from the coastal area to the mountain side. Second the dispersion curves of Rayleigh wave for array observation site were obtained by using the Spatial Autocorrelation (SPAC) Method. Then the inversion analysis was conducted to estimate the shear wave velocity profiles of the sites for at most 100m depth from the ground surface.

***Key Words :*** *Padang, seismicity, microtremor, array observation, Rayleigh wave, dispersion curve*

## 1. INTRODUCTION

Padang City is located in the high seismicity region along the western coast of Sumatra. It was known that there was the seismic gap off the coast of Padang and the occurrence of the inter plate earthquake with magnitude greater than 8.0 was expected(Aydan 2008). Although Padangwas struck by the massive earthquake with Mw 7.6 on 30 September 2009 and resulted in more than 1,000 casualties, this event was intra-plate type and one can say that the next inter-plate type earthquake is still expected. To reduce damages caused by the next destructive earthquake, the earthquake disaster mitigation program is needed. To develop the earthquake disaster mitigation program, prediction of earthquake ground motion distribution is essential information.

The intensity of ground motion is governed by not only magnitude of the event and the source distance but also the site amplification. To estimate the site amplification precisely, the subsurface structure under the region needs to be known. However the borehole testing technique provide the proper information of the subsurface structure, it is costly and

time-consuming. Therefore it is hardly possible to ensure numbers of borehole testing site enough especially in developing countries. In general, techniques by the use of microtremor measurement for estimating site amplification characteristics are considered easier and more cost-effective rather than the borehole testing methods.

Two methodologies are well known for investigating site amplification characteristics by using microtremor measurement. The first one is a technique using Horizontal to Vertical Spectrum Ratio (HVSR). Two orthogonal horizontal components and vertical component of microtremor are recorded at a site simultaneously and the spectrum ratio of the horizontal component to the vertical component is computed. It is known that a peak period of HVSR is approximately equal to dominant site period. On the other hands, the second technique is based on the dispersion characteristics of Rayleigh wave. The phase velocity of Rayleigh wave disperse and its characteristics reflects the soil at the site. The plot of phase velocity against frequency is called dispersion curve. One can draw a dispersion curve theoretically by using Haskell's matrix (Haskell, 1953) if soil profile is given. The soil profile at the site can be determined by finding a soil profile model which provides same characteristics of dispersion of Rayleigh wave by comparing to the observed one. To obtain a dispersion curve of Rayleigh wave, microtremor observation using an array of sensors is carried out. A dispersion characteristics of Rayleigh wave can be extracted from microtremor array records by using SPAC method (Aki, 1957).

## 2. GEOGRAPHY AND GEOLOGY

As described in the previous section, Padang City is located in the middle western coastal area of Sumatra Island. The Indo-Australia plate is subducting under the Eurasian plate at the offshore of the western Sumatra and earthquakes take place frequently in this region. Since 2000, Padang City has been affected by the 2000 Bengkulu earthquake, the 2004 great Sumatra earthquake, the 2005 great Nias earthquake and the 2007 Bengkulu earthquake.

The main part of Padang City is situated on the alluvium plain between the Indian Ocean and the mountains. The most part of the mountainous area is formed by Tertiary sediment rock and the outcrop of metamorphic rock is seen in some places. The alluvium plain spreads along the mountains with 10km in the east-west direction and 20km in the north-south direction. The topography around Padang City is shown in Fig. 1.

The rivers from the mountainous region reach the Indian Ocean after snaking several times and have formed the fens and deltas. Small villages are scattered in the mountainous region and moderate masonry house with single storey is typical in these villages. The dense populated zone is located in the flat area near the coast and modern style buildings with multiple stories are seen.

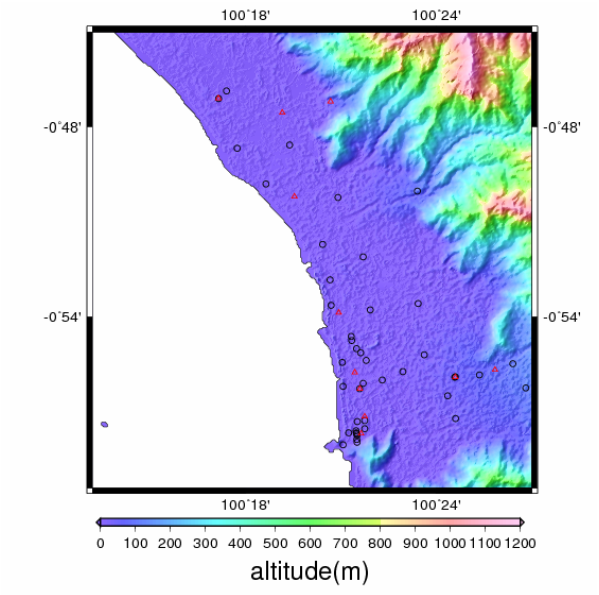


**Fig. 1** Topography of Padang City. The single station site and array site are indicated by a circle and a triangle respectively.

## 3. MICROTREMOR MEASUREMENT

The microtremor surveys with single station were carried out on November 2008, September 2009 and November 2009 at 50 locations covering Padang City. The locations are plotted in Fig. 2. The microtremor was measured by using GPL-6A3P sensor and the two horizontal(NS and EW) and the vertical(UD) components were recorded simultaneously for 10 minutes with 100Hz sampling frequency. In addition, the array observation with 4 stations were conducted at 11 sites on September and November 2009. Four sets of GPL-6A3P were used and three of them were arranged circularly and the other one was set at the center of the array. The radius of the array was varies from 1m to 30m depending on the situation of the site. The location of the array observation site is shown as a triangle in Fig. 2.

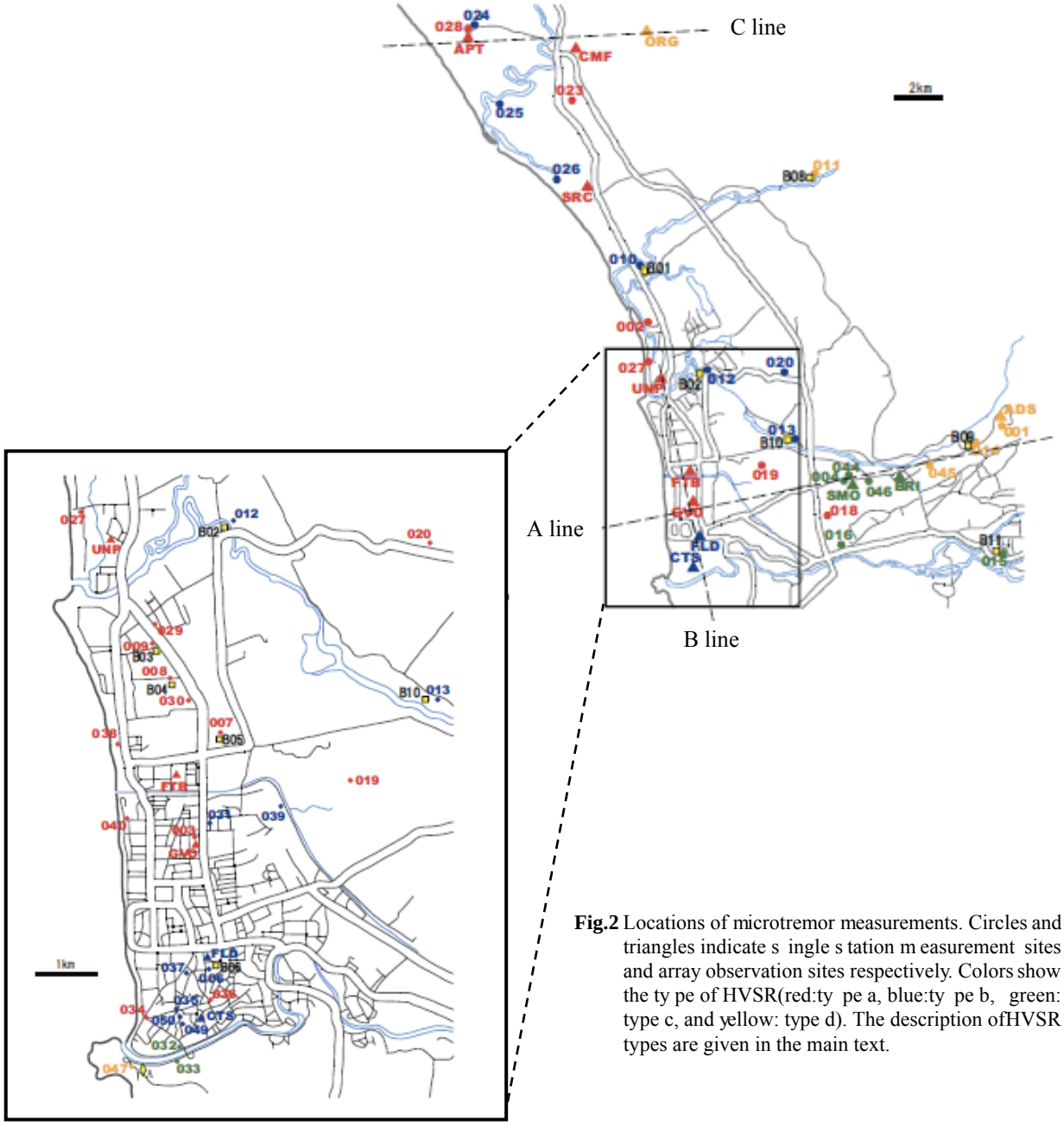


**Fig.2** Locations of microtremor measurements. Circles and triangles indicate s ingle s tation m easurement sites and array observation sites respectively. Colors show the ty pe of HVSR(red:ty pe a, blue:ty pe b, green: type c, and yellow: type d). The description ofHVSR types are given in the main text.

## 4. PEAK PERIOD DISTRIBUTION OF H/V

For each site, the tim e-series of the record is divided into at 5 to 10 intervals avoiding the infection of the strong noises caused by traffics et al. The Parzen ty pe window with 0.1-0.4Hz width was applied to the Fourier amplitude spectra of each interval for the purpose of sm oothing the signal. Then the HVSR of the individual interval was computed by

$$HVSR_i(\omega) = \sqrt{\frac{F_{NSi}(\omega)^2 + F_{FWi}(\omega)^2}{F_{UDi}(\omega)^2}} \qquad (1)$$

where $F_{NSi}(\omega)$, $F_{EWi}(\omega)$ and $F_{UDi}(\omega)$ denote the Fourier amplitude of the NS, EW and UD components of each interval respectively while $\omega$ is the frequency . Then the HVSR for each observation site was obtained by averaging of the *HVSRi* for all intervals.

The HVSRs were computed for 62 sites including 11 array observation sites. The HVSRs were classified into 4 types; (a) HVSR which showsa clear peak in the long period range(greater than 1.0s), (b) HVSR which has two peaks, (c) HVSR which has a clear peak in the short period range(smaller than 1.0s) and (d) HVSR which has no apparent peak.

The exam ples of these ty pes are shown in Fig. 3 and the type of each site is shown in Fig. 2.

The distribution of the HVSR' s peak period is shown in Fig. 4. To draw this figure, the Ordinary

Kriging technique was used for intepolation. In the case of type (b) spectrum, the longer peak period was taken. For the type (d), the peak period was assigned 0.1s. The HVSR of the coastal area have their peaks at 2.0s to 2.5s, whereas that of the mountainous area shows smaller peak period. This indicates that the sedimentary layer becomes thicker from mountain side to the coast.

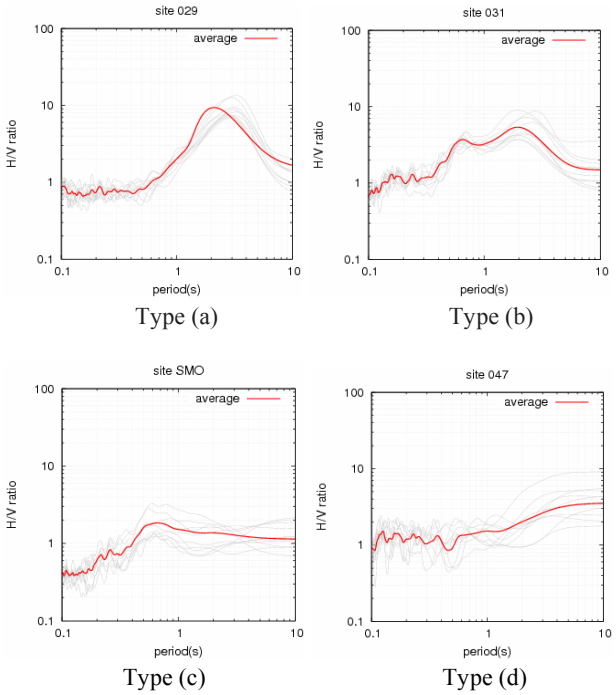


**Fig. 3** Four types of the measured HVSR

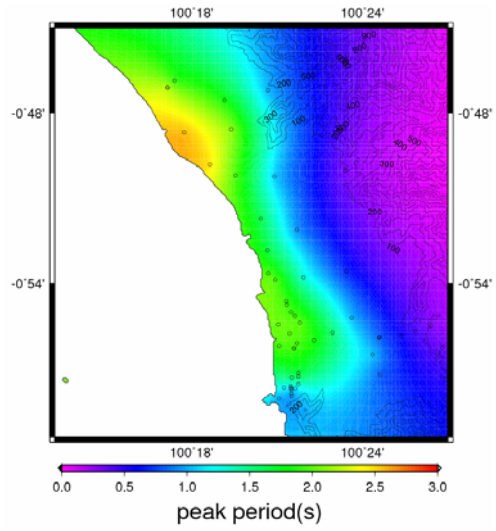


**Fig. 4** The distribution of the peak HVSR period. The altitude is also displayed by the solid contour lines.

## 5. S-WAVE VELOCITY PROFILE

The dispersion curves of Rayleigh wave were obtained for 11 array observation sites by using the SPAC method and shown in Fig. 5. By conducting the inversion analysis using these observed dispersion curves, the soil profiles for the 11 array observation sites were estimated. In the inversion analysis, Particle Swarm Optimization (PSO) algorithm was adopted. The PSO is a solver for non-linear optimization problem (Keneddy & Eberhart, 1995).

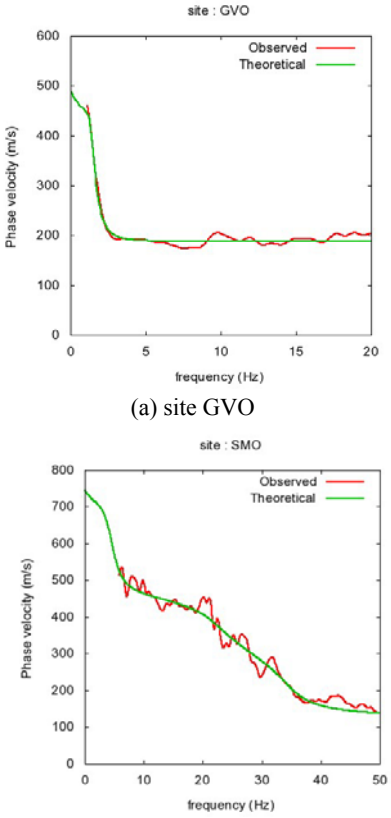


**Fig. 5** Disppersion curves of Rayleigh wave. The red lines are corresponding to the observed curve. The green lines are obtained from the soil profile models identified by the inversion analysis.

Before performing the inversion analysis, the subsurface structure was assumed to consist of horizontal layers of elastic and homogeneous mediums upon a semi-infinite elastic body. The shear wave velocity and thickness of each layer are the parameters which were determined by the inversion analysis. The theoretical dispersion curves of Rayleigh wave were computed for the obtained soil profiles and shown as the green solid lines in Fig. 5. As shown in Fig. 5, both dispersion curves showed good agreement each other.

The estimated shear wave profiles are summarized

in Fig. 6. The depth of the engineering base which defined as the soil layer with the shear wave velocity greater than 400m/s is depicted as broken linesin Fig. 6.

In the coastal area (GVO, APT, FTB and UNP), the depth of the engineering base is estimated approximately 100m to 180m although it becomes shallow in the southern part of the area(FLD and CTS).

As mentioned in the previous section, the HVSR for GVO has the perk at around 2.0. However, according to the quarter wavelength theory, it is estimated around 0.40s and 0.67s with 250m/s and 150m/s shear wave velocity respectively. This suggest that the peak of HVSR for GVO is governed by the deeper soil structure. Similar discussion can be made for all other site in the coastal area.

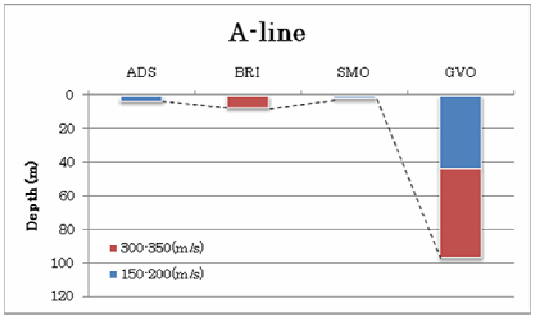


(a) A line

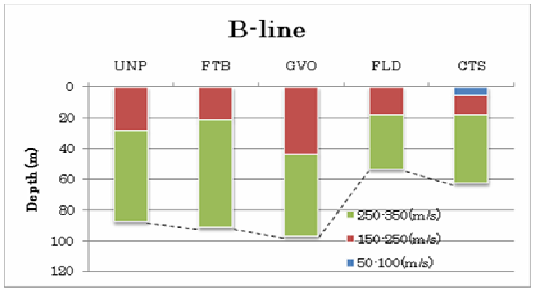


(b) B line

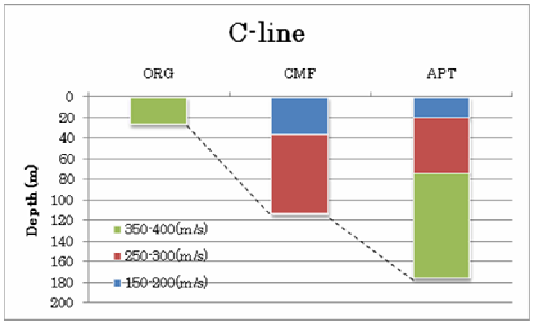


(c) C line

**Fig. 6** Obtained subsurface structures at array observation sites.

## 6. CONCLUSIONS

For estimating the site amplification of earthquake ground motion, the microtremor observation was performed at 62 sites in Padang City. The measurements for the analysis of HVSR were done at all sites whereas the array observations for obtaining the dispersion curves of Rayleigh wave were performed at 11 of 62 sites.

The HVSRs for the coastal area show the clear peaks at 2.0 to 2.5 seconds. On the other hand no clear peak is recognized in the HVSR for the mountainous area. In the intermediate area between the coastal and the mountain area, the HVSR has a dominant period at around 0.6 to 1.5 secondswhereas some sites show two peaks of the HVSR. These results suggest that the thick alluvium is situated in the coastal area of Padang City and its depth is decreasing from the coastal area to the mountain side.

The inversion analysis using the dispersion curve of Rayleigh wave showed that the shear wave velocity profiles of the array observation sites for at most 100m depth from the ground surface. However the peak period of the HVSR with 2.0 to 2.5 seconds cannot be reproduce by the estimated profiles. Therefore additional investigations for the deeper S-wave velocity structure estimation are required.

**ACKNOWLEDGMENT:** This research is done under the umbrella of Global COE Project for Education and Research on Human Security Engineeirng, Kyoto University (Project Leader: Prof. Yuzuru Matsuoka). Authors deeply appriciate strong and continuous supports to GCOE-HSE, Kyoto University. The authors thank to Mr. Kubo, ex-master course student in Kyoto University, for his assistance of observations and analyses.

## REFERENCES

Aydan, O. (2008): Seismic and tsunami hazard potentials in Indonesia with a special emphasis on Sumatra Island, Journal of the School of Marine Science and Technology, Tokai University, Vol.6, pp.19-38.

Aki, K. (1957): Space and time spectra of stationary stochastic waves, with special referent to microtremors, Bull. Earth. Res. Inst., Vol.35, No.3, pp.415-456.

Haskell, N. A. (1953): The dispersion of surface waves on multi-layered media, Bull. of the Seismological Society of America, Vol.43, No.1, pp.17-24.

Keneddy, J. and Eberhart, R. C. (1995): Particle swarm optimization, Proc. of IEEE International Conference on Neural Networks, Vol.4, pp.1942-1948.

2010 AIT-KU JOINT SYMPOSIUM ON HUMAN SECURITY ENGINEERING

Bangkok, Thailand, November 25-26, 2010

# Proposal of Seismic Hazard Map for Indonesia Based on the Latest Earthquake Catalogs

R.P. Rusnardi [1], J. Kiyono[1], Y. Ono[1]

[1] PhD Student, Graduate school of Engineering, Dept. of Urban Management., Kyoto University, Japan
(C1-146, Kyoto University Katsura Campus, Nishikyo-ku, Kyoto 615-8540, Japan)
E-mail: rusnardi@quake2.kuciv.kyoto-u.ac.jp
[1] Professor, Dept. of Urban Management, Kyoto University, Japan
E-mail: Kiyono@quake.kuciv.kyoto-u.ac.jp
[1] Assistant Professor, Department of Urban Management, Kyoto University, Japan
E-mail: ysk@quake2.kuciv.kyoto-u.ac.jp

**ABSTRACT**

Indonesian archipelago is located on the boundaries of the three major tectonic plates-India-Australian, Pacific, and Eurasian plates which extend from Sumatra in the west to Papua Island in the east. Thus it is a major source of subduction-related seismicity. Therefore tsunami and earthquake hazards are prone to occur. Based on complied data during the period 1779-2010, 48,000 earthquake events exceeding M4 had occurred in Indonesia. Since the earthquake data are available in various magnitudes scale, we converted all scales into moment magnitude. By using the catalogs compiled, we constructed area earthquake source model and estimated the frequency-magnitude relationship. From recorded data by accelerometers installed at four stations in Padang, we plotted observed data on the several existing attenuation equations and selected a suitable attenuation relationship for Indonesia. We calculated the peak ground acceleration at 2%, 5% and 10% probability of exceedance in 50 years for rock condition. We compared obtained ground motion acceleration probability with existing ones and discussed.

***Key Words:*** *seismic hazard, earthquake, faults, source zone, areal model*

## 1. INTRODUCTION

Indonesia is an archipelago located in Southeast Asia. Indonesia has approximately 17,504 islands with a total land area of 1,922,570 km$^2$ and 3,257,483 km$^2$ waters. Why does Indonesia often experience the earthquakes? Seen geographically, Indonesia is at the collision point of three crustal plates are the Eurasian Plate, the Pacific and Indian-Australian plate which stretches from Sumatra in the west to Papua in the east of the island (Figure 1). Thus it is a major source of subduction-related seismicity. According to catalog, the number of earthquakes considered in this study is the amount of 48,000 events with magnitude > 4.0. The data obtained is from year 1779 to year 2010, however, we only considered earthquake events from 1973 to 2010 for the calculation of an annual average number, because the number of seismic events in 1779-1973 is around 169 events, it represents only 0.35% of the total incidence of earthquakes. We obtained an average of 1,292 events/years. Most of the historical major earthquakes in Indonesia caused great damage to facilities as reported by Utsu (1992)[1)], Fauzi (1999)[2)] and EERI (2010)[3)]. In Figure 2, many large earthquakes in the shallow areas could produce a large tsunami like Aceh tsunami in 2004 which killed hundreds of thousands of people. In

this study, Indonesian region is clustered into two regions, west and east. The western islands cover Sumatera and Java, on the other hand eastern covers Bali, Flores, Timor, Ambon, Sulawesi and Papua.

In western Indonesia (i,e. Java and Sumatra), Sumatra subduction zone is formed by the subduction of the Indo-Australian plate beneath the Eurasian plate at a rate of about 67 mm per year and this is the main source of subduction-related seismicity[4]. A few giant earthquakes occur in this territory before like in 1779 ( Mw 8.4) , 1833 ( Mw 9.2) , 1861 (Mw8.3), in 2004 the largest (Mw 9.2), 2007 ( Mw 7.9) and the last incident occurred on 30 September 2009 (Mw 7.6) at 5.15 pm, it located -0.81 latitude, 99.65 longitude and depth of 80km. It produced a large shaking and severe damage to the region of Padang and Padang Pariaman. The location of Padang earthquake was at depth of about 80 km within the ocean slab of the Indo-Australian plate, and its epicenter was about 60km offshore from Padang. This earthquake was similar to intra-slab earthquake at intermediate depth with comparable magnitude, it did not generate a tsunami of significance. This earthquake caused 1,124 deaths, 1,214 severely injured, 1,688 minor injured, 3 people missing and significant damage to houses about 114,797 houses severe damaged, 67,198 houses moderate damaged, 67,837 minor damaged, Others 4,000 buildings and 93 schools in Padang city were damaged. Padang was sustained damage mostly to building. Higher number of causalities would happened if the earthquake struck earlier time when the school, office and others activities were in session.

The oblique convergence also results in lateral displacement along the Sumatera fault. This fault also generates large destructive earthquakes such as in 1892, 1943, 2007, Mw 7.1, 7.6, 6.4 respectively. These faults are capable of generating future strong ground motion that can affects to vulnerable structures. According to the catalogs, the tectonic of Sumatera produces a very high annual rate of earthquakes and many of the major earthquakes occurred in shallow region under the sea ( Figure 2). Those earthquakes cause large tsunami such as in 1833 and 2004 in eastern of Indonesia. Based primarily on record from 1608 to 1877, eastern Indonesia experienced over 30 significant earthquake events and 35 Tsunamis [5]. Probabilistic Seismic ysis (PSHA) aims to quantify the uncertainties and combine them to produce an explicit description of the distribution of future shaking that may occur at a site. We considered all possible earthquake events and estimate ground motions, along with their associated probabilities of occurrence. In order to assess the risk of structures due to earthquake shaking, we determine the annual probability ( or rate) of exceedance for some level of earthquake shaking at site. In this hazard assessment, we use the source modeling applied for the GSHAP map by compiling updated earthquake catalog. We here are interested in all earthquake sources capable of producing damaging ground motion at a site. In this study we consider magnitude larger than 4.0 in moment magnitude scale, and adopt new model such as area source because earthquake events may occur anywhere. For accelerometer records we compared attenuation equation and selected a suitable one for Indonesia. In addition, we calculated the seismic hazard for peak ground acceleration (PGA) with 1%, 5% and 10% probabilities of exceedance in 50 years.

## 2. PROBABILISTIC SEISMIC HAZARD ANALYSIS

### (1) Earthquake catalog

Estimation of future seismicity is based on the rate of past earthquake as determined from earthquake catalog. In this study, we compile a new catalog of instrumentally recorded by combining several sources such as USGS catalog, ISC catalog (various bulletin of the International Seismological), BMKG (Indonesia Meteorology agency) and Tsunami catalog and zone in Indonesia[6], we construct a new catalog by eliminating overlap according to both automatic and manual procedures that incorporate our judgment. Since the earthquake data have been reported in different magnitude and intensity scale by source catalogs, all data converted to moment magnitude[7]. Here we are interested in all earthquake source capable of producing damaging ground motions at site. These sources could be fault and subduction zone, which are typically planar surface indentified through various means such as observation of past earthquake location and geological evidence. If individual faults are not identifiable,

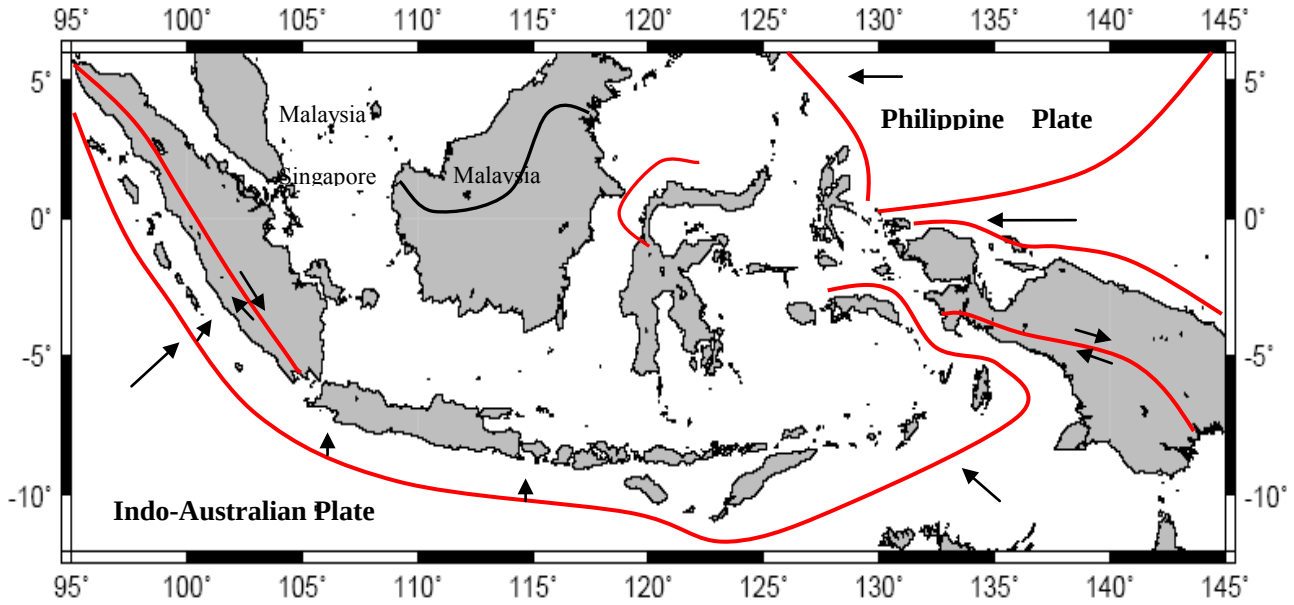


**Fig.1** Tectonic and Plate boundaries. Large arrows indicate the direction of plate motion

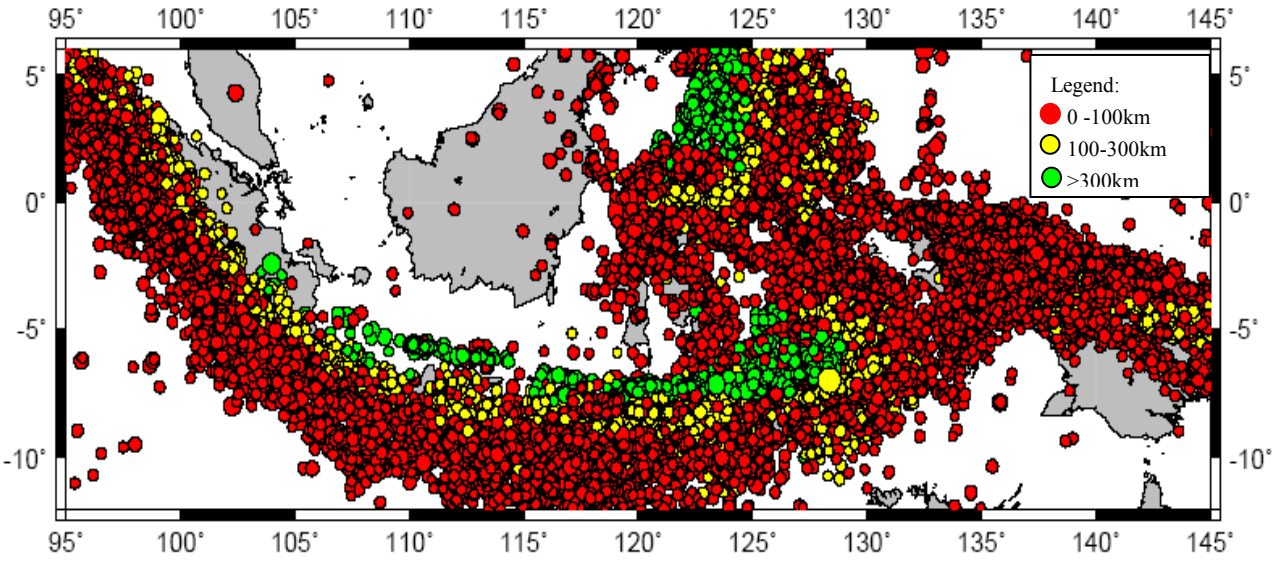


**Fig.2** Seismicity map of Indonesia region, Mw>4 . Data from USGS, ISC, Hamzah & Puspito, BMKG, the period 1779 – 2010

then earthquake sources may be described by areal region in which earthquake may occur any where[8]. For the accelerometer data the Engineer without Border Japan (EWBJ) was installed three accelerometers at 3 points in Padang city; government office, sub-district office and Andalas university, about 500m, 6km and 8 km from seaside respectively as shown in Fig. 3. These accelerometers were installed from the year of 2008

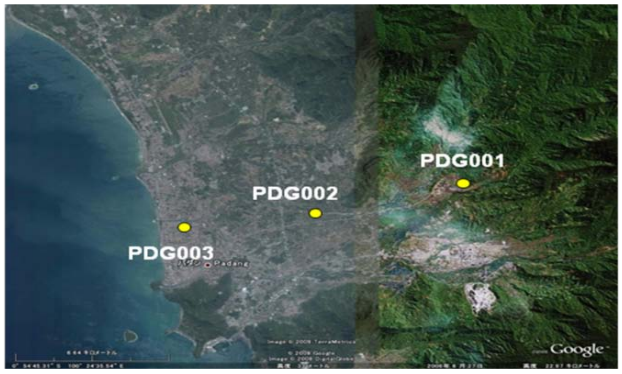


**Fig.3** Accelerometer stations at Padang city

### (2) Source Zones

In this study, we determine the earthquake sources described by areal region in which earthquake occurred within radius 150 km from a site. Indonesia located 95.E 145E and -9N 6N. The area divided into 1,400 meshes as showed in Figure 4. For each area, we calculated frequency-magnitude relationship, and determined an earthquake source capable of producing damaging ground motions at site. Probabilistic seismic hazard analysis was carried out and estimated the total probabilistic seismic hazard to a site.

### (3) Identify Earthquake Magnitudes

Tectonic faults are capable of producing earthquakes of various size (i.e., magnitude). The distribution of these earthquakes size in region generally follows a particular distribution[9], given as follow

$$\log\gamma_m = a - bm \qquad (1)$$

Where Log $\lambda_m$ is the rate of earthquake with $a$ value magnitude greater than $m$, and $a$ and $b$ are constants. Eq.(1) is estimated using statistical analysis of historical observation, with additional constraining data provided by other types of geological evidence indicate the overall rate of earthquake in a region, and $b$ value indicates the relative ratio of small and large magnitude (typical $b$ value are approximately equal to 1

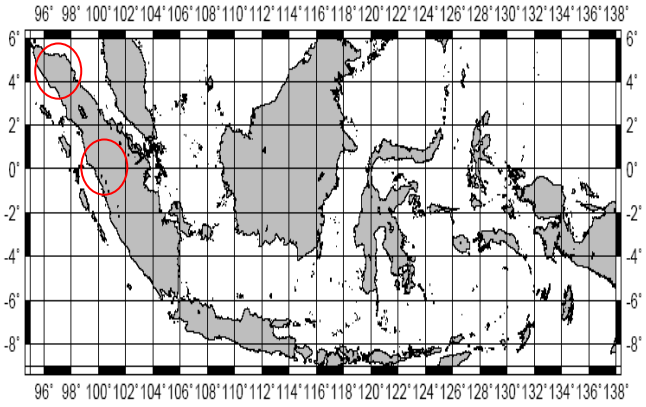


**Fig.4** Indonesia area analyzed and two red Circles are two samples of source zone with 150km radius for Padang city and Band Aceh

## 3. GROUND MOTION INTENSITY

The magnitude of ground motion at varying distance from the above earthquake source is determined from the comparison of several attenuations proposed by Fukushima (1999)[10], Young (1997)[11] and Megawati (2008)[12]. As no attenuation equation is currency existing in Indonesia, we plotted the recorded data of an observation site, and selected an appropriate attenuation (figure 5 and 6). From the comparison, we adopted Fukushima's attenuation as a suitable equation and applied to seismic hazard analysis.

$$\log A = 0.41*Mw - \log(R+0.032*10^{0.41Mw}) - 0.0034R + 1.3 \qquad (2)$$

Std = 0.21

Where logA is peak ground acceleration; Mw is moment magnitude; R is close distance to epicenter; and std is standard deviation. To estimate peak horizontal accelerations at site for rock and soft soil, the result from equation 2 multiplied by 0.60 and 1.4 respectively.

## 4. TOTAL HAZARD CURVE

The schematically illustrated attenuation model of probabilistic approach to estimating earthquake ground motion hazard, it shown in Figure 7. The seismic hazard *H (A)* is defined as the annual occurrence rate of earthquake that produces a ground motion exceeding a given level at a specific site, base on Cornel (1968)[13] and McGuire (1976)[14] the overall hazard in composed of the respective contribution *Hi (A)* from each source zones i out of the set of zone I. we will first consider one intermediate calculation as we build toward a PSHA equation that consider multi sources. Annual occurrence rate equation of Kramer (1996)[15].Where the range of possible $M_i$ and $R_i$ have been discretized into $n_M$ and $n_R$ interval, respectively, using the discretization technique.

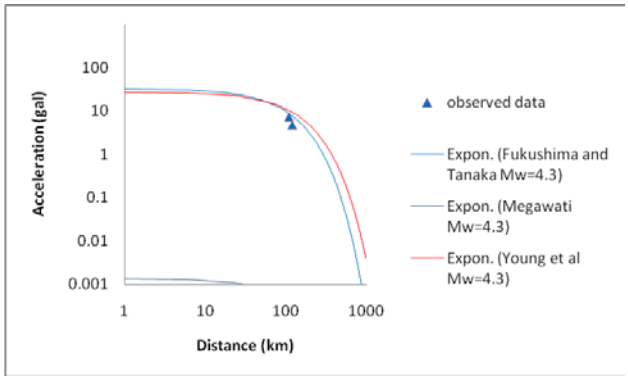


**Fig. 5** Comparison of attenuation relation for subduction zone and rock condition Mw=4.3

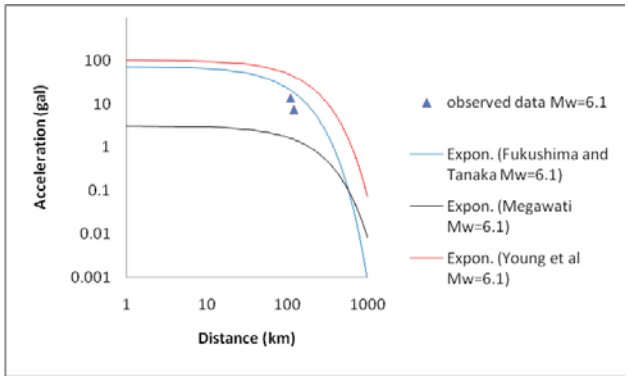


**Fig. 6** Comparison of attenuation relation for subduction zone and rock condition Mw=6.1

$$\lambda_m(IM>x)=\sum_{i=1}^{sources}\lambda_m(M_i>m_{min})\sum_{j=1}^{n_M}\sum_{k=1}^{n_R}P(IM>x|m_j,r_k) *P(M_i=m_j)P(R_j=r_k) \quad (3)$$

where $\lambda_m(IM>x)$ is the annual earthquake occurrence rate of which peak value exceeds a given level, x; $\lambda(M_i>m_{min})$ is the rate of earthquake with magnitude greater than *m*, $P(IM>x|m_j,r_k)$ is the probability of occurrence of the associated magnitude and distance; $P(M_i = m_j)$ is the probability associated with all magnitude between $m_j$ and $m_j+1$ to the discrete value $m_j$; $P(R_j=r_k)$ is the probability of occurrence of the associated distance.

## 5. CONCLUSION

From the comparison of proposed hazard map (Figure 7) and existing hazard map (Figure 8), the result of this study shows that the ground peak acceleration of 475 years at every site is higher about 30% through 55% compared with existing seismic hazard of Indonesia. Differences of the values might be mainly caused by the number of data collected, in which many earthquakes with magnitude greater than 6 occurred after 2002 are included and it might be difference on attenuation law.

**ACKNOWLEDGMENTS:** I would like to express my sincere gratitude to all those who helped me to complete this research, and to Directorate Jenderal of Higher Education of Indonesia Government (DIKTI) who was support in financial during studying Kyoto University, Thanks very much to the Engineer Without Border of Japan (EWBJ) which installed 3 accelerometers in Padang and we used this data in our study, thanks to Dr. Hakam, the person who helped me to collect investigation data in Padang. Thanks to Dr. Suharjono, Meteorology, Climatology and geophysical Agency (BMKG) of Indonesia government, for providing investigation data from accelerometers around Indonesia region.

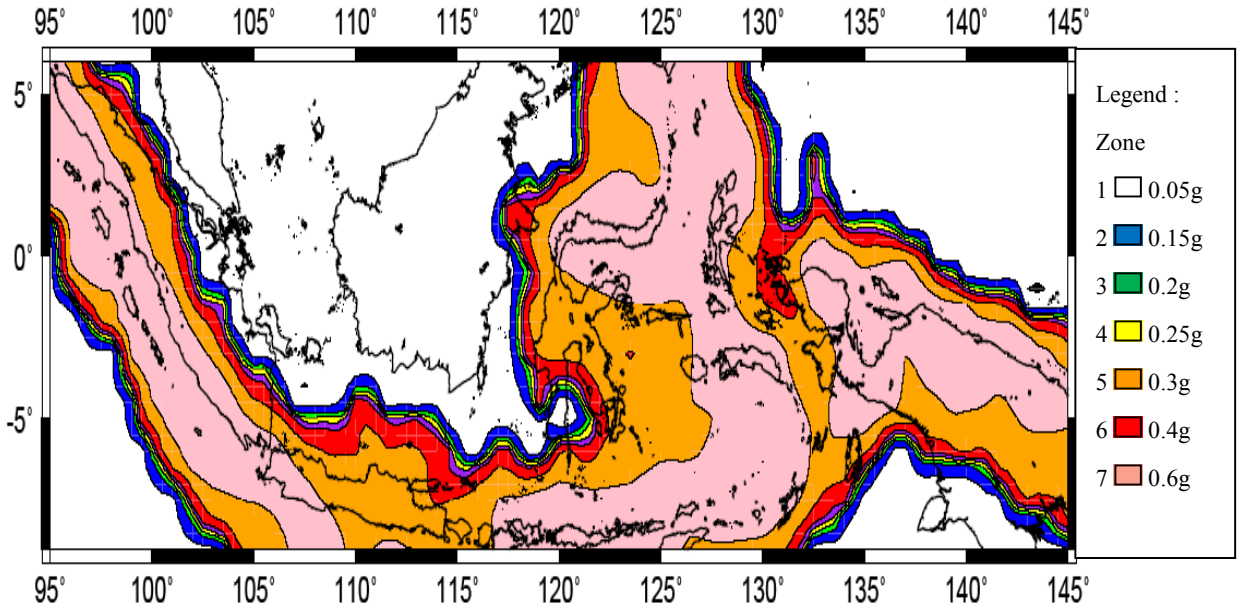


**Fig.7** The result of Seismic hazard of Indonesia return period 475 years for rock

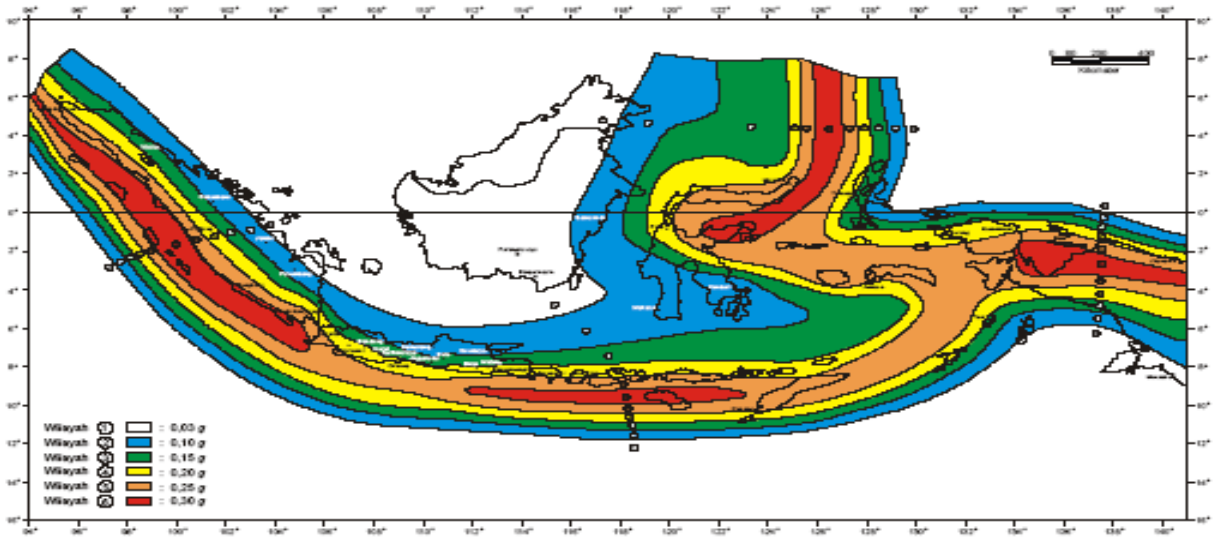

Gambar 2.1. Wilayah Gempa Indonesia dengan percepatan puncak batuan dasar dengan perioda ulang 500 tahun

**Fig.8** Copy of the existing Seismic hazard of Indonesia returns period 475 years for rock, made in 2002

## REFERENCES


1) Utsu, T. (1992), Catalog of Destructive Earthquake in the world 1500-1992, In the Disaster Reduction handbook, International Institude of seismology and earthquake Engineering, Tsuka Japan, I-24

2) Fauzi (1999), Private home page (http://www.gretchen.geo.rpi.edu/fauzi/txt/

3) EERI (2009)," The $M_w$ 7.6 Western Sumatra Earthquake of September 30, 2009, Special report

5) Major, J.R, Robinson, J.S. ; Harrris, R.A (2008), Earthquake and Tsunami History and Hazards of Eastern Indonesia, American Geophysical Union, Fall Meeting 2008

6) Hamzah and Puspito (2000)." Tsunami Catalog and zones in Indonesia, "Journal of natural disaster science, Volume 22, number 1, 2000, pp25-43

7) Hank,TC., and Kanamori,H. (1979)," A moment Magnitude Scale" Journal of Geophysics Res., vol. 84,2348-2350.

8) Jack W. Baker (2008)"Introduction Probabilistic Hazard Analysis" handbook. Version 1.3 oct 1st 2008.

9) Gutenber, B., and Ricther, C.F. (1944). "Frequency of Earthquake in California. "Bulletin of Seismological Society of America, 34(4), 185-188

10) Fukushima, Y., Tanaka, T. (1990). "Anew Attenuation Relation for Peak Horizontal Acceleration of Strong Earthquake Ground Motion in Japan". Bulletin of the Seismological Society of America. Soc. Am. 80, 757-783

11) Young, R.R., Chiou, S.J.< Silva, W.J., Humphrey, J.R. (1997)."Strong Ground Motion Attenuation Relationship for subduction zone. Seimol. Res. Lett. 68, 58-73

12) Megawati, (2008), "Seimic Hazard of Singapore and Malaysia." Earthquake engineering in low and moderate seismic region of southeast Asia and Australia, EJSE

13) Cornell, C.A., and Winterstein, S.R. (1988)." Temporal and Magnitude Dependence in Earthquake Recurrence Model." Bulletin of the Seismological Society of America, 78(4), 1522-1537

14] Mcguire, R.K (2004)." Seismic Hazard and Risk Analysis" Earthquake engineering institute, MNO-10

[15] Kramer, S.L (1996) " Geotechnical Earthquake Engineering", Prentice-Hall International series in civil engineering and engineering mechanic


**Kyoto University Global COE Program**
**Global Center for Education and Research on**
**Human Security Engineering for Asian Megacities**

**京都大学グローバル COE プログラム**
**アジア・メガシティの人間安全保障工学拠点**